Mukesh G. Harisinghani
Editor

Atlas of Lymph Node Anatomy

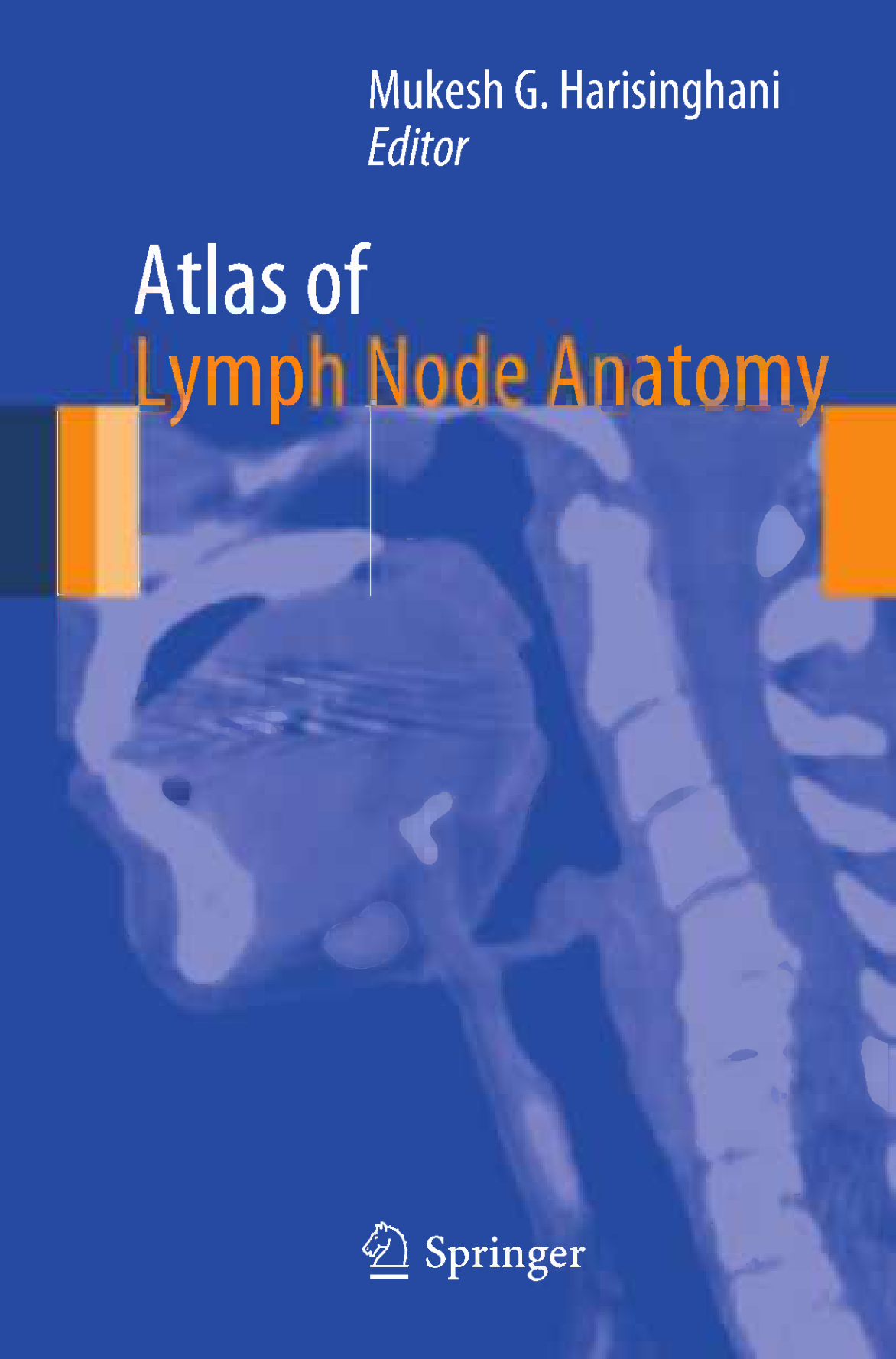

Springer

Atlas of Lymph Node Anatomy

Mukesh G. Harisinghani
Editor

Atlas of Lymph Node Anatomy

This publication was developed through an unrestricted educational grant from Siemens.

Springer

Editor
Mukesh G. Harisinghani
Massachusetts General Hospital,
Department of Radiology
Harvard Medical School
Boston
Massachusetts
USA

ISBN 978-1-4419-9766-1 ISBN 978-1-4419-9767-8 (eBook)
DOI 10.1007/978-1-4419-9767-8
Springer New York Heidelberg Dordrecht London

Library of Congress Control Number: 2012951645

Printed on acid-free paper

Springer is part of Springer Science+Business Media (www.springer.com)

For my wife, Alpana, and my children,
Puneet and Ayesha

Mukesh G. Harisinghani

Preface

Nodal staging is an integral part of determining therapy and prognosis in most primary tumors and the evaluation of lymph nodes involves accurate anatomical localization followed by characterization. While there is an abundance of surgical literature highlighting the distribution of regional lymph nodes in various primary tumors, a comprehensive imaging text highlighting the anatomical nodal stations and their involvement in various primary tumors is lacking. The current atlas attempts to highlight nodal anatomy by way of color illustrations and color-coded topographical depiction on cross-sectional imaging studies. We hope the content will be useful and informative to a wide range of readers filling in the void about nodal anatomy.

Mukesh G. Harisinghani

Acknowledgments

First, I would like to acknowledge my mentors for stimulating my interest and fostering my enthusiasm during my early academic years. This project would not have been possible without their guidance and constant encouragement. I have to thank the contributors who helped me realize this atlas by providing ideas and enabling me to complete this project in a timely fashion. A special note of appreciation to my family for tolerating my time away to complete this book.

Mukesh G. Harisinghani

Contents

Contributors

Suzanne Aquino, M.D. Radiologist, Honolulu, HI, USA

Kai Cao, BME Department of Radiology, Massachusetts General Hospital, Boston, MA, USA

Subba R. Digumarthy, M.D. Department of Radiology, Massachusetts General Hospital, Boston, MA, USA

Azadeh Elmi, M.D. Department of Radiology, Massachusetts General Hospital, Boston, MA, USA

Alpana M. Harisinghani, M.D. Medical Research Associate, Perceptive Informatics, Billerica, MA, USA

Sandeep S. Hedgire, M.D. Department of Radiology, Massachusetts General Hospital, Boston, MA, USA

Susanne Loomis, MS, FBCA Radiology Education Media Services (REMS), Massachusetts General Hospital, Boston, MA, USA

Shaunagh McDermott, M.D. Department of Radiology, Massachusetts General Hospital, Boston, MA, USA

Nishad D. Nadkarni, M.D. Department of Radiology, Massachusetts General Hospital, Boston, MA, USA

Vivek K. Pargaonkar, M.D. Department of Radiology, Massachusetts General Hospital, Boston, MA, USA

Zena Patel, M.D. Department of Radiology, PD Hinduja National Hospital, Mumbai, Maharashtra, India

Anuradha Shenoy-Bhangle, M.D. Department of Radiology, Massachusetts General Hospital, Boston, MA, USA

Patrick D. Sutphin, M.D., Ph.D. Department of Radiology, Massachusetts General Hospital, Boston, MA, USA

Head and Neck Lymph Node Anatomy

1

Cancers of the head and neck—including cancers of the buccal cavity, head and neck subset, larynx, pharynx, thyroid, salivary glands, and nose/nasal passages—account for approximately 6 % of all malignancies in the United States [1]. Careful analysis of nodes in the neck and knowledge of the various compartments is critical in the assessment and staging of primary head and neck malignancies. Regardless of the site of the primary tumor, the presence of a single metastatic lymph node in either the ipsilateral or contralateral side of the neck reduces the 5-year survival rate by about 50 %. The risk of cervical metastasis depends on the site of origin of the primary tumor [2].

Classification

The classification of cervical lymph nodes is complicated by the use of several different systems and the rather loose intermixing of specific names for a particular node from one system to another [3]. Of the approximately 800 lymph nodes in the body, about 300 are located in the neck. Thus, between one fifth and one sixth of all the nodes in the body are located in either side of the neck, making development of a classification system very complex [4].

For nearly four decades, the most commonly used classification for the cervical lymph nodes was that developed by Rouvière in 1938 who described the "collar" (including occipital, mastoid, parotid, facial, retropharyngeal, submaxillary, submental, and sublingual nodes), anterior and lateral cervical groups. The direction of nodal classification changed from that of a pure anatomic study to a nodal mapping guide for selecting the most appropriate surgical procedure among the various types of neck dissections [5].

In 1981, Shah et al. [6] suggested that the anatomically based terminology be replaced with a simpler classification based on levels. Since then, a number of classifications have been proposed that use such level, region, or zone terminology. In the past few decades, the simple level-wise classification (*see* Tables 1.1 and 1.2; Figs. 1.1 and 1.2) has been in use widely [7]. This system

M.G. Harisinghani (ed.), *Atlas of Lymph Node Anatomy*,
DOI 10.1007/978-1-4419-9767-8_1, © Springer Science+Business Media New York 2013

of division of neck nodes was supported by American Head and Neck Society and neck classification project [2]. However, it did not recommend adding additional levels and stated that the nodes involving regions outside the VI levels should be referred to by the name of their specific nodal group (*e.g.*, retropharyngeal/periparotid nodes).

Table 1.1 Numeric classification system of cervical nodes

Level	Location
I	Submandibular and submental nodes (all nodes in floor of mouth)
II	Internal jugular chain (or deep cervical chain) nodes; nodes about internal jugular vein from skull base to hyoid bone (same level as carotid bifurcation)
III	Nodes about internal jugular vein from hyoid bone to cricoid cartilage (same level that omohyoid muscle crosses internal jugular chain)
IV	Infraomohyoid nodes about internal jugular vein between cricoid cartilage and supradavicular fossa
V	Posterior triangle nodes (deep to sternocleidomastoid muscle)
VI	Nodes related to thyroid gland
VII	Nodes in tracheoesophageal groove, about esophagus extending down to superior mediastinum.

The ad hoc committee of the neck classification project introduced the concept of sublevels in the neck nodes as the nodes in particular zone in a level had different risk of metastatic involvement compared to the other zones in the same level [2]

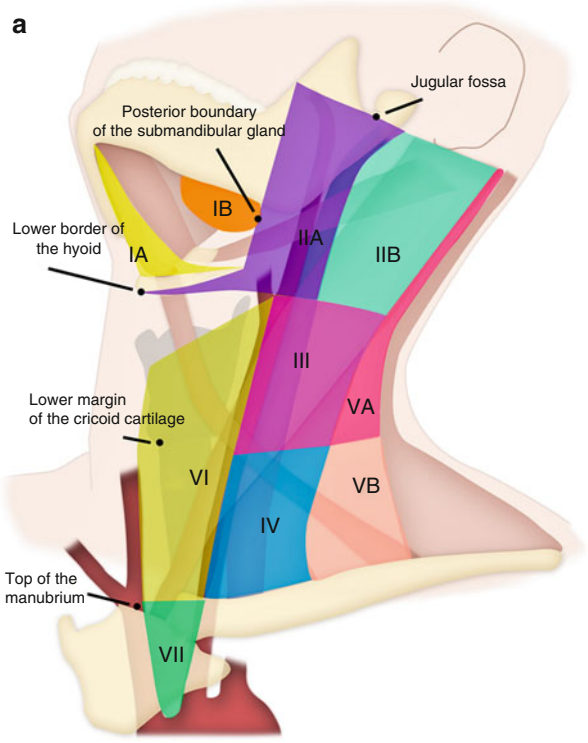

Fig. 1.1 (**a**) Important anatomical landmarks in the neck dividing the region into nodal levels. (**b**) Individual nodal groups are depicted (refer to color scheme)

Fig. 1.1 (continued)

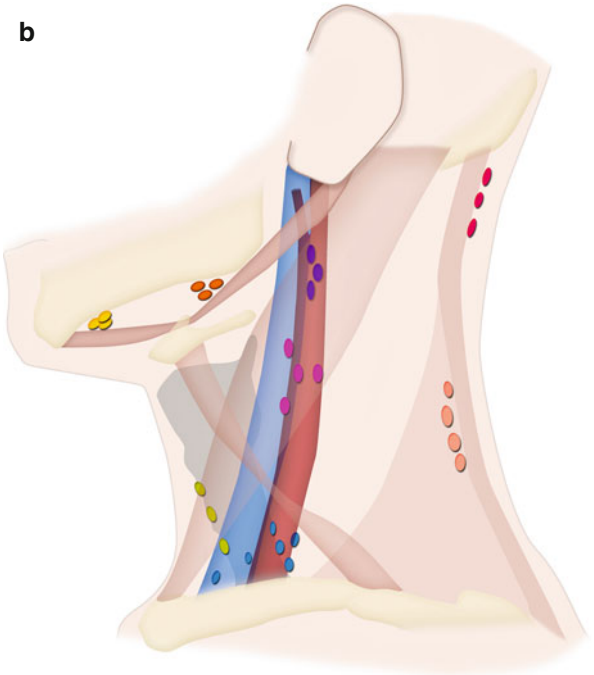

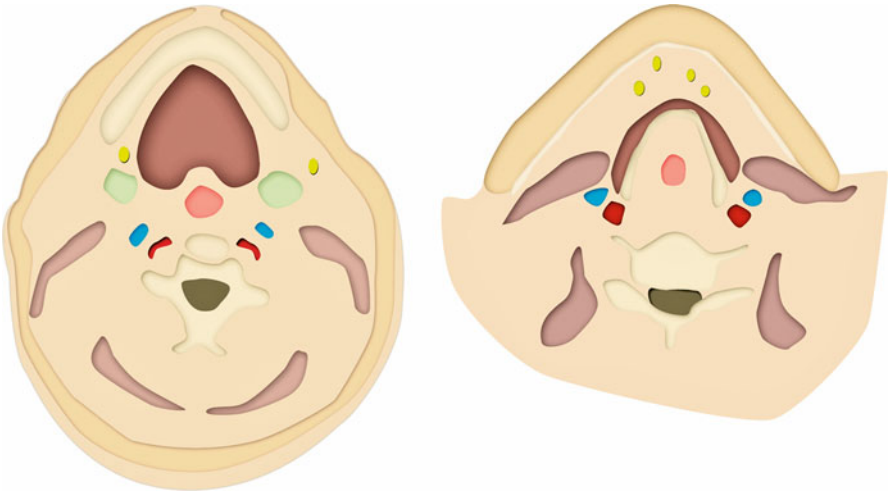

Fig. 1.2 Level IB submandibular (*left*) and level IA submental group of nodes (*right*)

Table 1.2 Levels and sublevels of cervical lymph nodes with their anatomical boundaries

Level	Superior	Inferior	Anterior (medial)	Posterior (lateral)
IA	Symphysis of mandible	Body of hyoid	Anterior belly of contralateral digastric muscle	Anterior belly of ipsilateral digastric muscle
IB	Body of mandible	Posterior belly of muscle	Anterior belly of digastric muscle	Stylohyoid muscle
IIA	Skull base	Horizontal plane defined by the inferior body of the hyoid bone	Stylohyoid muscle	Vertical plane defined by the spinal accessory nerve
IIB	Skull base	Horizontal plane defined by the inferior body of the hyoid bone	Vertical plane defined by the spinal accessory nerve	Lateral border of the sternocleidomastoid muscle
III	Horizontal plane defined by inferior body of hyoid	Horizontal plane defined by the inferior border of the cricoid cartilage	Lateral border of the sternohyoid muscle	Lateral border of the sternocleidomastoid or sensory branches of cervical plexus
IV	Horizontal plane defined by the inferior border of the cricoid cartilage	Clavicle	Lateral border of the sternohyoid muscle	Lateral border of the sternocleidomastoid or sensory branches of cervical plexus
VA	Apex of the convergence of the sternocleidomastoid and trapezius muscles	Horizontal plane defined by the lower border of the cricoid cartilage	Posterior border of the sternocleidomastoid muscle or sensory branches of cervical plexus	Anterior border of the trapezius muscle
VB	Horizontal plane defined by the lower border of the cricoid cartilage	Clavicle	Posterior border of the sternocleidomastoid muscle or sensory branches of cervical plexus	Anterior border of the trapezius muscle
VI	Hyoid bone	Suprasternal	Common carotid artery	Common carotid artery

Table 1.3 Summary of cervical lymph node involvement in various primaries

Site of primary carcinoma	Lymph nodes commonly involved	Not so commonly involved
Oral portion of tongue	I, II, III	
Floor of mouth	I, II	
Anterior faucial pillar-retromolar trigone	I, II, III	
Soft palate	II	
Nasopharynx	II, III, IV	V
Oropharynx	II,III	V
Tonsillar fossa	I, II, III, IV	V
Hypopharynx	II, III, IV	V
Base of tongue	II, III, IV	V
Supraglottic larynx	II, III, IV	
Thyroid	VI	II–V if V is clinically +
Stomach and testis		IV

Criteria for Enlargement

The size criteria for the cervical lymph nodes has been proposed as short axis diameter greater than 11 mm in jugulodigastric and greater than 10 mm in all other cervical nodes [8]. At the time of this writing, the criteria to define cervical lymphadenopathy are (1) a discrete mass great than 1.0–1.5 cm; (2) an ill-defined mass in a lymph node area; (3) multiple nodes of 6–15 mm; and (4) obliteration of tissue planes around vessels in a nonirradiated neck. A nodal mass with central low density is specifically indicative of tumor necrosis [7, 9–11].

Level I: Submental (IA) and Submandibular (IB)

Metastatic Involvement

These nodes contain metastatic disease when the primary site is lip, buccal mucosa, anterior nasal cavity, and soft tissue of cheek (*see* Table 1.3; Figs. 1.3 and 1.4). Of course it is important to distinguish between level IA and IB as IA is likely to contain metastatic disease associated with floor of mouth, lower lip, ventral tongue, and anterior nasal cavity tumors [12], whereas lesions from oral cavity subsite are likely to spread to level IB, II, and III. In the 1990 study by Candela et al. [13], level I metastases were frequent in oral cavity tumors, with a mean prevalence of 30.1 %. The corresponding figure for oropharyngeal cancer was 10.3 %, largely because of the high prevalence in N + disease [13].

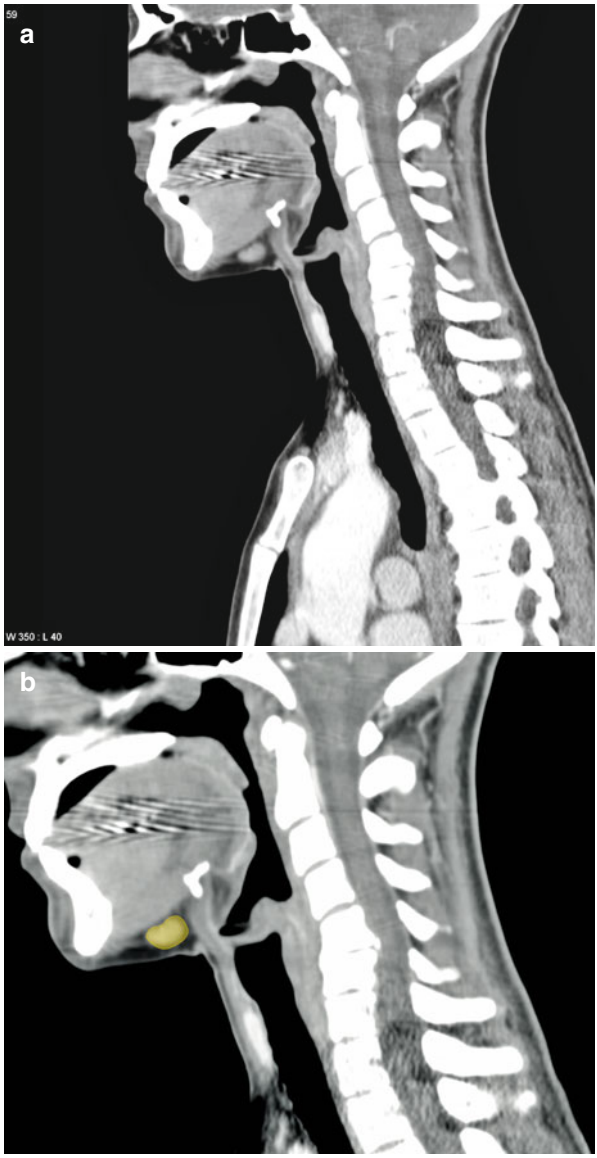

Fig. 1.3 (**a**) Sagittal CECT scans showing an enlarged level IA (submental) node in this patient with lymphoma. The node is outlined in (**b**)

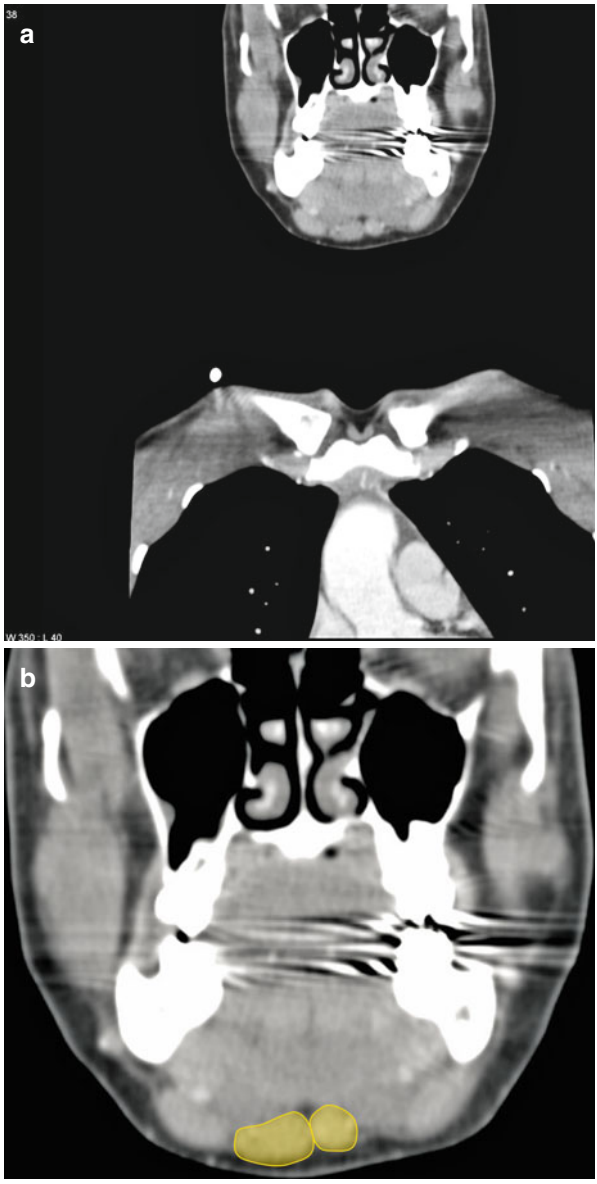

Fig. 1.4 (**a**) Coronal CECT scans showing an enlarged Level IB (submandibular) node in this patient with lymphoma. The node is outlined in (**b**)

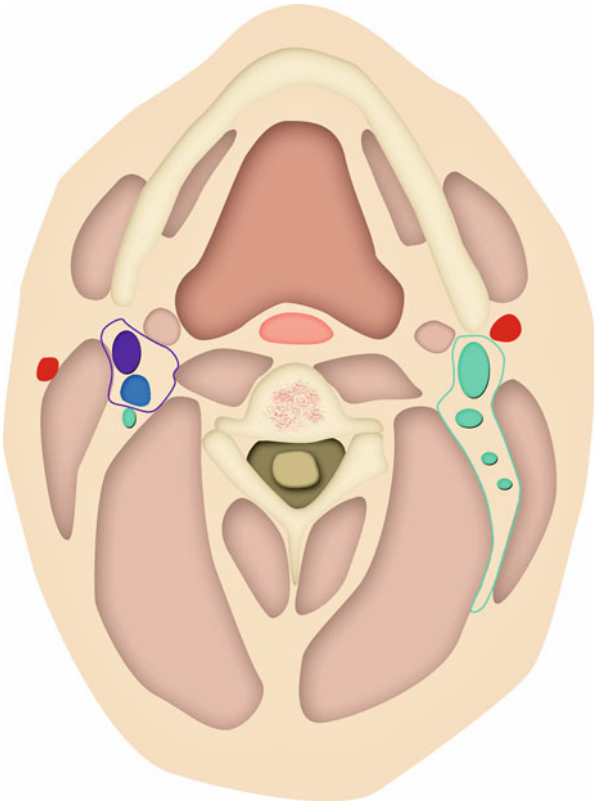

Fig. 1.5 Internal jugular chain of lymph nodes (level II). These nodes can be further divided into IIA and IIB by spinal accessory nerve The red colors represent branches of external carotid artery

Unusual Site of Metastasis

They do not form part of the primary drainage pathway of nasopharyngeal carcinomas but may be the sole site of tumour recurrence after radiotherapy. This is thought to be due to fibrosis of the lymphatic vessels in the irradiated regions resulting in diversion of lymph drainage to the submental nodes [14].

Level II

Internal jugular chain lymph nodes (*see* Fig. 1.5) are frequently divided into IIA (*see* Fig. 1.6) and IIB by spinal accessory nerve [2]. As the nerve cannot be identified on the CT scan, the Brussels guidelines used a criteria from radiological point of view proposed by Som et al. [15], which takes the posterior edge of the internal jugular vein (IJV) for subdivisions between levels IIA and IIB (*see* Figs. 1.7 and 1.8).

Fig. 1.6 (**a**) Axial CECT showing enlarged IIA level nodes. Note central hypodensity in these nodes which represent necrosis. The node is outlined in (**b**)

Fig. 1.6 (continued)

Fig. 1.7 (**a**) Axial CECT showing enlarged level II nodes. These are further divided into IIA and IIB based on the posterior edge of internal jugular vein. The nodes are outlined in (**b**)

Fig. 1.7 (continued)

Fig. 1.8 (**a**) Axial CECT showing single level IIA and multiple level IIB nodes. The nodes are outlined in (**b**)

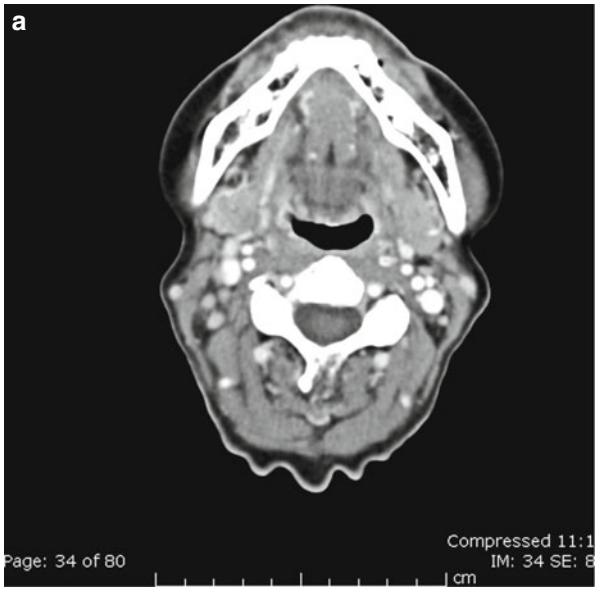

Fig. 1.8 (continued)

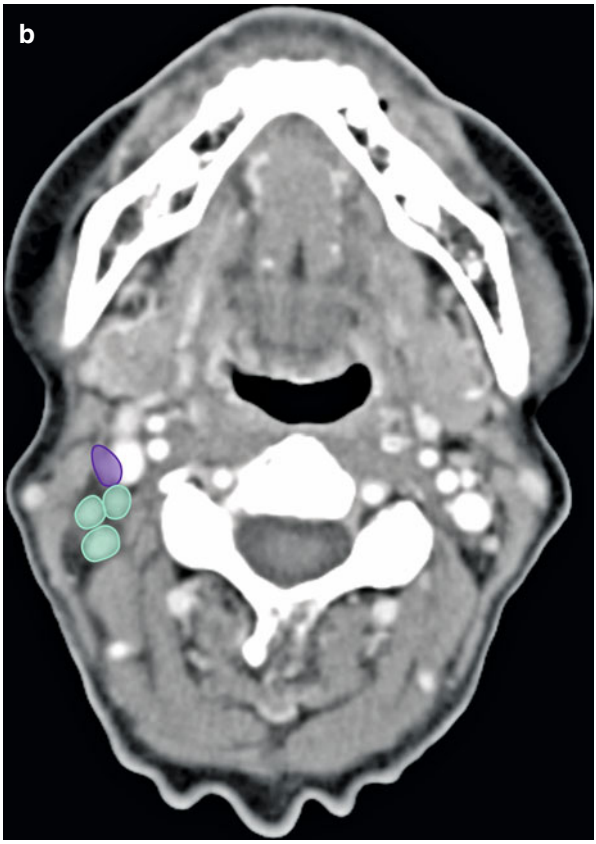

Metastatic Involvement

Level II is arbitrarily divided into IIA and IIB by spinal accessory nerve. They drain lymph from oral cavity, nasal cavity, nasopharynx, oropharynx, hypopharynx, larynx, and parotid gland (*see* Figs. 1.9 and 1.10).

The first draining lymph node station of supraglottic carcinomas is located in level IIA. Involvement in papillary thyroid carcinoma is not uncommon especially of level IIB nodes. Neck dissection should include the level IIB lymph node whenever level IIA lymph node metastasis is found. Level IIB dissection is probably unnecessary when level IIA lymph nodes are uninvolved because the incidence of metastasis to level IIB is low if level IIA is not involved [16].

Unusual Site of Metastasis

Intraparotid lymph nodes may be involved by lymphoma or metastatic spread from tumors of the scalp and face region [17].

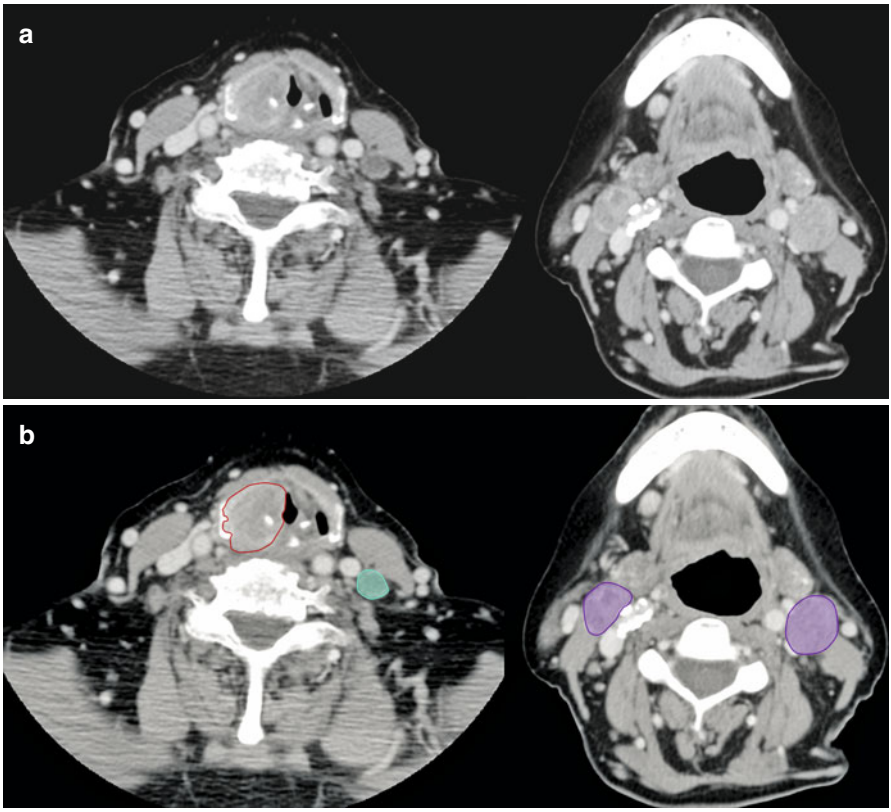

Fig. 1.9 (**a**) Axial CECT showing bilateral enlarged level II nodes in this patient with poorly differentiated right pyriform sinus carcinoma. The tumor and the nodes are outlined in (**b**)

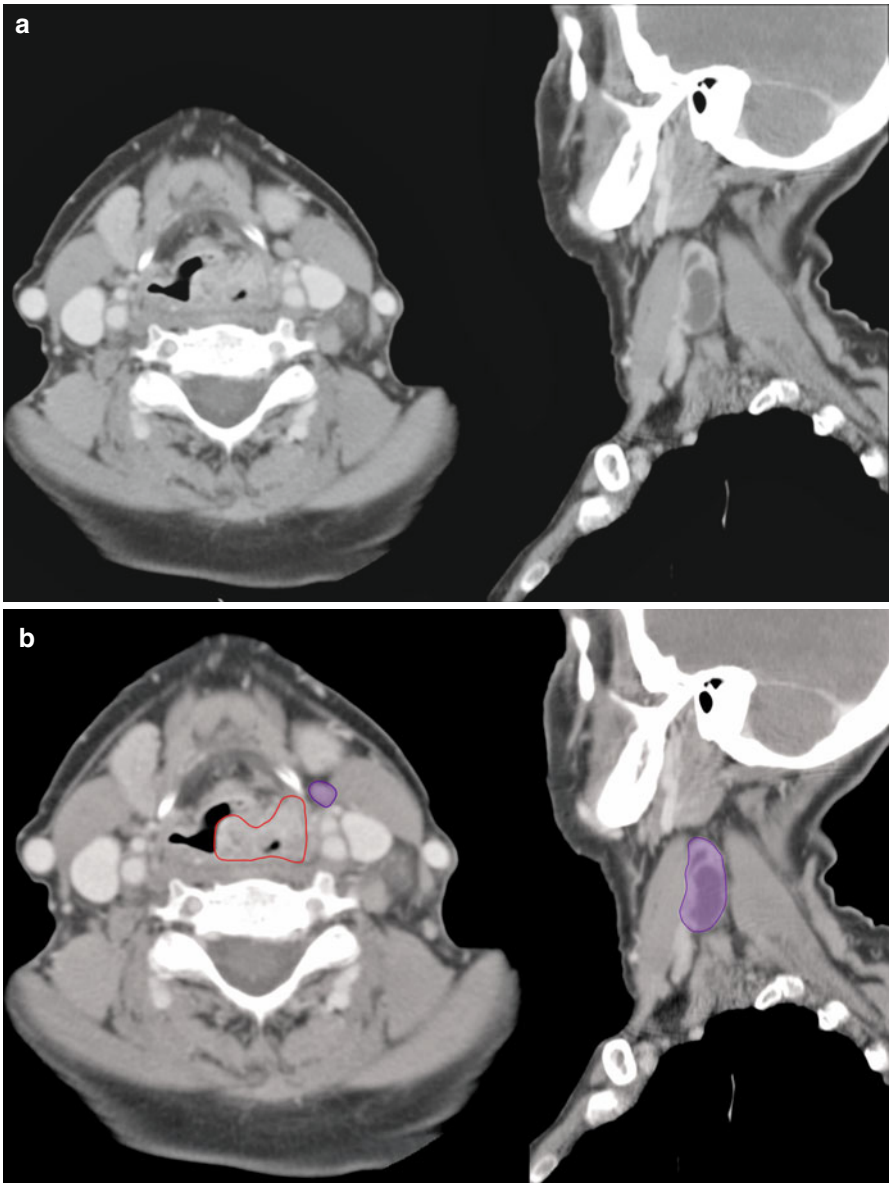

Fig. 1.10 (**a**) Axial CECT showing bilateral enlarged level II nodes in this patient with squamous cell carcinoma of the supraglottic larynx and enlarged level II nodes. Sagittal image shows necrotic level IIA node. The tumor and the nodes are outlined in (**b**)

Level III

Level III nodes drain lymph from the oral cavity, nasopharynx, oropharynx, hypopharynx, and larynx and can harbor metastatic spread from primaries located at these locations [2] (*see* Figs. 1.11, 1.12, and 1.13). Skip metastasis from carcinoma tongue is not unusual in this group [18].

Fig. 1.11 (**a**) Enlarged right-sided level III nodes seen on axial CECT. The nodes are outlined in (**b**)

Fig. 1.11 (continued)

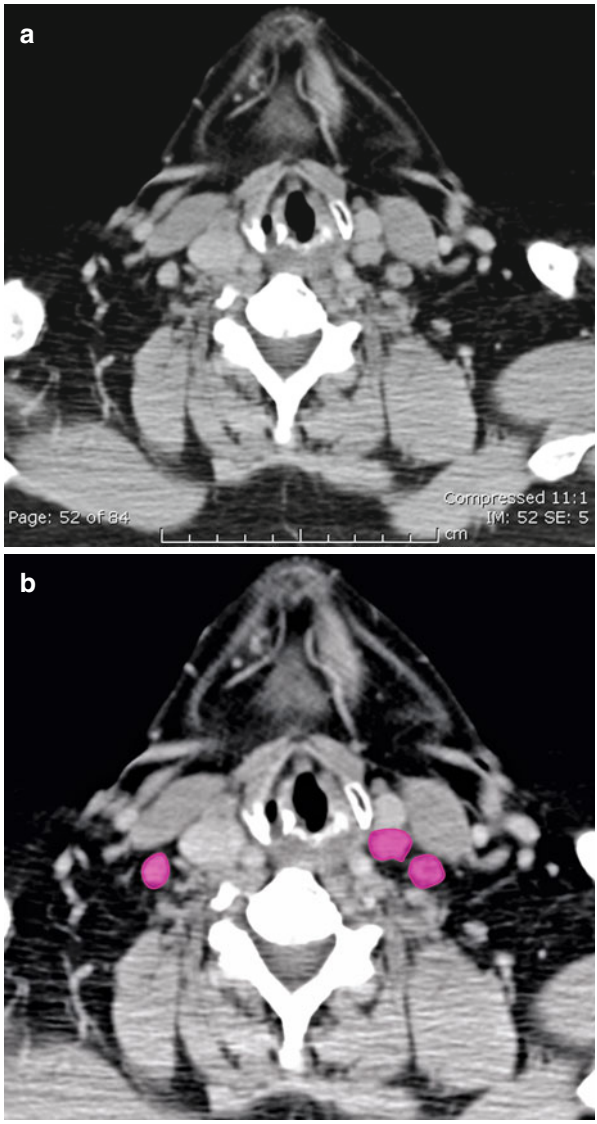

Fig. 1.12 (**a**) Enlarged bilateral level III nodes seen on axial CECT. The nodes are outlined in (**b**)

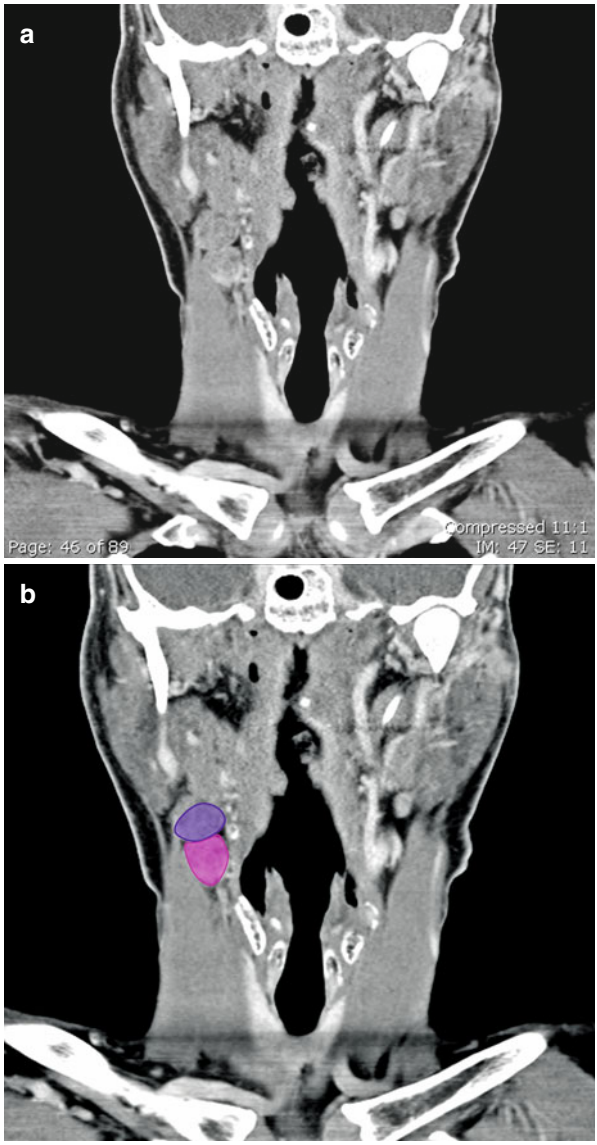

Fig. 1.13 (**a**) Hyoid bone as anatomical landmark separating enlarged level IIA node (superiorly) and level III node (inferiorly) on this coronal CECT. Part of the inferior body of hyoid bone is seen medial to these nodes. The nodes are outlined in (**b**)

Level IV

These groups of lymph nodes drain the following sites: hypopharynx, thyroid, cervical esophagus, and larynx. The classical Virchow node hails from this group. Involvement of level V nodes precedes their involvement in thyroid malignancies (*see* Figs. 1.14, 1.15, 1.16, and 1.17) [2, 19]. These nodes accompany level III nodes in skip metastasis from carcinoma tongue [18]. Involvement of Virchow node in carcinoma stomach is attributed to the predominant drainage by thoracic duct and partial filtration by Virchow node. This is considered as an ominous sign and changes the staging of carcinoma stomach to stage IV/M1b [20]. Level IV can be an unusual site of testicular metastasis [21].

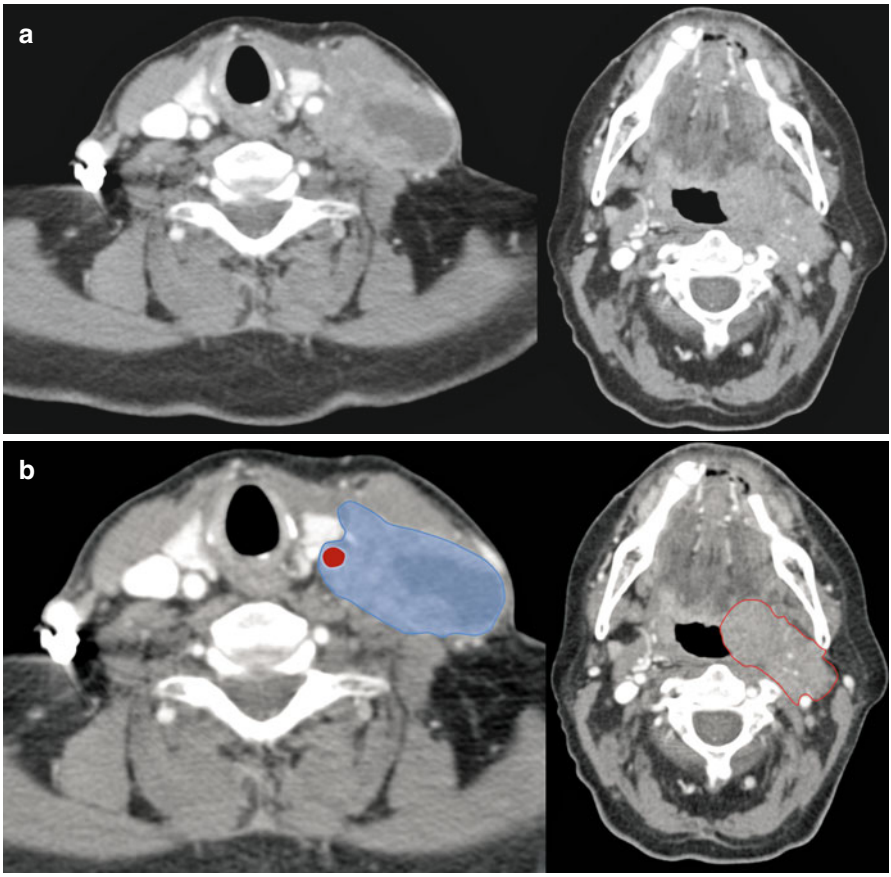

Fig. 1.14 (**a**) Axial CECT demonstrates an enlarged necrotic level IV node abutting the internal carotid artery in this patient with oropharyngeal carcinoma. The tumor and the node are outlined in (**b**)

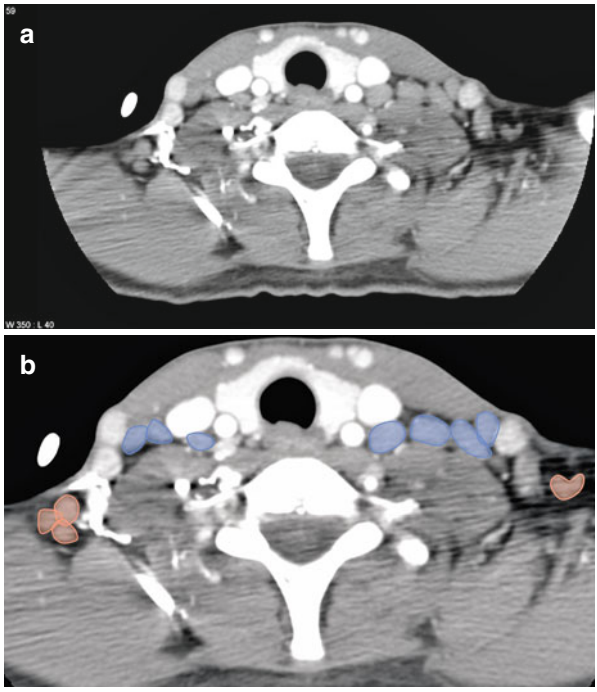

Fig. 1.15 (**a**) Multiple bilateral enlarged level IV and VB nodes noted on this axial CECT in this patient with lymphoma. The nodes are outlined in (**b**)

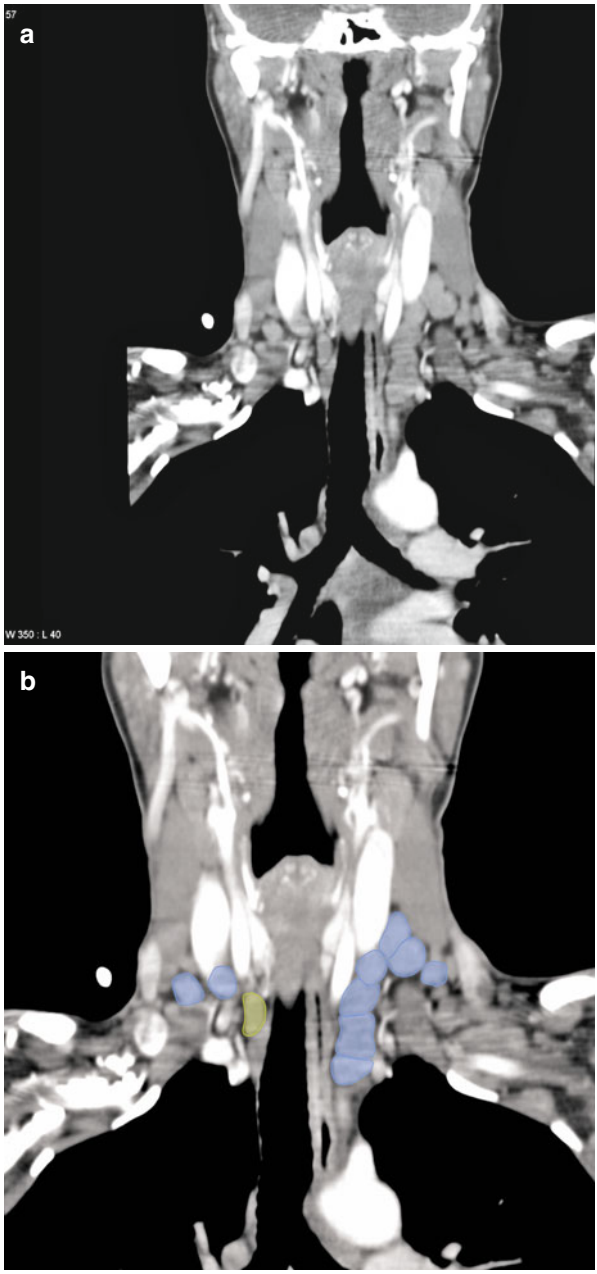

Fig. 1.16 (**a**) Coronal CECT image showing enlarged bilateral level IV and level VI nodes, which are outlined in (**b**)

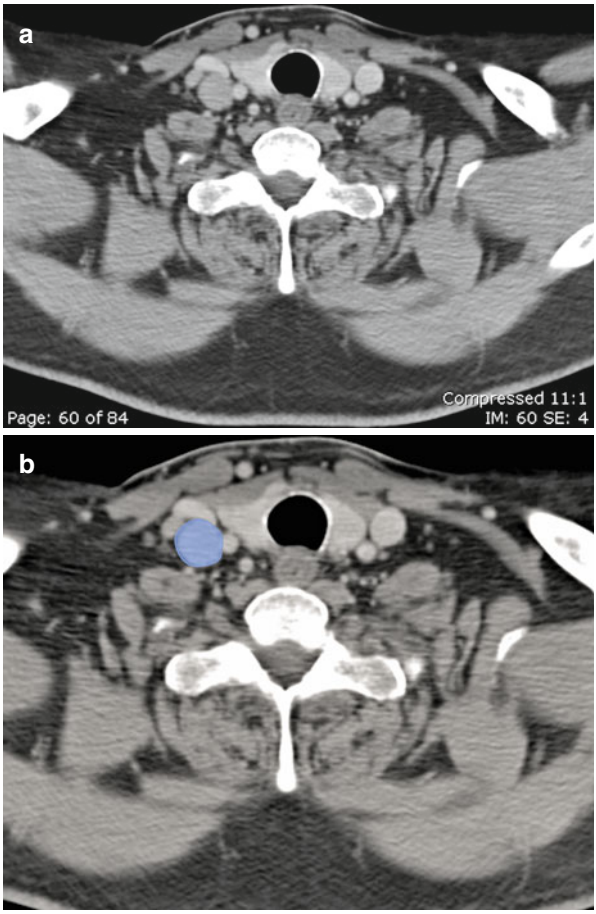

Fig. 1.17 (**a**) Axial CECT in this patient with lymphoma showing enlarged right-sided level IV node, which is outlined in (**b**)

Level V (A + B)

Lymphatics from nasopharynx and cutaneous tissue of posterior scalp and neck drain in to group V. Level VA (*see* Fig. 1.18) primarily contains nodes along the spinal accessory nerve and level VB contains transverse cervical and supraclavicular nodes (*see* Fig. 1.19).

Metastatic involvement of this group alone is seen in a small subset of patients but occurs commonly if group I to IV harbor the tumor spread. Level VB (*see* Fig. 1.20) is known to be associated with primary tumor located in the thyroid gland [5]. Involvement of level VB is an ominous sign in aerodigestive tract malignancies. Level VB nodes should be carefully identified and differentiated from Virchow nodes [2].

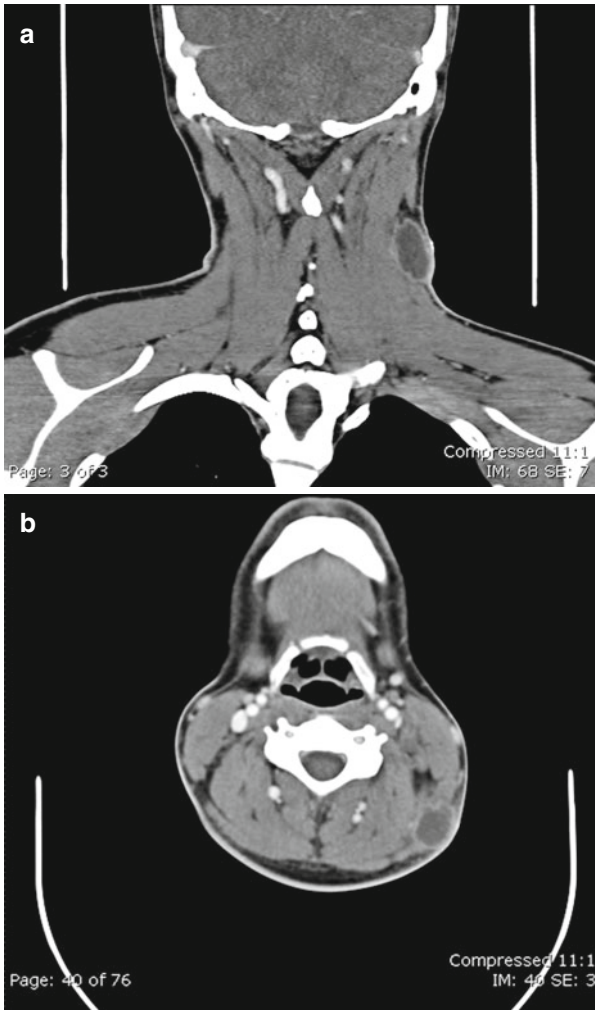

Fig. 1.18 Coronal (**a**) and axial (**b**) CECT image showing an enlarged necrotic level VA node noted at the convergence of trapezius and sternocleidomastoid muscles, which forms superior margin for this group. The nodes are outlined on (**c**, **d**)

Fig. 1.18 (continued)

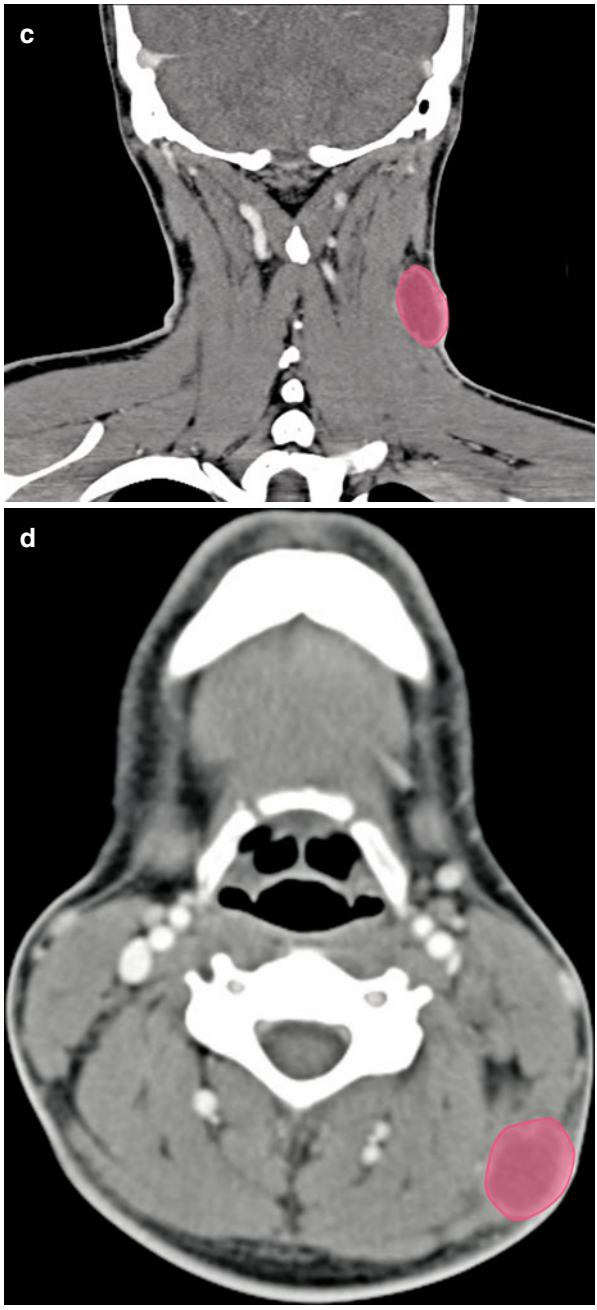

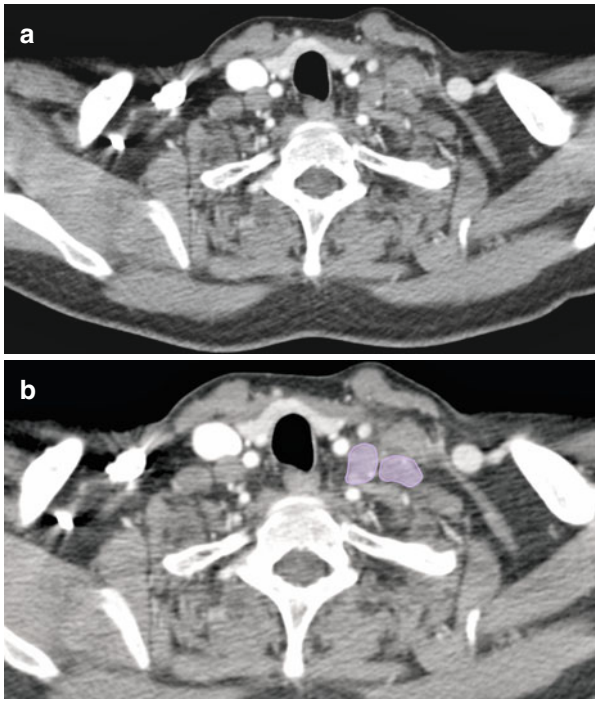

Fig. 1.19 (**a**) Enlarged supraclavicular nodes noted on this axial CECT image. Involvement of these nodes is considered as a bad prognostic sign in aerodigestive tract malignancies. The nodes are depicted in (**b**)

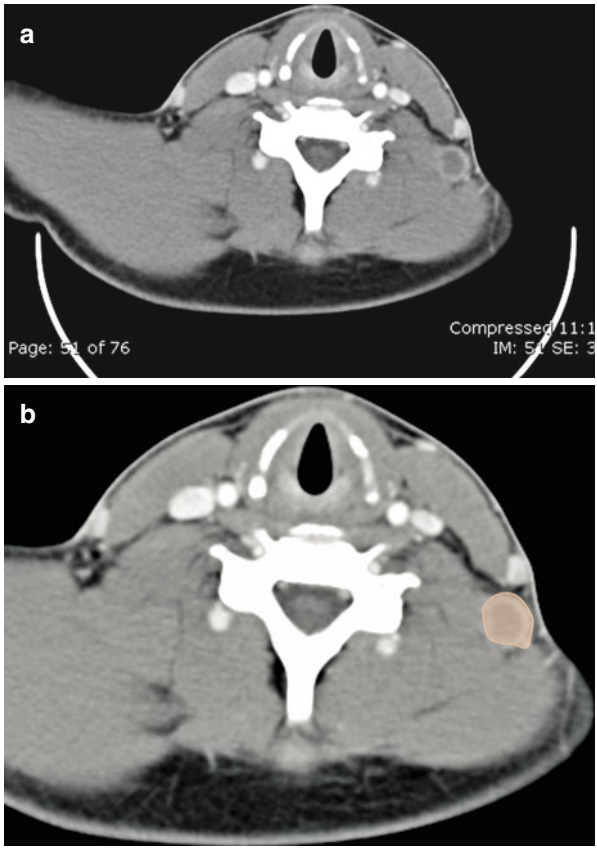

Fig. 1.20 (**a**) Axial CECT image showing an enlarged level VB node with central necrosis and peripheral enhancement. The node is depicted in (**b**)

Level VI

Pre- and paratracheal (*see* Fig. 1.21), precricoid, and perithyroid lymph nodes constitute this group and drains lymph from thyroid gland, glottic/subglottic larynx, apex of pyriform sinus, and cervical esophagus [13].

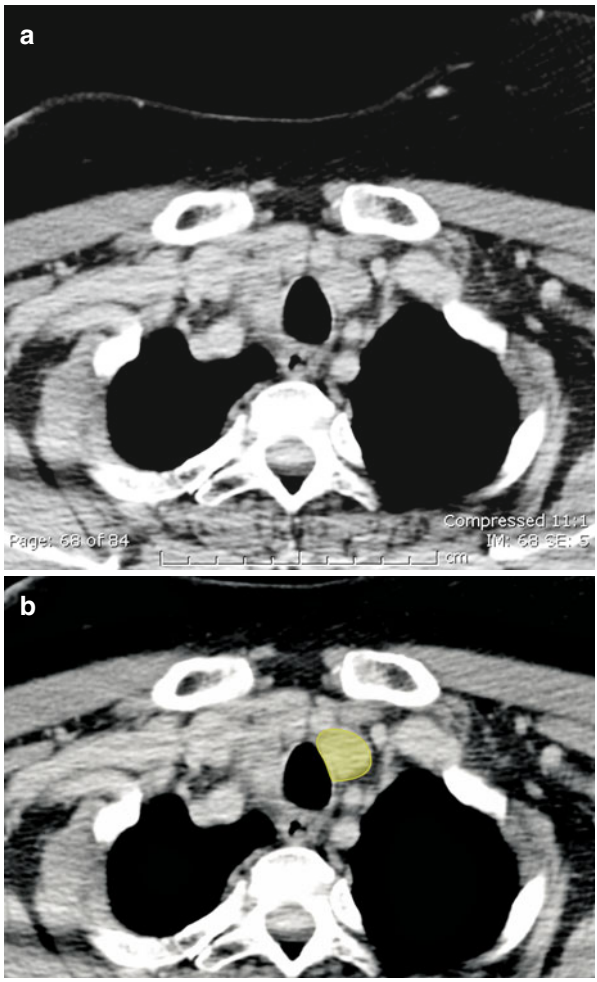

Fig. 1.21 (**a**) Axial CECT showing an enlarged level VI node in left paratracheal location, which is outlined in (**b**)

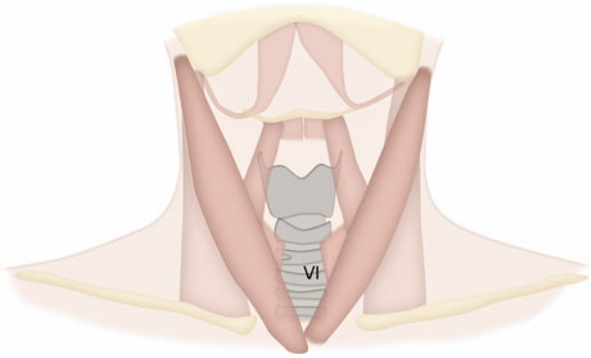

Fig. 1.22 Anatomical location of level *VI* nodes

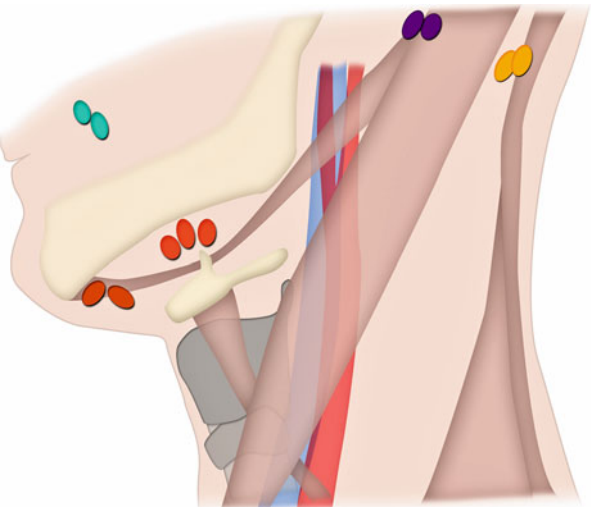

Fig. 1.23 Occipital, facial, and mastoid groups of nodes are depicted. These nodes are not included in the level system

The facial, mastoid occipital, and retropharyngeal nodes (*see* Fig. 1.22) are not included in the level system and are designated by their names if they are enlarged. The American Academy Otolaryngology–Head and Neck Surgery (AAO-HNS) believes that level VII (*see* Table 1.1) should be included in mediastinal nodal groups instead of cervical nodes. Facial nodal group is a blanket term applied for nodes at mandibular, buccinators, infraorbital, retrozygomatic, and malar nodes. These nodes are rarely identified and their metastatic involvement is seen in nasopharyngeal and epidermal malignancies [17].

Medial and lateral retropharyngeal nodes may be involved in pharyngeal and sinonasal, thyroid and cervical, esophageal primaries and are considered abnormal if larger than 5 mm [22, 23].

Occipital, facial, and mastoid groups of nodes are not included in the level system (Fig. 1.23).

References

1. Altekruse SF KC, Krapcho M, Neyman N, Aminou R, Waldron W, Ruhl J, Howlader N, Tatalovich Z, Cho H, Mariotto A, Eisner MP, Lewis DR, Cronin K, Chen HS, Feuer EJ, Stinchcomb DG, Edwards BK, editors. SEER Cancer Statistics Review. 1975–2007. Bethesda: National Cancer Institute. Accessible at: http://seer.cancer.gov/csr/1975_2007/, based on November 2009 SEER data submission, posted to the SEER web site, 2010. Accessed 17 May 2012.
2. Robbins KT, Clayman G, Levine PA, et al. Neck dissection classification update: revisions proposed by the American Head and Neck Society and the American Academy of Otolaryngology-Head and Neck Surgery. Arch Otolaryngol Head Neck Surg. 2002;128:751–8.
3. Paff GH. Anatomy of the head and neck. Philadelphia: Saunders; 1973.
4. Schuller DE. Management of cervical metastasis in head and neck cancer. Washington, D.C.: American Academy of Otolaryngology, Head and Neck Surgery Foundation; 1982.
5. Robbins KT. Classification of neck dissection: current concepts and future considerations. Otolaryngol Clin North Am. 1998;31:639–55.
6. Shah JP, Strong E, Spiro RH, Vikram B. Surgical grand rounds. Neck dissection: current status and future possibilities. Clin Bull. 1981;11:25–33.
7. Som PM. Detection of metastasis in cervical lymph nodes: CT and MR criteria and differential diagnosis. AJR Am J Roentgenol. 1992;158:961–9.
8. van den Brekel MW, Stel HV, Castelijns JA, et al. Cervical lymph node metastasis: assessment of radiologic criteria. Radiology. 1990;177:379–84.
9. Rouviere H. Lymphatic system of the head and neck. Ann Arbor: Edwards Brothers; 1938.
10. Suojanen JN, Mukherji SK, Dupuy DE, et al. Spiral CT in evaluation of head and neck lesions: work in progress. Radiology. 1992;183:281–3.
11. van den Brekel MW, Castelijns JA, Snow GB. Detection of lymph node metastases in the neck: radiologic criteria. Radiology. 1994;192:617–8.
12. van den Brekel MW, Castelijns JA. Imaging of lymph nodes in the neck. Semin Roentgenol. 2000;35:42–53.
13. Buckley JG, Feber T. Surgical treatment of cervical node metastases from squamous carcinoma of the upper aerodigestive tract: evaluation of the evidence for modifications of neck dissection. Head Neck. 2001;23:907–15.
14. Ahuja AT, Leung SF, Teo P, et al. Submental metastases from nasopharyngeal carcinoma. Clin Radiol. 1999;54:25–8.
15. Som PM, Curtin HD, Mancuso AA. An imaging-based classification for the cervical nodes designed as an adjunct to recent clinically based nodal classifications. Arch Otolaryngol Head Neck Surg. 1999;125:388–96.
16. Lee BJ, Wang SG, Lee JC, et al. Level IIb lymph node metastasis in neck dissection for papillary thyroid carcinoma. Arch Otolaryngol Head Neck Surg. 2007;133:1028–30.
17. Moulding FJ, Roach SC, Carrington BM. Unusual sites of lymph node metastases and pitfalls in their detection. Clin Radiol. 2004;59:558–72.
18. Byers RM, Weber RS, Andrews T, et al. Frequency and therapeutic implications of "skip metastases" in the neck from squamous carcinoma of the oral tongue. Head Neck. 1997;19:14–9.
19. Seethala RR. Current state of neck dissection in the United States. Head Neck Pathol. 2009;3:238–45.
20. Bhatia KS, Griffith JF, Ahuja AT. Stomach cancer: prevalence and significance of neck nodal metastases on sonography. Eur Radiol. 2009;19:1968–72.
21. van Vledder MG, van der Hage JA, Kirkels WJ, et al. Cervical lymph node dissection for metastatic testicular cancer. Ann Surg Oncol. 2010;17:1682–7.
22. Ozlugedik S, Ibrahim Acar H, Apaydin N, et al. Retropharyngeal space and lymph nodes: an anatomical guide for surgical dissection. Acta Otolaryngol. 2005;125:1111–5.
23. Mancuso AA, Harnsberger HR, Muraki AS, Stevens MH. Computed tomography of cervical and retropharyngeal lymph nodes: normal anatomy, variants of normal, and applications in staging head and neck cancer. Part II: pathology. Radiology. 1983;148:715–23.

Chapter 2 Chest Lymph Node Anatomy

Mediastinal Lymph Nodes

In 2009, a new lung cancer lymph node map was proposed by the International Association for the Study of Lung Cancer (IASLC) to reconcile the difference between the Naruke [1] and the Mountain–Dresler–American Thoracic Society (ATS) [2] maps and redefine the definitions of the anatomical boundaries of each lymph node station [3].

Supraclavicular Nodes 1

1R and 1L. *Low cervical, supraclavicular, and sternal notch nodes* (*see* Figs. 2.1–2.5).
Upper border: Lower margin of cricoid cartilage.
Lower border: Clavicles bilaterally and, in the midline, the upper border of the manubrium; 1R designates right-sided nodes; 1L designates left-sided nodes in this region.
For lymph node station 1, the midline of the trachea serves as the border between 1R and 1L.

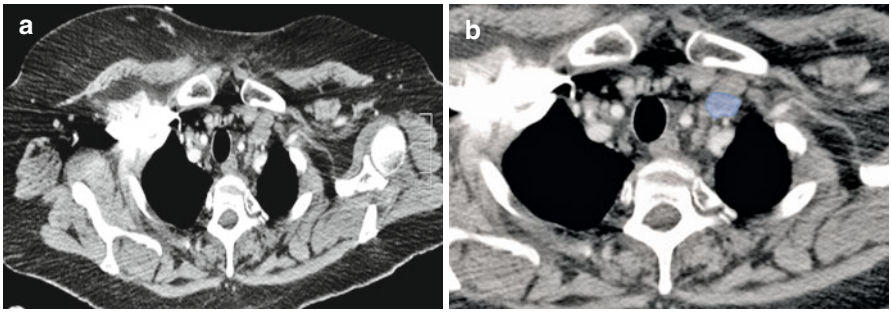

Fig. 2.1 (**a**, **b**) Axial CT scan through the lung apices shows enlarged left supraclavicular lymph node (*blue*)

M.G. Harisinghani (ed.), *Atlas of Lymph Node Anatomy*,
DOI 10.1007/978-1-4419-9767-8_2, © Springer Science+Business Media New York 2013

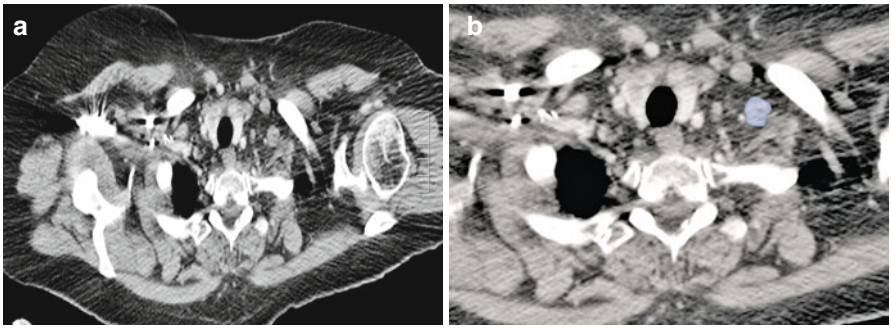

Fig. 2.2 (**a**, **b**) Axial CT scan through the lung apices shows enlarged left supraclavicular lymph node (*blue*)

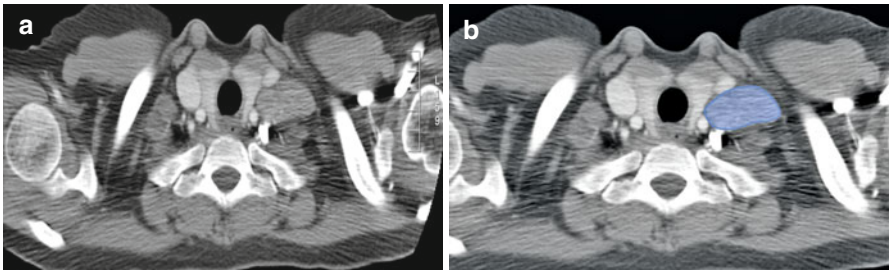

Fig. 2.3 (**a**, **b**) Axial CT scan through the lung apices shows enlarged left supraclavicular lymph node (*blue*)

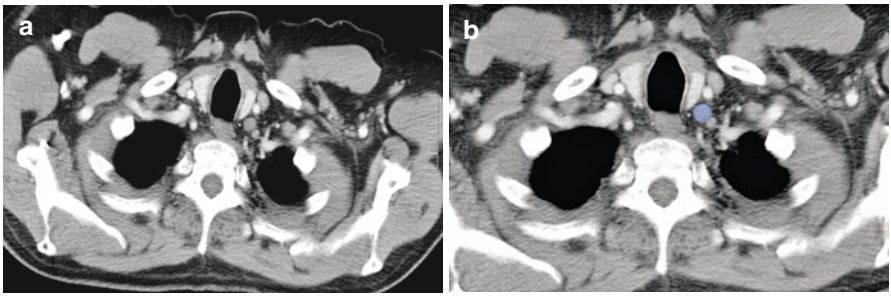

Fig. 2.4 (**a**, **b**) Axial CT scan through the lung apices shows enlarged left supraclavicular lymph node (*blue*)

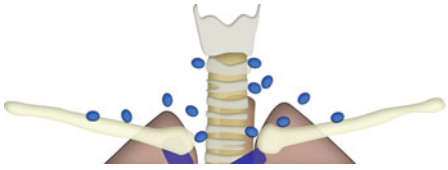

Fig. 2.5 Schematic diagram showing the anatomic locations of the low cervical, supraclavicular and sternal notch node stations, which together comprise the supraclavicular lymph nodes

Superior Mediastinal Nodes 2–4

2R. *Upper paratracheal.* Includes nodes extending to the left lateral border of the trachea.

Upper border: Apex of the right lung and pleural space and in the midline, the upper border of the manubrium.

Lower border: Intersection of caudal margin of innominate vein with the trachea.

2L. *Upper paratracheal.*

Upper border: Apex of the left lung and pleural space and in the midline, the upper border of the manubrium.

Lower border: Superior border of the aortic arch (*see* Figs. 2.6 and 2.7).

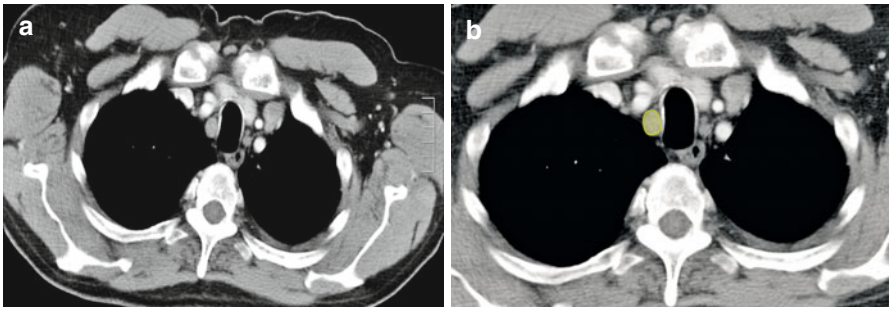

Fig. 2.6 (**a**, **b**) Axial CT scan showing an enlarged right upper paratracheal lymph node (*green*)

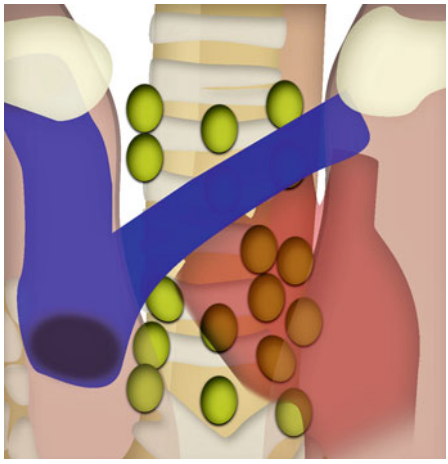

Fig. 2.7 Schematic illustration showing anatomic locations for paratracheal lymph nodes

3A. *Prevascular* (*see* Figs. 2.8–2.10).
On the right:
Upper border: Apex of chest.
Lower border: Level of carina.
Anterior border: Posterior aspect of sternum.
Posterior border: Anterior border of superior vena cava.
On the left:
Upper border: Apex of chest.
Lower border: Level of carina.
Anterior border: Posterior aspect of sternum.
Posterior border: Left carotid artery.

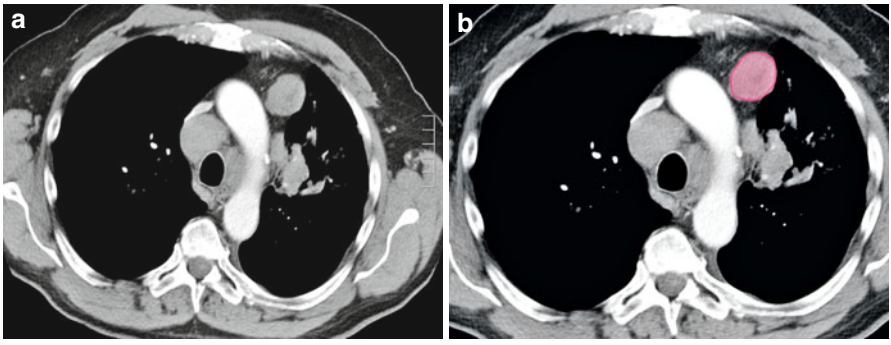

Fig. 2.8 (**a**, **b**) Contrast-enhanced axial CT scan shows an enlarged lymph node in the prevascular space on the left side, anterior to the arch of aorta (*red*)

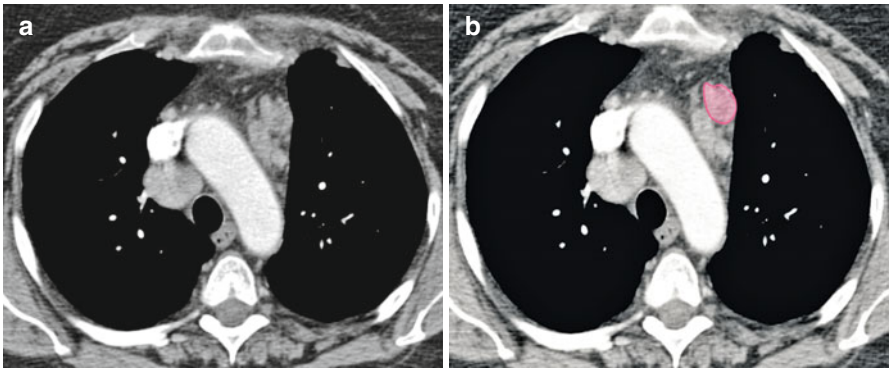

Fig. 2.9 (**a**, **b**) Contrast-enhanced axial CT scan shows an enlarged lymph node in the prevascular area on the left side, anterior to the descending aorta (*red*)

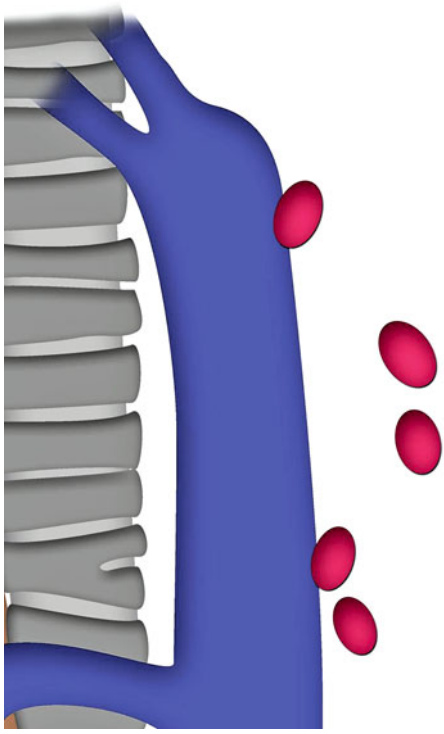

Fig. 2.10 Schematic illustration shows the anatomic location of prevascular group of lymph nodes

3P. *Retrotracheal* (*see* Fig. 2.11).
Upper border: Apex of chest.
Lower border: Carina.

4R. *Lower paratracheal.* Includes right paratracheal nodes, and pretracheal nodes extending to the left lateral border of trachea (*see* Figs. 2.12–2.14).
Upper border: Intersection of caudal margin of innominate veins with the trachea.
Lower border: Lower border of azygos vein.

4L. *Lower paratracheal.* Includes nodes to the left of the left lateral border of the trachea, medial to the ligamentum arteriosum.
Upper border: Upper margins of the aortic arch.
Lower border: Upper rim of the left main pulmonary artery.

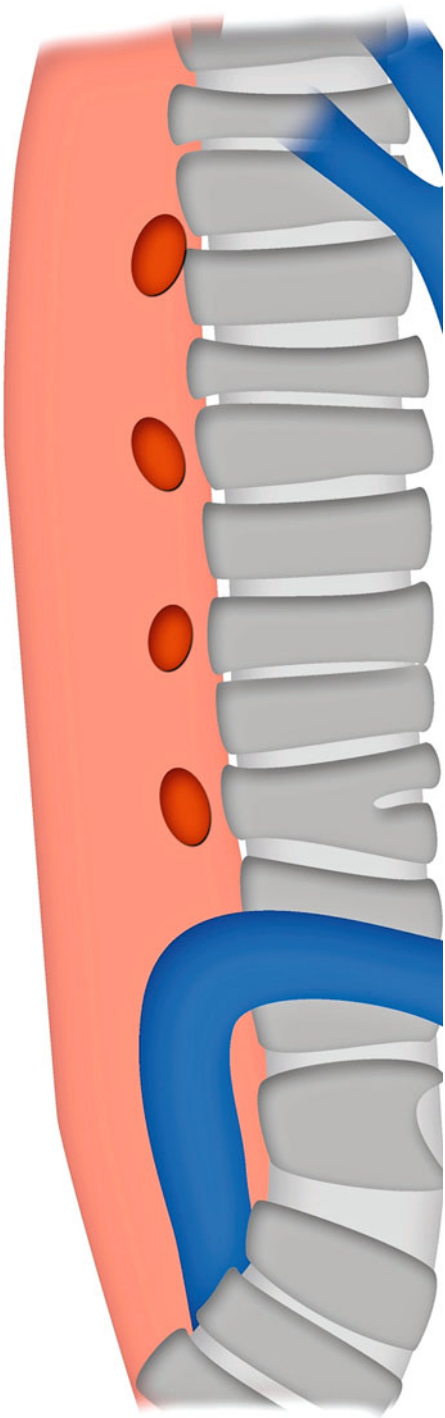

Fig. 2.11 Schematic illustration shows the anatomic location and distribution of retrotracheal group of lymph nodes (*dark red*)

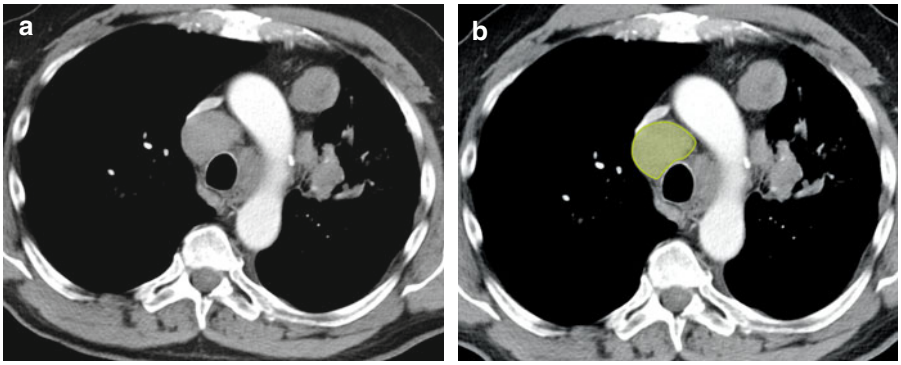

Fig. 2.12 (**a**, **b**) Axial contrast-enhanced CT image through the upper thorax shows an enlarged right-sided lower pretracheal lymph node (*green*)

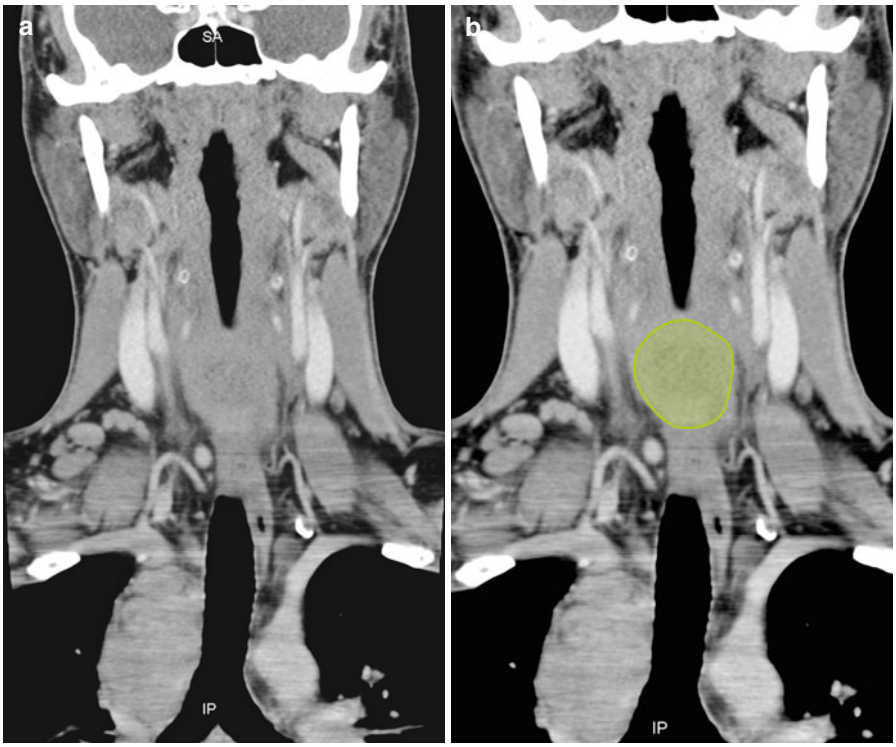

Fig. 2.13 (**a**, **b**) Coronal reformatted CT scan image of the same patient shows enlarged right lower pretracheal lymph node (*green*)

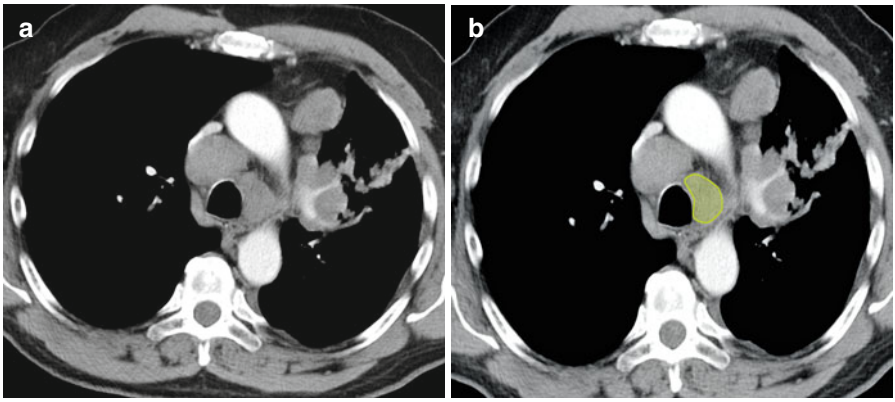

Fig. 2.14 (**a**, **b**) Axial contrast-enhanced CT scan through upper thorax shows an enlarged left lower paratracheal lymph node abutting the left lateral wall of the trachea (*green*)

Aortic Nodes 5–6

5. *Subaortic*. Lymph nodes lateral to the ligamentum arteriosum (*see* Fig. 2.15).
Upper border: The lower border of the aortic arch.
Lower border: Upper rim of the left main pulmonary artery.
6. *Para-aortic.* Lymph nodes anterior and lateral to the ascending aorta and aortic arch (*see* Figs. 2.16 and 2.17).
Upper border: A line tangential to the upper border of the aortic arch.
Lower border: The lower border of the aortic arch.

Inferior Mediastinal Nodes 7–9

7. *Subcarinal* (*see* Fig. 2.18).
Upper border: The carina of the trachea.
Lower border: The upper border of the lower lobe bronchus on the left; the lower border of the bronchus intermedius on the right.
8. *Paraesophageal.* Lymph nodes adjacent to the wall of the esophagus and to the right or left of the midline, excluding subcarinal nodes (*see* Figs. 2.19–2.22).
Upper border: The upper border of the lower lobe bronchus on the left; the lower border of the bronchus intermedius on the right.
Lower border: The diaphragm.
9. *Pulmonary ligament.* Lymph nodes lying within the pulmonary ligament (*see* Fig. 2.23).
Upper border: The inferior pulmonary vein.
Lower border: The diaphragm.

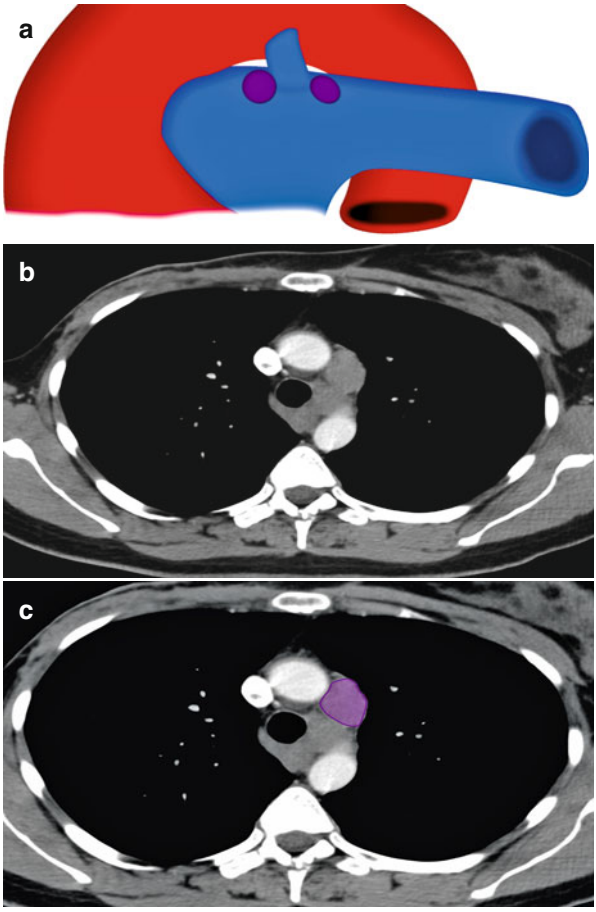

Fig. 2.15 (**a**) Schematic illustration shows the anatomic location of subaortic lymph nodes. (**b**, **c**) Axial contrast-enhanced CT scan image of the thorax shows an enlarged subaortic lymph node (*purple*)

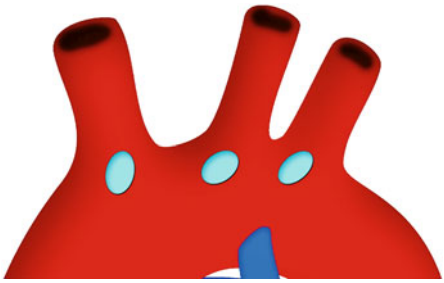

Fig. 2.16 Schematic illustration shows the anatomic location for paraaortic group of lymph nodes

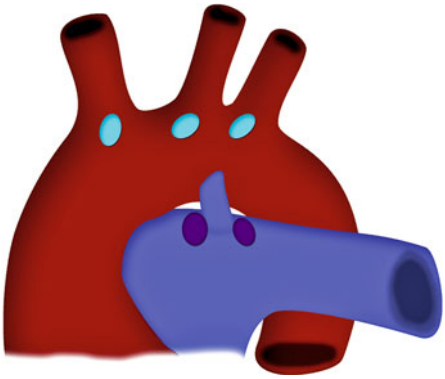

Fig. 2.17 Schematic illustration shows the anatomic locations of the para-aortic and retroaortic group of lymph nodes using color coding scheme

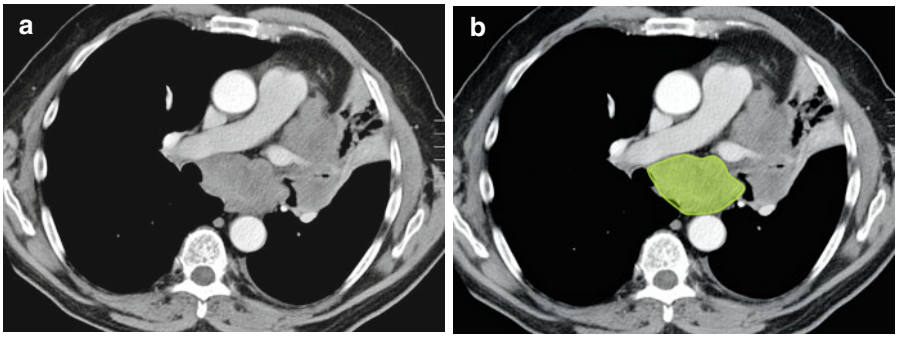

Fig. 2.18 (**a**, **b**) Axial contrast-enhanced CT scan of the thorax shows enlarged subcarinal group of lymph nodes (*green*)

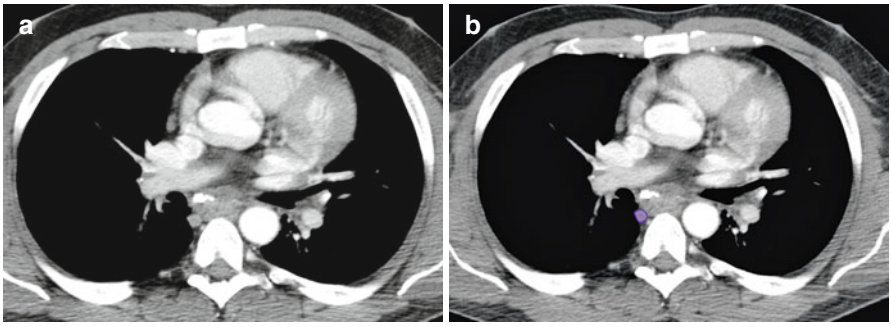

Fig. 2.19 (**a**, **b**) Axial contrast-enhanced CT scan of the thorax shows enlarged paraesophageal group of lymph nodes (*purple*)

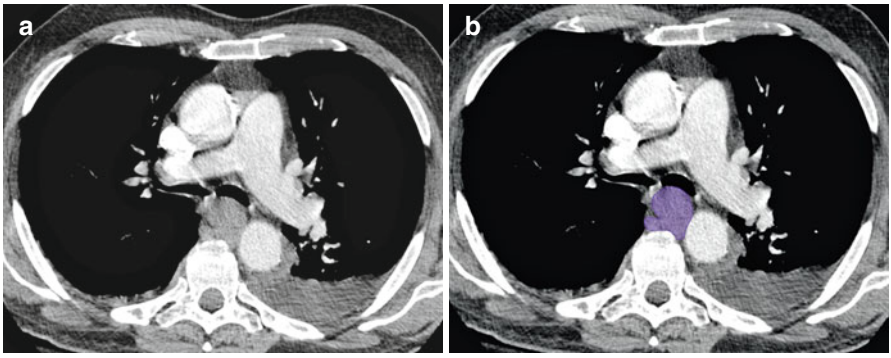

Fig. 2.20 (**a**, **b**) Axial contrast-enhanced CT scan of the thorax shows enlarged paraesophageal group of lymph nodes (*purple*)

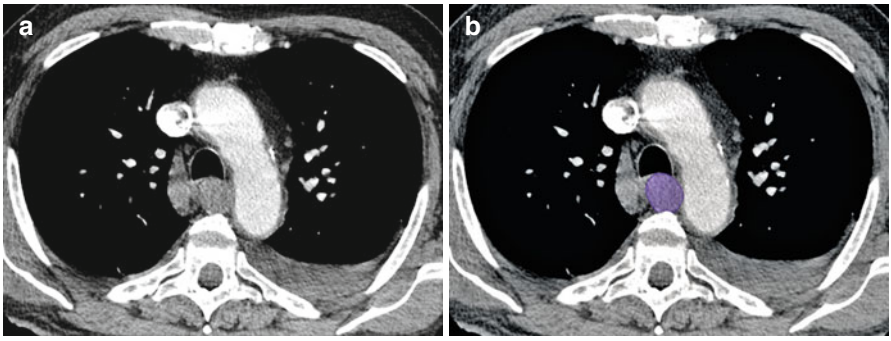

Fig. 2.21 (**a**, **b**) Axial contrast-enhanced CT scan of the thorax shows enlarged paraesophageal group of lymph nodes (*purple*)

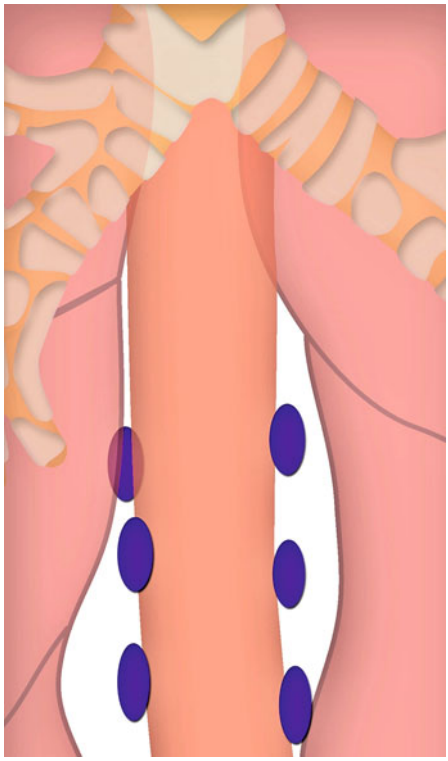

Fig. 2.22 Schematic illustration shows the anatomic location and distribution of the paraesophageal group of lymph nodes using color-coding scheme

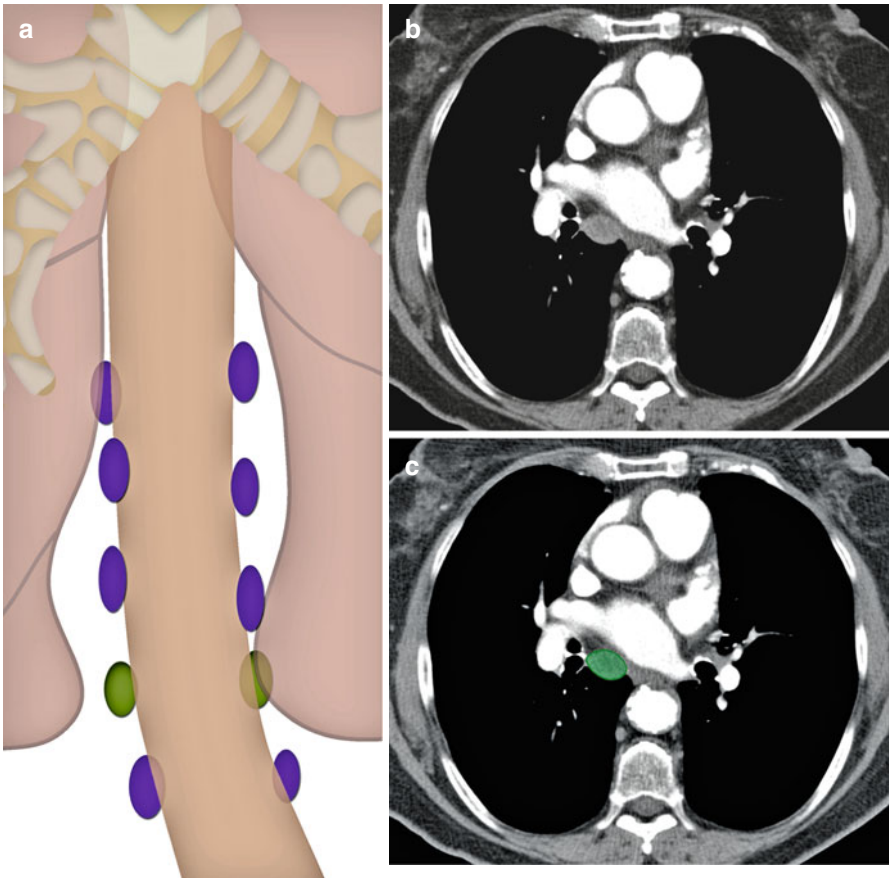

Fig. 2.23 (**a**) Schematic illustration shows the anatomic location and distribution of lymph nodes lying within the pulmonary ligament (*green*). These are seen interspersed between the paraesophageal group of lymph nodes (*violet*). (**b**, **c**) Axial contrast-enhanced CT scan of the thorax shows an enlarged right-sided pulmonary ligament lymph (*green*)

Hilar, Lobar, and (Sub)Segmental Nodes 10–14

These are all N1 nodes:

10. *Hilar.* Includes lymph nodes immediately adjacent to the mainstem bronchus and hilar vessels, including the proximal portions of the pulmonary veins and the main pulmonary artery (*see* Fig. 2.24).

Upper border: The lower rim of the azygos vein on the right; upper rim of the pulmonary artery on the left.

Lower border: Interlobar region bilaterally.

11. *Interlobar.* Between the origin of the lobar bronchi (*see* Fig. 2.25).

11s: Between the upper lobe bronchus and bronchus intermedius on the right.

11i: Between the middle and lower lobe bronchus on the right.

12. *Lobar.* Adjacent to the lobar bronchi (*see* Fig. 2.26).

13. *Segmental.* Adjacent to the segmental bronchi.

14. *Subsegmental*. Adjacent to the subsegmental bronchi.

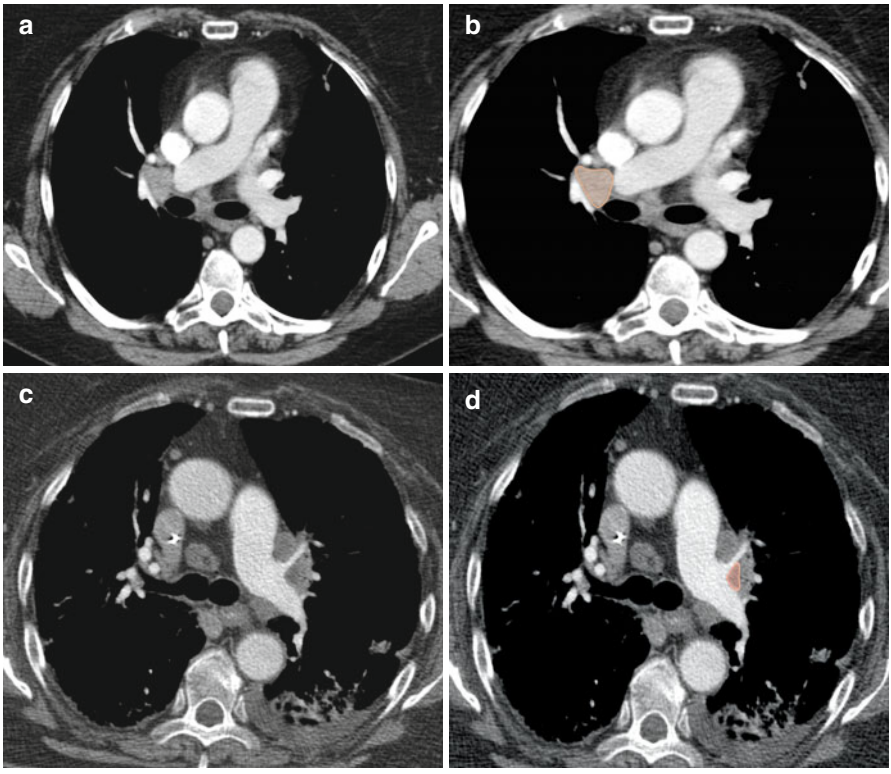

Fig. 2.24 (**a**, **b**) Axial contrast-enhanced CT scan of the thorax shows enlarged right hilar group of lymph nodes (*orange*). (**c**, **d**) Axial contrast-enhanced CT scan of the thorax shows enlarged left hilar group of lymph nodes (*orange*)

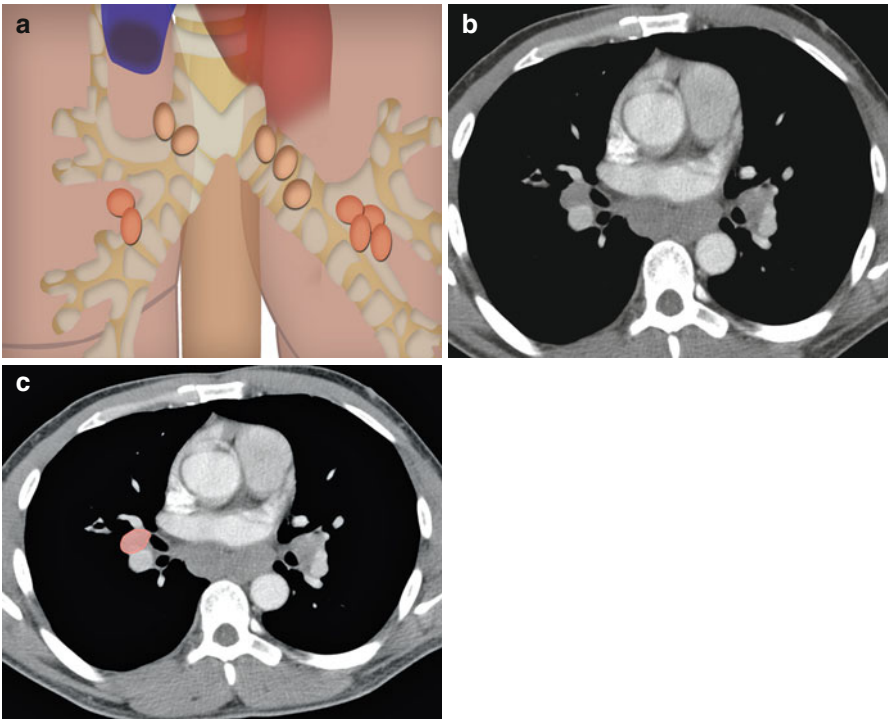

Fig. 2.25 (**a**) Schematic illustration shows the anatomic location and distribution of the hilar and interlobar group of lymph node. (**b**, **c**) An axial CT scan image of the thorax shows an enlarged right interlobar lymph node (*orange*)

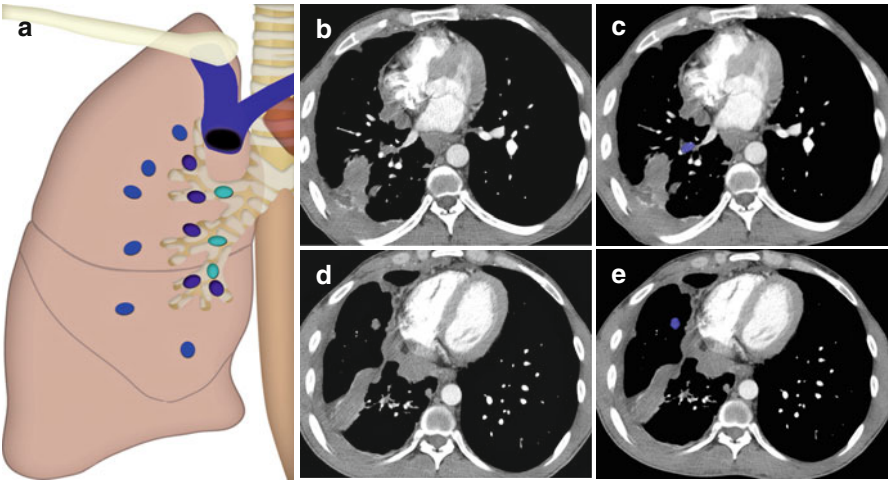

Fig. 2.26 (**a**) Schematic illustration shows the anatomic location and distribution of the lobar, segmental, and subsegmental group of lymph nodes using color-coding scheme. (**b**, **c**) Axial CT scan of the thorax shows an enlarged right segmental lymph node (*blue*). (**d**, **e**) Axial CT scan of the thorax shows enlarged right subsegmental lymph node (*blue*)

Malignant Causes of Enlargement

A study was performed to look at the appearance of the lymph node at CT to improve specificity for detecting malignant nodes in bronchogenic carcinoma. The four parameters evaluated were (1) node location, (2) homogenicity, (3) border delineation, and (4) delineation by fat. Of 54 carcinoma patients, nodes were pathologically malignant in 21. CT showed enlarged lymph nodes (>1 cm) in 20 of these (true-positive rate, 96 %), but also in 13 of the 33 patients with pathologically benign lymph nodes (false-positive rate, 39 %). A combination of all four CT parameters reduced the false-positive rate from 39 to 21 % and decreased the true-positive rate from 96 to 86 % [4].

The most common cause of malignant lymph node enlargement in the mediastinum is lung cancer. It has been reported that 20–25 % of clinical stage I disease have mediastinal lymph node disease [5–7].

In patients with esophageal cancer, location of mediastinal lymph nodes depend on the location of the primary tumor. Thoracic mediastinal lymph nodes were involved in 19.44 % of patients with upper thoracic esophageal carcinoma; in 34.7 % of patients with middle thoracic esophageal carcinomas; and in 34.1 % of patients with lower thoracic esophageal carcinoma [8].

Another cause of thoracic lymphadenopthy is lymphoma, in which mediastinal lymph node involvement is more frequent than hilar, which is usually asymmetrical and accompanied by mediastinal involvement [9] (*see* Figs. 2.27–2.32).

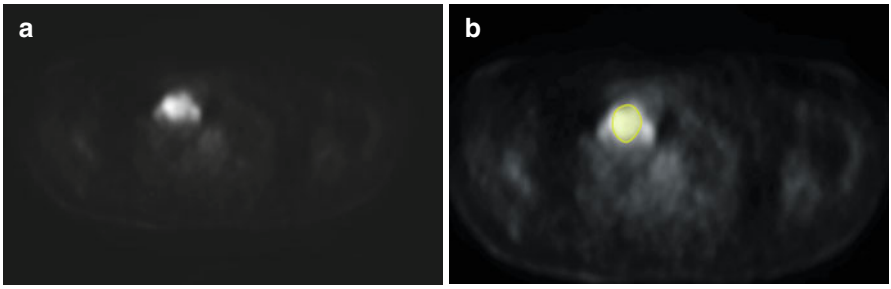

Fig. 2.27 (**a**, **b**) Axial positron emission tomography (PET) scan of the thorax shows fluorodeoxy-glucose (FDG) avid uptake by mediastinal lymph nodes in a case of lymphoma (*green*)

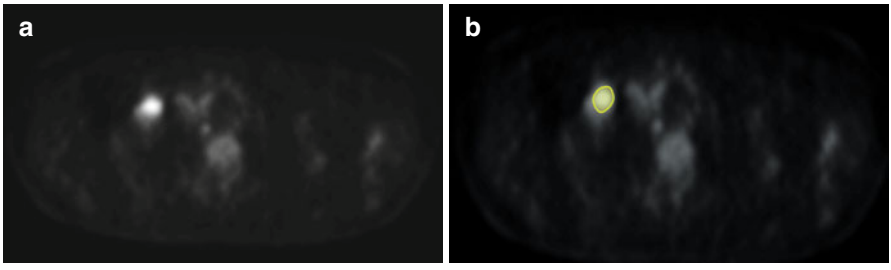

Fig. 2.28 (**a**, **b**) Axial PET scan of the thorax shows FDG avid uptake by mediastinal lymph nodes in a case of lymphoma (*green*)

Lymphoma tends to expand along or around rather than invade existing structures. In Hodgkin's disease, upwards of 85 % of patients have intrathoracic involvement on CT, compared with approximately 50 % with non-Hodgkin's lymphoma [9, 10]. Hodgkin's disease tends to spread contiguously between lymph node groups, while non-Hodgkin's lymphoma more frequently involves atypical lymph node sites, such as posterior mediastinal and anterior diaphragmatic nodes [9, 10].

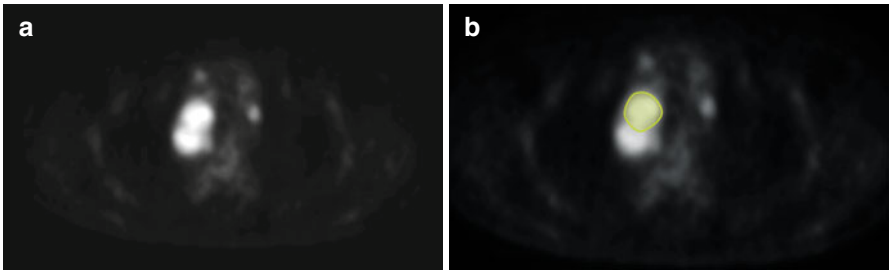

Fig. 2.29 (**a**, **b**) Axial PET scan of the thorax shows FDG avid uptake by mediastinal lymph nodes in a case of lymphoma (*green*)

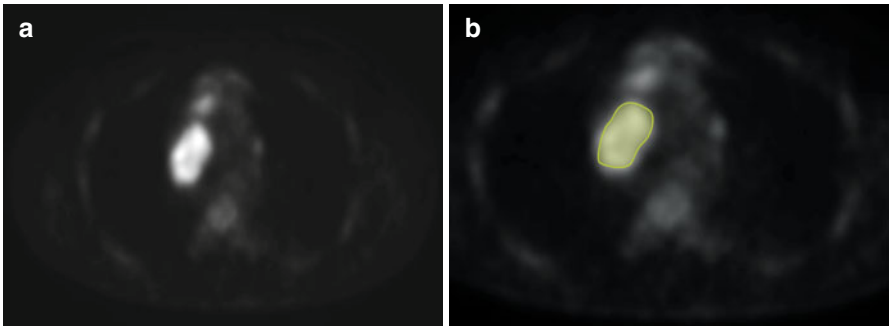

Fig. 2.30 (**a**, **b**) Axial PET scan of the thorax shows FDG avid uptake by mediastinal lymph nodes in a case of lymphoma (*green*)

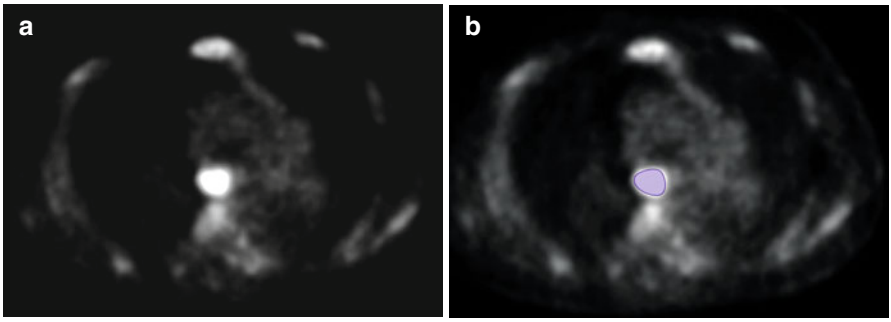

Fig. 2.31 (**a**, **b**) Axial PET scan of the thorax shows FDG avid uptake by mediastinal lymph nodes in a case of lymphoma (*purple*)

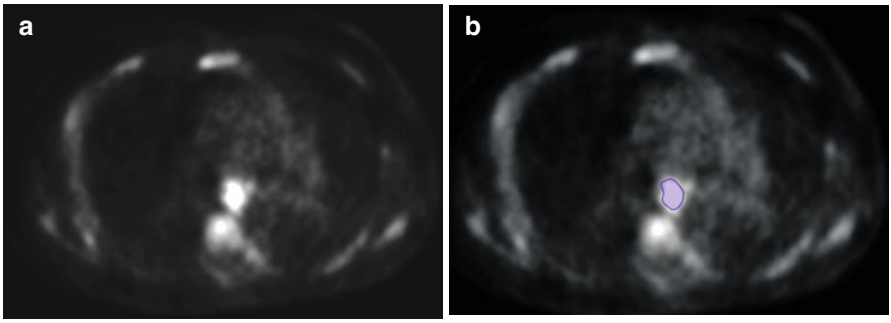

Fig. 2.32 (**a**, **b**) Axial PET scan of the thorax shows FDG avid uptake by mediastinal lymph nodes in a case of lymphoma (*purple*)

Intrathoracic lymph node metastases from extrathoracic carcinomas are infrequent. They were detected on chest radiograph in 25 of 1,071 patients (2.3 %) by McLoud and colleagues [11]. The primary malignancies included eight tumors of the head and neck, 12 genitourinary malignancies, three carcinomas of the breast, and two malignant lymphomas. The most frequently detected lymph node group was the right paratracheal 4R and 2R (60 %).

Mabon and Libshitz [12] analyzed 50 mediastinal metastases of infradiaphragmatic malignancies on computed tomodensitography, a technique allowing a better visualization of all nodal groups in the mediastinum. Several lymph node stations were commonly involved, and only one single station was involved in only 6 %. Besides a majority of genitourinary malignancies (kidney, 25; testis, 7; prostate, 4; ovary, 3; bladder, 2), they also observed metastases from carcinoma of the colon or rectum in 6 and stomach in 3. Libson and colleagues [13] reported 12 cases of mediastinal metastases in 19,994 patients (1 %) with carcinomas of the stomach, pancreas, colon, and rectum.

In a recent study on the role of surgery in intrathoracic lymph node metastases from extrathoracic carcinoma [14], 26 of 565 patients with mediastinal lymph node enlargement had a history of extrathoracic carcinoma (breast, 7; kidney, 5; testis, 3; prostate, 2; bladder, 1; head and neck, 3; thyroid gland, 2; rectum, 1; intestine, 1; melanoma, 1).

Axillary Lymph Nodes

Axillary lymph nodes are divided into five groups according to their afferent vessels and respective relationships with the vascular structures of the axilla [15] (*see* Figs. 2.33–2.35).

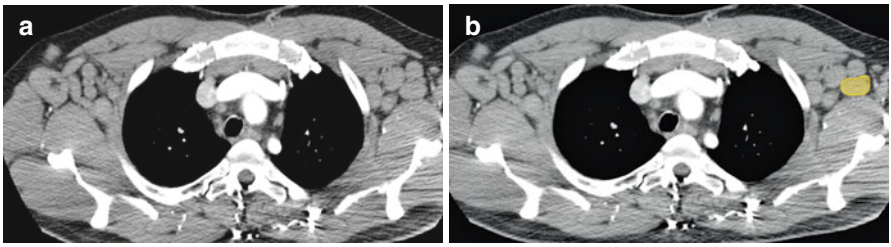

Fig. 2.33 (**a**, **b**) Axial contrast-enhanced CT scan of the thorax shows enlarged axillary group of lymph nodes (*yellow*)

Fig. 2.34 Schematic illustration shows different subgroups of the axillary lymph nodes using a color-coding scheme

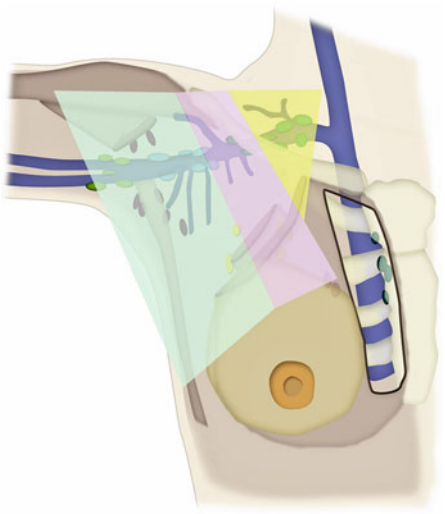

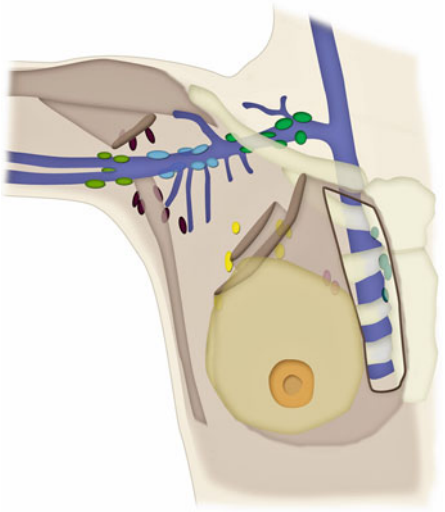

Fig. 2.35 Schematic illustration shows different subgroups of the axillary lymph nodes using a color-coding scheme

Lateral or Brachial Group

Nodes situated to the inferomedial side of the axillary vein.

Afferent vessels: Drain the lymph from the superficial and deep compartments of upper lymph, except for the superficial vessels of the arm that run along the cephalic vein.

Efferent vessels: Most terminate in the central or apical groups, whereas others pass into the supraclavicular nodes.

Anterior or Pectoral Group

Nodes located behind the pectoralis major muscle and along the lower border of the pectoralis minor, forming a chain along and behind the lateral thoracic vessels.

Afferent vessels: From the skin and muscles of the anterior and lateral walls of the trunk above the umbilicus, and the lateral parts of the breast.

Efferent vessels: Extend to the central and apical groups of axillary nodes.

Posterior or Subscapular Group

Nodes arranged in a chain that follows the subscapular vessels in the groove that separates the teres minor and subscapularis muscles.

Afferent vessels: Collect the lymph nodes arising from the muscles and skin of the back and from the scapular area down to the iliac crest.

Efferent vessels: Drain into the central and apical lymph nodes

Central Group

Located in the central part of the adipose tissue of the axilla between the preceding chains that progressively converge toward them.

Efferent vessels: Extend into the apical group.

Apical Group

Nodes that occupy the apex of the axilla, behind the upper portion of the pectoralis minor and partly above this muscle. The majority of these nodes rest on the inferomedial side of the proximal part of the axillary vein, in close contact with the upper digitations of serratus anterior.

Afferent vessels: From all other axillary nodes; they also drain some superficial vessels running along the cephalic vein.

Efferent vessels: The efferent vessels of this group unite to form the subclavian trunk, which finally opens into the right lymphatic duct on the right side or into the thoracic duct on the left side.

The inferior border of the pectoralis major and the inferolateral and superomedial edges of the pectoralis minor can be used as anatomical landmarks to separate the inferior (I), middle (II), and superior (III) levels of the axillary space. Narrowing progressively, these levels contain the anterior (pectoral), lateral (brachial), posterior (subscapular), and central groups of nodes (level I), and then the central and apical groups (levels II and III).

Malignant Causes of Enlargement

The most common cause of malignant axillary lymph node enlargement is breast cancer. The relationship between the tumor diameter and the probability of nodal involvement in all tumor sizes appears linear. For patients with cancer 5 cm or greater, 71.1 % are expected to have at least one node involved [16]. Other common causes include lymphoma and malignant melanoma.

Rare causes would include basal cell carcinoma [17] and ovarian cancer [18].

Chest Wall Nodes

Internal Mammary (Internal Thoracic or Parasternal) Nodes

These nodes lie at the anterior ends of the intercostal spaces, along the internal mammary (internal thoracic) vessels (*see* Figs. 2.36 and 2.37).

Afferent vessels: These nodes receive lymphatic drainage from the anterior diaphragmatic nodes, anterosuperior portions of the liver, medial part of the breasts, and deeper structures of the anterior chest and upper anterior abdominal wall.

Efferent vessels: May empty into the right lymphatic duct, the thoracic duct, or the inferior deep cervical nodes [19].

Malignant Causes of Enlargement

One of the commonest causes of internal mammary lymph node enlargement is breast cancer. In a study on patients undergoing free flap breast reconstruction, 43 patients had internal mammary lymph node sampling and six patients had positive lymph nodes [20].

Posterior Intercostal Nodes

These nodes are located near the heads and necks of the posterior ribs.

Afferent vessels: They receive lymphatic drainage from the posterolateral intercostal spaces, posterolateral breasts, parietal pleura, vertebrae, and spinal muscles.

Efferent vessels: From the upper intercostal spaces end in the thoracic duct on the left, and in one of the lymphatic ducts on the right. Those from the lower four to seven intercostal spaces unite to form a common trunk, which empties into the thoracic duct or cisterna chyli [19].

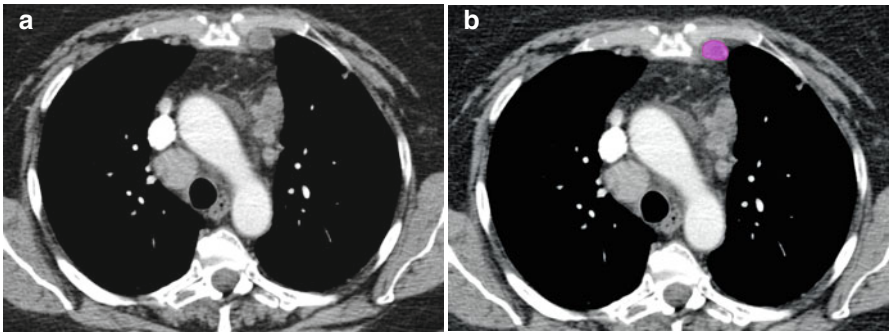

Fig. 2.36 (**a**, **b**) Axial contrast-enhanced CT scan of the thorax shows enlarged left internal mammary lymph nodes (*pink*)

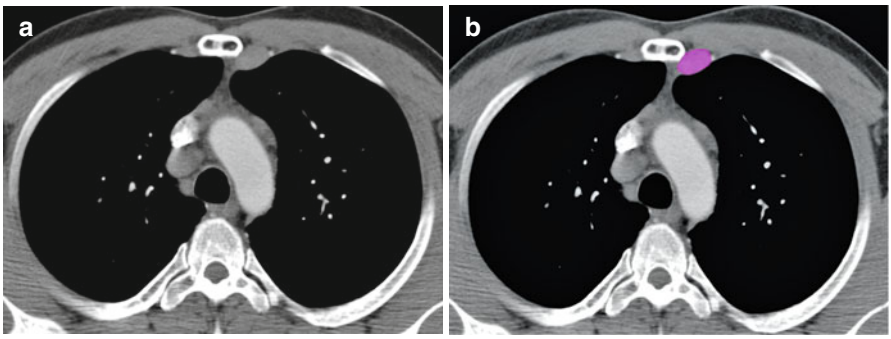

Fig. 2.37 (**a**, **b**) Axial contrast-enhanced CT scan of the thorax shows enlarged left internal mammary lymph nodes (*pink*)

Juxtavertebral (Pre-vertebral or Paravertebral) Nodes

These lie along the anterior and lateral aspects of the vertebral bodies, most common from T8 to T12. They communicate with posterior mediastinal lymph nodes and the posterior intercostal nodes, and similarly drain to the right lymphatic duct or thoracic duct [19].

Diaphragmatic Nodes

They are located on or just above the thoracic surface of the diaphragm and are divided into three groups [21].

Anterior (Pre-pericardial or Cardiophrenic) Group

These are located anterior to the pericardium, posterior to the xiphoid process, and in the right and left cardiophrenic fat (*see* Figs. 2.38–2.41).

Afferent vessels: From the anterior part of the diaphragm and its pleura, and the anterosuperior portion of the liver.

Efferent vessels: They drain to the internal mammary nodes alongside the xiphoid and can provide a route for retrograde spread of breast cancer to the liver via lymphatics of the rectus abdominis muscle when the upper internal thoracic trunks are blocked.

Middle (Juxtaphrenic or Lateral) Group

This group receives lymph from the central diaphragm and from the convex surface of the liver on the right.

Posterior (Retrocrural) Group

These nodes lie behind diaphragmatic crura and anterior to the spine.

Afferent vessels: Lymph from the posterior part of the diaphragm.

Efferent vessels: They communicate with the posterior mediastinal and para-aortic nodes in the upper abdomen.

Figure 2.42 represents the schematic illustration of all major groups of lymph nodes in the chest using a color-coding scheme. The color coding is also depicted on Fig. 2.43.

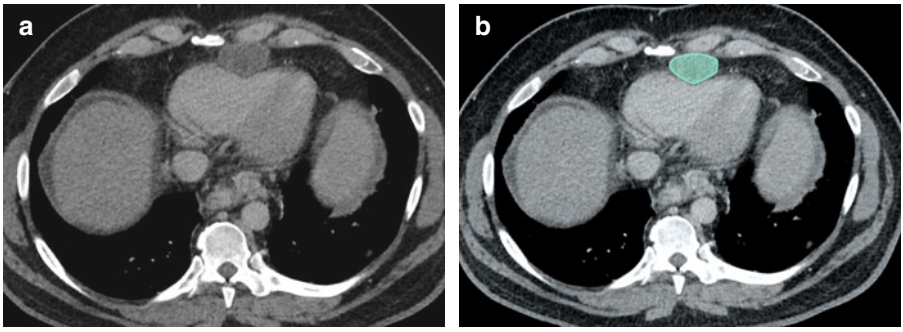

Fig. 2.38 (**a**, **b**) Axial contrast-enhanced CT scan of the thorax shows enlarged pericardial lymph node in a case of hepatocellular carcinoma (*green*)

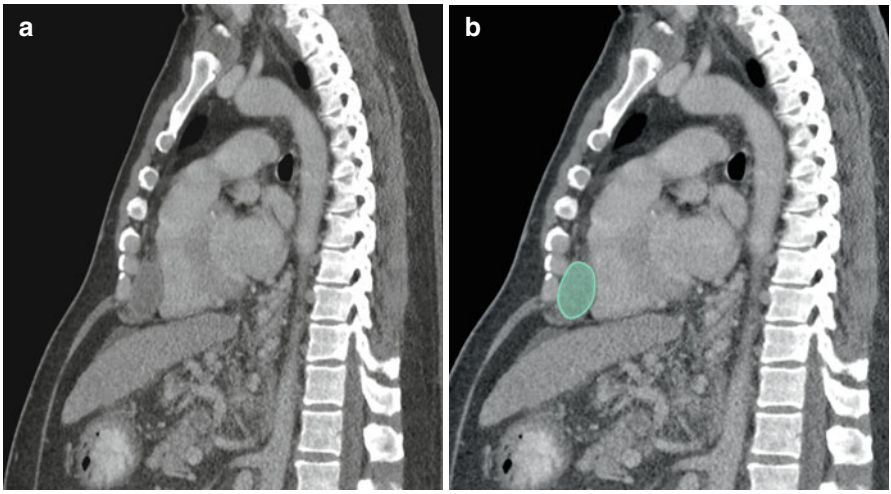

Fig. 2.39 (**a**, **b**) Sagittal reformatted CT scan of the thorax and upper abdomen shows enlarged pericardial lymph node in a case of hepatocellular carcinoma (*green*)

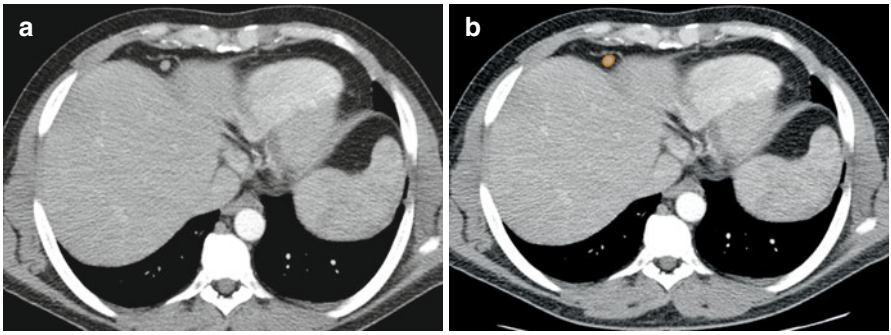

Fig. 2.40 (**a**, **b**) Axial contrast-enhanced CT scan of the thorax shows enlarged anterior diaphragmatic lymph node (*orange*)

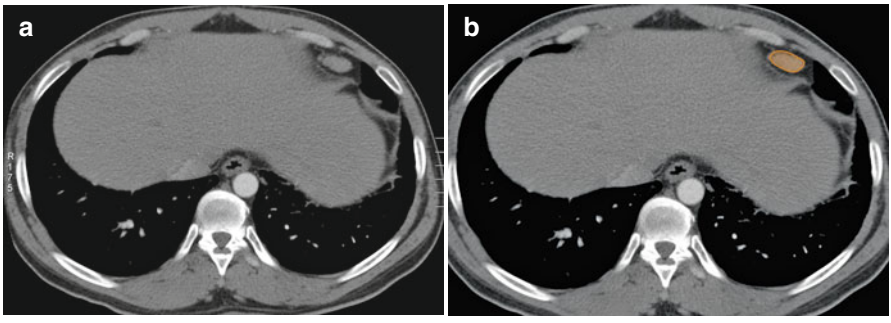

Fig. 2.41 (**a**, **b**) Axial contrast-enhanced CT scan of the thorax shows enlarged anterior diaphragmatic lymph node in a case of sarcoidosis (*orange*)

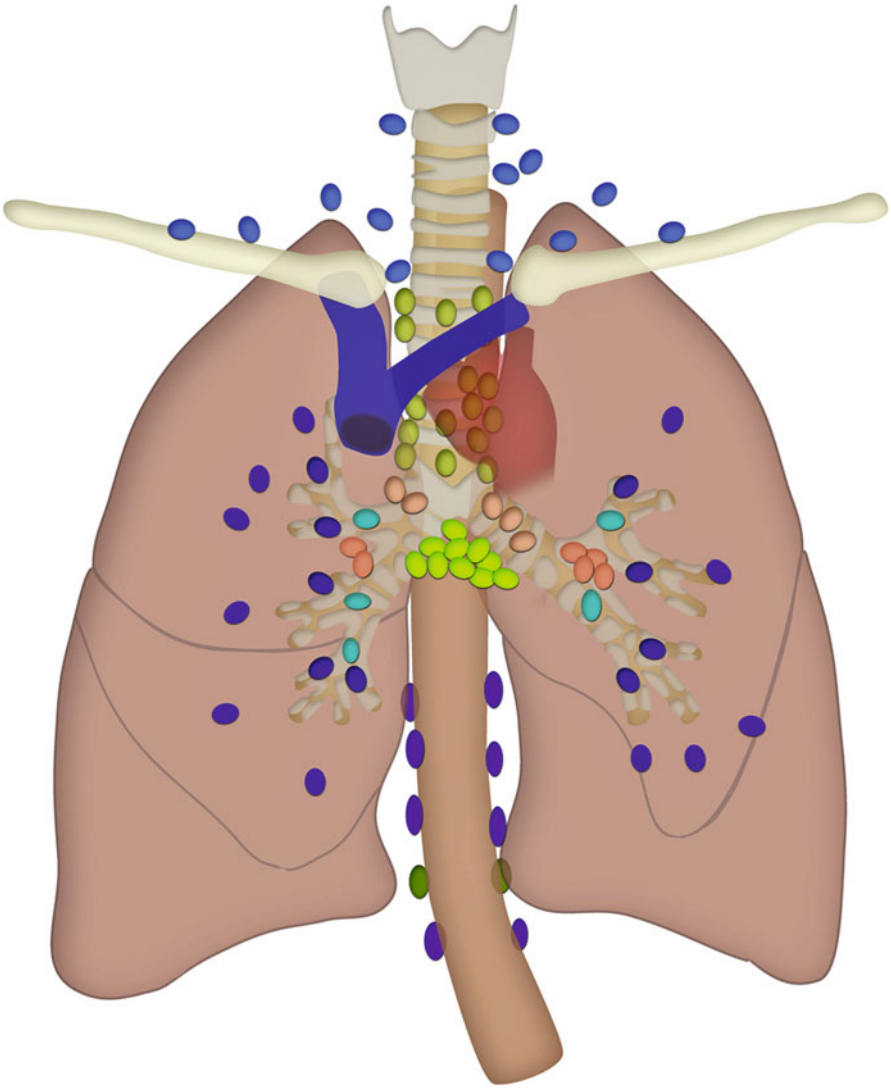

Fig. 2.42 Schematic illustration shows all major groups of lymph nodes in the chest using a color-coding scheme

Fig. 2.43 Diagram showing the color-coding scheme used to identify various groups of lymph nodes in the chest

References

1. Naruke T, Suemasu K, Ishikawa S. Lymph node mapping and curability at various levels of metastasis in resected lung cancer. J Thorac Cardiovasc Surg. 1978;76:832–9.
2. Mountain CF, Dresler CM. Regional lymph node classification for lung cancer staging. Chest. 1997;111:1718–23.
3. Rusch VW, Asamura H, Watanabe H, et al. The IASLC lung cancer staging project: a proposal for a new international lymph node map in the forthcoming seventh edition of the TNM classification for lung cancer. J Thorac Oncol. 2009;4:568–77.
4. Feigin DS, Friedman PJ, Liston SE, et al. Improving specificity of computed tomography in diagnosis of malignant mediastinal lymph nodes. J Comput Tomogr. 1985;9:21–32.
5. Seely JM, Mayo JR, Miller RR, Muller NL. T1 lung cancer: prevalence of mediastinal nodal metastases and diagnostic accuracy of CT. Radiology. 1993;186:129–32.

6. Heavey LR, Glazer GM, Gross BH, et al. The role of CT in staging radiographic T1N0M0 lung cancer. AJR Am J Roentgenol. 1986;146:285–90.
7. Conces Jr DJ, Klink JF, Tarver RD, Moak GD. T1N0M0 lung cancer: evaluation with CT. Radiology. 1989;170(3 Pt 1):643–6.
8. Li H, Zhang Y, Cai H, Xiang J. Pattern of lymph node metastases in patients with squamous cell carcinoma of the thoracic esophagus who underwent three-field lymphadenectomy. Eur Surg Res. 2007;39:1–6.
9. Castellino RA, Blank N, Hoppe RT, Cho C. Hodgkin disease: contributions of chest CT in the initial staging evaluation. Radiology. 1986;160:603–5.
10. Castellino RA. The non-Hodgkin lymphomas: practical concepts for the diagnostic radiologist. Radiology. 1991;178:315–21.
11. McLoud TC, Kalisher L, Stark P, Greene R. Intrathoracic lymph node metastases from extrathoracic neoplasms. AJR Am J Roentgenol. 1978;131:403–7.
12. Mahon TG, Libshitz HI. Mediastinal metastases of infradiaphragmatic malignancies. Eur J Radiol. 1992;15:130–4.
13. Libson E, Bloom RA, Halperin I, et al. Mediastinal lymph node metastases from gastrointestinal carcinoma. Cancer. 1987;59:1490–3.
14. Riquet M, Berna P, Brian E, et al. Intrathoracic lymph node metastases from extrathoracic carcinoma: the place for surgery. Ann Thorac Surg. 2009;88:200–5.
15. Lengele B, Hamoir M, Scalliet P, Gregoire V. Anatomical bases for the radiological delineation of lymph node areas. Major collecting trunks, head and neck. Radiother Oncol. 2007;85:146–55.
16. Carter CL, Allen C, Henson DE. Relation of tumor size, lymph node status, and survival in 24,740 breast cancer cases. Cancer. 1989;63:181–7.
17. Berlin JM, Warner MR, Bailin PL. Metastatic basal cell carcinoma presenting as unilateral axillary lymphadenopathy: report of a case and review of the literature. Dermatol Surg. 2002;28:1082–4.
18. Hockstein S, Keh P, Lurain JR, Fishman DA. Ovarian carcinoma initially presenting as metastatic axillary lymphadenopathy. Gynecol Oncol. 1997;65:543–7.
19. Suwatanapongched T, Gierada DS. CT of thoracic lymph nodes. Part I: anatomy and drainage. Br J Radiol. 2006;79:922–8.
20. Yu JT, Provenzano E, Forouhi P, Malata CM. An evaluation of incidental metastases to internal mammary lymph nodes detected during microvascular abdominal free flap breast reconstruction. J Plast Reconstr Aesthet Surg. 2011;64:716–21.
21. Aronberg DJ, Peterson RR, Glazer HS, Sagel SS. Superior diaphragmatic lymph nodes: CT assessment. J Comput Assist Tomogr. 1986;10:937–41.

Abdominal Lymph Node Anatomy

3

Lymph node metastasis is frequently seen in most primary abdominal malignant tumors. The tumor cells enter lymphatic vessels and travel to the lymph nodes along lymphatic drainage pathways. The lymphatic vessels and lymph nodes generally accompany the blood vessels supplying or draining the organs. They are all located in the subperitoneal space within the ligaments, mesentery, mesocolon, and extra peritoneum. Metastasis to the lymph nodes generally follows the nodal station in a stepwise direction—*i.e.*, from the primary tumor to the nodal station that is closest to the primary tumor and then progresses farther away but within the lymphatic drainage pathways. Metastasis to a nodal station that is farther from the primary tumor without involving the nodal station close to the primary tumor ("skip" metastasis) is rare. The key to understanding the pathways of lymphatic drainage of each individual organ is to understand the ligamentous, mesenteric, and peritoneal attachments and the vascular supply of that organ [1].

The benefits of understanding the pathways of lymphatic drainage of each individual organ are threefold. First, when the site of the primary tumor is known, it allows identification of the expected first landing site for nodal metastases by following the vascular supply to that organ [2, 3]. Second, when the primary site of tumor is not clinically known, identifying abnormal nodes in certain locations allows tracking the arterial supply or venous drainage in that region to the primary organ. Third, it also allows identification of the expected site of recurrent disease or nodal metastasis or the pattern of disease progression after treatment by looking at the nodal station beyond the treated site. The location of drainage pattern of abdominal lymphatics is outlined in Table 3.1.

The accuracy for characterizing malignant lymph nodes based on size criteria (Table 3.2) is low and has been described in published reports.

Normal-sized lymph nodes can be malignant and enlarged lymph nodes can be nonmalignant (*see* Fig. 3.1) [6–8]. Newer imaging technology such as positron emission tomography (PET)/computed tomography (CT) or magnetic resonance imaging (MRI) with nanoparticles may be superior for accurate nodal characterization [9–11].

M.G. Harisinghani, (ed.), *Atlas of Lymph Node Anatomy*,
DOI 10.1007/978-1-4419-9767-8_3, © Springer Science+Business Media New York 2013

Table 3.1 Lymphatics of the abdomen [4]

Structure	Location	Afferents from	Efferents to	Regions drained	Notes
Paracardial nodes	Around the esophago-gastric junction	Lymphatic vessels of the fundus and cardia of the stomach	Left gastric nodes	Fundus and cardia of the stomach	Paracardial nodes are 5 or 6 in number
Gastric nodes, left	On the lesser curvature of the stomach, along the course of the left gastric vessels	Lymphatic vessels from the lesser curvature of the stomach	Celiac nodes	Lesser curvature of the stomach	Left gastric nodes are 10–20 in number
Gastric nodes, right	On the lesser curvature of the stomach, along the course of the right gastric vessels	Lymphatic vessels from the lesser curvature of the stomach	Celiac nodes	Lesser curvature of the stomach	Right gastric nodes are two to three in number
Gastro-omental nodes, left	On the greater curvature of the stomach, along the left gastro-omental vessels	Lymphatic vessels from the greater curvature of the stomach	Splenic nodes	Left half of the greater curvature of the stomach	Left gastro-omental nodes are 1 or 2 in number
Gastro-omental nodes, right	On the greater curvature of the stomach, along the right gastro-omental vessels	Lymphatic vessels from the greater curvature of the stomach	Pyloric nodes	Greater curvature of the stomach	Right gastro-omental nodes are 6–12 in number
Hepatic nodes	Along the course of the common hepatic artery	Right gastric nodes, pyloric nodes	Celiac nodes	Liver and gall bladder; extrahepatic biliary apparatus; respiratory diaphragm; head of pancreas and duodenum	Hepatic nodes drain a portion of the respiratory diaphragm because of the common embryonic origin of the diaphragm and the liver (septum transversum)
Cystic node	Near the neck of the gall bladder	Lymphatic vessels of the gall bladder	Hepatic nodes	Gall bladder	Cystic node drains to the node of the omental foramen, then to hepatic nodes

Pyloric nodes	Near the termination of the gastroduodenal artery.	Pancreaticoduodenal nodes	Hepatic nodes	Head of pancreas and duodenum; right half of greater curvature of stomach	Pyloric nodes are six to eight in number
Pancreaticoduodenal nodes	Along the pancreaticoduodenal arcade of vessels	Lymphatic vessels from the duodenum and pancreas	Pyloric nodes	Duodenum and head of the pancreas	Lymph from the pancreas is drained in three different directions: pancreaticoduodenal nodes, pancreaticosplenic nodes, superior mesenteric nodes
Pancreaticosplenic nodes	Along the splenic vessels	Lymphatic vessels from the pancreas and greater curvature of the stomach	Celiac nodes	Neck, body and tail of the pancreas; left half of the greater curvature of the stomach	Lymph from the pancreas is drained in three different directions: pancreaticoduodenal nodes, pancreaticosplenic nodes, superior mesenteric nodes
Celiac nodes	Around the celiac arterial trunk	Hepatic nodes, gastric nodes, pancreaticosplenic nodes	Intestinal lymph trunk	Liver, gall bladder, stomach, spleen, pancreas	Celiac nodes are from three to six in number
Mesenteric nodes	Along the vasa recta and branches of the superior mesenteric a. Between the leaves of peritoneum forming the mesentery	Peripheral nodes located along the attachment of the mesentery	Superior mesenteric nodes	Small intestine	Mesenteric nodes may number as many as 200; an important node group in cases of intestinal cancer
Mesenteric nodes, superior	Along the course of the superior mesenteric artery	Mesenteric nodes, ileocolic nodes, right colic nodes, middle colic nodes	Celiac nodes, intestinal lymph trunk	Gut and viscera supplied by the superior mesenteric artery	Superior mesenteric nodes are important in the spread of cancer from the small and large intestine

(continued)

Table 3.1 (continued)

Structure	Location	Afferents from	Efferents to	Regions drained	Notes
Inferior mesenteric nodes	Around the root of the inferior mesenteric artery.	Peripheral nodes located along the marginal artery.	Lumbar chain of nodes, superior mesenteric nodes	Distal one-third of the transverse colon, descending colon, sigmoid colon, rectum	Inferior mesenteric nodes may number as high as 90; an important node group in cases of cancer of the colon and rectum
Ileocolic nodes	Along the origin and terminal end of the ileocolic vessels	Peripheral nodes located along the attachment of the mesentery	Superior mesenteric nodes	Ileum, cecum, appendix	Ileocolic nodes located near the ileocecal junction may be divided into two subsidiary groups: cecal nodes and appendicular nodes
Colic nodes, right	Along the course of the right colic vessels	Peripheral nodes located along the marginal a.	Superior mesenteric nodes	Ascending colon, cecum	Right colic nodes are approximately 70 in number
Colic nodes, middle	Along the course of the middle colic vessels	Peripheral nodes located along the attachment of the mesentery	Superior mesenteric nodes	Transverse colon	Middle colic nodes are approximately 40 in number
Colic nodes, left	Along the course of the left colic vessels	Peripheral nodes located along the marginal a.	Inferior mesenteric nodes	Descending colon, sigmoid	Left colic nodes are approximately 30 in number
Pararectal nodes	Along the course of the superior rectal vessels	Lymphatic vessels from the rectum and anal canal	Inferior mesenteric nodes	Rectum and anal canal	Pararectal nodes are small lymph nodes that are not well localized
Lateral aortic nodes	Along the inferior vena cava and abdominal aorta from the aortic bifurcation to the aortic hiatus of the diaphragm	Common iliac nodes; lymphatic vessels from the posterior abdominal wall and viscera	Efferents form one lumbar trunk on each side	Lower limb; pelvic organs; perineum; anterior and posterior abdominal wall; kidney; suprarenal gland; respiratory diaphragm	Also known as: lumbar nodes; the intestinal trunk drains into to the left lumbar trunk; the lumbar trunks unite to form the thoracic duct/ cisterna chili

Table 3.2 Size criteria for detecting abdominal malignant lymph nodes [5]

Location	Short axis nodal diameter, mm
Retrocrural	>6
Paracardiac	>8
Mediastinal	≥10
Gastrohepatic ligament	>8
Upper paraaortic	>9
Portacaval	>10
Portahepatis	> 7
Lower paraaortic	> 11

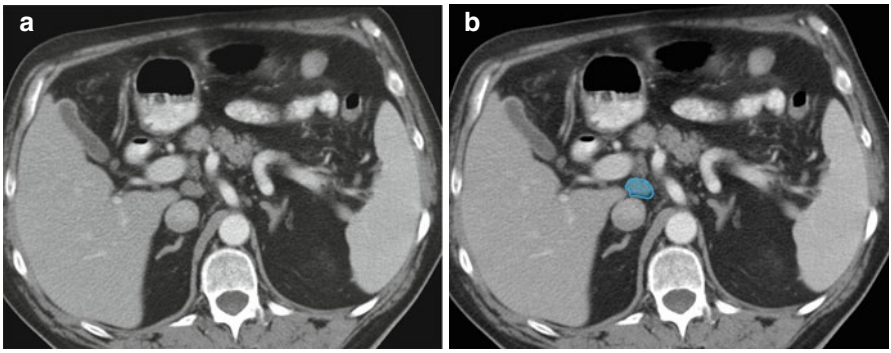

Fig. 3.1 (**a**, **b**) Axial CT image in a patient with cirrhosis shows a prominent portocaval lymph node (*blue*)

Lymphatic Spread of Malignancies

Liver

Hepatocellular carcinoma (HCC) is the most common primary visceral malignancy [12]. Lymph node metastases (LNM) are rare and generally associated with poor prognosis in hepatocellular carcinoma (*see* Fig. 3.2). The median survival time of patients with single and multiple LNM after surgery was 52 and 14 months, respectively [13].

Table 3.4 outlines the regional lymph nodes for hepatocellular carcinoma. There are several potential pathways for tumor spread, including superficial and deep pathways, below and above the diaphragm. The superficial lymphatic network (*see* Fig. 3.3) is extensive and is located beneath Glisson's capsule. The drainage of superficial lymphatics can be classified into three major groups:

1. Through the hepatoduodenal and gastrohepatic ligament pathway, it is the most common distribution of lymph node metastasis.
2. The diaphragmatic lymphatic plexus is another important pathway of drainage because a large portion of the liver is in contact with the diaphragm either directly at the bare area or indirectly through the coronary and triangular ligaments. However, nodal metastasis through this pathway is often overlooked.

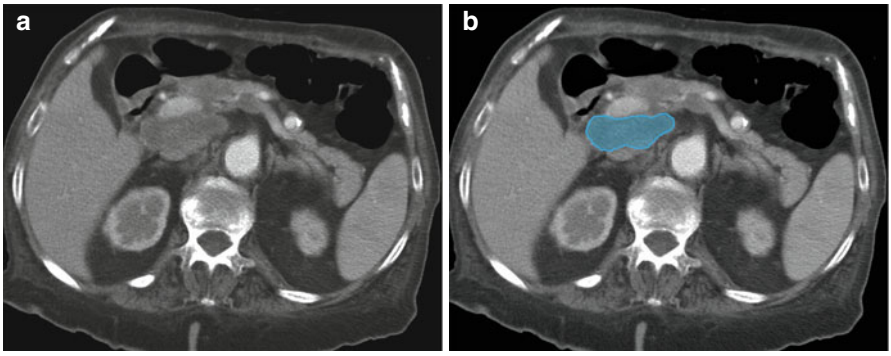

Fig. 3.2 (**a**, **b**) Axial CT image in a patient with hepatoma shows a metastatic low density portocaval lymph node (*blue*)

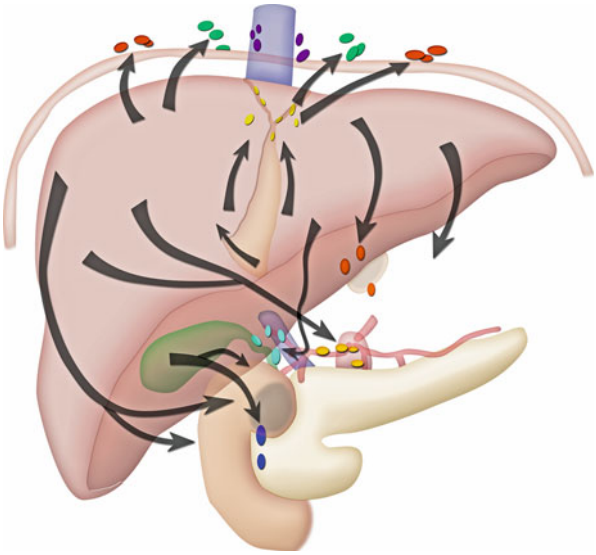

Fig. 3.3 Superficial pathways of lymphatic drainage for the liver. The anterior diaphragmatic nodes consist of the lateral anterior diaphragmatic group and the medial group, which includes the pericardiac nodes and the subxiphoid nodes behind the xiphoid cartilage. The nodes in the falciform ligament drain into the anterior abdominal wall along the superficial epigastric and deep epigastric lymph nodes. The epigastric and the subxiphoid nodes drain into the internal mammary nodes

3. The rare pathway for nodal metastasis is along the falciform ligament to the deep superior epigastric node in the anterior abdominal wall along the deep superior epigastric artery below the xiphoid cartilage.

The deep lymphatic network follows the portal veins, drains into the lymph nodes at the hilum of the liver, the hepatic lymph nodes, then to the nodes in the hepatoduodenal ligament. The nodes in the hepatoduodenal ligament can be separated into two major chains: the hepatic artery chain and posterior periportal chain (*see* Figs. 3.4 and 3.5). The hepatic artery chain follows the common hepatic artery to the node at the celiac axis and then into the cisterna chyli. The posterior periportal chain is located posterior to the portal vein in the hepatoduodenal ligament (*see* Fig. 3.6).

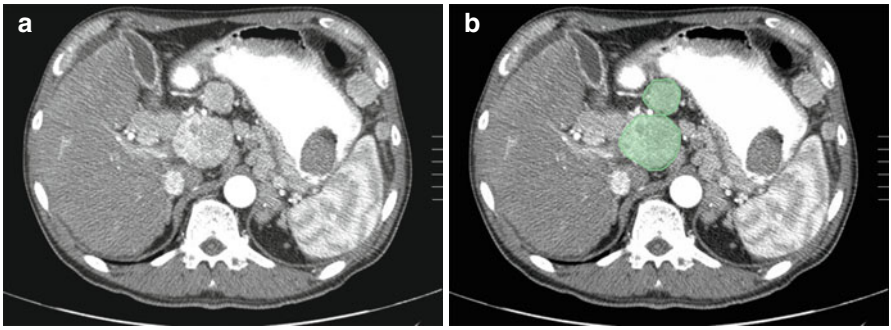

Fig. 3.4 (**a**, **b**) Axial CT image in a patient with hepatocellular carcinoma shows enlarged hypervascular nodes (*green*) in the periportal locations

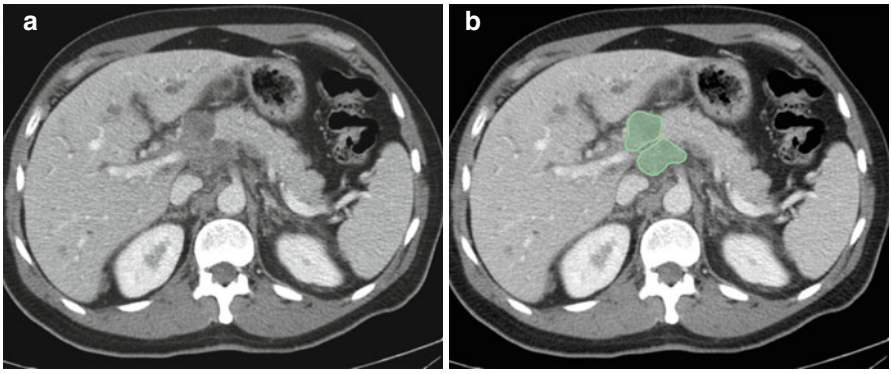

Fig. 3.5 (**a**, **b**) Axial CT image in a patient with hepatoma shows enlarged nodes in the periportal (*green*) and peripancreatic location causing secondary biliary obstruction

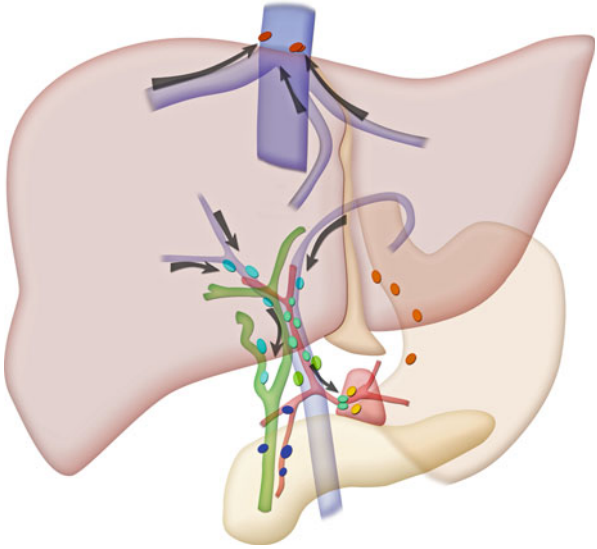

Fig. 3.6 Deep pathways of lymphatic drainage for the liver. The deep pathways follow the hepatic veins to the inferior vena cava nodes and the juxtaphrenic nodes that follow along the phrenic nerve. The pathways that follow the portal vein drain into the hepatic hilar nodes and the nodes in the hepatoduodenal ligament, which then drain into the celiac node and the cisterna chyli

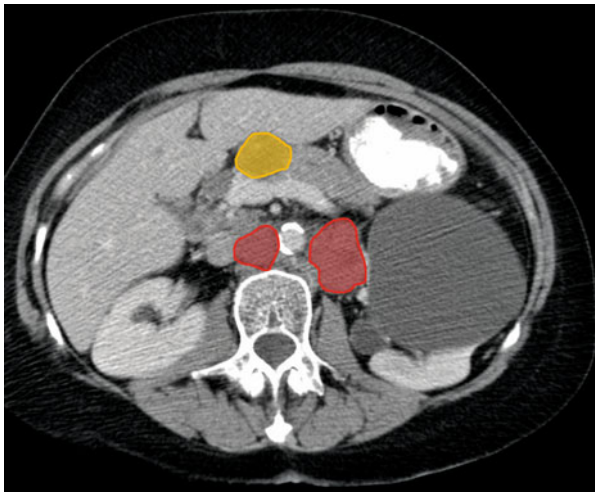

Fig. 3.7 Axial CT image in a patient with cholangiocarcinoma shows enlarged prepancreatic (*yellow*) and retroperitoneal lymph nodes (*red*)

Table 3.3 N-stage classification for hepatocellular carcinoma

Stage	Findings
NX	Regional nodes cannot be assessed
N0	No regional nodal metastasis
N1	Metastasis in regional lymph nodes

Table 3.4 Regional lymph nodes for hepatocellular carcinoma (7)

Hepatocellular carcinoma
Hepatoduodenal ligament
Caval lymph nodes
Hepatic artery

It drains into the retropancreatic nodes and the aortocaval node (*see* Fig. 3.7) and then into the cisterna chyli and the thoracic duct [1].

Tables 3.3 and 3.4 list the N staging for hepatocellular carcinoma and the regional lymph nodes for hepatocellular carcinoma. No consensus has yet been reached on the treatment strategy for LNM from HCC. Long-term survival can be expected after selective lymphadenectomy, especially in patients with a single LNM. On the other hand, efficacy of selective lymphadenectomy for multiple LNM seemed equivocal due to its advanced and systemic nature of the disease [13].

Stomach

Gastric cancer is the third most common gastrointestinal malignancy [7]. Lymph node metastasis in gastric cancer is common and the incidence increases with advanced stages of tumor invasion [14].

The lymphatic drainage of the stomach consists of intrinsic and extrinsic systems (*see* Fig. 3.8). The intrinsic system includes intramural submucosal and subserosal

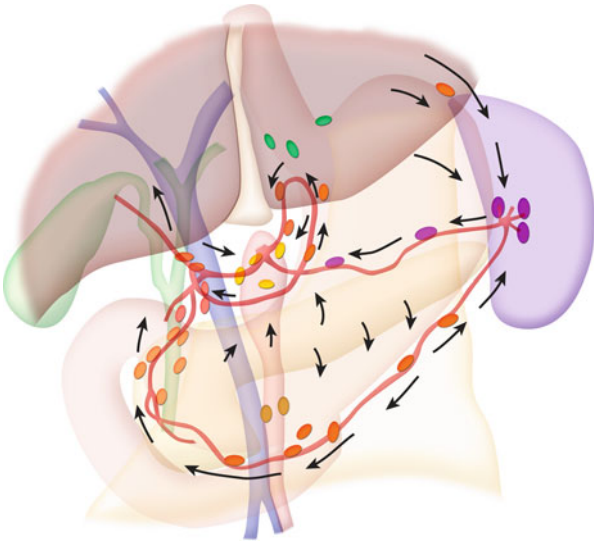

Fig. 3.8 Lymphatic drainage pathways for the stomach

Table 3.5 N-stage classification for gastric cancer

Stage	Findings
NX	Regional lymph node(s) cannot be assessed
N0	No regional lymph node metastasis
N1	Metastasis in one to six regional lymph nodes
N2	Metastasis in 7–15 regional lymph nodes
N3	Metastasis in more than 15 regional lymph nodes

networks and the extrinsic system forms lymphatic vessels outside the stomach and generally follows the course of the arteries in various peritoneal ligaments around the stomach. These lymphatic vessels drain into the lymph nodes at nodal stations in the corresponding ligaments and drain into the central collecting nodes at the root of the celiac axis and the superior mesenteric artery [1].

Tables 3.5 and 3.6 list the nodal staging for gastric carcinoma and the regional draining lymph nodes. The extent of nodal metastasis as defined by pathologic staging on surgical specimens has been used as prognostic indicators based on the number of positive nodes. However, the nodal groups described in this section are based on anatomic locations according to the Japanese Classification of Gastric Cancer (JCGC).

The JCGC classified the nodes into three groups (*see* Fig. 3.9):

- Group 1 are lymph nodes around the stomach including the left cardiac, right cardiac, greater and lesser curvature, and supra- and infrapyloric nodes. Resection of these nodes is defined as D1 category (*see* Fig. 3.10).
- Group 2 are lymph nodes away from the perigastric lymph nodes. They include the left gastric, common hepatic, splenic artery, splenic hilum, proper hepatic, and celiac nodes. Resection of nodes in group 1 and group 2 is defined as D2 category.

Table 3.6 Regional lymph nodes for gastric cancer [7]

Gastric cancer
Greater curvature of stomach
Greater curvature
Greater omental
Gastroduodenal
Gastroepiploic
Pyloric
Pancreaticoduodenal lymph nodes
Pancreatic and splenic area
Pancreaticolienal
Peripancreatic
Splenic
Lesser curvature of stomach
Lesser curvature
Lesser omental
Left gastric
Cardio-oesophageal
Common hepatic
Hepatoduodenal ligament

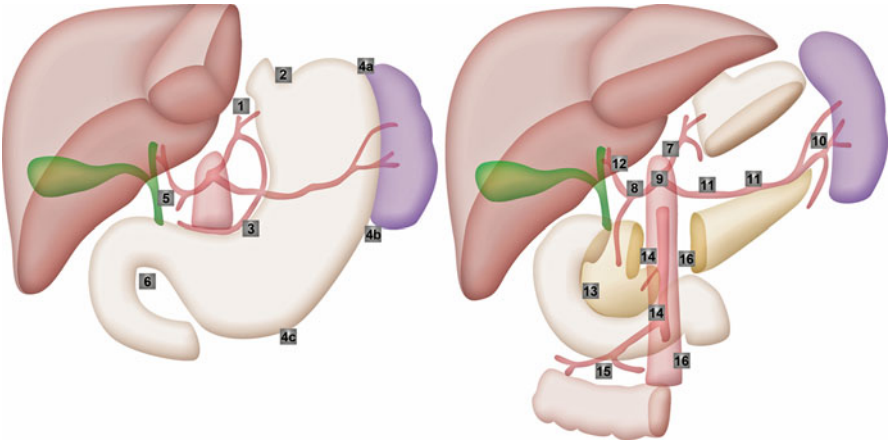

Fig. 3.9 The JCGC classification for perigastric lymph nodes. *Group 1*: *1* Right cardial nodes, *2* left cardial nodes, *3* nodes along the lesser curvature, *4* nodes along the greater curvature, *5* suprapyloric nodes, *6* infrapyloric nodes. *Group 2*: *7* nodes along the left gastric artery, 8 nodes along the common hepatic artery, *9* nodes around the celiac axis, *10* nodes at the splenic hilus, *11* nodes along the splenic artery. *Group 3*: *12* nodes in the hepatoduodenale ligament, *13* nodes at the posterior aspect of the pancreas head, *14* nodes at the root of the mesenterium, *15* nodes in the mesocolon of the transverse colon, *16* para-aortic nodes

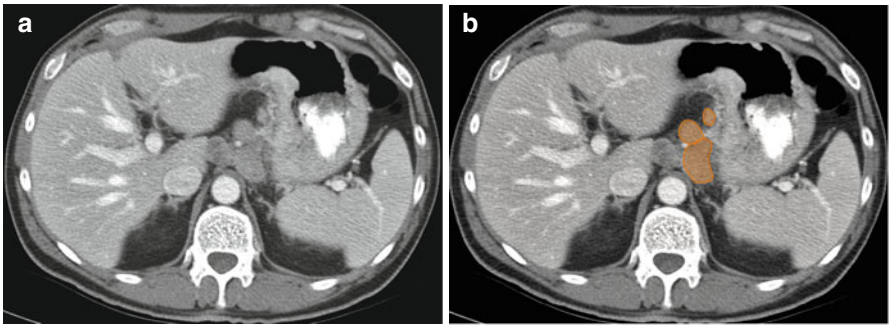

Fig. 3.10 (**a**, **b**) Axial CT image in a patient with gastric carcinoma shows enlarged gastrohepatic lymph nodes (*orange*) along the lesser curvature

- Group 3 are lymph nodes in the hepatoduodenal ligament, posterior pancreas, root of the mesentery, paraesophageal, and diaphragmatic nodes. Resection of the three nodal groups and paraaortic nodes is defined as D3 category.

Paraesophageal and Paracardiac Nodes

The lymph from the distal esophagus and the cardiac orifice of the stomach drains to the paraesophageal lymph nodes around the esophagus above the diaphragm and the paracardiac nodes below the diaphragm. They can spread upward along the esophagus to the mediastinal lymph nodes and along the thoracic duct to the left or right supraclavicular nodes or downward along the esophageal branches of the left gastric artery to the left gastric nodes and the celiac nodes (*see* Fig. 3.11) [1].

Nodal Metastases in the Gastrohepatic Ligament

Tumors arising from the area of the stomach along the lesser curvature and the esophagogastric junction, supplied by the left gastric artery, generally metastasize to the lymph nodes in the gastrohepatic ligament (*see* Fig. 3.12). The primary nodal group (group 1) consists of nodes along the left and right gastric artery anastomosis along the lesser curvature. Group 2 nodes include the nodes along the left gastric artery and vein in the gastropancreatic fold that drain toward the nodes at the celiac axis. Tumors arising from the area of the stomach in the distribution of the right gastric artery along the lesser curvature of the gastric antrum drain into the perigastric nodes and the suprapyloric nodes near the pylorus (group 1). They then drain into the nodes at the common hepatic artery (group 2), from where the right gastric artery originates or the area where the right gastric vein drains into the portal vein. From these nodes, drainage continues along the hepatic artery toward the celiac axis (group 2). The lymphatic anastomoses in the gastrohepatic ligament along the lesser

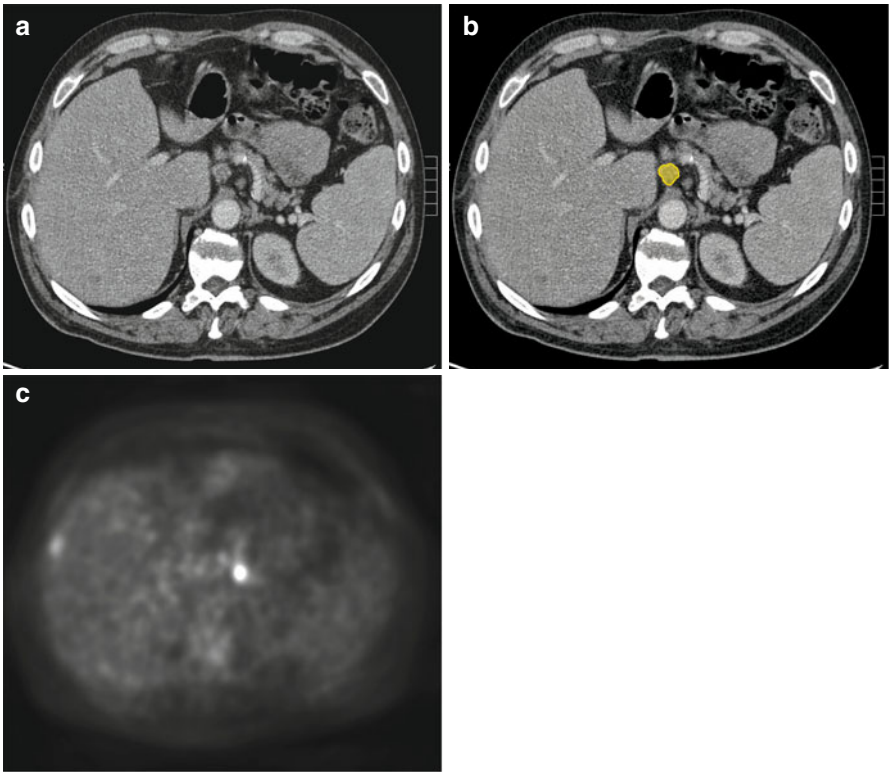

Fig. 3.11 (**a–c**) Axial CT image in a patient with esophageal cancer shows enlarged celiac lymph node (*yellow*). The node shows FDG activity on a PET scan

curvature form the alternate drainage pathways for the tumors arising from this region. Less commonly they are involved in pancreatic cancer due to retrograde tumor extension from the celiac nodes [1].

Nodal Metastases in the Gastrosplenic Ligament

Lymphatic drainage of tumors at the posterior wall and the greater curvature of the gastric fundus spreads to the perigastric nodes (group 1) in the superior segment of the gastrosplenic ligament, then follows along the branches of the short gastric artery to the nodes at the hilum of the spleen (group 2). The tumors from the greater curvature of the body of the stomach also spread to the perigastric nodes (group 1) and then advance along the left gastroepiploic vessels and drain into the lymph nodes in the splenic hilum (group 2). From the splenic hilum, they may spread to the nodes along the splenic artery to the nodes at the celiac axis (group 2). In addition, the tumors from the posterior wall of the gastric fundus and upper segment of the body may drain along the posterior gastric artery to the nodes along the splenic

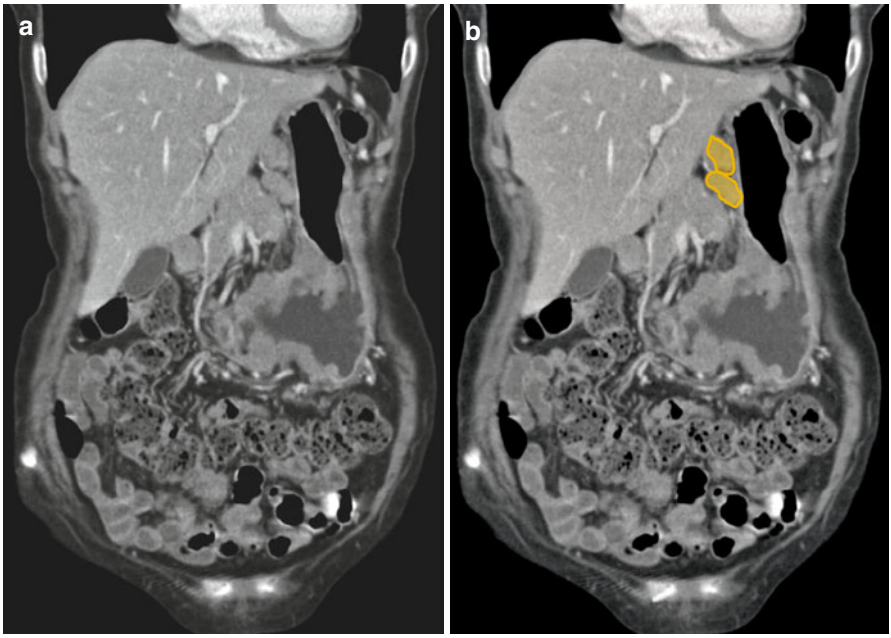

Fig. 3.12 (**a**, **b**) Coronal reformatted CT image in a patient with stomach cancer show prominent gastrohepatic ligament lymph nodes (*orange*)

artery that are known as the suprapancreatic nodes or the nodes in the splenorenal ligament and then to the nodes at the celiac axis [1].

Nodal Metastases in the Gastrocolic Ligament

Primary tumors involving the greater curvature of the antrum of the stomach in the distribution of the right gastroepiploic artery spread to the perigastric nodes (group 1) accompanying the right gastroepiploic vessels that course along the greater curvature of the stomach. They drain into the nodes at the gastrocolic trunk (group 2) (*see* Fig. 3.13) or the nodes at the origin of the right gastroepiploic artery and the nodes along the gastroduodenal artery (the subpyloric or infrapyloric node). From there, they may proceed to the celiac axis or the root of the superior mesenteric artery [1].

Inferior Phrenic Nodal Pathways

Tumors involving the esophagogastric junction or the gastric cardia may invade the diaphragm as they penetrate beyond its wall. The lymphatic drainage of the peritoneal surface of the diaphragm is via the nodes along the inferior phrenic artery and veins that course along the left crus of the diaphragm toward the celiac axis or the left renal vein [1].

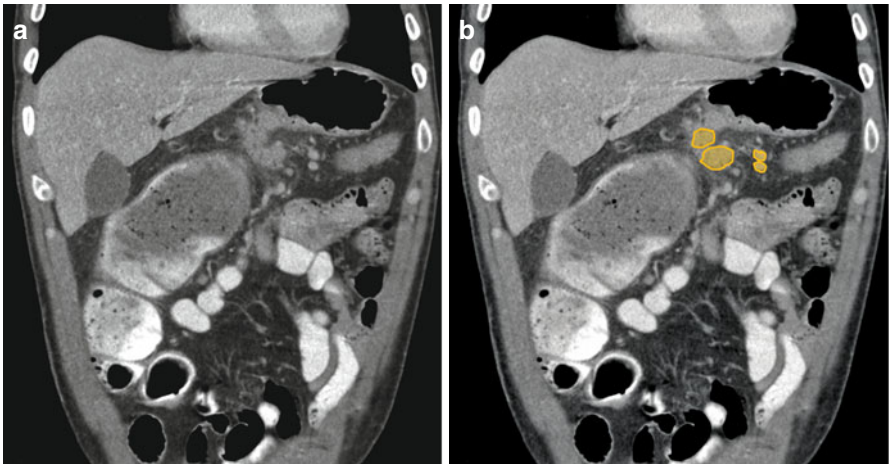

Fig. 3.13 (**a**, **b**) Coronal reformatted CT image in a patient with stomach cancer shows prominent gastrocolic ligament lymph nodes (*orange*)

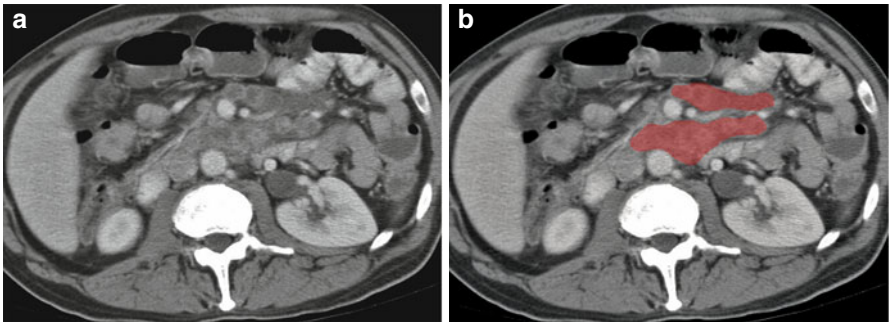

Fig. 3.14 (**a**, **b**) Axial CT image in a patient with lymphoma shows enlarged, clustered mesenteric root lymph nodes (*red*)

A CT scan of the abdomen and pelvis is the most widely recommended method for preoperative staging of gastric cancer [15]. The accuracy of MRI is considered to be inferior to CT for examining LN involvement, but may be more accurate than CT for non-nodal metastatic disease [16]. Further diagnostic imaging via 18 F-fluoro-deoxy-D-glucose (FDG) PET is not a replacement for CT in gastric cancer cases, but can complement CT for staging and prognostic information [15].

Small Intestine

The three most common malignant tumors of the small intestine are lymphoma, adenocarcinoma, and carcinoid tumor. The path of regional nodal metastasis follows the vessels of the involved segment to the root of the superior mesentery artery (SMA) (*see* Fig. 3.14) near the head of the pancreas and to the extra peritoneum [1].

Table 3.7 N-stage classification for colorectal cancer

Stage	Findings
NX	Regional nodes cannot be assessed
N1	Metastasis in one to three regional lymph nodes
N2	Metastasis in four or more regional lymph nodes

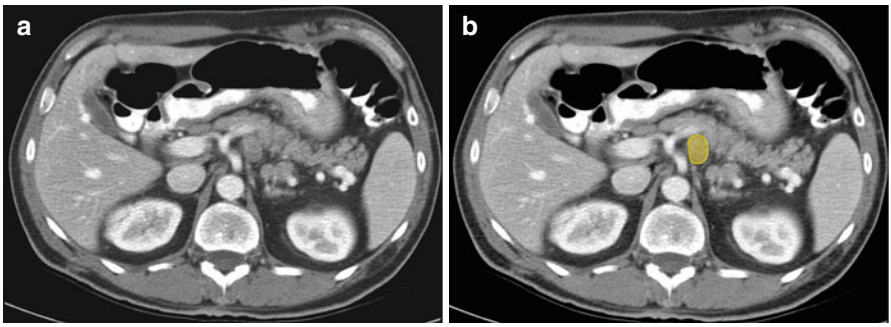

Fig. 3.15 (**a**, **b**) Axial CT image in a patient with primary colon cancer shows an enlarged celiac lymph node (*yellow*)

Appendix

Similar to the small intestine, carcinoid tumor, noncarcinoid epithelial tumor, and lymphoma are the three most common tumors of the appendix. Lymph node metastasis is rare in the tumors of the appendix. Generally, nodal metastasis follows the ileocolic vessels along the root of the mesentery to the origin of the SMA and the paraaortic region [1].

Colorectal

Colorectal adenocarcinoma is the third most common cancer and the third most common cause of cancer deaths [7]. Lymph node metastasis is one of the most important prognostic factors in the TNM classification—defining the number of positive nodes in stepwise incremental groups—that correlates with poorer outcome (Table 3.7) (*see* Fig. 3.15) [1]. Accurate identification of abnormal lymph nodes is important as it aids in preoperative planning of the extent of surgery. Patients with T1–T2 rectal tumors can be treated with resection alone. If there are nodal metastases (or if the tumor is T3), neoadjuvant treatment is required. It also helps in identifying regions of possible recurrence in treated cases, in the clinical setting of increasing carcinoembryonic antigen levels [17–19].

Table 3.8 lists regional lymph nodes for colorectal cancer. Lymph from the wall of the large intestine and rectum drains into the lymph nodes accompanying the arteries and veins of the corresponding colon and rectum [19–21]. The nodes can be classified according to the location as follows (*see* Fig. 3.16).

Table 3.8 Regional lymph nodes for colorectal cancer [7]

Colorectal cancer
Pericolic/perirectal
Ileocolic
Right colic
Middle colic
Left colic
Inferior mesenteric artery
Superior rectal (hemorrhoidal)

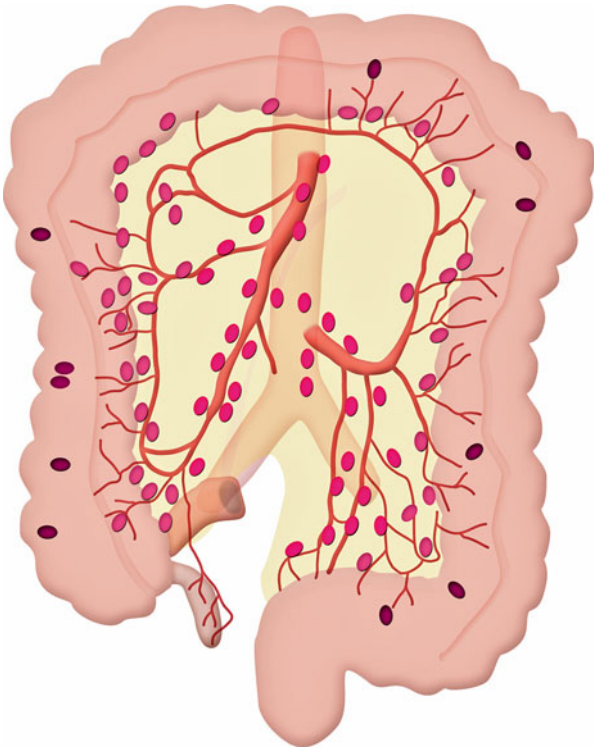

Fig. 3.16 Lymphatic drainage pathways for the colon

- The epicolic nodes accompanying the vasa recta outside the wall.
- The paracolic nodes along the marginal vessels.
- The intermediate mesocolic nodes along the ileocolic, right colic, middle colic, left ascending and descending colic, left colic, and sigmoidal arteries.
- The principal nodes at the gastrocolic trunk, the origin of the middle colic artery, and the origin of the inferior mesenteric artery.

Caecum and ascending colon. The lymphatic drainage is via the epicolic nodes and the paracolic nodes, which are seen in proximity with the marginal vessels along the mesocolic side of the colon. From the paracolic nodes (*see* Fig. 3.17), lymphatic drainage follows the vessels in the ileocolic (*see* Fig. 3.18) and right colic

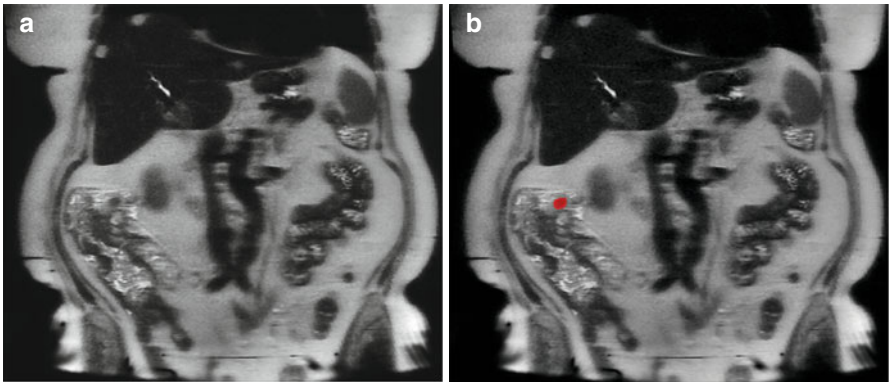

Fig. 3.17 (**a**, **b**) Coronal T2-weighted image in a patient with ascending colon adenocarcinoma with metastatic pericolic lymph node (*red*)

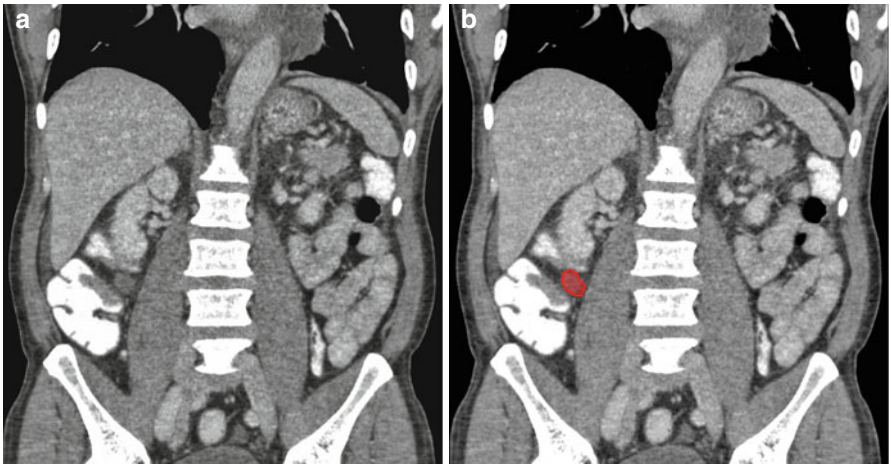

Fig. 3.18 (**a**, **b**) Coronal reformatted CT image in a patient with cecal cancer shows prominent ileocolic lymph node (*red*)

mesentery, where the intermediate nodal group is located and drains into the principal nodes at the root of the SMA.

Transverse colon. The lymphatic drainage is from the epicolic nodes and the paracolic nodes (along the marginal vessels) to the intermediate nodal group situated along the middle colic vessels and then into the principal node at the root of the SMA (*see* Fig. 3.19).

Left side of colon and upper rectum. The lymphatic drainage is from the epicolic and the paracolic (along the marginal vessels) group to the intermediate mesocolic nodes including the left colic nodes, and then to the principal inferior mesenteric artery (IMA) nodes (*see* Fig. 3.20).

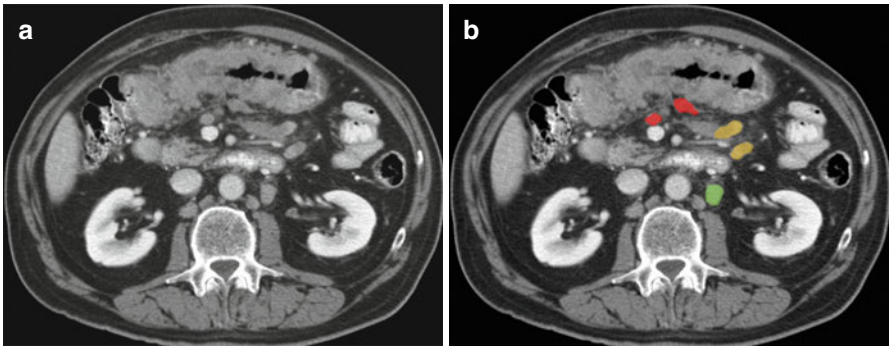

Fig. 3.19 (**a**, **b**) Axial CT image in a patient with malignancy in the transverse colon shows pericolonic (*red*), mesenteric (*yellow*), and left periaortic (*green*) lymph nodes

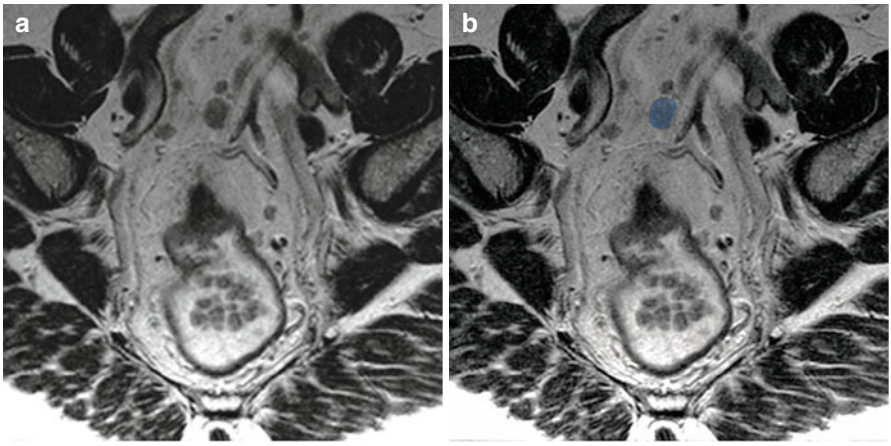

Fig. 3.20 (**a**, **b**) Axial oblique T2-weighted images in a patient with rectal cancer shows metastatic inferior mesenteric lymph node (*blue*)

Lower rectum. There are two different lymphatic pathways: one is along the superior hemorrhoidal vessels toward the mesorectum (*see* Figs. 3.21, 3.22, 3.23, and 3.24) and mesocolon; the other is the lateral route, along the middle and inferior hemorrhoidal vessels toward the hypogastric and obturator nodes, and then to the paraaortic nodes (*see* Figs. 3.25 and 3.26).

Anus. Anal tumors usually spread to the superficial inguinal nodes and then to the deep inguinal nodes along the common femoral vessels. From here they ascend to the external iliac, common iliac, and paraaortic groups (*see* Figs. 3.27 and 3.28).

A key pathologic characteristic in determining the stage of disease in colon cancer is the status of the draining lymph nodes [22]. The criteria for distance between tumor and mesorectal fascia in case of T3 tumors, also applies for mesorectal nodes lying within the mesorectal fat (*see* Fig. 3.29). Nodes are more than 3 mm in size,

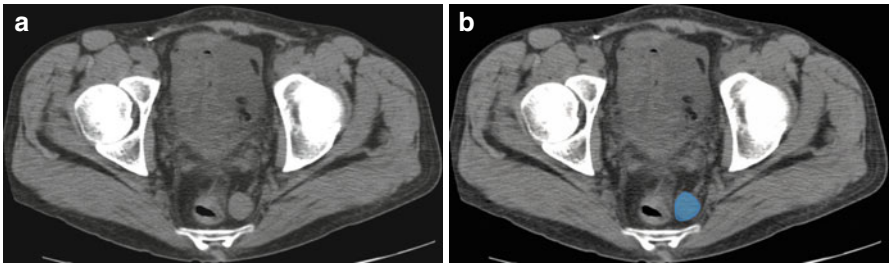

Fig. 3.21 (**a**, **b**) Axial CT image in a patient with primary rectal cancer shows an enlarged left perirectal lymph node (*blue*)

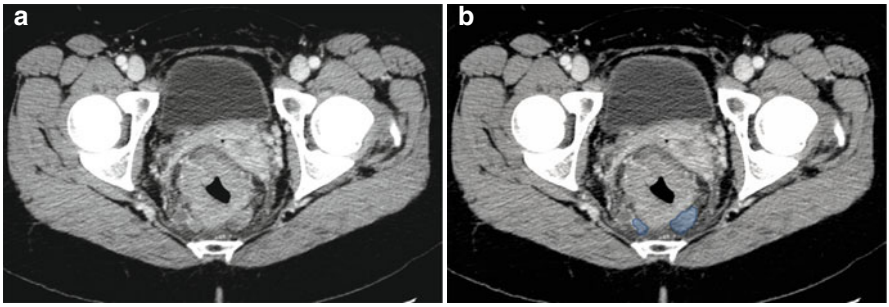

Fig. 3.22 (**a**, **b**) Axial CT image in a patient with rectal cancer showing metastatic perirectal lymph nodes (*blue*)

whereas tumor deposits are smaller. If lymph nodes are involved with tumor (Stage III disease), 5-fluorouracil–based adjuvant therapy improves survival [23]. However, for node-negative disease (stage II disease), the benefits of adjuvant chemotherapy are not well-established.

MRI with the use of ultrasmall superparamagnetic iron oxide (USPIO) contrast agents has a promising role, however further evaluation in rectal cancer needs to be assessed [24]. Because of the nonspecificity on anatomic imaging, additional imaging studies and aspiration biopsy are frequently used to establish the diagnosis of metastatic disease before treatment decision.

Retroperitoneal Lymph Nodes

Renal, Upper Urothelial, and Adrenal Malignancies

Lymphatics draining the kidney are derived from three plexuses: one beneath the renal capsule, the second around the renal tubules, and the third in the perirenal fat. These plexuses drain into lymphatic trunks that run from the renal hilum along the renal vein

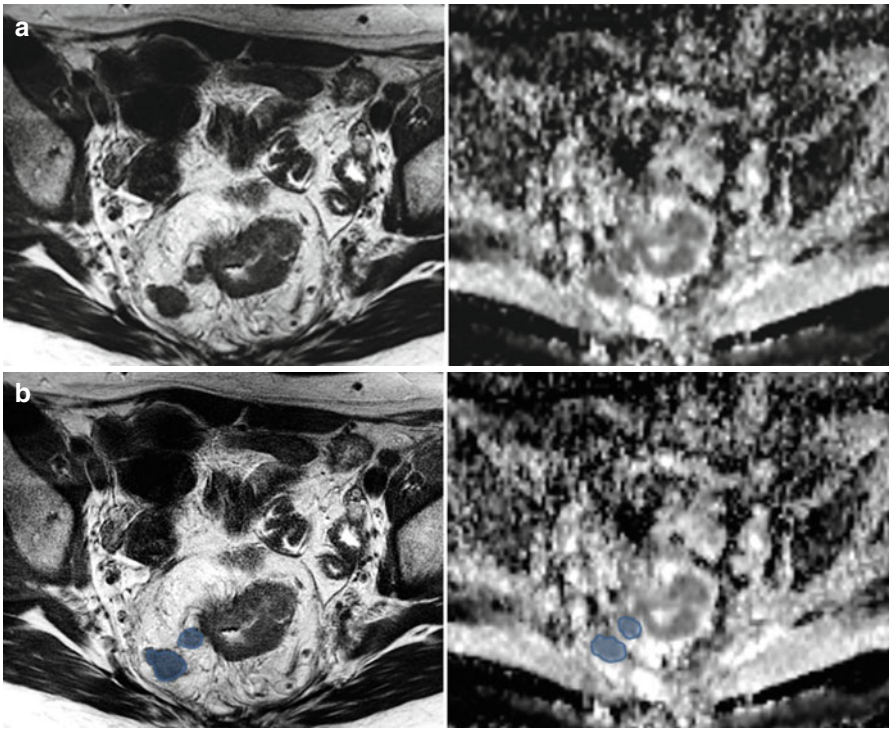

Fig. 3.23 (**a**, **b**) Axial T2-weighted image (*left*) and Apparent Diffusion Coefficient (ADC) map (*right*) of a patient with rectal cancer showing metastatic perirectal lymph nodes (*blue*) with restricted diffusion and dark signal on ADC

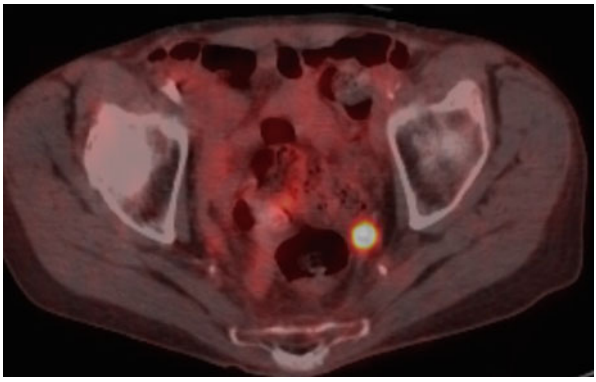

Fig. 3.24 Fused axial PET-CT image shows FDG avid metastatic left perirectal lymph node

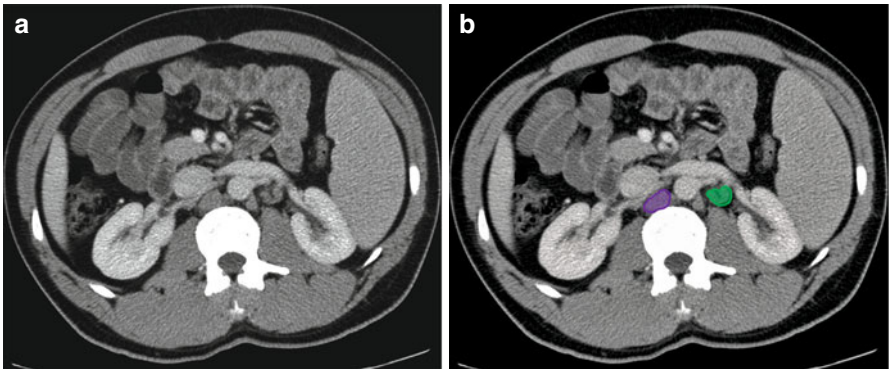

Fig. 3.25 (**a**, **b**) Axial CT image in a patient with rectal cancer (*not shown*) shows metastatic retrocaval (*purple*) and left periaortic lymph node (*green*)

Fig. 3.26 Coronal reformatted CT image in a patient with primary colonic mucinous adenocarcinoma shows calcified metastatic left periaortic lymph nodes (*arrows*)

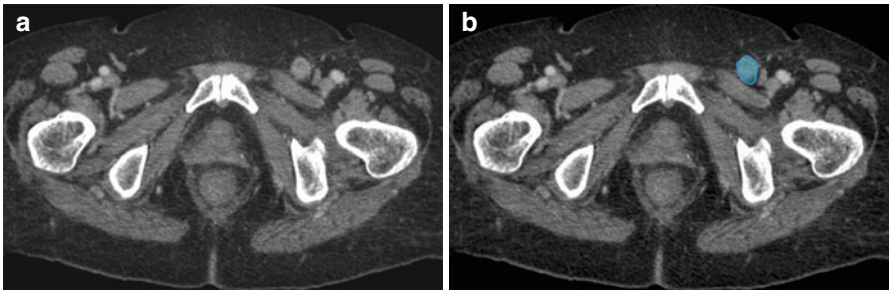

Fig. 3.27 (**a**, **b**) Axial CT image in a patient with anal cancer shows metastatic left inguinal lymph node (*blue*)

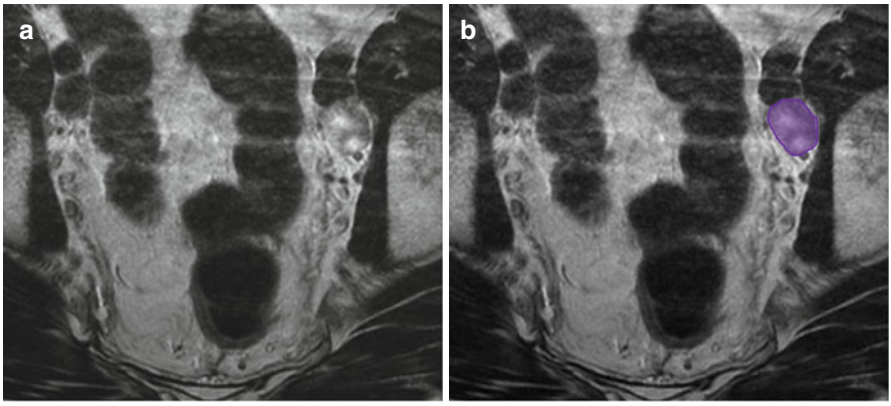

Fig. 3.28 (**a**, **b**) Axial T2-weighted image in a patient with anal cancer shows metastatic left external iliac lymph node (*purple*)

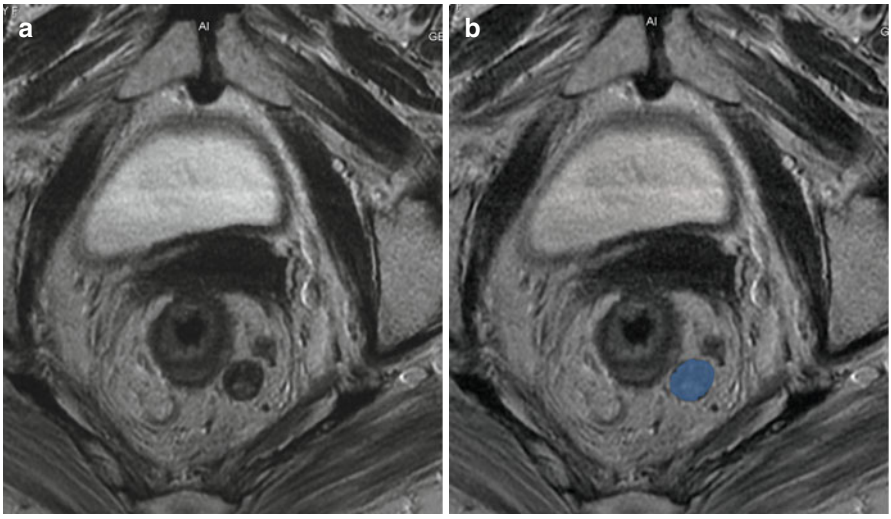

Fig. 3.29 (**a**, **b**) Axial T2-weighted image in a patient with rectal cancer shows heterogenous metastatic perirectal lymph node (*blue*)

to the paraaortic nodes, which then drain into the cisterna chyli and predominantly the left supraclavicular nodes via the thoracic duct. The lymphatic drainage for the proximal ureters is to the paraaortic nodes in the region of the renal vessels and gonadal artery. The middle ureteral lymphatics drain to the common iliac nodes and the lower ureteral lymphatics to the external and internal iliac nodes. All the iliac nodes drain to the paraaortic nodes, cisterna chyli, and predominantly the left supraclavicular nodes via the thoracic duct. The adrenal lymphatics drain to the paraaortic nodes [1].

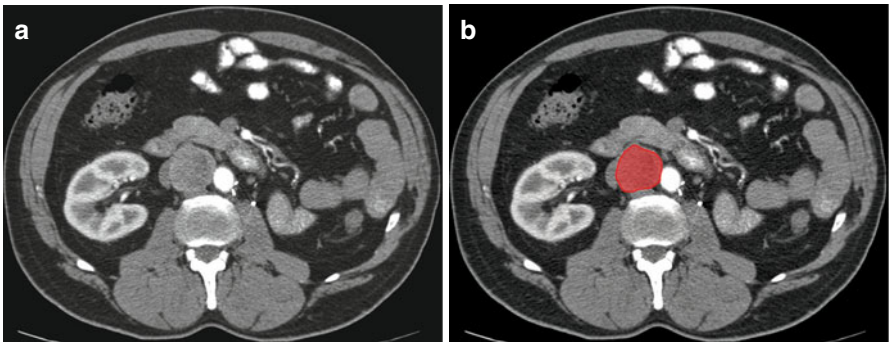

Fig. 3.30 (**a**, **b**) Axial CT image in a patient with left nephrectomy for renal cell cancer shows enlarged aortocaval (*red*) lymph node with biopsy-proven recurrent RCC

Table 3.9 N-stage classification for renal cancer

Stage	Findings
NX	Regional nodes cannot be assessed
N0	No regional nodal metastases
N1	Metastases in a single regional lymph node
N2	Metastasis in more than one regional lymph node

Lymphatic Spread of Malignancies

Renal Tumor

Renal tumors account for 3 % of all cancer cases and deaths [25]; the majority of these are renal cell carcinomas. Lymph node status is a strong prognostic indicator in patients with kidney cancer [26, 27] with 5-year disease-specific survival for patients with node-positive disease reported between 21 % and 38 % [28, 29].

Lymphatic spread of renal cell carcinomas (RCC) is initially to regional lymph nodes. These include nodes along the renal arteries from the renal hilum to the paraaortic nodes at this level (*see* Fig. 3.30). Ten to fifteen percent of patients have regional nodal involvement without distant spread. Lymphatic spread may continue above or below the level of the renal hilum, with subsequent spread to the cisterna chyli and to the left supraclavicular nodes via the thoracic duct. Occasionally, there is spread from these nodes to the mediastinum and pulmonary hilar nodes [1].

Table 3.9 lists the N-Stage classification for kidney cancer. Diagnosis of pathologic lymph nodes is problematic, as approximately 50 % of enlarged regional nodes are hyperplastic [30]. Criteria currently used for suspect nodes are those 1 cm or

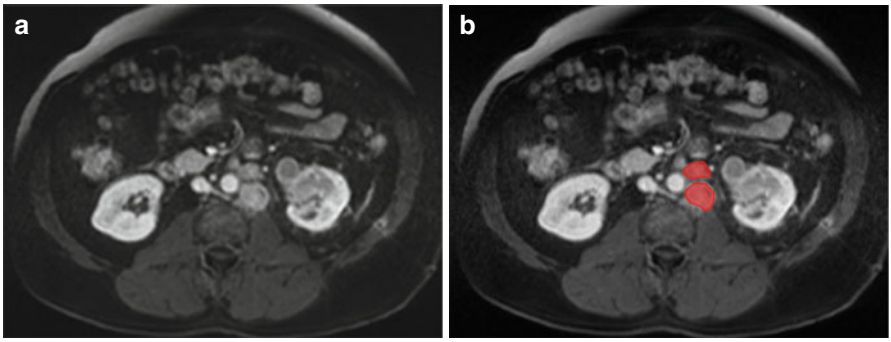

Fig. 3.31 (**a**, **b**) Axial post gadolinium-enhanced T1-weighted image shows metastatic left periaortic lymph nodes (*red*) in a patient with left transitional cell carcinoma

more in short axis and loss of oval shape and fatty hilus. Clustering of three or more nodes in the regional area is also suggestive of metastatic spread.

Urothelial Tumors

Periureteral extension from ureteral transitional cell carcinoma (TCC) is secondary to growth through the ureteral wall and involvement of the extensive lymphatic drainage. The sites of regional lymphatic spread are dependent on the location of the tumor. The paraaortic nodes are involved initially in the renal pelvic and upper ureteral tumors (*see* Fig. 3.31). If the origin is from the middle ureter, metastases are to the common iliac nodes, whereas lower ureteral tumors involve the internal and external nodes initially. The iliac nodes drain into the para-aortic nodes. Lymphatics within the wall of the ureter allow for direct extension within the wall [1].

Adrenal Tumors

Primary malignant tumors of the adrenal gland arise from the cortex as adrenocortical carcinomas or from the medulla as pheochromocytomas or in the spectrum of the neuroblastoma ganglioneuroma complex. Most of these tumors spread by lymphatic spread to the para-aortic lymph nodes [1].

Pancreatic Cancer

Pancreatic cancer is the second most common gastrointestinal malignancy and is the fifth leading cause of cancer-related death. The majority of cases are ductal adenocarcinomas (exocrine ductal epithelium, 95 % of cases). Up to two thirds may be located in the head of the pancreas. Lymph node metastases are common in pancreatic and duodenal cancer and they carry a poor prognosis [31, 32].

Lymphatic Spread and Nodal Metastasis

Lymphatic drainage of the head of the pancreas is different from that of the body and tail (Table 3.10; *see* Fig. 3.32).

The head of the pancreas and the duodenum share similar drainage pathways by following arteries around the head of the pancreas [32, 33]. They can be divided into three major routes: the gastroduodenal, the inferior pancreaticoduodenal, and the dorsal pancreatic:

1. Around the head of the pancreas, multiple lymph nodes can be found between the pancreas and duodenum above and below the root of the transverse mesocolon and anterior and posterior to the head of the pancreas. Although many names are used for these nodes such as the inferior and superior pancreaticoduodenal nodes (*see* Fig. 3.33), they can be designated peripancreatic nodes (*see* Fig. 3.34). The gastroduodenal route collects lymphatics from the anterior pancreaticoduodenal nodes (*see* Figs. 3.35, 3.36, and 3.37), which drain lymphatics along the anterior surface of the pancreas, and the posterior pancreaticoduodenal nodes, which follow the bile duct along the posterior pancreaticoduodenal vein to the posterior periportal node.
2. The inferior pancreaticoduodenal route also receives lymphatic drainage from the anterior and posterior pancreaticoduodenal nodes by following the inferior pancreaticoduodenal artery to the superior mesenteric artery node. Occasionally, they may also drain into the node at the proximal jejunal mesentery.

Table 3.10 Lymph node groups in tumors of the pancreatic head, body, and tail

Lymph node station group	Tumor of head	Tumor of body/tail
1	13a, 13b, 17a, 17b	8a, 8p, 10, 11p, 11d, 18
2	6, 8a, 8p, 12a, 12b, 12p, 14p, 14d	7, 9, 14p, 14d, 15
3	1, 2, 3, 4, 5, 7, 9, 10, 11p, 11d, 15, 16a2, 16bl, 18	5, 6, 12a, 12b, 12p, 13a, 13b, 17a, 17b, 16a2, 16b1

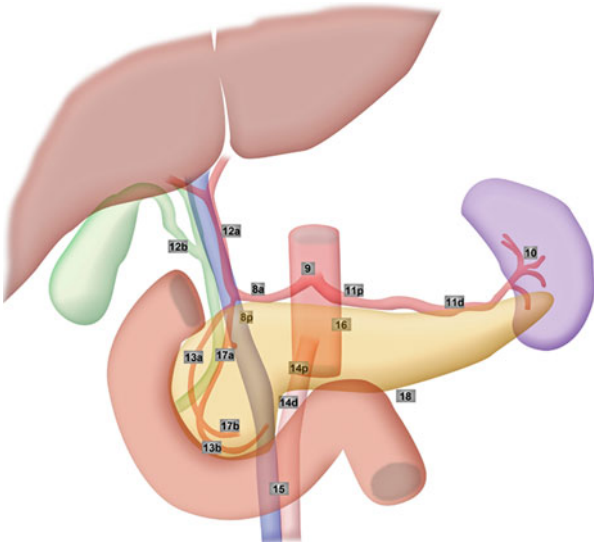

Fig. 3.32 Lymph node stations according to the classification of pancreatic carcinoma proposed by the Japan Pancreas Society (*see* Table 3.11)

Table 3.11 Lymph node stations in pancreatic carcinoma as proposed by the Japan Pancreas Society

Station	Name
1	Right cardial lymph nodes
2	Left cardial lymph nodes
3	Lymph nodes along the lesser curvature of the stomach
4	Lymph nodes along the greater curvature of the stomach
5	Suprapyloric lymph nodes
6	Infrapyloric lymph nodes
7	Lymph nodes along the left gastric artery
8a	Lymph nodes in the anterosuperior group along the common hepatic artery
8p	Lymph nodes in the posterior group along the common hepatic artery
9	Lymph nodes around the celiac artery
10	Lymph nodes at the splenic hilum
11p	Lymph nodes along the proximal splenic artery
11d	Lymph nodes along the distal splenic artery
12a	Lymph nodes along the hepatic artery
12p	Lymph nodes along the portal vein
12b	Lymph nodes along the bile duct
13a	Lymph nodes on the posterior aspect of the superior portion of the head of the pancreas
13b	Lymph nodes on the posterior aspect of the inferior portion of the head of the pancreas
14p	Lymph nodes on the proximal superior mesenteric artery
14d	Lymph nodes along the distal superior mesenteric artery
15	Lymph nodes along the middle colic artery
16	Lymph nodes around the abdominal aorta
16a1	Lymph nodes around the aortic hiatus of the diaphragm
16b1	Lymph nodes around the abdominal aorta (from the superior margin of the celiac trunk to the inferior margin of the inferior mesenteric artery)
16b2	Lymph nodes around the abdominal aorta (from the superior margin of the inferior mesenteric artery to the aortic bifurcation)
17a	Lymph nodes on the anterior surface of the superior portion of the head of the pancreas
17b	Lymph nodes on the anterior surface of the inferior portion of the head of the pancreas
18	Lymph nodes along the inferior margin of the pancreas

3. The dorsal pancreatic route is uncommon. It collects lymphatics along the medial border of the head of the pancreas and follows the branch of the dorsal pancreatic artery to the superior mesenteric artery or celiac node. The lymphatic drainage of the body and tail of the pancreas follows the dorsal pancreatic artery, the splenic artery, and vein to the celiac lymph node.

The lymphatic drainage of the body and tail of the pancreas follows the dorsal pancreatic artery, the splenic artery, and vein to the celiac lymph node. The nodal staging for pancreatic cancer based on American Joint Committee on Cancer (AJCC) criteria is listed in Table 3.12. Table 3.13 lists the regional lymph nodes for pancreatic cancer.

Table 3.12 N-stage classification for pancreatic cancer

Stage	Findings
NX	Regional nodes cannot be assessed
N0	No regional nodal metastases
N1	Regional lymph node metastasis

Table 3.13 The regional lymph nodes for pancreatic cancer

Pancreatic cancer
Peripancreatic
Hepatic artery
Celiac axis
Pyloric
Splenic region

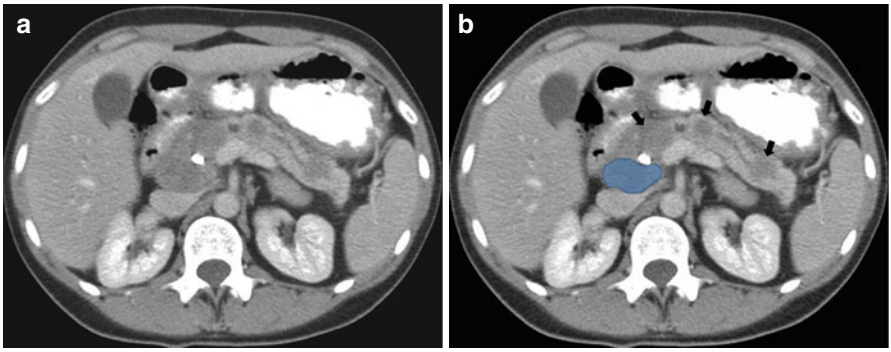

Fig. 3.33 (**a**, **b**) Axial CT image in a patient with metastatic sarcoma with multiple metastases to the pancreas (*arrows*) and to the superior pancreaticoduodenal lymph node (*blue*)

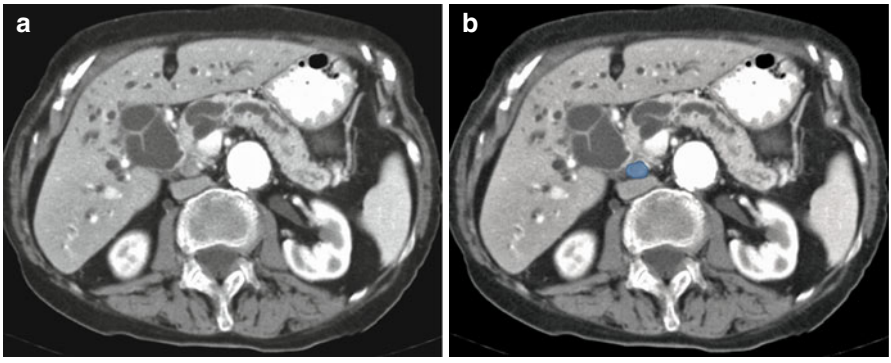

Fig. 3.34 (**a**, **b**) Axial CT image in a patient with primary pancreatic adenocarcinoma shows metastatic retropancreatic lymph node (*blue*)

Fig. 3.35 Axial CT image in a patient with healed tuberculosis shows a calcified lymph node in superior pancreaticoduodenal location

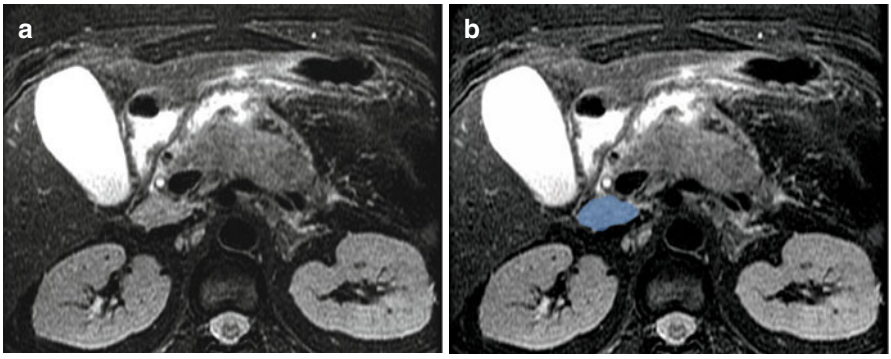

Fig. 3.36 (**a, b**) Axial T2-weighted image in a patient with pancreatitis shows an enlarged superior pancreaticoduodenal lymph node (*blue*)

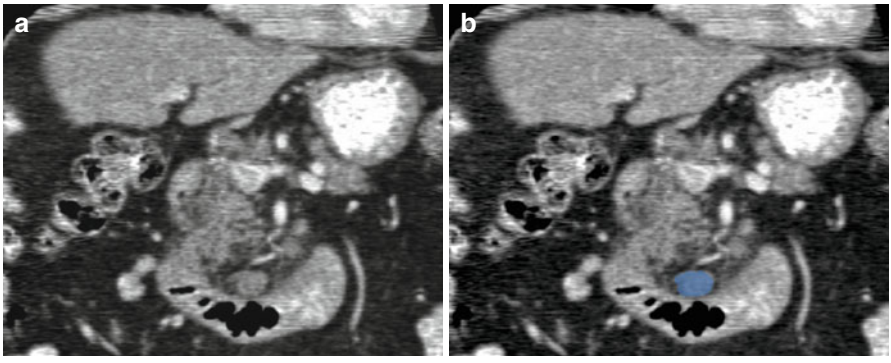

Fig. 3.37 (**a**, **b**)Coronal reformatted image in a patient with primary pancreatic adenocarcinoma (*not shown*) shows a prominent inferior pancreaticoduodenal lymph node (*blue*)

Preoperative imaging studies, using the size of the nodes as diagnostic criteria, are not accurate for the diagnosis of nodal metastasis. Because of the lack of accuracy, peripancreatic lymph nodes and the nodes along the gastroduodenal artery and inferior pancreaticoduodenal artery are included in radiation field, and they are routinely resected at the time of pancreaticoduodenectomy. However, it is important to note when an abnormal node, such as one with low density and/or irregular border, is detected beyond the usual drainage basin and outside the routine surgical or radiation field, such as in the proximal jejunal mesentery or at the base of the transverse mesocolon, as these can be the site of recurrent disease [1].

References

1. Meyers MA, Charnsangavej C, Oliphant M. Meyers' dynamic radiology of the abdomen: normal and pathologic anatomy. New York: Springer; 2010.
2. McDaniel KP, Charnsangavej C, DuBrow RA, et al. Pathways of nodal metastasis in carcinomas of the cecum, ascending colon, and transverse colon: CT demonstration. AJR Am J Roentgenol. 1993;161:61–4.
3. Granfield CA, Charnsangavej C, Dubrow RA, Varma DG, et al. Regional lymph node metastases in carcinoma of the left side of the colon and rectum: CT demonstration. AJR Am J Roentgenol. 1992;159:757–61.
4. Gest TPP. Anatomy: Medcharts. New York: Iloc; 1994.
5. Dorfman RE, Alpern MB, Gross BH, Sandler MA. Upper abdominal lymph nodes: criteria for normal size determined with CT. Radiology. 1991;180:319–22.
6. Dodd 3rd GD, Baron RL, Oliver 3rd JH, et al. Enlarged abdominal lymph nodes in end-stage cirrhosis: CT-histopathologic correlation in 507 patients. Radiology. 1997;203:127–30.
7. Morón FE, Szklaruk J. Learning the nodal stations in the abdomen. Br J Radiol. 2007;80: 841–8.
8. Harisinghani MG, Barentsz J, Hahn PF, et al. Noninvasive detection of clinically occult lymph-node metastases in prostate cancer. N Engl J Med. 2003;348:2491–9.
9. Torabi M, Aquino SL, Harisinghani MG. Current concepts in lymph node imaging. J Nucl Med. 2004;45:1509–18.
10. Frija J, Bourrier P, Zagdanski AM, De Kerviler E. Diagnosis of a malignant lymph node. J Radiol. 2005;86:113–25.
11. Harisinghani MG, Saksena MA, Hahn PF, et al. Ferumoxtran-10-enhanced MR lymphangiography: does contrast-enhanced imaging alone suffice for accurate lymph node characterization? AJR Am J Roentgenol. 2006;186:144–8.
12. Egner JR. AJCC cancer staging manual. JAMA. 2010;304:1726–7.
13. Kobayashi S, Takahashi S, Kato Y, et al. Surgical treatment of lymph node metastases from hepatocellular carcinoma. J Hepatobiliary Pancreat Sci. 2011;18:559–66.
14. Hartgrink HH, van de Velde CJH, Putter H, et al. Extended lymph node dissection for gastric cancer: who may benefit? Final results of the randomized Dutch gastric cancer group trial. J Clin Oncol. 2004;22:2069–77.
15. Coburn NG. Lymph nodes and gastric cancer. J Surg Oncol. 2009;99:199–206.
16. Dicken BJ, Bigam DL, Cass C, et al. Gastric adenocarcinoma. Ann Surg. 2005;241:27–39.
17. Taylor FGM, Swift RI, Blomqvist L, Brown G. A systematic approach to the interpretation of preoperative staging MRI for rectal cancer. AJR Am J Roentgenol. 2008;191:1827–35.
18. Steup WH, Moriya Y, van de Velde CJH. Patterns of lymphatic spread in rectal cancer. A topographical analysis on lymph node metastases. Eur J Cancer. 2002;38:911–8.

19. Granfield CA, Charnsangavej C, Dubrow RA, et al. Regional lymph node metastases in carcinoma of the left side of the colon and rectum: CT demonstration. AJR Am J Roentgenol. 1992;159: 757–61.
20. McDaniel K, Charnsangavej C, DuBrow R, et al. Pathways of nodal metastasis in carcinomas of the cecum, ascending colon, and transverse colon: CT demonstration. Am J Roentgenol. 1993;161:61–4.
21. Granfield C, Charnsangavej C, Dubrow R, et al. Regional lymph node metastases in carcinoma of the left side of the colon and rectum: CT demonstration. Am J Roentgenol. 1992;159:757–61.
22. Rajput A, Romanus D, Weiser MR, et al. Meeting the 12 lymph node (LN) benchmark in colon cancer. J Surg Oncol. 2010;102:3–9.
23. Wolpin BM, Meyerhardt JA, Mamon HJ, Mayer RJ. Adjuvant treatment of colorectal cancer. CA Cancer J Clin. 2007;57:168–85.
24. Iafrate F, Laghi A, Paolantonio P, et al. Preoperative staging of rectal cancer with MR imaging: correlation with surgical and histopathologic findings. Radiographics. 2006;26:701–14.
25. American Cancer Society. Cancer facts and figures. 2011. Accessible at: http://www.cancer.org/Research/CancerFactsFigures/CancerFactsFigures/cancer-facts-figures-2011. Accessed 31 May 2012.
26. Karakiewicz PI, Lewinshtein DJ, Chun FK-H, et al. Tumor size improves the accuracy of TNM predictions in patients with renal cancer. Eur Urol. 2006;50:521–8. discussion 529.
27. Lughezzani G, Capitanio U, Jeldres C, et al. Prognostic significance of lymph node invasion in patients with metastatic renal cell carcinoma: a population-based perspective. Cancer. 2009;115: 5680–7.
28. Capitanio U, Jeldres C, Patard J-J, et al. Stage-specific effect of nodal metastases on survival in patients with non-metastatic renal cell carcinoma. BJU Int. 2009;103:33–7.
29. Pantuck AJ, Zisman A, Dorey F, et al. Renal cell carcinoma with retroperitoneal lymph nodes: role of lymph node dissection. J Urol. 2003;169:2076–83.
30. Israel GM, Bosniak MA. Renal imaging for diagnosis and staging of renal cell carcinoma. Urol Clin North Am. 2003;30:499–514.
31. Takahashi T, Ishikura H, Motohara T, et al. Perineural invasion by ductal adenocarcinoma of the pancreas. J Surg Oncol. 1997;65:164–70.
32. Kayahara M, Nakagawara H, Kitagawa H, Ohta T. The nature of neural invasion by pancreatic cancer. Pancreas. 2007;35:218–23.
33. Pawlik TM, Gleisner AL, Cameron JL, et al. Prognostic relevance of lymph node ratio following pancreaticoduodenectomy for pancreatic cancer. Surgery. 2007;141:610–8.

Pelvic Lymph Nodes

4

A good basic understanding of the anatomy and nomenclature of the inguino-pelvic nodal groups is essential for accurate staging of male and female urogenital pelvic neoplasms. Lymph nodes are not only crucial for staging and management but are also important factors in prognosticating the disease.

Classification and Anatomical Location of Pelvic Lymph Nodes

Common Iliac Nodal Group

The common iliac nodal group consists of three subgroups: lateral, middle, and medial (*see* Fig. 4.1). The lateral subgroup is an extension of the lateral chain of external iliac nodes located lateral to the common iliac artery (*see* Figs. 4.2 and 4.3). The medial subgroup occupies the triangular area bordered by both common iliac arteries from the aortic bifurcation to the bifurcation of common iliac artery into external and internal iliac arteries. Nodes at the sacral promontory are included in this chain (*see* Fig. 4.4). The middle subgroup is located in the lumbosacral fossa (the area bordered posteromedially by the lower lumbar or upper sacral vertebral bodies, anterolaterally by the psoas muscle, and anteromedially by the common iliac vessels) and between the common iliac artery and common iliac vein [1].

M.G. Harisinghani, (ed.), *Atlas of Lymph Node Anatomy*,
DOI 10.1007/978-1-4419-9767-8_4, © Springer Science+Business Media New York 2013

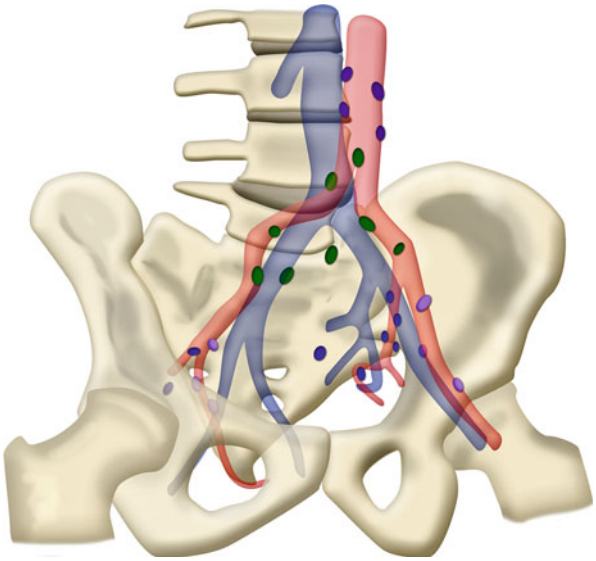

Fig. 4.1 The paraaortic nodes are outlined in *deep purple*, *green* nodes are common iliac, external iliac nodes are *light purple* and internal iliac nodes are *blue*. Schematic shows the common iliac nodal group, which consists of three chains: (1) the lateral chain, which is located lateral to the common iliac artery and forms an extension from the lateral external iliac nodal chain; (2) the medial chain, which occupies the triangular area bordered by both common iliac arteries and includes nodes at the sacral promontory; and (3) the middle chain, which consists of nodes within the lumbosacral fossa. The relation of these nodes to the common iliac vein is also shown

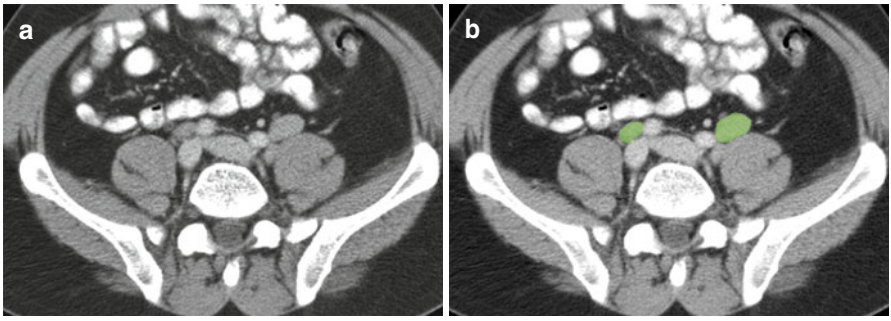

Fig. 4.2 (**a**, **b**) Axial CT image shows bilateral common iliac lymph nodes (*green*)

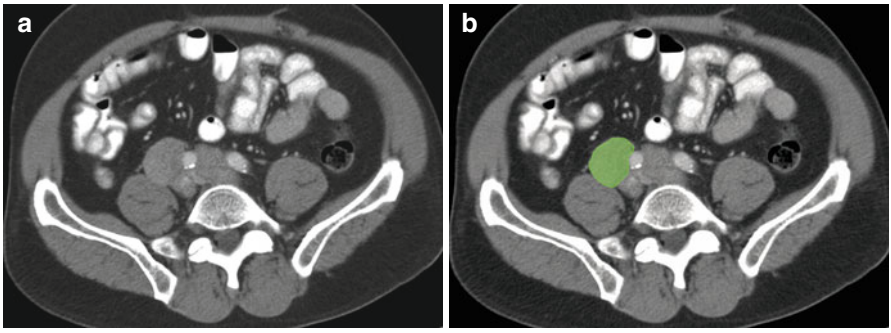

Fig. 4.3 (**a**, **b**) Axial CT image shows enlarge common iliac lymph nodes (*green*)

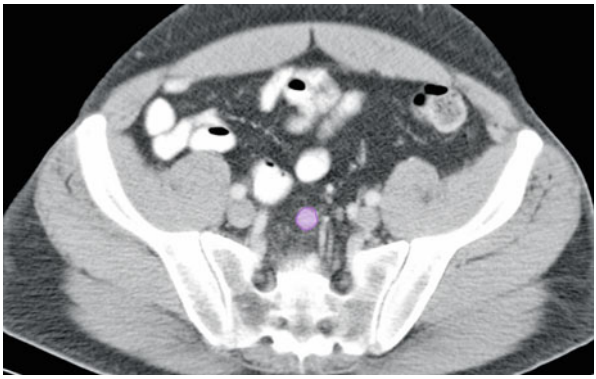

Fig. 4.4 Axial CT image shows the node at the sacral promontory (*purple*), which are included in medial subgroup of the common iliac group

External Iliac Nodal Group

The external iliac nodal group consists of three subgroups: lateral, middle, and medial (*see* Figs. 4.5 and 4.6). The lateral subgroup includes nodes that are located along the lateral aspect of the external iliac artery (*see* Fig. 4.7). The middle subgroup comprises nodes located between the external iliac artery and the external iliac vein (*see* Fig. 4.8). The medial subgroup contains nodes located medial and posterior to the external iliac vein. The medial subgroups are also known as the obturator nodes (*see* Figs. 4.9 and 4.10) [2].

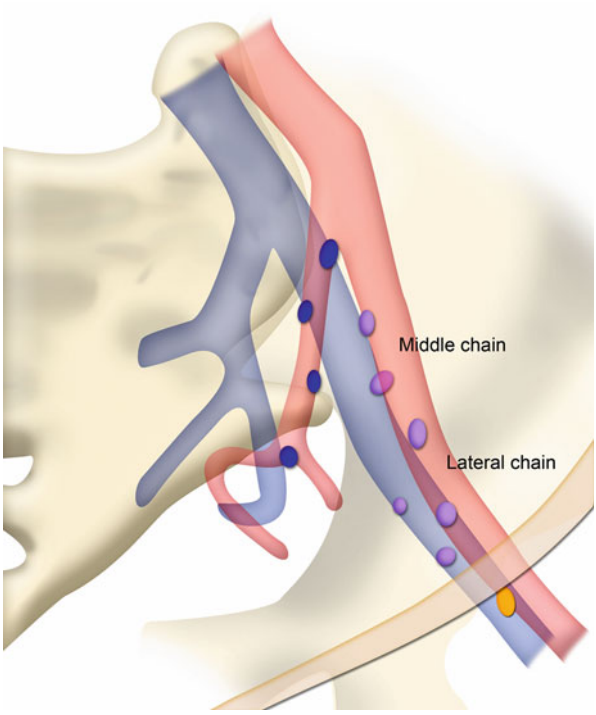

Fig. 4.5 External iliac lymph nodes (*purple*). Schematic shows the external iliac nodal group comprising the lateral chain, positioned laterally along the external iliac artery; the middle chain, situated between the external iliac artery and external iliac vein; and the medial chain (also known as obturator nodes), positioned medial and posterior to the external iliac vein

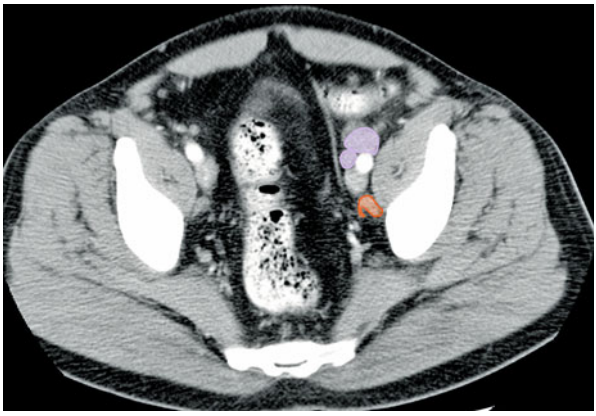

Fig. 4.6 Axial contrast-enhanced CT image shows the three chains of the external iliac nodal group. These are, as depicted, the lateral (*big purple*) chain, the middle (*small purple*) chain, and the medial (*orange*) chain

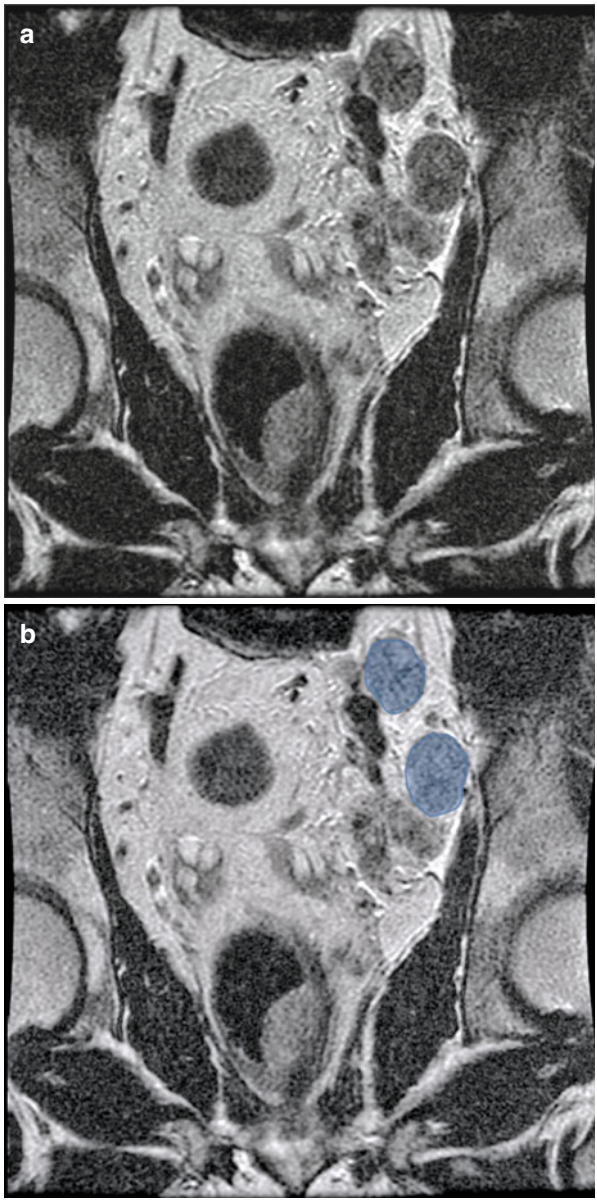

Fig. 4.7 (**a**, **b**) Coronal T2-weighted image in a patient with rectal cancer showing enlarged left external iliac lymph nodes (*blue*)

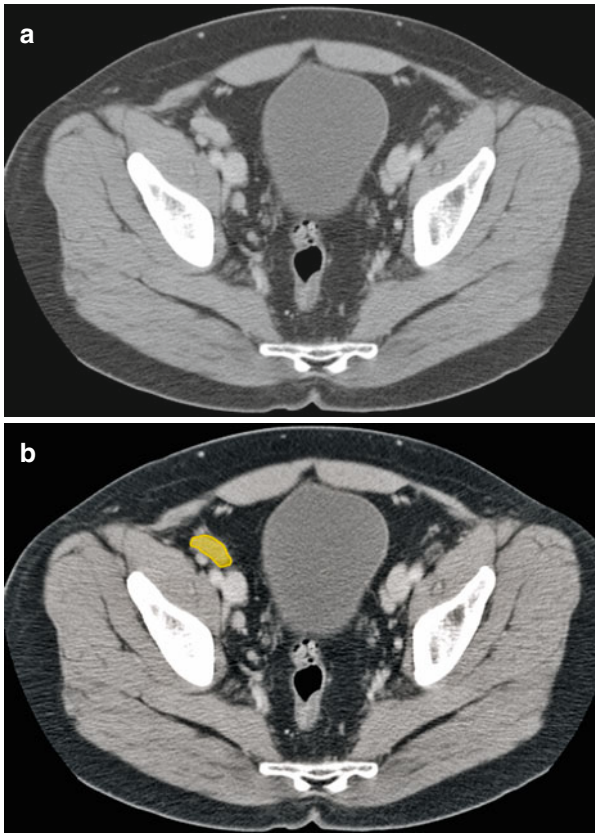

Fig. 4.8 (**a**, **b**) Axial CT image shows right external iliac lymph node (*orange*)

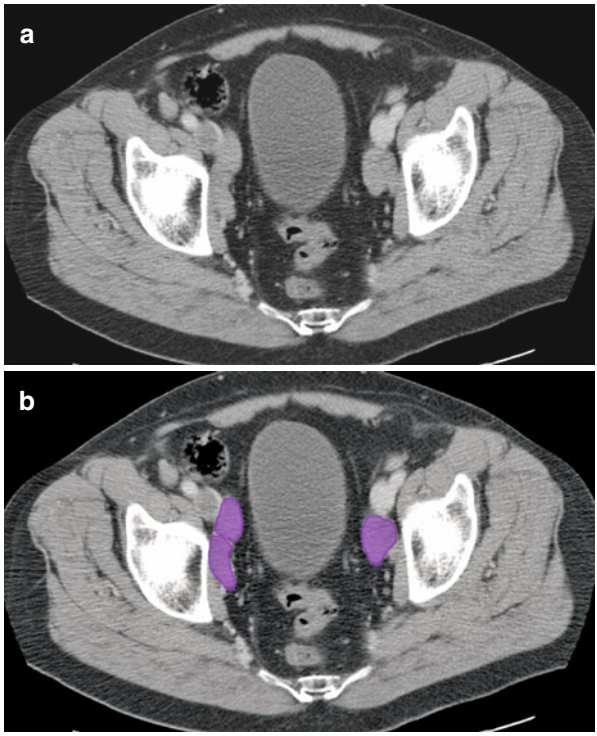

Fig. 4.9 (**a**, **b**) Axial CT image shows enlarged bilateral obturator lymph nodes (*purple*)

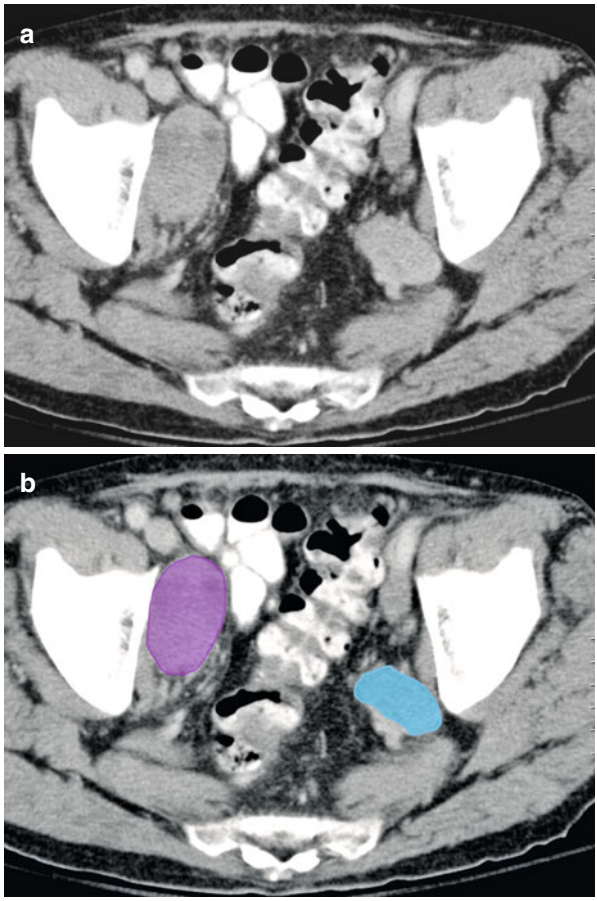

Fig. 4.10 (**a**–**d**) Axial and coronal reformatted CT images shows enlarged right obturator (*purple*) and left internal iliac (*blue*) lymph nodes

Fig. 4.10 (continued)

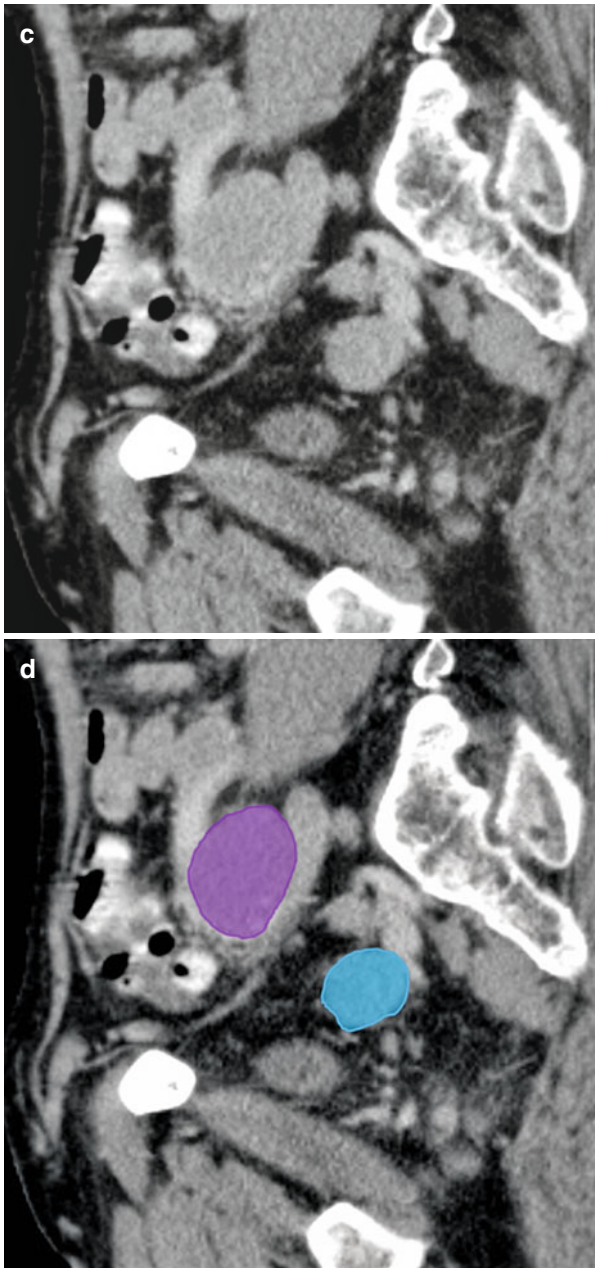

Internal Iliac (Hypogastric) Nodal Group

The internal iliac nodal group, also known as the hypogastric nodal group, consists of several nodal chains accompanying each of the visceral branches of the internal iliac artery (*see* Figs. 4.11 and 4.12). Among the nodes of this group, the junctional nodes are located at the junction between the internal and external iliac nodal groups [2].

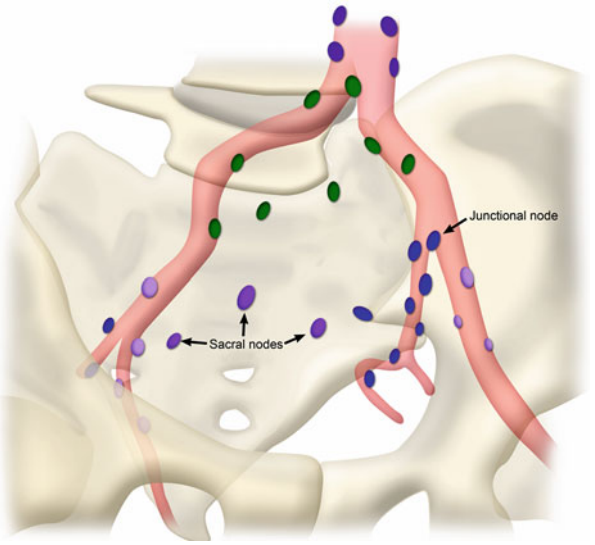

Fig. 4.11 The *light purple* nodes are external iliac, *blue* are internal iliac, *green* are common iliac and deep *purple* are paraaortic nodes. Schematic shows the chains of internal iliac lymph nodes that accompany the visceral branches of the internal iliac vessels. The central location of the sacral nodes within the pelvis and the position of the junctional nodes between the internal and external iliac arteries are clearly visible

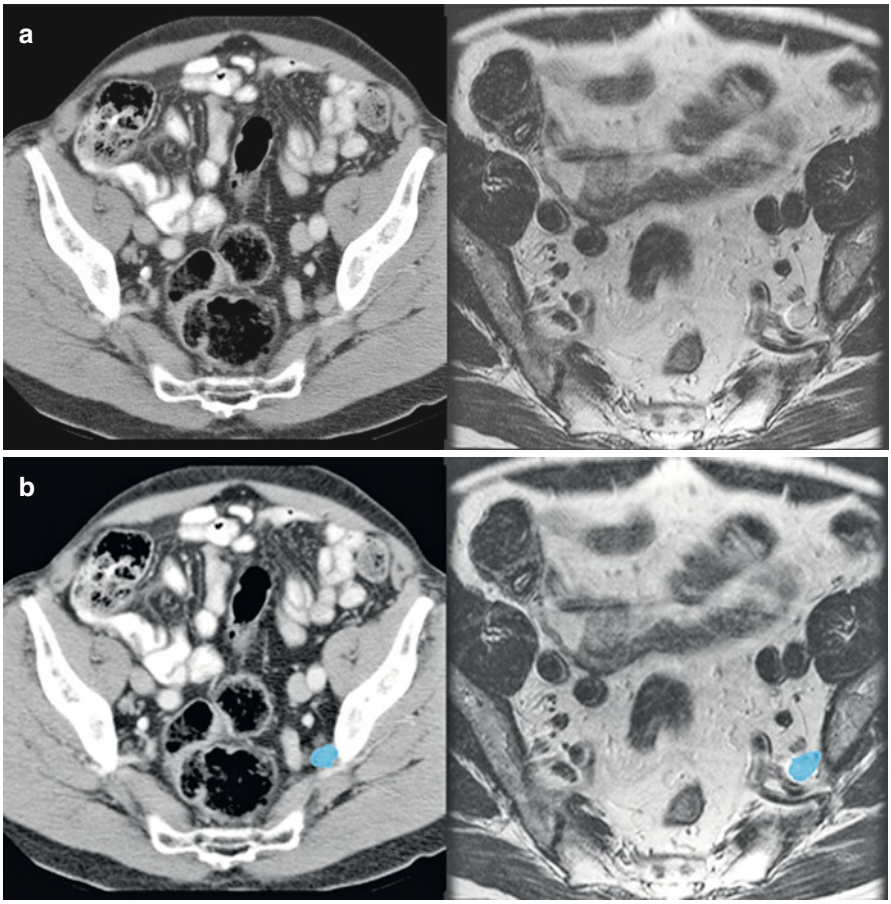

Fig. 4.12 (**a**, **b**) Axial CT (*right*) and axial T2-weighted MR images (*left*) shows a prominent left internal iliac lymph node (*blue*) nestled anterior to the internal iliac vessels

Inguinal Nodes

This group consists of superficial inguinal and deep inguinal nodes (*see* Fig. 4.13). The superficial inguinal nodes, which are located in the subcutaneous tissue anterior to the inguinal ligament, accompany the superficial femoral vein and the saphenous vein (*see* Figs. 4.14, 4.15 and 4.16). The sentinel nodes for the superficial subgroup are those situated at the saphenofemoral junction, where the great saphenous vein drains into the common femoral vein.

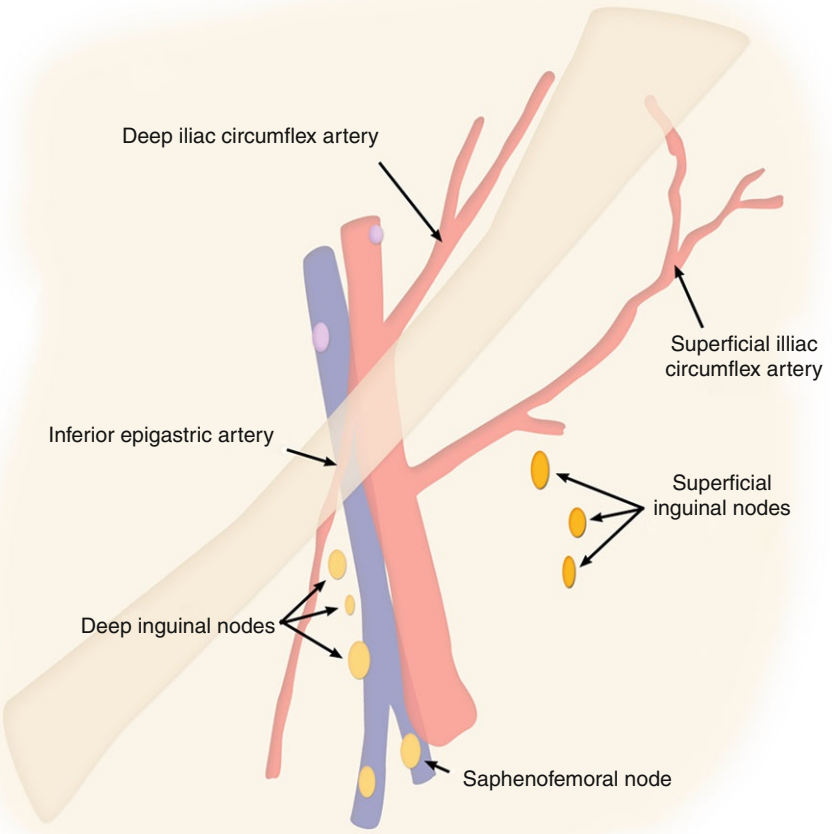

Fig. 4.13 Inguinal lymph nodes. Schematic show the locations of the superficial and deep inguinal nodes in relation to the common femoral artery, common femoral vein, and saphenous vein. The sentinel nodes in the superficial inguinal group are those located at the saphenofemoral junction

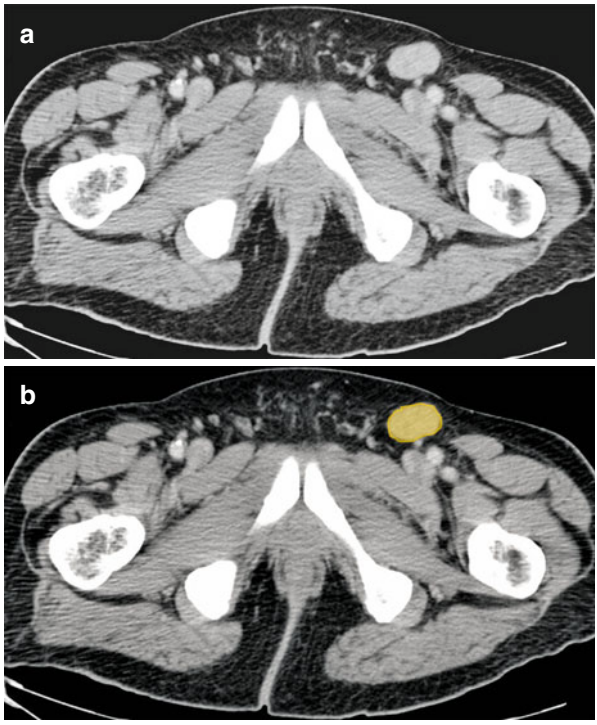

Fig. 4.14 (**a**, **b**) Axial CT image shows an enlarged left inguinal lymph node (*orange*)

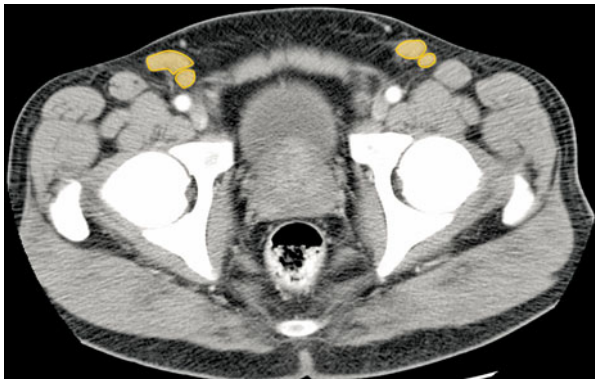

Fig. 4.15 Axial CT image shows the locations of the superficial inguinal nodes (*orange*)

The deep inguinal nodes are those located along the common femoral vessels (*see* Fig. 4.17). The anatomical landmarks that mark the boundary between the deep inguinal nodes and the medial chain of the external iliac nodes are the inguinal ligament and the origins of the inferior epigastric and circumflex iliac vessels [2].

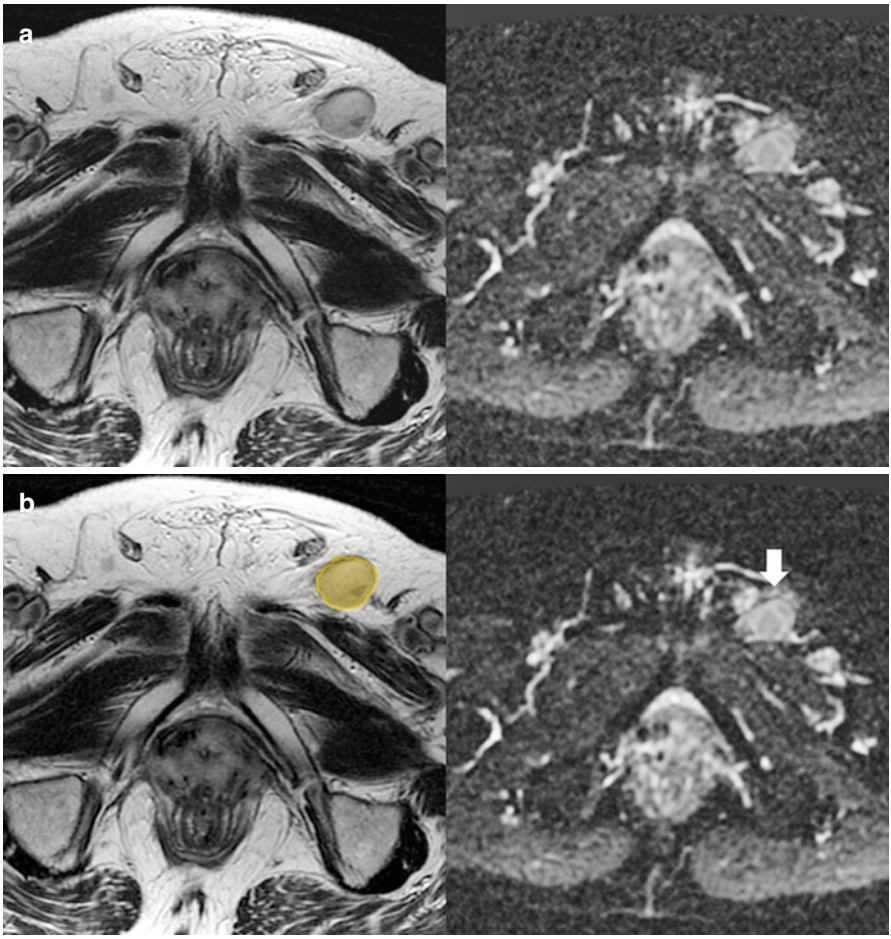

Fig. 4.16 (**a**, **b**) Axial T2-weighted MR image (*left image*) and Apparent Diffusion Coefficient (ADC) map (*right image*) shows presence of an enlarged left inguinal node (*orange*) showing restricted diffusion and dark on ADC map (*arrow*)

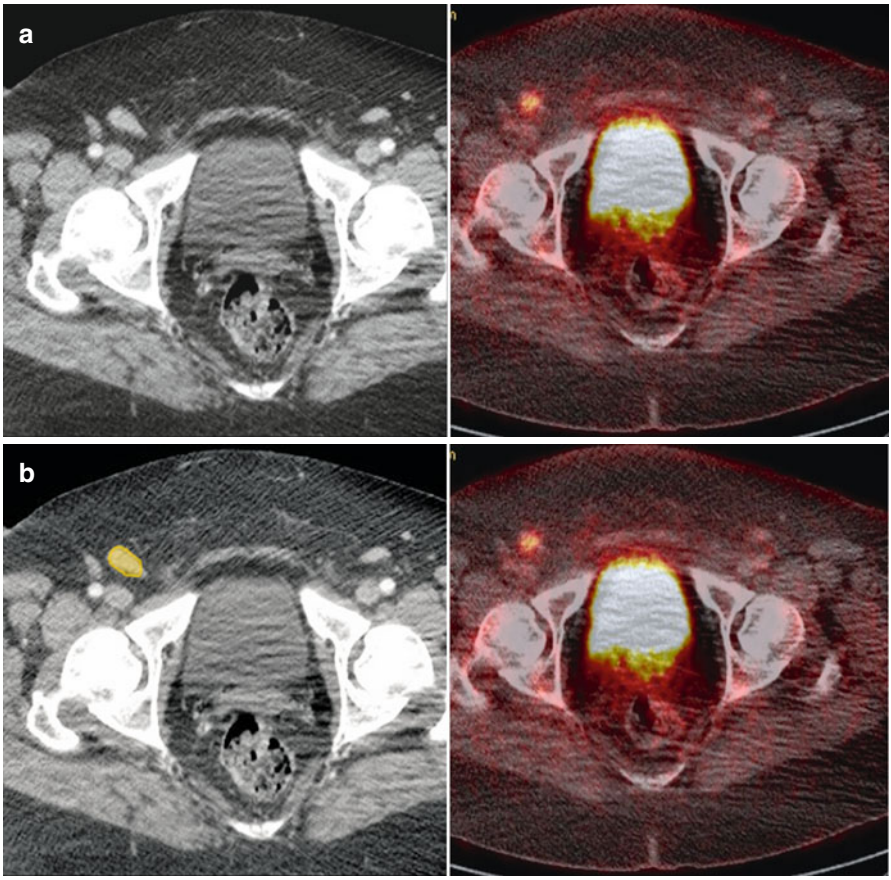

Fig. 4.17 (**a**, **b**) Axial CT and PET-CT–fused images show FDG avid right inguinal lymph node (*orange*) in a patient with vulvar cancer

Perivisceral Nodes

These nodes are seen adjacent to the pelvic organs and are regional nodes for the respective organ adjacent to which they lie:

- Perirectal, within the mesorectal fat (*see* Fig. 4.18), drain along the superior hemorrhoidal vessels into the inferior mesenteric vessel nodal group
- Perivesical, around the urinary bladder
- Periprostatic, adjacent to the prostate gland

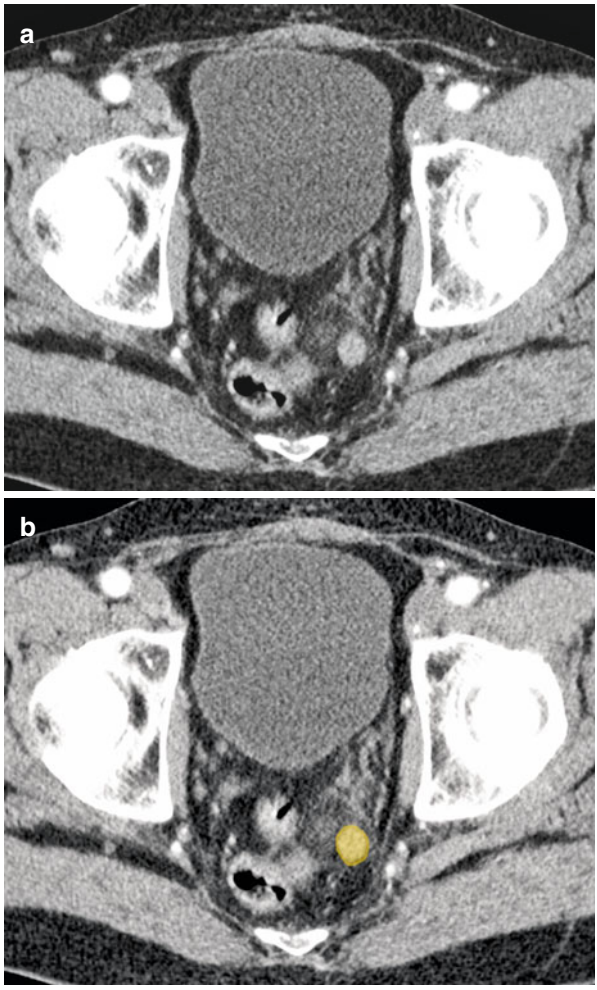

Fig. 4.18 (**a**, **b**) Axial CT image in a patient with prostate cancer shows metastatic perirectal lymph node (*orange*)

Criteria for Diagnosing Abnormal Lymph Nodes

Size

Multiple studies have been performed to decide the cut-off size for distinguishing normal from abnormal nodes. Due to varied results, there is lack of consensus for the size criteria. In addition, the size criteria vary for different tumors. Generally, nodes larger than 10 mm in short-axis diameter are considered enlarged for the iliac nodes and 15 mm for inguinal nodes.

Shape and Margin

Ovoid lymph nodes with a fatty central hilum favor a benign etiology. Nodes with a higher short-axis to long-axis ratio (*i.e.*, rounded nodes) are more likely to be malignant [3]. It has also been shown that nodes with an irregular margin are more likely to be metastatic [4].

Internal Architecture

Heterogeneous signal intensity of the node on T2-weighted magnetic resonance (MR) images has been shown to indicate malignant infiltration. Similarly, the presence of central low density on computed tomography (CT), suggestive of necrosis is also seen in metastases. Mucinous primary tumors can be associated with subtle calcification within metastatic lymph nodes.

Nodal Staging

It is important to note whether the nodes involved are regional or nonregional for the particular organ as lymphatic pathways and N staging varies for different tumor origins. A positive nonregional node upstages the disease to M-metastatic node, stage IV, and changes the management completely. Table 4.1 illustrates the regional and nonregional lymph nodes for common pelvic malignances.

Gynecologic Malignancies

Lymph nodes, either locoregional or distant, are common sites of metastatic disease in gynecologic tumor and the nodal status is the single most important prognostic factor in most gynecologic malignancies.

Table 4.1 The regional and nonregional lymph nodes for common pelvic malignances

Nodes	Anus	Bladder	Cervix	Endometrium	Ovary	Penis	Prostate	Rectum	Testis	Vagina	Vulva
Pervisceral	Regional	Regional	Regional	Regional	Regional	Regional	Regional	Regional	Regional	Regional	Regional
Inguinal	Regional	Non	Non	Non	Non	Regional	Non	Non	Regional*	Regional	Regional
Internal Iliac	Regional	Regional	Regional	Regional	Regional	Regional	Regional	Regional	Non	Regional	Non
External Iliac	Non	Regional	Regional	Regional	Regional	Regional	Regional	Non	Regional*	Regional	Non
Common Iliac	Non	Non	Regional	Regional	Regional	Non	Non	Non	Non	Non	Non
Para-aortic	Non	Non	Non	Regional	Regional	Non	Non	Non	Regional	Non	Non

Asterisk indicates regional only in the setting of previous inguinal/scrotal surgery. *Non* nonregional

Pattern of Lymphatic Drainage of the Female Pelvis

Superficial and deep inguinal nodes receive drainage from the vulva and lower vagina. The upper vagina, cervix, and lower uterine body drain laterally to the broad ligament, obturator, internal and external iliac nodes, and posteriorly to the sacral nodes. The upper uterine body primary drains to the iliac nodes. The ovaries and fallopian tubes drain along the ovarian artery to the para-aortic nodes, with the lower uterine drainage, or along the round ligament. Less frequently drainage from the upper uterine body is to the iliac nodes and inguinal nodes (Table 4.2).

Cephalic to the pelvis, the nodal drainage is to the bilateral para-aortic nodes to the cisterna chyli at the L2 level to the right of the abdominal aorta (*see* Fig. 4.19). Lymphatic drainage proceeds through the aortic hiatus within the thoracic duct, with the next nodal station in the supraclavicular region [1].

Table 4.2 Pelvic lymphatic drainage of genital structures

Nodes	Pelvic structures drained
Inguinal	Vulva, lower vagina (ovary, fallopian tube, uterus rare)
Sacral	Upper vagina, cervix
Internal iliac	Upper vagina, cervix, lower uterine body (vulva rare)
External iliac	Upper vagina, cervix, upper uterine body, inguinal nodes
Common iliac	Internal iliac nodes, external iliac nodes
Para-aortic	Ovary, fallopian tube, uterus, common iliac nodes

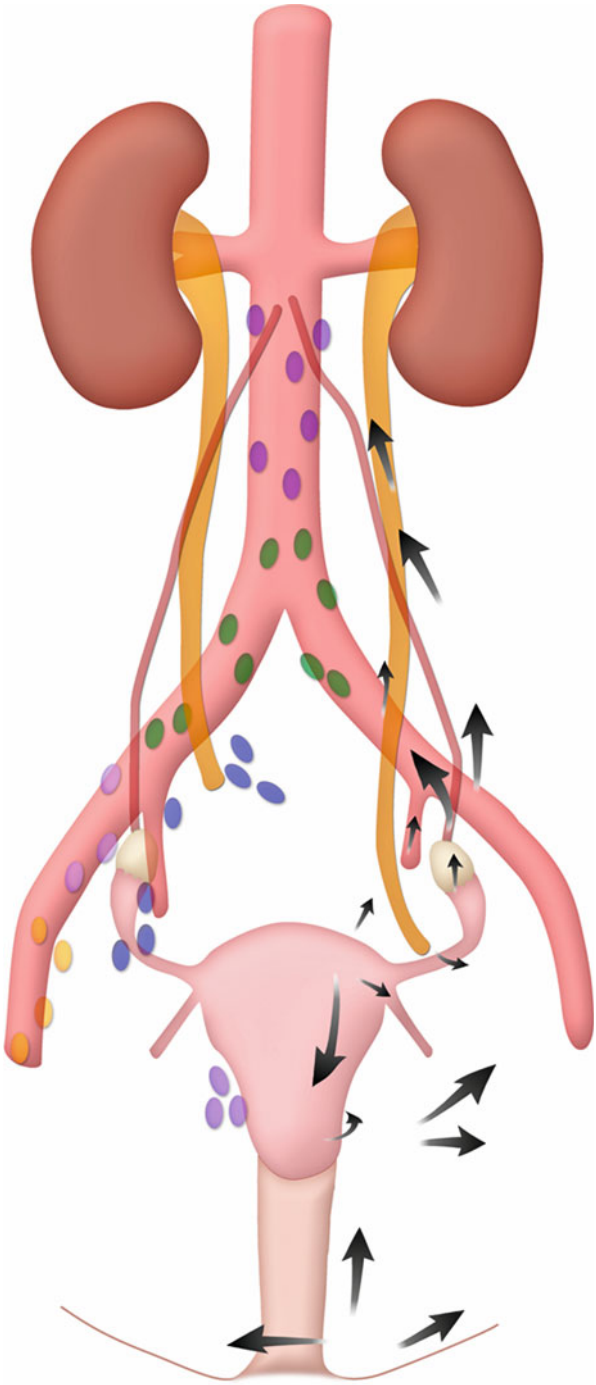

Fig. 4.19 Patterns of lymphatic drainage of the female pelvis. *Arrows* from vulva and vaginal region show lateral spread to superficial and deep inguinal nodes on either side and sometimes directly to iliac nodes. *Arrows* from cervix and upper vagina show pathway of spread to parametrial, obturator and external iliac nodes and along the uterosacral ligament to sacral nodes. *Arrows* from ovary and fallopian tubes drain show their pathway of spread to paraaortic nodes

Lymphatic Spread of Malignancies

Vulva

Although an uncommon gynecologic malignancy, 10–25 % of patients in early-stage disease have node involvement [5]. In vulvar cancer, the 5-year survival rate of a node-negative patient is approximately 90 %, whereas patients with nodal disease have a 5-year survival rate of 50 % [6].

Superficial inguinal nodes are the most common site of spread (*see* Fig. 4.20). Lateral vulvar tumors metastasize to the ipsilateral nodes (*see* Fig. 4.21); it is rare for contralateral node involvement in early tumors. Also in the absence of ipsilateral groin node involvement, contralateral groin or deep pelvic involvement is unusual. Lesions involving the clitoris can metastasize initially to the deep or superficial inguinal nodes [1].

Nodal status markedly affects overall staging. In patients with vulvar cancer, nodal spread occurs to regional inguinal and femoral lymph nodes, whereas metastases to deep pelvic nodes such as the internal or external iliac nodes are considered distant metastases. Unilateral regional nodal spread constitutes N1 disease (overall stage III), whereas bilateral regional nodal spread represents N2 disease (overall stage IV). Table 4.3 outlines the N-stage classification system for vulvar cancer.

Routine cross-sectional imaging relies on size and morphology has minimal impact on the nodal staging of vulvar cancer [7]. The use of positron emission tomography (PET) for patients with vulvar cancer is evolving but yet undefined [8]. Ultrasound combined with fine-needle aspiration (FNA) is an alternative imaging technique to assess inguinal lymph nodes with sensitivity and specificity values up to 93 and 100 %, respectively [9].

Vagina

Like vulvar tumors, vaginal carcinomas are rare, accounting for fewer than 3 % of gynecologic malignancies [10]. It is more common for the vagina to be a site of metastasis especially from direct extension from extragenital sites, such as the rectum, bladder, or other genital sites such as cervix or endometrium [1].

Table 4.3 N-stage classification for vulvar cancer

Stage	Findings
NX	Regional nodes cannot be assessed
N0	No regional nodal metastasis
N1	Metastasis in unilateral regional lymph nodes
N2	Metastasis in bilateral regional lymph nodes

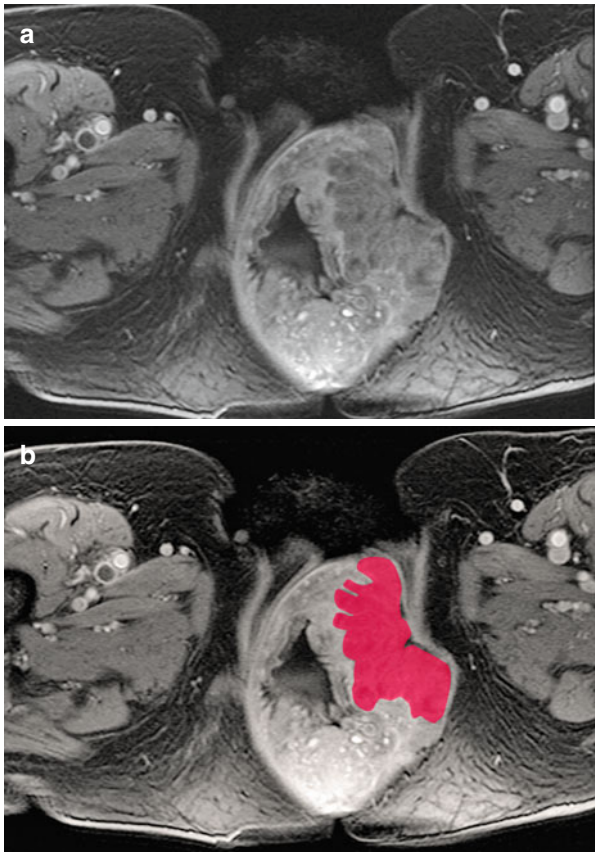

Fig. 4.20 (**a**–**d**) Axial contrast-enhanced T1-weighted MR image (**a**) shows the vulva cancer (*red*). The upper level of axial contrast-enhanced MRI images (**c**, **d**) metastatic superficial inguinal node (*orange*)

Fig. 4.20 (continued)

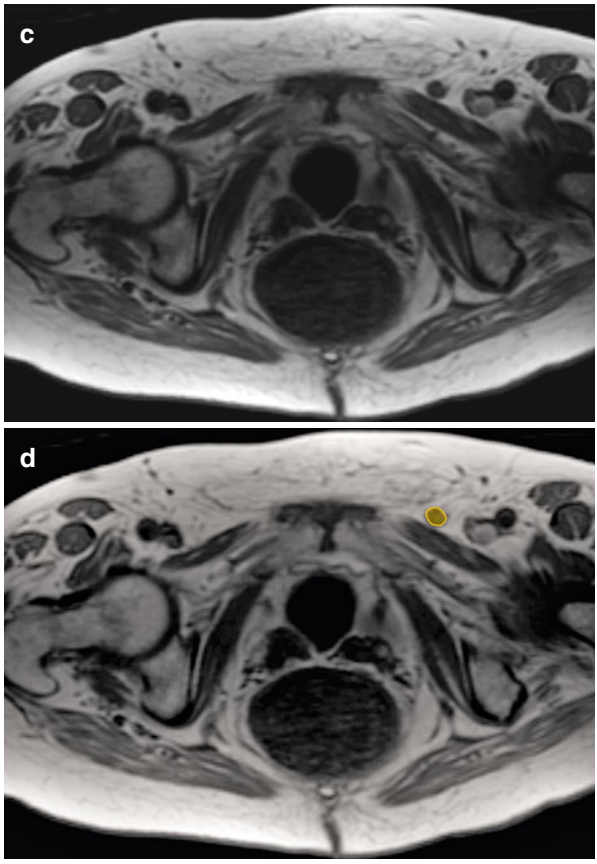

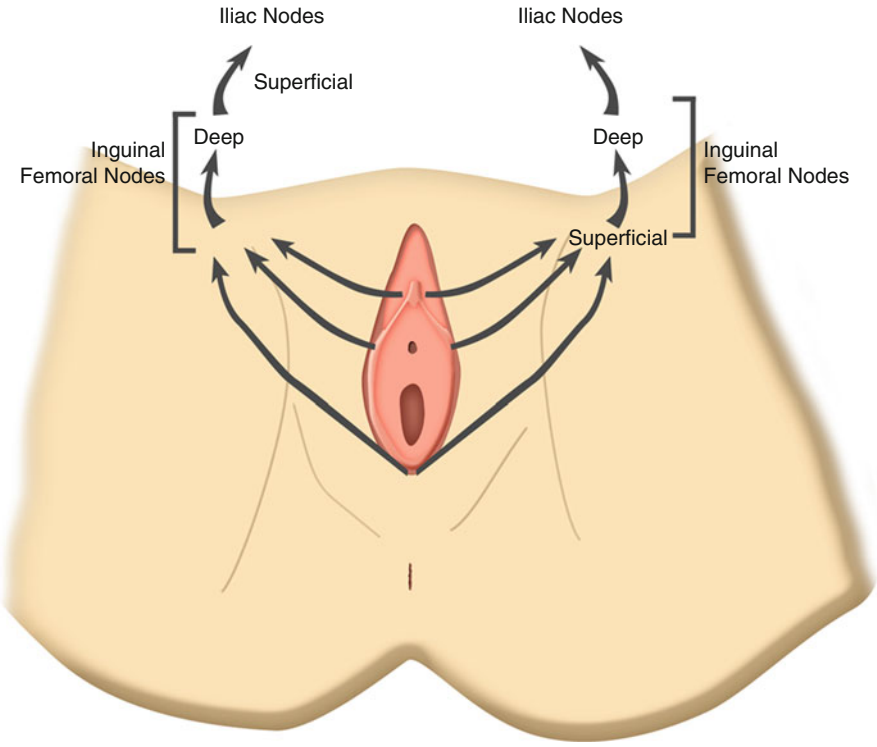

Fig. 4.21 Lymphatic drainage of the vulva

Nodal metastases follow the lymphatic drainage pathways from the vagina. Tumors of the lower third of the vagina involve inguinal nodes (*see* Fig. 4.22); tumors of the vaginal vault involve the hypogastric and obturator nodes; and tumors of the posterior wall involve the gluteal nodes.

Nodal metastasis affects the management of vaginal cancer. The American Joint Committee on Cancer staging system classifies metastasis to regional lymph nodes as stage III. Stage I–II vaginal tumors are treated with external beam radiation therapy (EBRT) targeted to the primary lesion, as well as to the expected lymphatic drainage sites of the tumor (inguinal and/or lateral pelvic nodes). For stage III or IVA tumors, radiation therapy, including node directed EBRT, is standard [10]. Table 4.4 outlines the N-stage classification system for vaginal cancer.

Although cross-sectional imaging has limited value, 18F-fluoro-deoxy-D-glucose (FDG)–PET scanning can be used to stage lymph nodes in these patients.

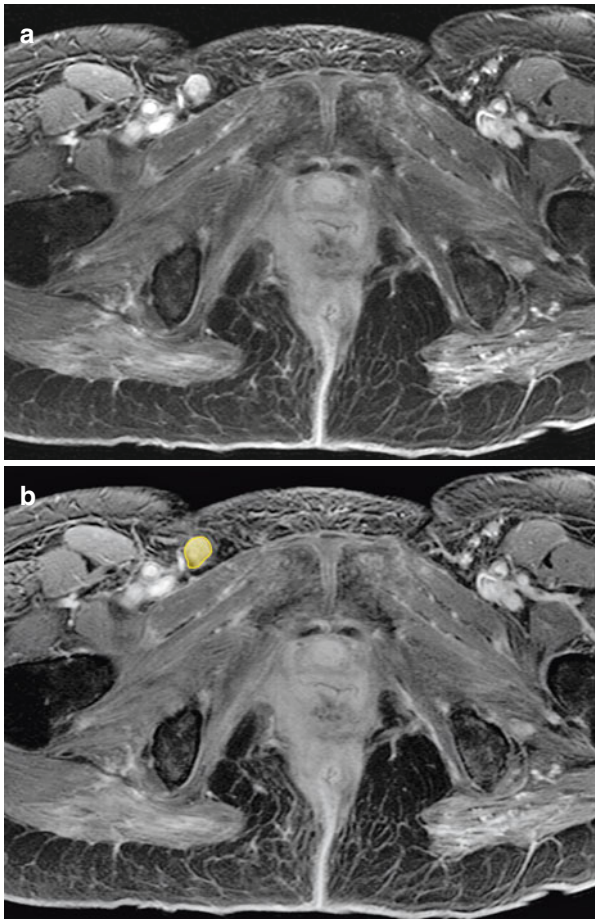

Fig. 4.22 (**a**, **b**) Axial contrast-enhanced T1-weighted MR image show the metastatic right inguinal node (*orange*) in the patient with vaginal cancer

Table 4.4 N-stage classification for vaginal, cervical, endometrial, ovarian cancer

Stage	Findings
NX	Regional nodes cannot be assessed
N0	No regional nodal metastasis
N1	Metastasis in regional lymph nodes

Uterus

The uterus is located in the lower pelvis, anterior to the rectum and posterior to the urinary bladder. It is divisible by the internal os into two regions, the cervix and body.

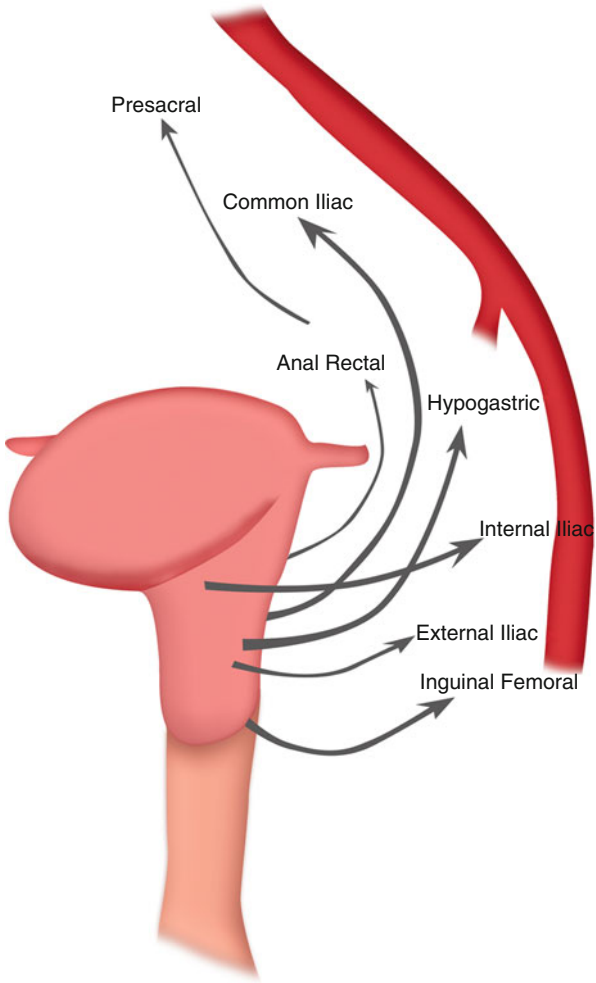

Fig. 4.23 Lymphatic drainage of the vagina

Invasive Cervical Cancer

Lymph node involvement is a poor prognostic indicator in cervical cancer patients with 5-year survival rate dropping to 71 % from 85 % in those patients with pelvic nodal metastases versus no nodal metastases. Those with para-aortic nodes have a 20–45 % 5-year survival [11].

Lymphatic spread within the subperitoneal space occurs from the cervical lymphatic plexus to the lower uterine segment to three groups of draining lymphatics. The upper lymphatics follow the uterine artery, cross the uterus, and drain to the upper internal iliac (hypogastric) nodes. The middle lymphatics drain to the obturator nodes (*see* Figs. 4.24, 4.25 and 4.26). The lower lymphatics drain to the superior

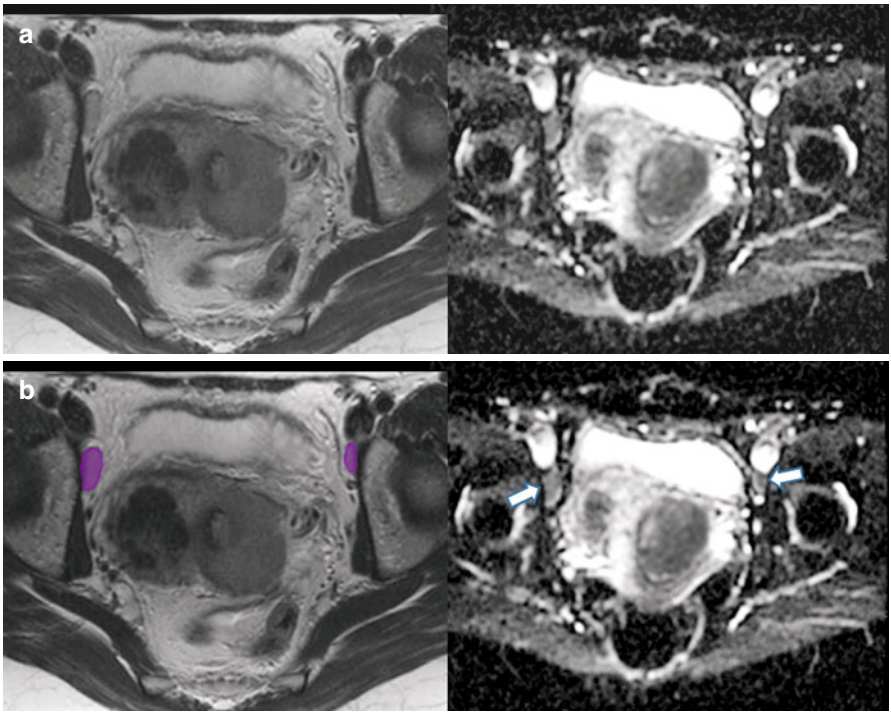

Fig. 4.24 (**a**, **b**) Axial T2-weighted (*left image*) and ADC images (*right image*) showing bilateral metastatic obturator lymph nodes (*purple*) showing restricted diffusion in a patient with cervical cancer

and inferior gluteal nodes. All groups drain cephalad to the common iliac nodes and para-aortic nodes [12]. Supraclavicular node involvement is frequent and represents nodal spread from the para-aortic nodes to the cisterna chyli via the thoracic duct. There is usually an orderly pattern of nodal progression cephalad.

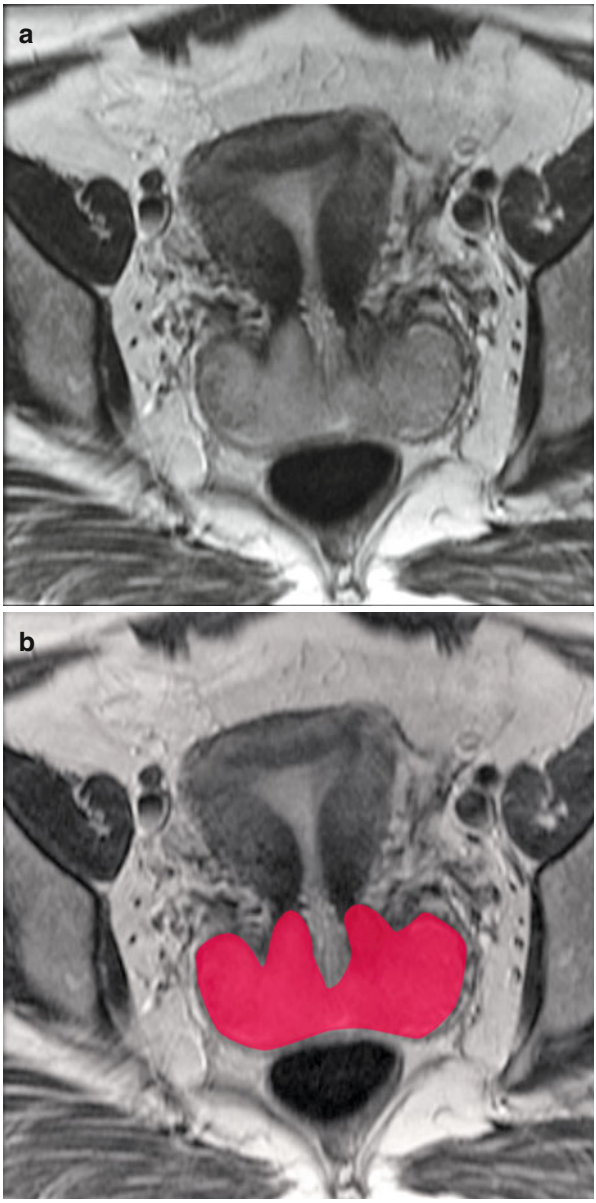

Fig. 4.25 (**a**–**d**) Axial T2-weighted MR image shows the cervical cancer (*red*). Axial contrast-enhanced CT image in the same patient (**c**, **d**) shows the enlarged metastatic left external iliac lymph node (*orange*)

Fig. 4.25 (continued)

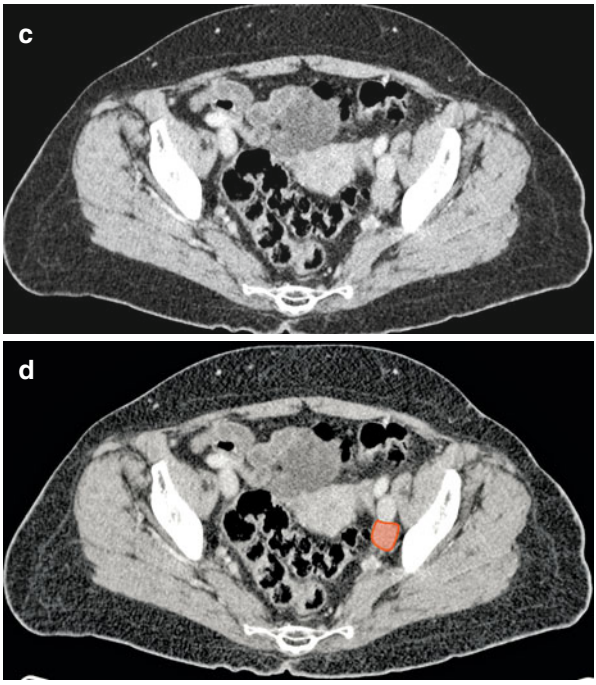

Fig. 4.26 (**a**, **b**) Reformatted coronal CT image shows metastatic left external iliac node (*purple*) in a patient with cervical cancer

Fig. 4.26 (continued)

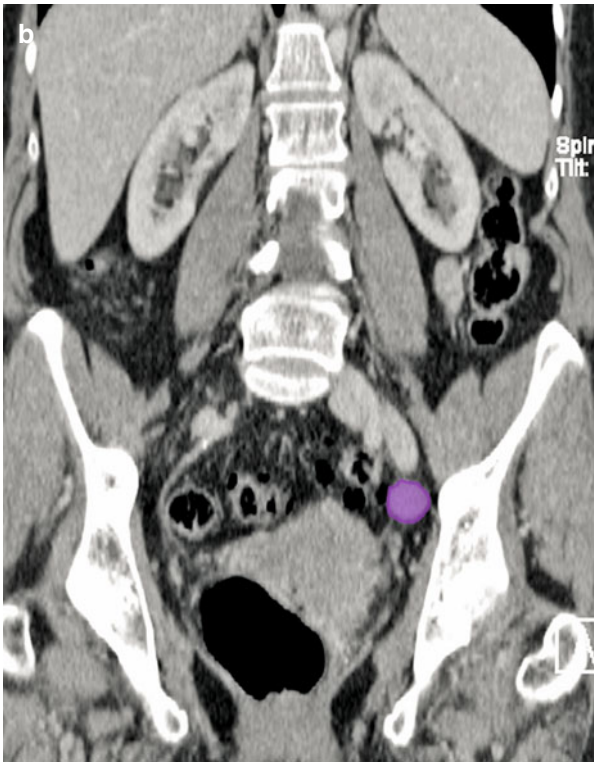

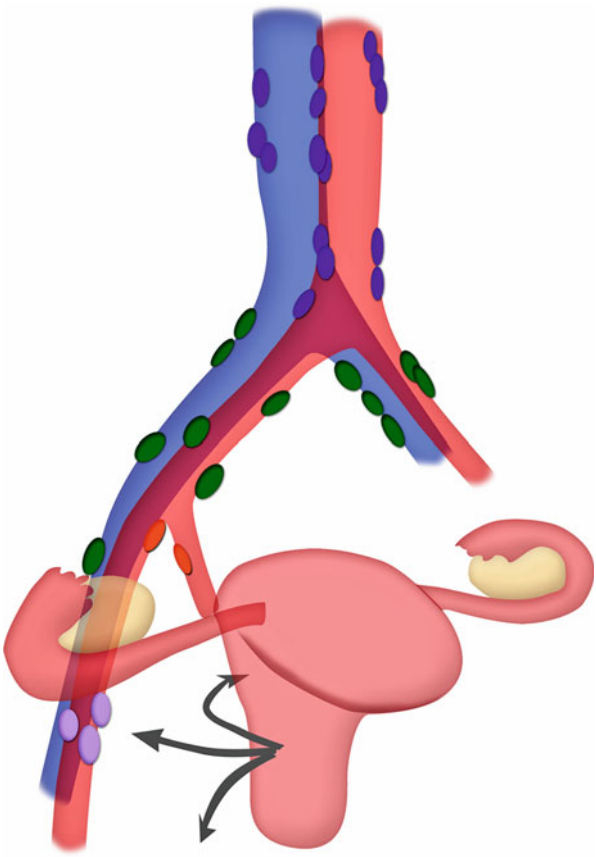

Fig. 4.27 Lymphatic drainage of the cervix

Cancer of the Uterine Body

Cancer of the uterine body is the most common gynecologic malignancy. Ninety percent of endometrial cancers arise from the epithelial lining. Retroperitoneal nodal involvement is a prognostic indicator. In endometrial carcinoma, the 5-year survival rate of a patient with more than one positive node is 55 % [13].

Subperitoneal spread via the lymphatics follows several routes. The fundus and superior portion of the uterus drain with the ovarian vessels and lymphatics to the upper abdominal para-aortic nodes. The middle and lower regions drain through the broad ligament along uterine vessels to the internal and external iliac nodes (see Figs. 4.28, 4.29 and 4.30). Occasionally, disease spreads to the superficial inguinal nodes by lymphatics along the round ligament (*see* Fig. 4.31).

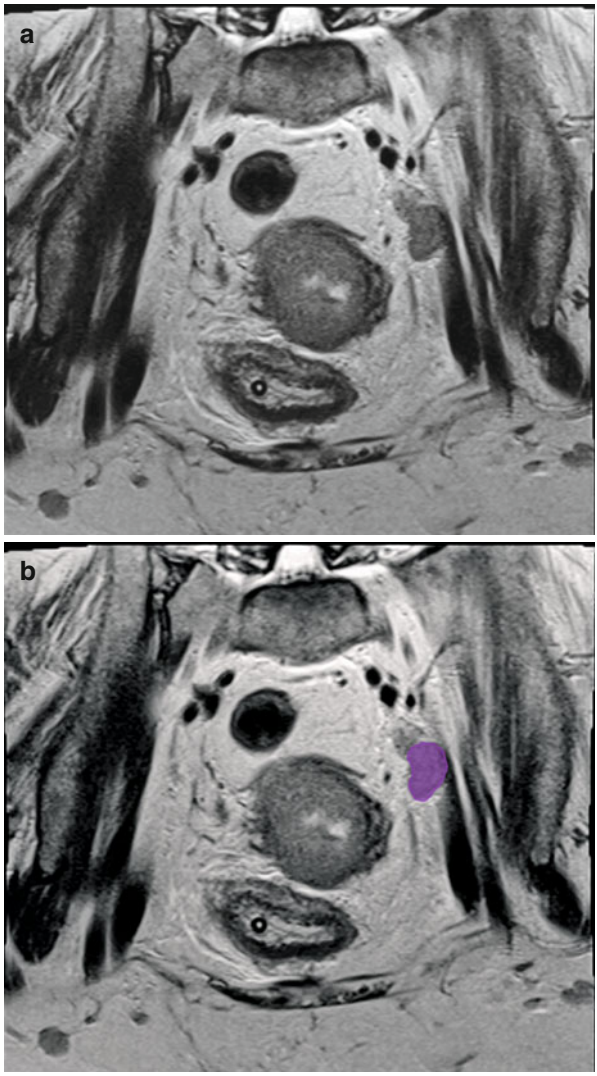

Fig. 4.28 (**a**, **b**) Oblique coronal MR image showing metastatic left external iliac lymph node (*purple*) in a patient with endometrial cancer

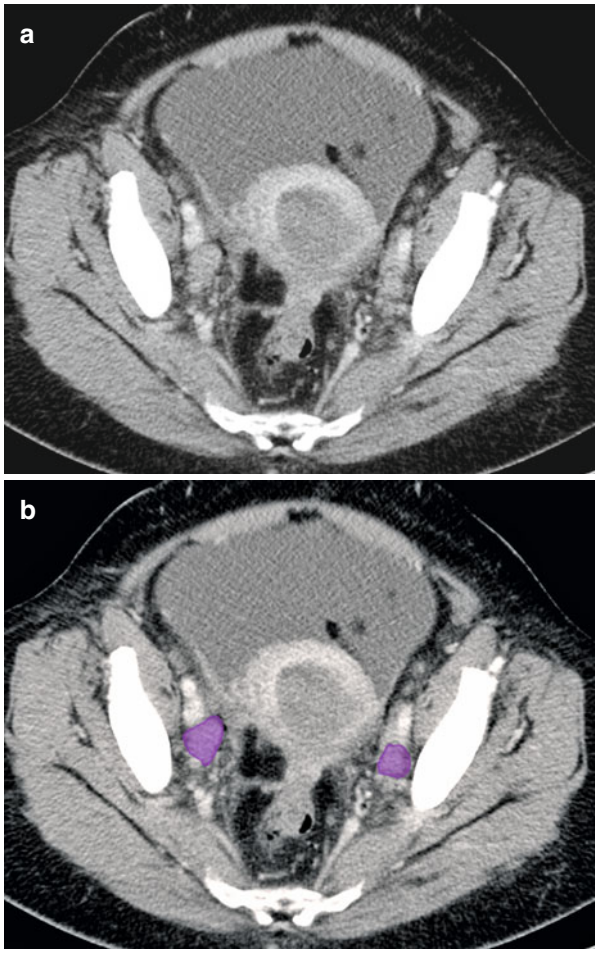

Fig. 4.29 (**a**, **b**) Axial CT image shows bilateral external iliac metastatic nodes (*purple*) in a patient with endometrial cancer

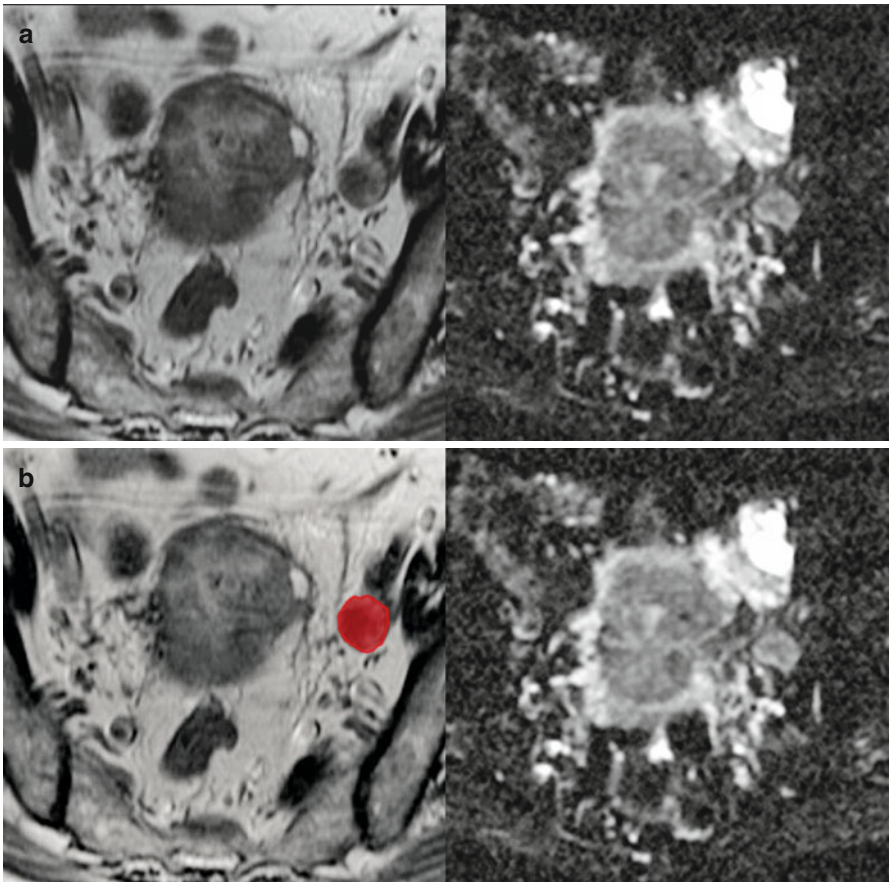

Fig. 4.30 (**a**, **b**) Axial T2-weighted image (*left*) and ADC map (*right*) showing metastatic left external iliac lymph node (*red*)

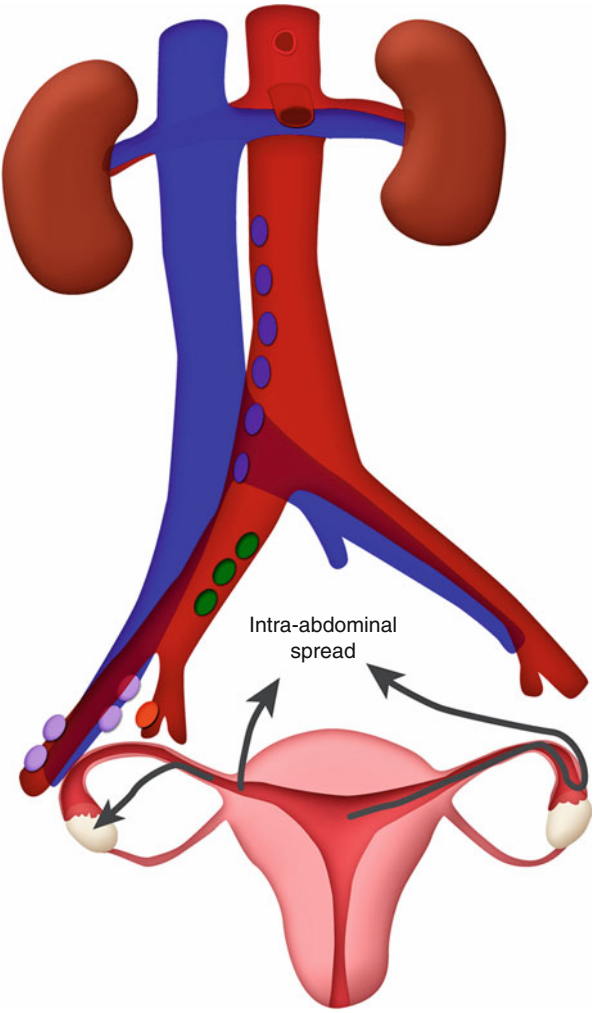

Fig. 4.31 Patterns of lymphatic dissemination of endometrial cancer

Fallopian Tube

The lymphatics of the fallopian tubes accompany the ovarian lymphatics to the para-aortic nodes in the upper abdomen. There is drainage along the uterine vessels in the broad ligament to the iliac nodes.

Patterns of lymphatic spread are similar to ovarian cancer. There is a high propensity for lymphatic spread to the para-aortic nodes and pelvic nodes.

Ovary

In ovarian cancer, confirmed nodal metastases upstages a patient to a higher stage (stage IIIC) regardless of tumor extent. Patients with lower-stage ovarian cancers

have 5-year survival rates of 57–89 %, whereas the survival rate of patients with stage III ovarian cancer is only 34 % [14].

Lymphatic spread of ovarian tumors is along three routes. The most frequent route is the lymphatics along the ovarian vessels to the para-aortic lymph nodes (*see* Figs. 4.32 and 4.33). The second in frequency is along the ovarian branches from the uterine vessels to the broad ligament and parametria and then to the external iliac nodes, obturator nodes, and common iliac nodes. The least frequent lymphatic spread is along the lymphatics of the round ligament to the superficial and deep inguinal nodes (*see* Fig. 4.34).

Multidetector computed tomography (MDCT) is unable to detect cancer in normal size nodes and cannot discriminate reactive nodes from metastases. CT criteria for nodal disease are based on size (*i.e.*, 1 cm or more in short axis being abnormal). Unfortunately, this has a sensitivity of 40–50 % and a specificity of 85–95 % [15]. Nodal necrosis and clusters of small lymph nodes along expected drainage routes may indicate metastases [16]. PET-CT for lymph node staging is under evaluation [17].

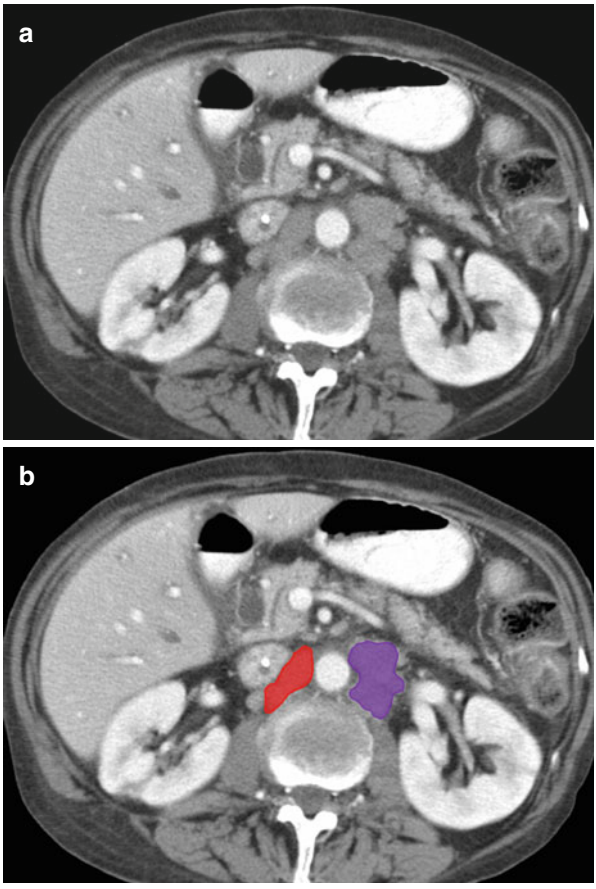

Fig. 4.32 (**a**, **b**) Axial CT image in a patient with ovarian cancer shows metastatic aortocaval (*red*) and left periaortic lymph node (*purple*)

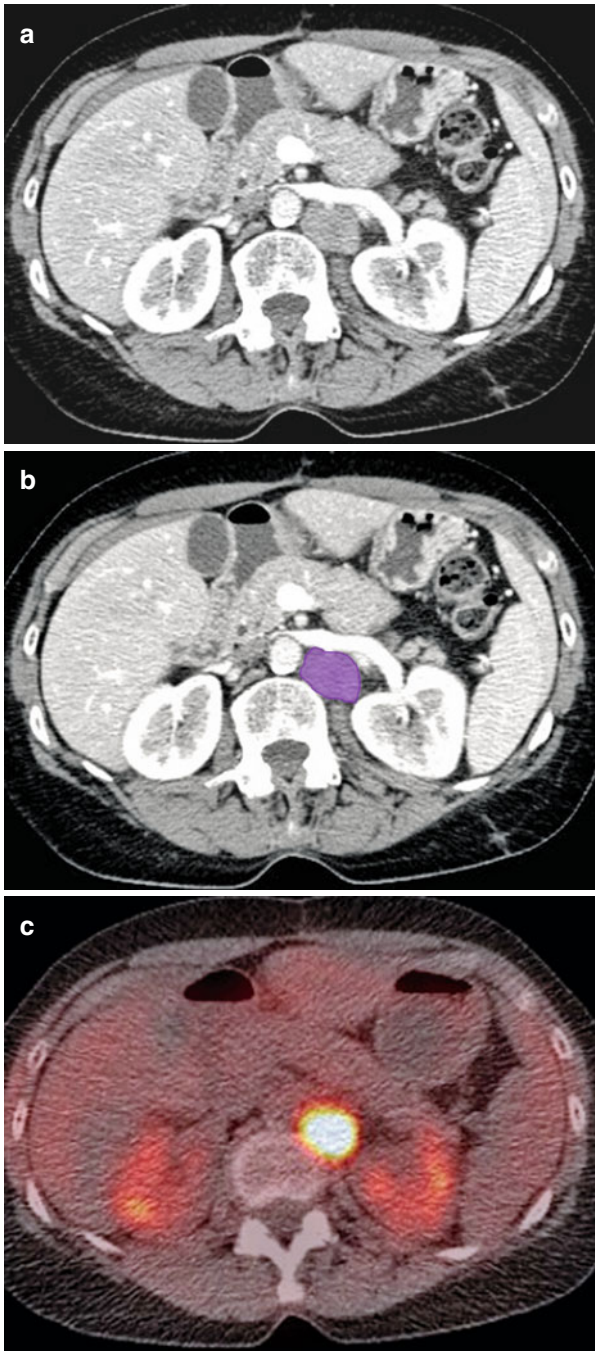

Fig. 4.33 (**a–c**) Axial CT and fused PET-CT images in a patient with ovarian cancer showing FDG avid metastatic left periaortic lymph node (*purple*)

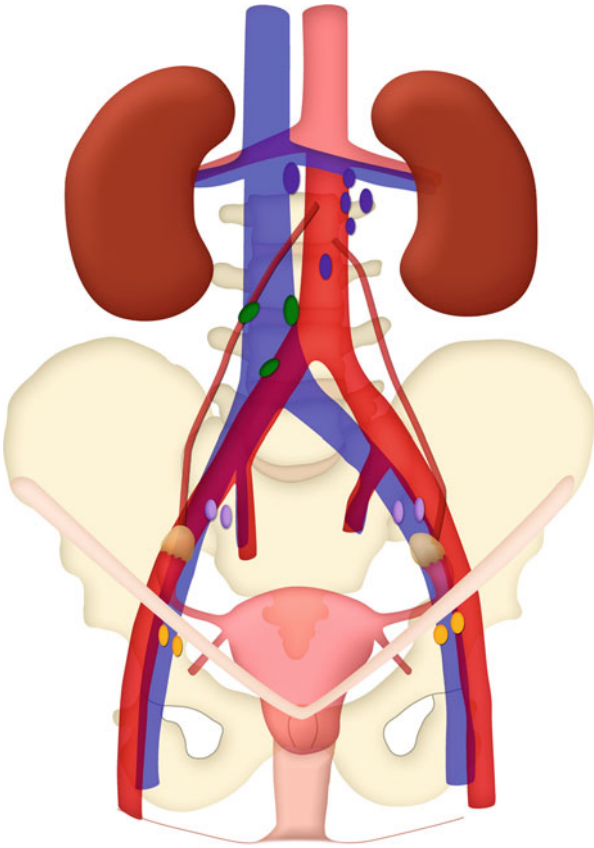

Fig. 4.34 Lymphatic drainage of the ovary

Male Urogenital Pelvic Malignancies

Male urogenital pelvic cancers commonly spread to iliopelvic or retroperitoneal lymph nodes by following pathways of normal lymphatic drainage from the pelvic organs. The most likely pathway of nodal spread (superficial inguinal, pelvic, or para-aortic) depends on the location of the primary tumor and whether surgery or other therapy has disrupted normal lymphatic drainage from the tumor site. Knowledge of both factors is essential for accurate disease staging.

Superficial Inguinal Pathway

The superficial inguinal pathway is the primary route of metastasis from perineal tumors, including penile cancer (*see* Fig. 4.35). The saphenofemoral junction node is the sentinel node along this pathway (*see* Fig. 4.36); from that node, metastatic tumor cells may ascend to the deep inguinal and external iliac nodes [18].

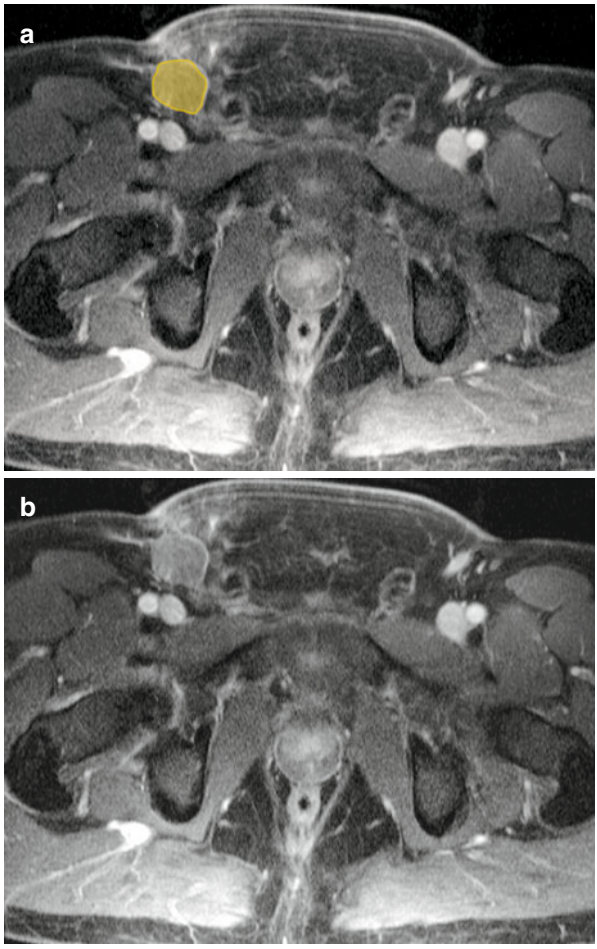

Fig. 4.35 (**a**, **b**) Axial contrast-enhanced T1-weighted MR image showing metastatic right inguinal lymph node (*orange*) in a patient with penile cancer

Pelvic Pathways

Pelvic tumors may metastasize along four pelvic lymphatic drainage pathways (*see* Fig. 4.37): (1) the anterior pelvic route, which drains lymph from the anterior wall of the bladder along the obliterated umbilical artery to the internal iliac (hypogastric) nodes; (2) the lateral route, which drains lymph from the pelvic organs to the medial chain of the external iliac nodal group (a characteristic route of spread from carcinomas at the lateral aspect of the bladder and from prostate adenocarcinomas); (3) the internal iliac (hypogastric) route, which drains lymph from most of the pelvic organs along the visceral branches of the internal iliac lymphatic ducts to the junctional nodes located at the junction between the internal and external iliac vessels; and (4) the presacral route, which includes the lymphatic plexus anterior to the sacrum and coccyx and extending upward to the common iliac nodes (*see* Fig. 4.38). Late-stage tumors of lower pelvic organs such as the prostate may spread to the presacral space either via the perirectal lymphatics or by direct extension [18].

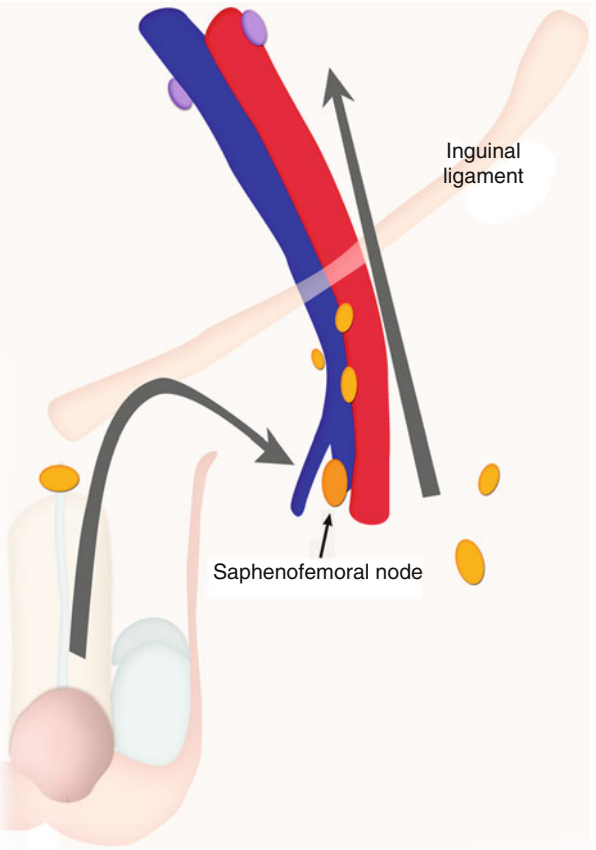

Fig. 4.36 Superficial inguinal lymphatic drainage pathway. Schematic shows the location of the saphenofemoral junction nodes, sentinel nodes for the superficial inguinal pathway, along which metastatic tumor cells from the penis can ascend toward the deep inguinal and external iliac nodes

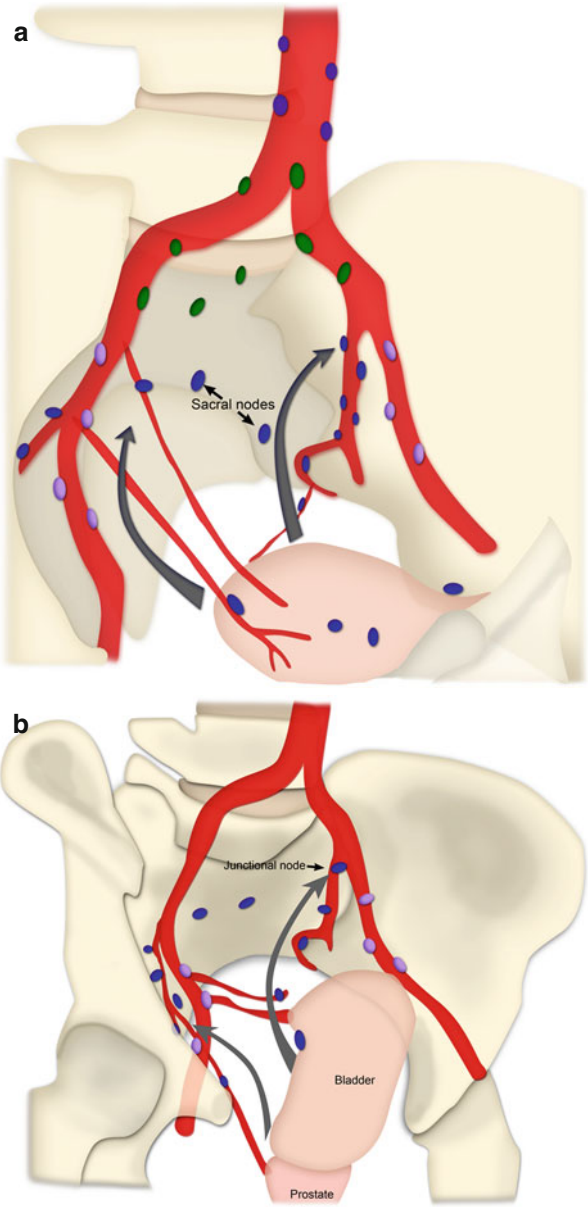

Fig. 4.37 Schematics show pelvic pathways of nodal metastasis: (**a**) by the anterior route (*arrows*), lymph drains from the anterior wall of the bladder along the obliterated umbilical artery to the internal iliac or hypo-gastric nodes; (**b**) by the lateral route (*small arrow*), lymph drains from the pelvic organs to the external iliac (*purple*) nodes; by the internal iliac or hypogastric route (*big arrow*), it drains along the visceral branches of the internal iliac vessels to the junctional nodes; and by the presacral route, it drains through the lymphatic plexus anterior to the sacrum and coccyx

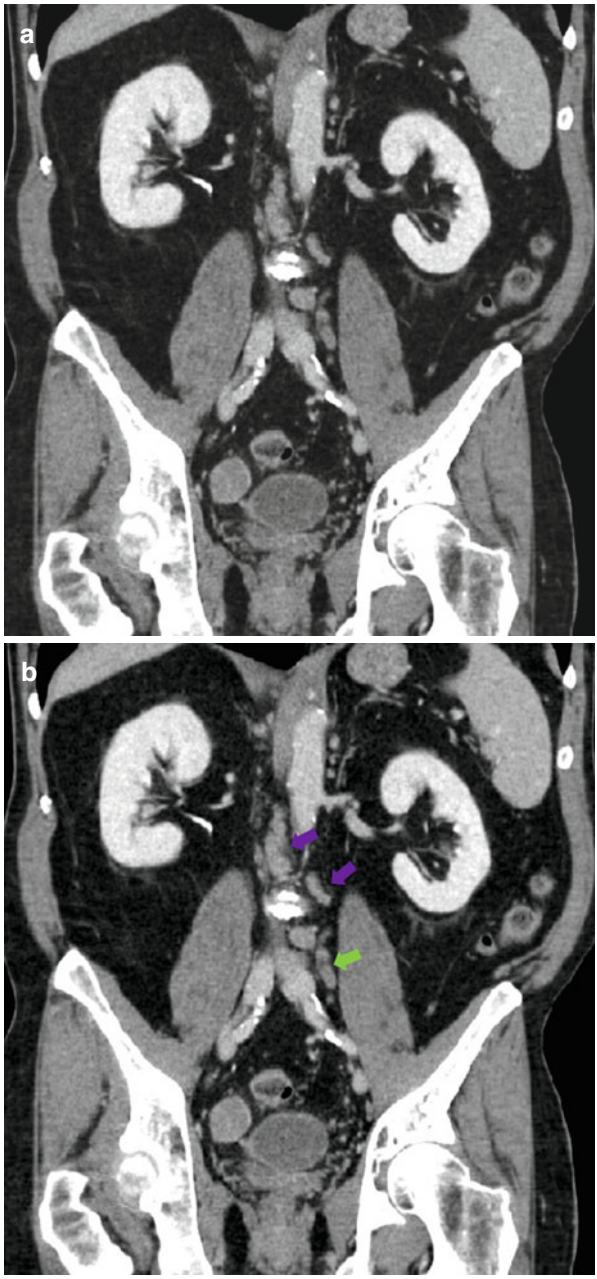

Fig. 4.38 (**a**, **b**) Coronal reformatted CT image shows ascending metastatic lymph nodes. Adenopathy is seen in common iliac (*green arrow*) and left periaortic (*purple arrow*) lymph nodes

Para-aortic Pathway

Metastases from testicular carcinoma spread commonly through the para-aortic pathway (*see* Fig. 4.39), a route that bypasses the pelvic lymph nodes. The lymphatic

vessels of the testis follow the gonadal blood vessels. At the inguinal ring the lymphatic vessels continue upward along the gonadal blood vessels, anterior to the psoas muscle, ending in the para-aortic and paracaval nodes at the renal hilum (*see* Fig. 4.40). From these nodes, metastatic disease may spread downward in a retrograde fashion toward the aortic bifurcation [18].

Modified Post-therapeutic Pathways

Knowledge about any previous treatment of the primary tumor is important because surgery, chemotherapy, and radiation therapy may modify the pattern of nodal disease. Nodal dissemination follows a different pathway when normal lymphatic drainage has been disrupted by nodal dissection or therapeutic irradiation, as often occurs in the treatment of germ cell tumors of the testis. Pelvic nodes are not usually involved in testicular cancer unless scrotal surgery or retroperitoneal nodal dissection has taken place. After radical cystectomy for bladder cancer, metastatic disease is seen more frequently in the common iliac and para-aortic nodes than in the expected nodal chains. Similarly, after therapeutic irradiation of the prostate or radical prostatectomy, recurrent disease usually is seen in extrapelvic nodes [18].

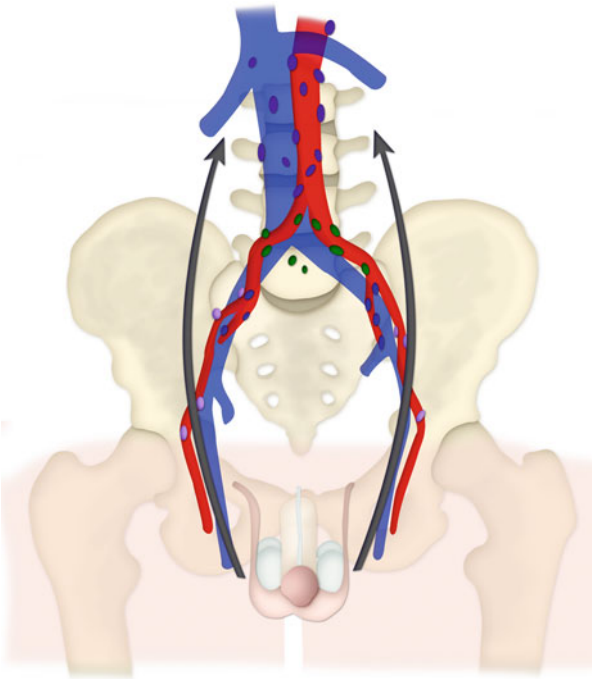

Fig. 4.39 Schematic shows the para-aortic pathway of metastasis (*arrows*), by which malignant cells from testicular tumors can proceed upward through lymphatic ducts that follow the gonadal vessels to nodes at the renal hilum, completely bypassing the pelvic nodes

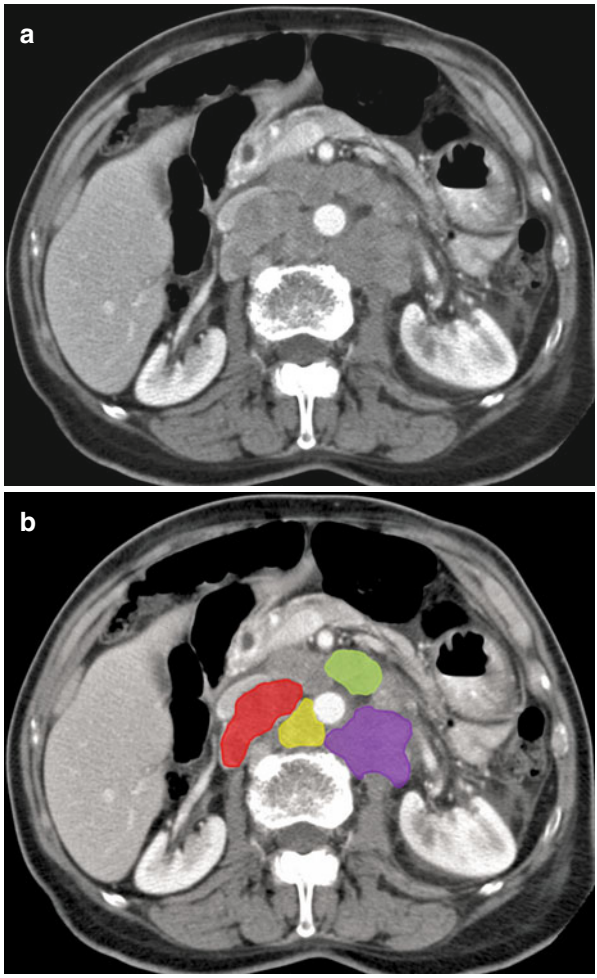

Fig. 4.40 (**a**, **b**) Axial CT image shows retroperitoneal nodal group. These are, as depicted, the retrocaval (*red*) chain, aortocaval (*yellow*), pre-aortic (*green*), and left periaortic chain (*purple*)

Pathways of Nodal Spread in Urogenital Pelvic Malignancies

Urogenital tumors usually spread first to regional lymph nodes (Table 4.1). The specific nodal groups most likely to be affected by metastatic disease vary according to the location of the primary tumor (prostate, penis, testis, or bladder). In the TNM classification system, regional nodal metastases are categorized as N lesions, and metastases to lymph nodes outside the regional groups are categorized as M lesions.

Prostate Cancer

Prostate cancer is the most common cancer in men. At radical prostatectomy, nodal involvement is found in 5–10 % of patients with prostate carcinoma. The 5-year

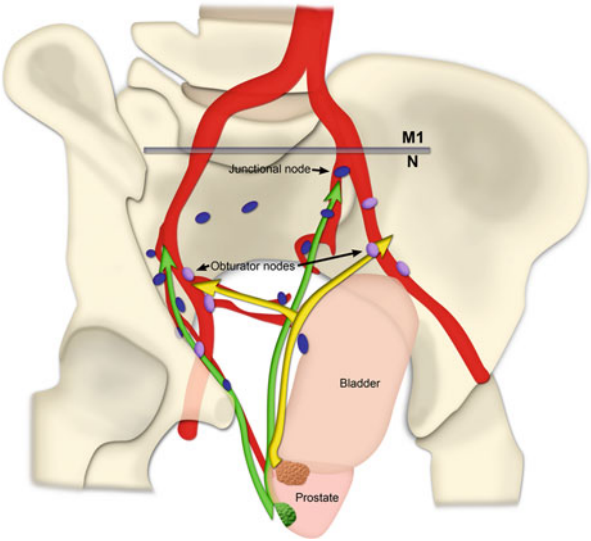

Fig. 4.41 Schematic shows common pathways of metastasis from prostate cancer. The obturator nodes in the external iliac (*purple*) nodal group are the lateral route (*yellow arrows*), and the junctional nodes in the internal iliac (*blue*) nodal group are the hypogastric route (*green arrows*). Nodal metastases to the common iliac chain are considered distant metastases

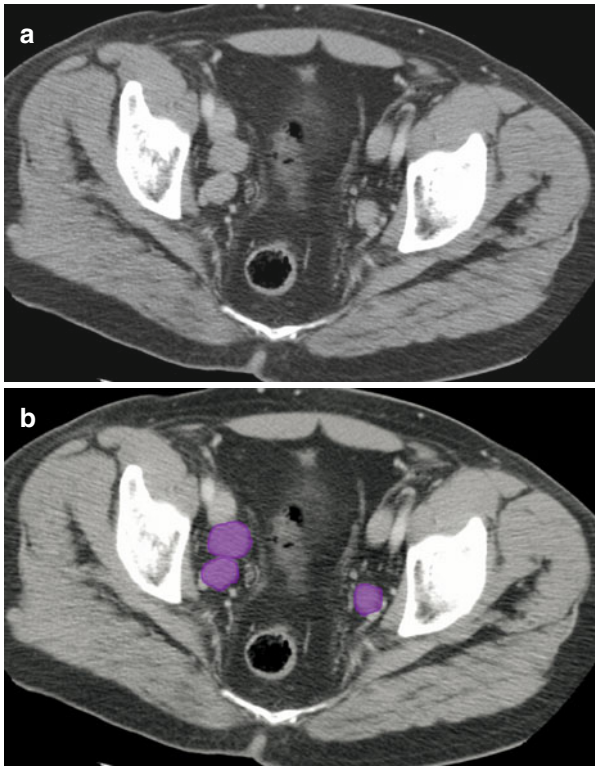

Fig. 4.42 (**a**, **b**) Axial CT image show bilateral metastatic obturator lymph nodes (*purple*) in a patient with prostate cancer

relative survival rate for patients with a single nodal metastasis is 75–80 %, whereas that for patients with multiple nodal metastases is only 20–30 % [18].

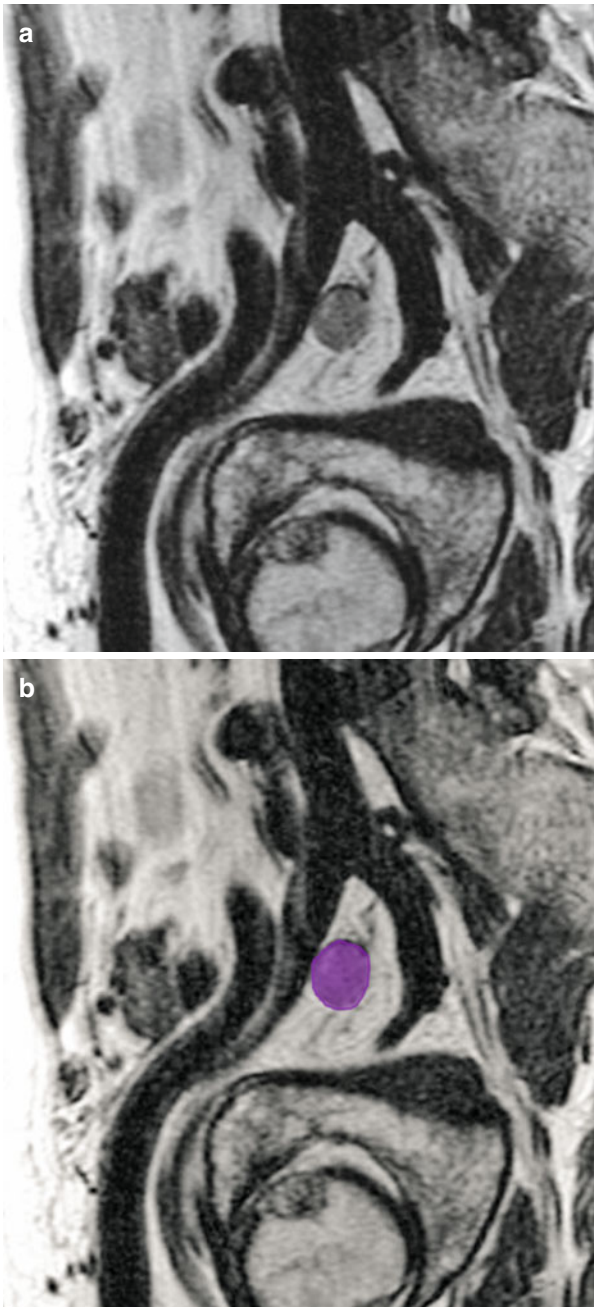

Fig. 4.43 (**a**, **b**) Oblique sagittal T2-weighted MR image shows metastatic obturator lymph node (*purple*) in a patient with prostate cancer

Prostate cancers spread via the pelvic lymphatic drainage pathways (*see* Fig. 4.41). The main route of drainage from the prostate gland is the lateral route, for which the sentinel nodes are the obturator nodes (*see* Figs. 4.42 and 4.43) (medial chain of the external iliac nodal group). From there, the tumor may spread to the middle and lateral chains of the external iliac nodes (*see* Fig. 4.44). The second most common route of drainage is the internal iliac (hypogastric) route, via the lymph nodes positioned along the visceral branches of the internal iliac (hypogastric) vessels (*see* Fig. 4.45). For this route, the sentinel nodes are the junctional nodes located at the junction of the internal and external iliac vessels.

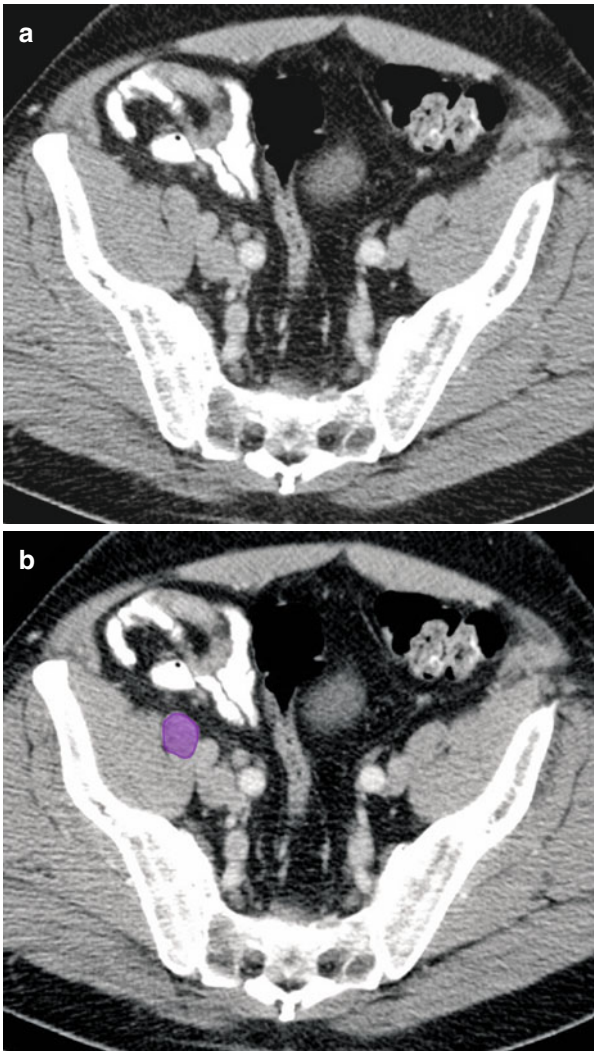

Fig. 4.44 (**a**, **b**) Axial CT image shows metastatic right external iliac lymph node (*purple*) in a patient with prostate cancer

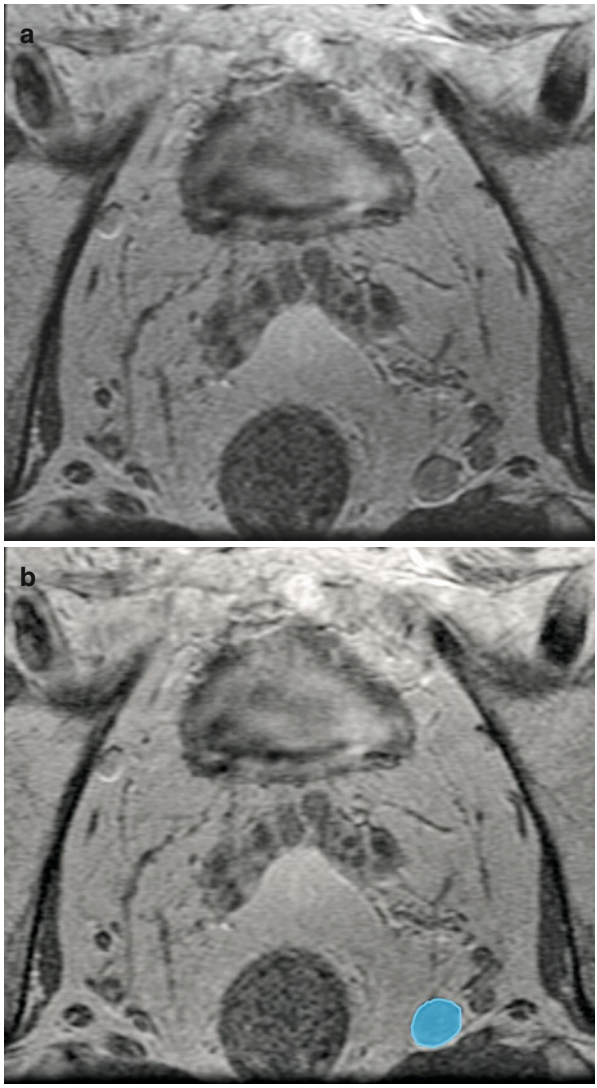

Fig. 4.45 (**a**, **b**) Axial T2-weighted MR image showing metastatic left internal iliac node (*blue*) in a patient with prostate cancer

Some lymphatic drainage occurs along an anterior route, via lymph nodes located anterior to the urinary bladder. From these nodes, metastases can spread to the internal iliac nodes. There is also a presacral route anterior to the sacrum and the coccyx (*see* Fig. 4.46); via this route, prostate cancer may metastasize to the perirectal lymphatic plexus, subsequently ascending to the lateral sacral nodes and those at the sacral promontory (medial chain of the common iliac nodes) [19, 20]. In patients with a primary tumor that affects only one lobe of the prostate, nodal metastases tend to be ipsilateral [21].

In the characterization of nodal metastases from prostate cancer, the regional lymph nodes are the pelvic nodes located below the bifurcation of the common

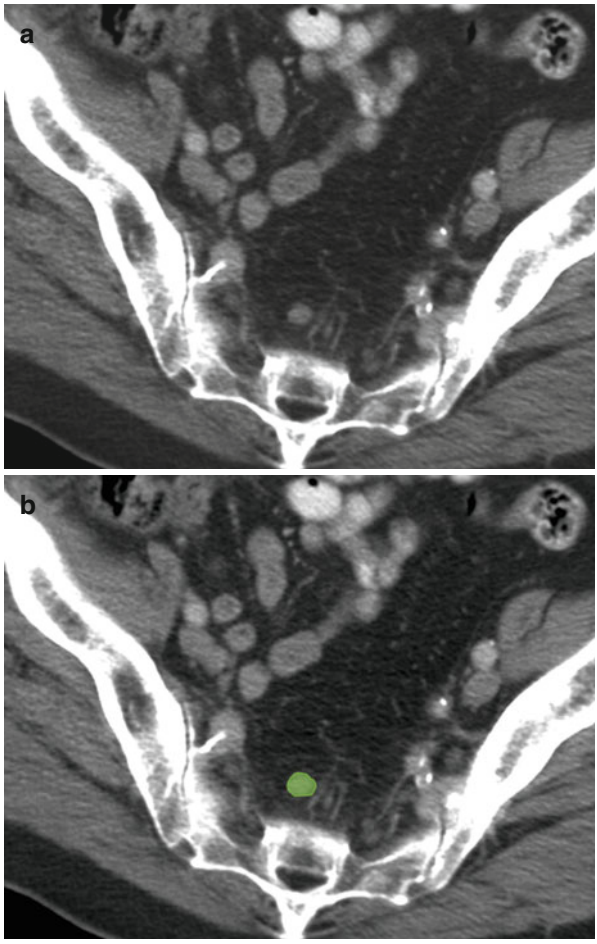

Fig. 4.46 (**a**, **b**) Axial CT image showing metastatic presacral lymph node (*green*) in a patient with prostate cancer

iliac arteries (*see* Fig. 4.47): the internal iliac nodes (including the sacral nodes) and the external iliac nodes (including the obturator nodes) (Table 4.1). The laterality of nodal metastases (*i.e.*, whether they are bi- or unilateral, left- or right-sided) does not affect their categorization as N lesions (Table 4.4). However, metastases to common iliac nodes are categorized as M1 lesions (*see* Fig. 4.48) [46].

Efficacy data for MR imaging and CT in the evaluation of lymph node metastases are similar. However, neither modality allows reliable detection of small nodal metastases, with reported accuracy ranging from 67 to 93 % and sensitivity ranging from 27 to 75 % [22]. High-resolution MR imaging with ultrasmall superparamagnetic iron oxide (USPIO) nanoparticles shows considerable promise for improving the detection of lymph node metastases that are occult at CT or standard MR imaging [23].

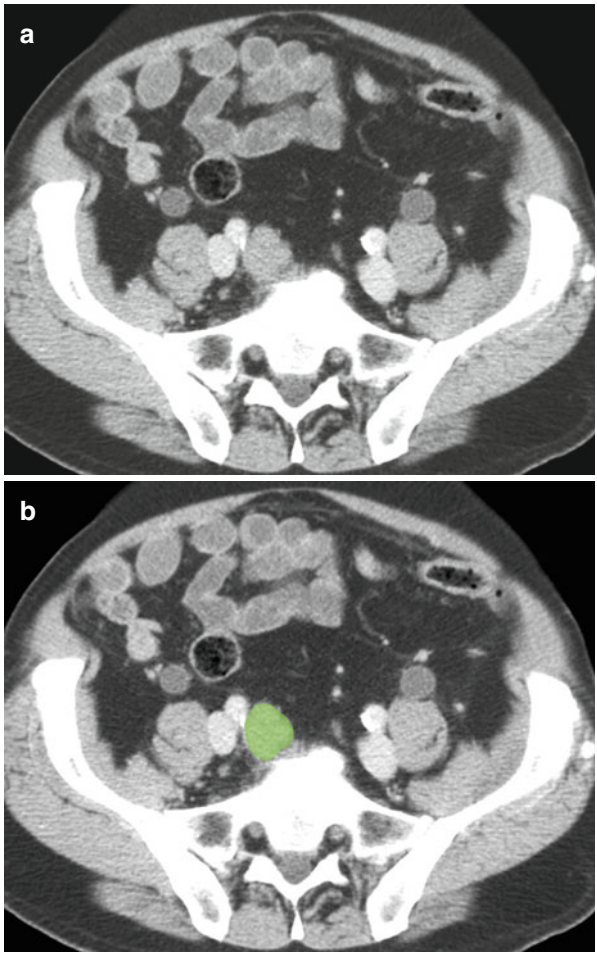

Fig. 4.47 (**a**, **b**) Axial CT image showing metastatic right common iliac lymph node (*green*) in a patient with prostate cancer

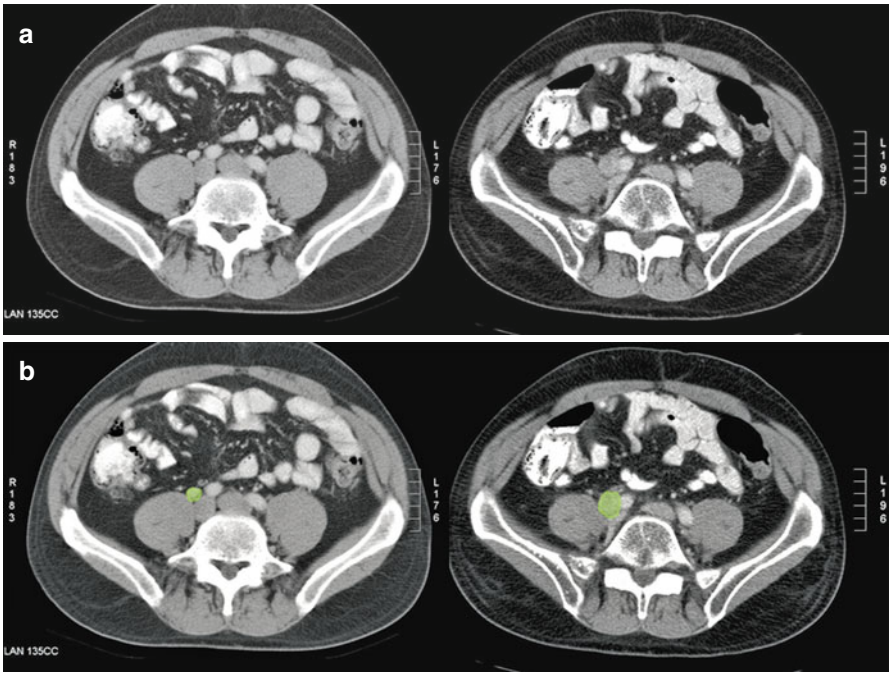

Fig. 4.48 (**a**, **b**) Axial CT images in a patient with prostate cancer showing progressive nodal enlargement with time. The earlier time point (*left image*) shows a small right common iliac lymph node (*green*) progressively enlarging over 6 months (*right image*)

Penile Cancer

Penile carcinoma accounts for ≤10 % of all male malignancies [24]. At the time of presentation, up to 96 % of patients with penile cancer will have palpable inguinal lymph nodes (*see* Fig. 4.49), and 45 % will have nodal metastases. Among those with only one or two involved nodes, the 5-year survival rate is 82–88 %, whereas it drops to 7–50 % among those with more than two [25].

Lymph from the penis has multiple drainage routes. The external pudendal pathway drains the skin of the penis and perineum to the nodes at the saphenofemoral venous junction; the deep inguinal pathway drains the glans penis to the deep inguinal and external iliac nodes (*see* Fig. 4.49); and the internal iliac pathway drains the erectile tissue to the internal iliac nodes [1]. Lymphatic drainage of the penile urethra is to the internal iliac group of lymph nodes via inguinal lymphatics (*see* Fig. 4.50).

Penile cancers commonly metastasize to lymph nodes along the superficial inguinal pathway (*see* Fig. 4.51). The saphenofemoral junction node is the sentinel node for this group of cancers. From there, metastatic tumor cells may ascend toward the deep inguinal nodes. Metastases to the external iliac nodes also may

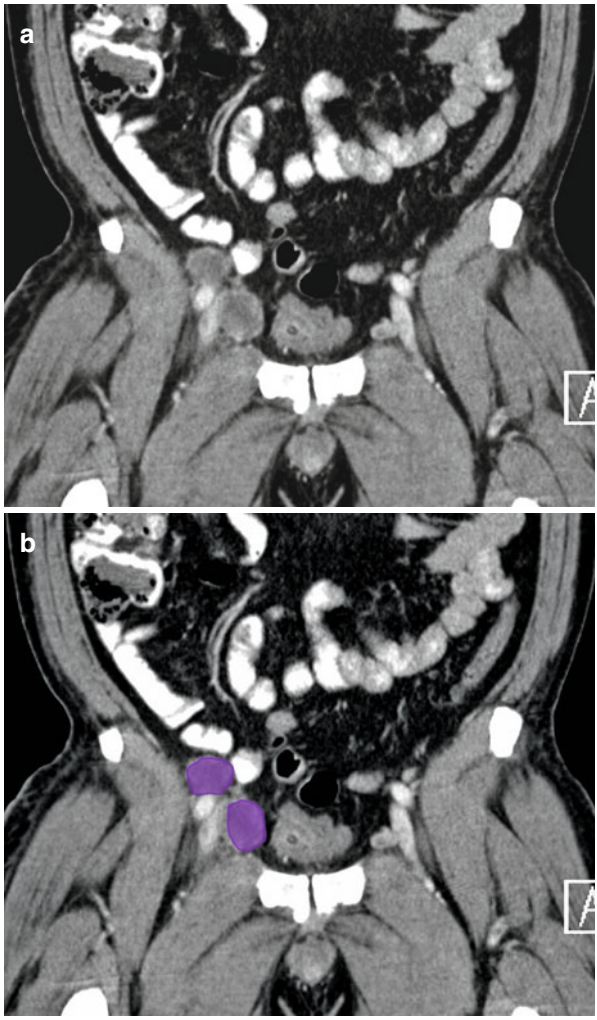

Fig. 4.49 (**a**, **b**) Coronal reformatted CT image shows metastatic right external iliac lymph nodes (*purple*) in a patient with penile cancer

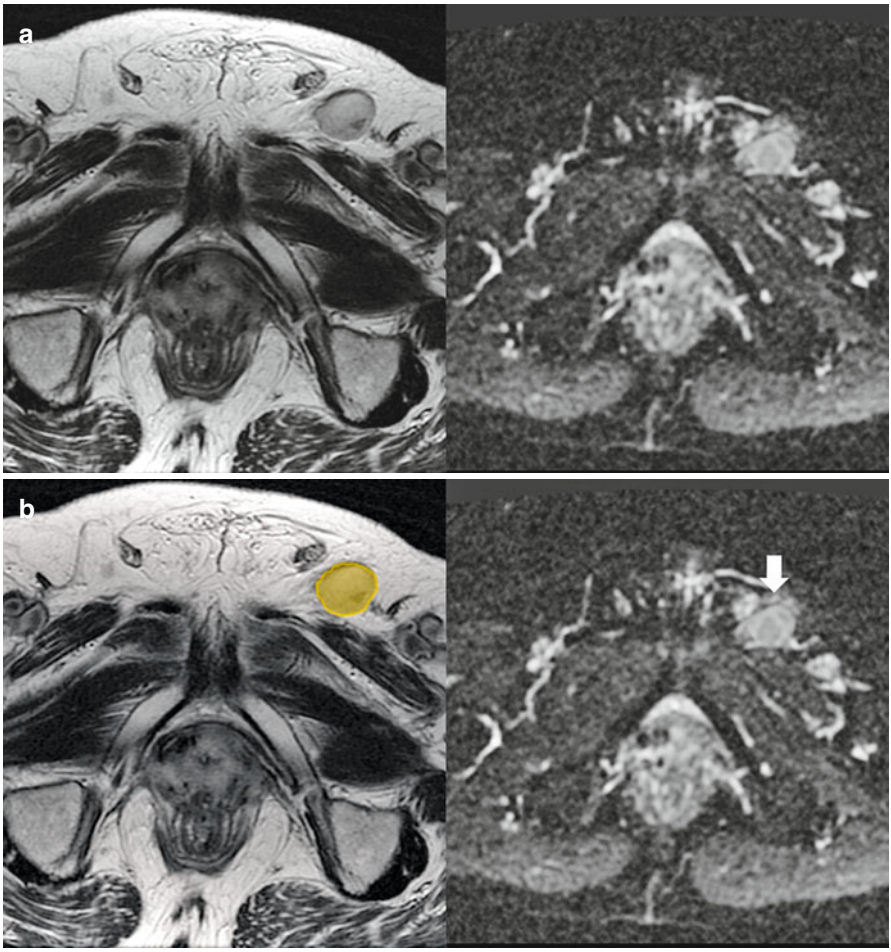

Fig. 4.50 (**a**, **b**) Axial T2-weighted image (*left image*) and ADC map (*right image*) in a patient with transitional cell cancer of urethra showing metastatic left inguinal node (*orange*) with restricted diffusion (*arrow*)

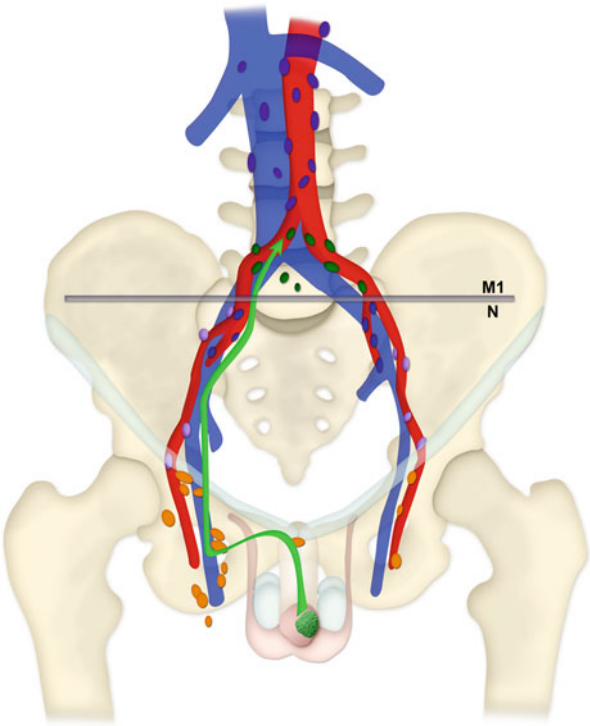

Fig. 4.51 Schematic shows the most common pathway of metastasis from penile cancer: the superficial inguinal lymphatic drainage pathway (*green arrow*). The saphenofemoral (*orange*) nodes are sentinel nodes along this pathway. Involvement of the common iliac (*green*) nodes is indicative of *M1* disease

Table 4.5 N-stage classification for penile cancer

Stage	Findings
NX	Regional nodes cannot be assessed
N0	No regional nodal metastasis
N1	Metastasis in single superficial inguinal lymph node
N2	Metastasis in multiple and/or bilateral superficial inguinal lymph nodes
N3	Metastasis in deep inguinal or pelvic lymph nodes

occur via a secondary pathway; however, direct (so-called skip) metastases to this nodal group are rare. Nodal dissemination of penile cancer is frequently bilateral because of the complex lymphatic network and lateral crossover of lymphatic ducts at the base of the penis. Periprostatic and peri-seminal vesicle lymph nodes are rarely involved [19].

In patients with penile cancer, metastases to superficial inguinal, deep inguinal, internal iliac, or external iliac (including obturator) nodes are categorized as N lesions (regional nodal metastases) (Table 4.5), whereas metastases to common iliac nodes are categorized as M1 lesions (nonregional nodal metastases) (Table 4.1).

Although the capacity of CT and MR imaging to depict small lymph node metastases is limited, these modalities have an advantage over clinical examination in that they allow the assessment of nonpalpable deep pelvic and retroperitoneal nodes. The utility of PET for TNM classification of penile cancer is under investigation [26].

Testicular Cancer

Testicular cancer accounts for about 1 % of all neoplasms in men [27, 28]. Testicular cancer spreads more frequently through the lymphatic system than by local extension, because the tunica albuginea forms a natural barrier to infiltration [1]. The prognosis is generally good for patients with testicular cancer, even for those with distant metastases, for whom the 5-year survival rate is more than 80 % [20].

Testicular cancer spreads via the para-aortic pathway (*see* Fig. 4.52). Testicular lymphatic drainage follows the testicular veins. For metastases from the right testis, the sentinel nodes are those in the aortocaval chain at the level of the second lumbar vertebral body (*see* Fig. 4.53). For metastases from the left testis, the sentinel nodes are usually those in the left para-aortic nodal group just below the left renal vein (*see* Figs. 4.54 and 4.55). Some right-to-left crossover of lymphatic involvement may occur, following the normal drainage pathway to the cisterna chyli and thoracic duct (13 % of cases); however, metastases in contralateral nodes alone (without

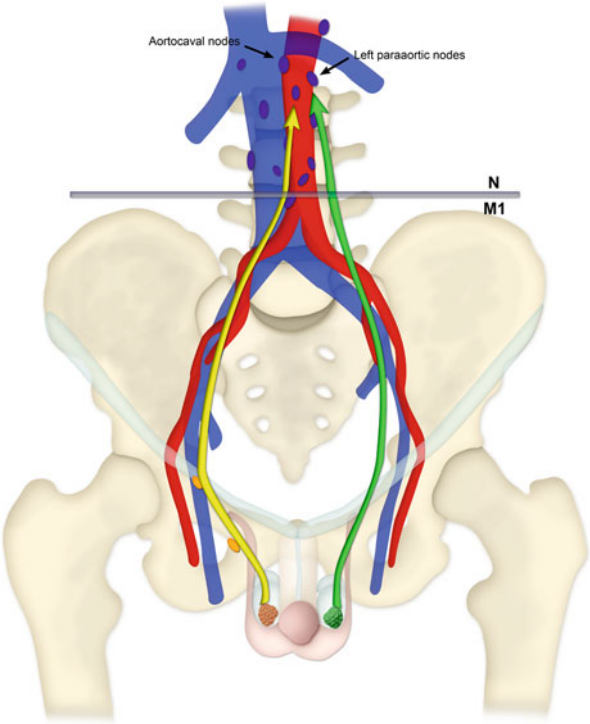

Fig. 4.52 Drawing shows common routes of nodal metastasis from testicular cancer along the para-aortic pathway. In metastases from the right testis (*yellow arrow*), the sentinel nodes are in the aortocaval chain at the level of the second lumbar vertebral body. In metastases from the left testis (*green arrow*), the sentinel nodes are usually the left para-aortic nodes located just inferior to the left renal vein

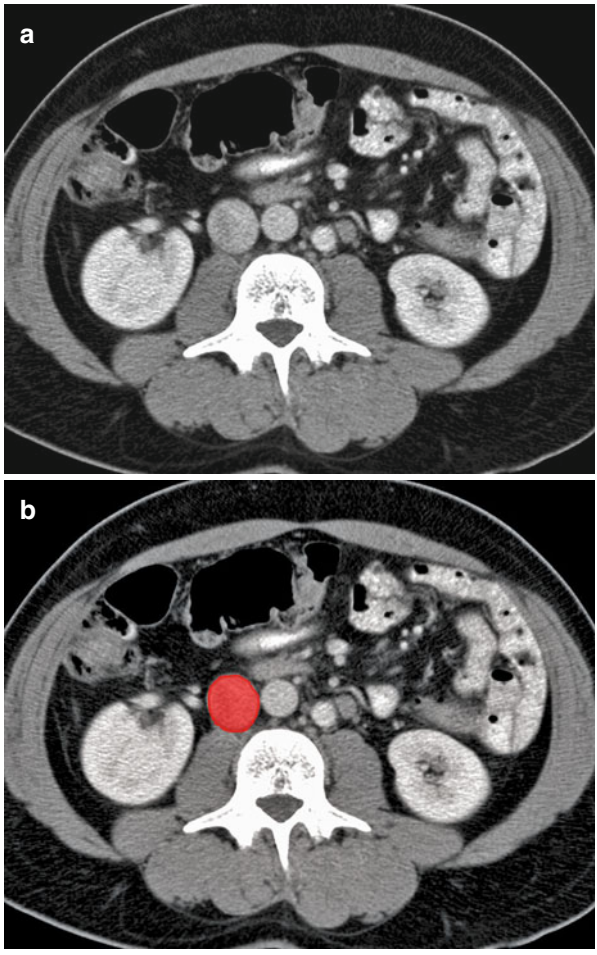

Fig. 4.53 (**a**, **b**) Axial CT image shows metastatic right para-aortic lymph node (*red*) in a patient with testicular cancer

involvement of the ipsilateral nodes) are rare (<2 % of cases). From the thoracic duct, a tumor can spread to the left supraclavicular nodes and subsequently to the lungs. Left-to-right crossover also can occur (20 % of cases), but, as with right-to-left crossover, the presence of contralateral nodal metastases without involvement of the ipsilateral nodes is infrequent [20, 28, 29]. As the volume of the tumor increases, it may spread from the sentinel nodes to involve the common iliac, internal iliac and external iliac nodes. Tumors within the epididymis can spread directly to the external iliac nodes. After orchiectomy, the pelvic and inguinal nodes should be assessed as regional nodes because the normal lymphatic drainage pathways are disrupted by surgery.

The importance of nodal metastasis is integral to the management of testicular cancer. N stage (Table 4.6) subdivides overall stage II disease into IIA, IIB, and IIC on the basis of the presence of N1, N2, and N3 disease, respectively. In patients with

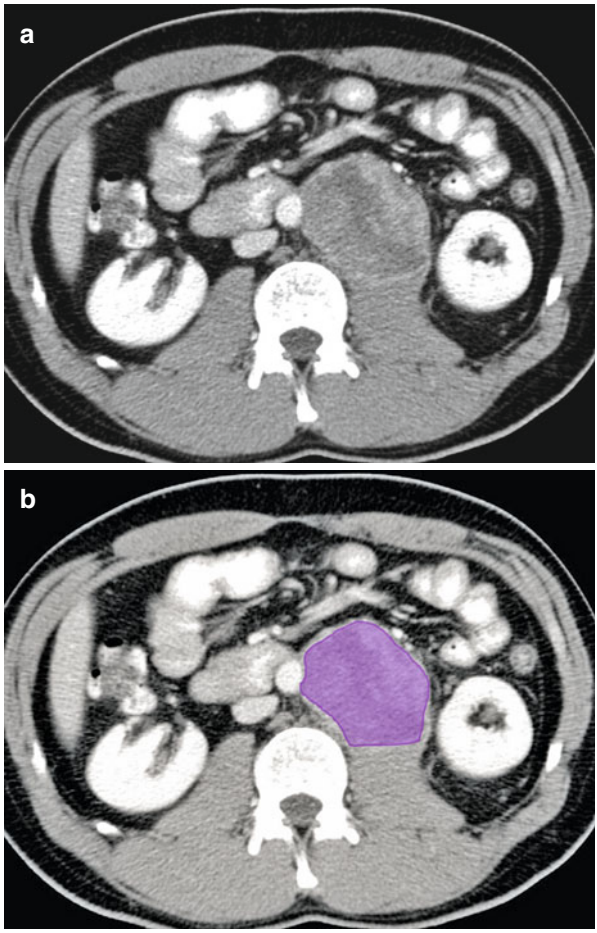

Fig. 4.54 (**a**, **b**) Axial CT image shows metastatic left para-aortic lymph node (*purple*) in a patient with testicular cancer

seminomas, stage IIA and IIB disease, including that in ipsilateral iliac nodes, can be treated with infradiaphragmatic EBRT. For stage IIC (nodes >5 cm) and III seminomas, systemic chemotherapy is advocated, with further management dependent on treatment response. For stage IIA or IIB nonseminomatous germ cell tumors, treatment options include chemotherapy followed by retroperitoneal lymph node dissection. Stage IIC (nodes >5 cm) and III (including nonregional nodal metastasis) nonseminomatous germ cell tumors are primarily treated with chemotherapy, with entry into clinical trials considered for stage IIIC disease [10].

Reported sensitivity and specificity of CT for detection of nodal metastases vary widely (65–96 % and 85–100 %, respectively) and may depend on the nodal size criterion used [30]. MR imaging of the abdomen and pelvis may not provide any additional information beyond that obtained with CT. Higher accuracy in the detection of residual tumor tissue is reported to be achievable with the use of FDG-PET than with CT [31].

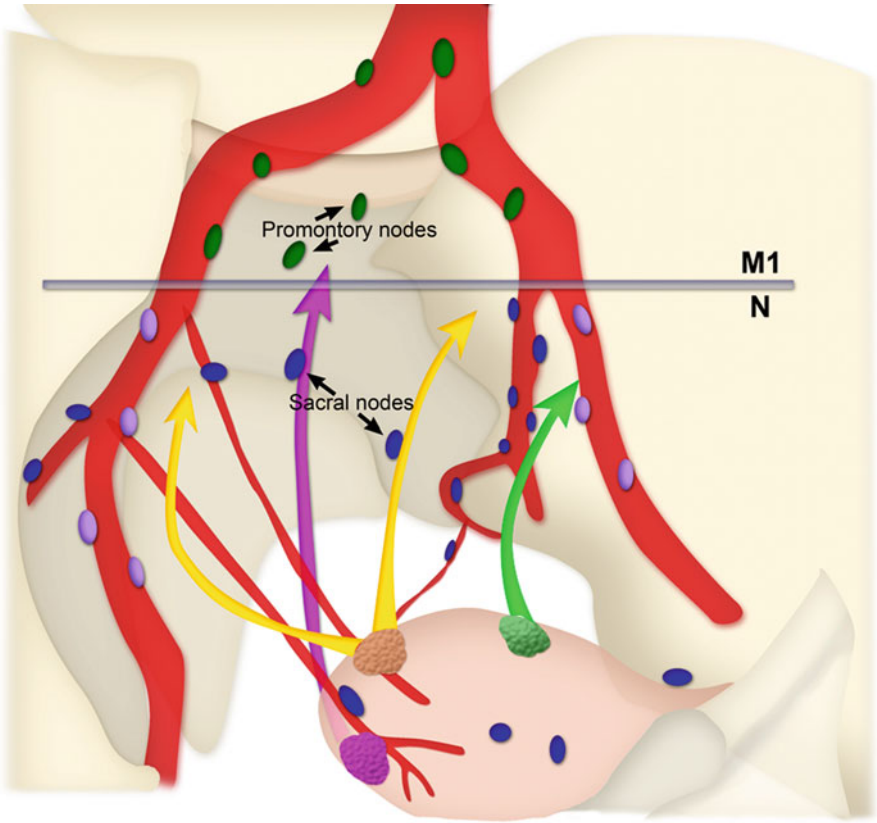

Fig. 4.55 Schematic shows common routes of metastasis from bladder cancer along lymphatic drainage pathways in the pelvis. Cancers in the bladder fundus metastasize mainly via an anterior route (*yellow arrows*), whereas those in upper or lower lateral parts of the bladder can metastasize via a lateral route (*green arrow*) directly to the external iliac (*purple*) nodes. Cancer in the bladder neck metastasizes via the presacral route (*pink arrow*)

Table 4.6 N-stage classification for testicular cancer

Stage	Findings
NX	Regional nodes cannot be assessed
N0	No regional nodal metastasis
N1	Metastasis in node or nodal mass <2 cm in greatest dimension; <5 nodes involved
N2	Metastasis in node or nodal mass >2 cm but <5 cm or >5 nodes involved, each <5 cm
N3	Metastasis in lymph node or nodal mass >5 cm in greatest dimension

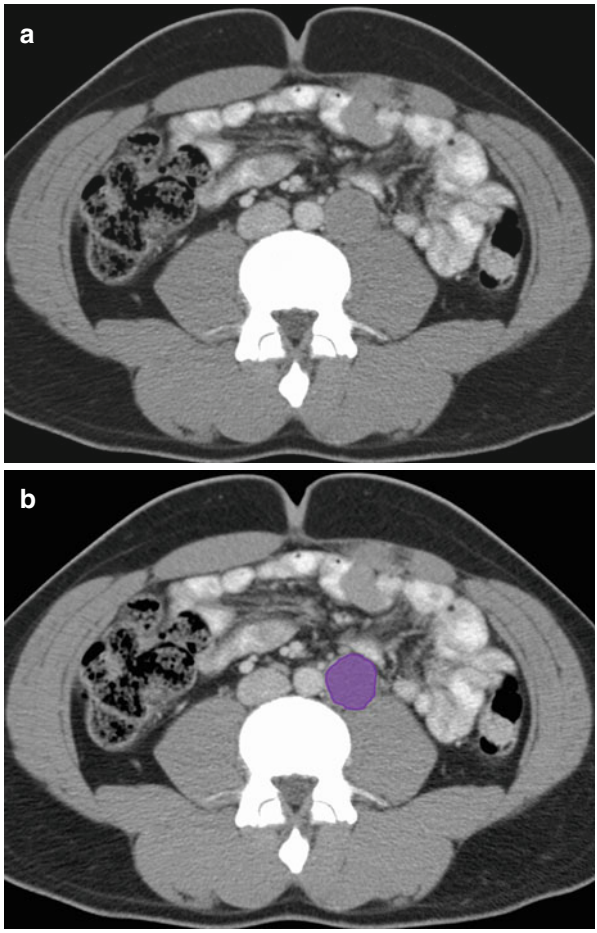

Fig. 4.56 (**a**, **b**) Axial CT image shows metastatic left para-aortic lymph node (*purple*) in a patient with testicular cancer

Bladder Cancer

Bladder cancer is the sixth most prevalent malignancy in the United States [32]. A major adverse prognostic feature is the presence of any nodal metastases. The 3-year survival rate among patients with involvement of a solitary node is about 50 %, but the rate decreases to about 25 % when multiple nodes are involved. By contrast, the 3-year survival rate among patients with no detectable nodal involvement is about 70 % [33–35].

Bladder cancer commonly spreads via a pelvic pathway (*see* Fig. 4.56). The specific route of nodal metastasis may vary according to the site of the primary cancer. If the tumor is located in the fundus (*i.e.*, the base or posterior wall) of the bladder, the preferential sites of metastasis are the obturator and internal iliac nodes, which are reached via an anterior route; tumors in the upper and lower lateral parts of the bladder

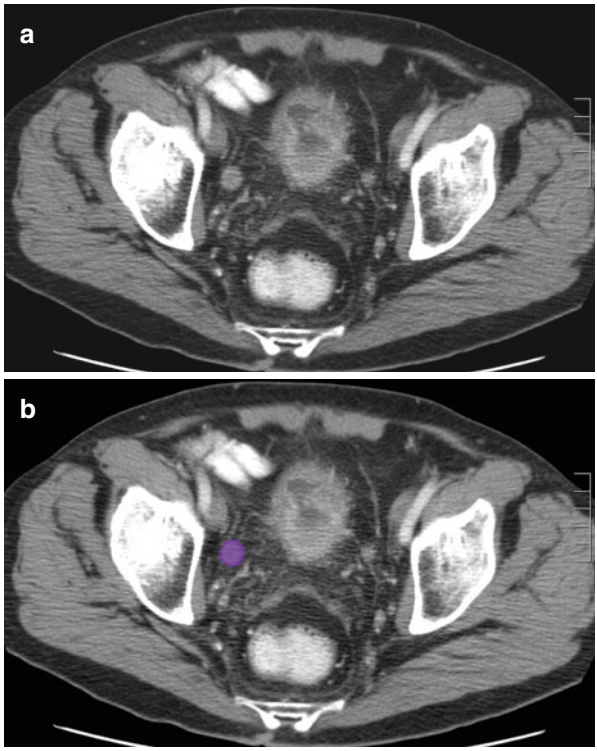

Fig. 4.57 (**a**, **b**) Axial CT image in a patient with bladder cancer shows metastatic right external iliac lymph node (*purple*)

may directly metastasize to the external iliac nodes via a lateral route (*see* Figs. 4.57, 4.58 and 4.59); and bladder neck cancers may metastasize via a presacral route to the presacral nodes and, from there, to the common iliac nodes [19, 20].

Nodal metastasis from bladder cancer most commonly occurs in the obturator and internal iliac nodes. If these nodes are free of tumor, nodal metastasis to more cranial node groups is extremely unlikely [34]. Four additional points should be kept in mind when categorizing nodal metastases from bladder cancer: first, the laterality of enlarged regional nodes does not affect their classification as N lesions (Table 4.1). Second, the involvement of common iliac lymph nodes is considered indicative of M1 disease (Table 4.1) (*see* Fig. 4.60). Third, the maximum diameter (not the maximum short-axis diameter) of the largest regional node determines the N classification (Table 4.7). Last, the presence of any nodal metastases is regarded as an indicator of stage IV disease (Table 4.7).

In patients with bladder carcinoma, multidetector CT is the imaging technique of choice for disease staging, although MR imaging is also useful for assessing local invasion and detecting metastases to obturator and presacral nodes. By contrast, FDG-PET is of limited value because the radiotracer is excreted into the urinary bladder [1].

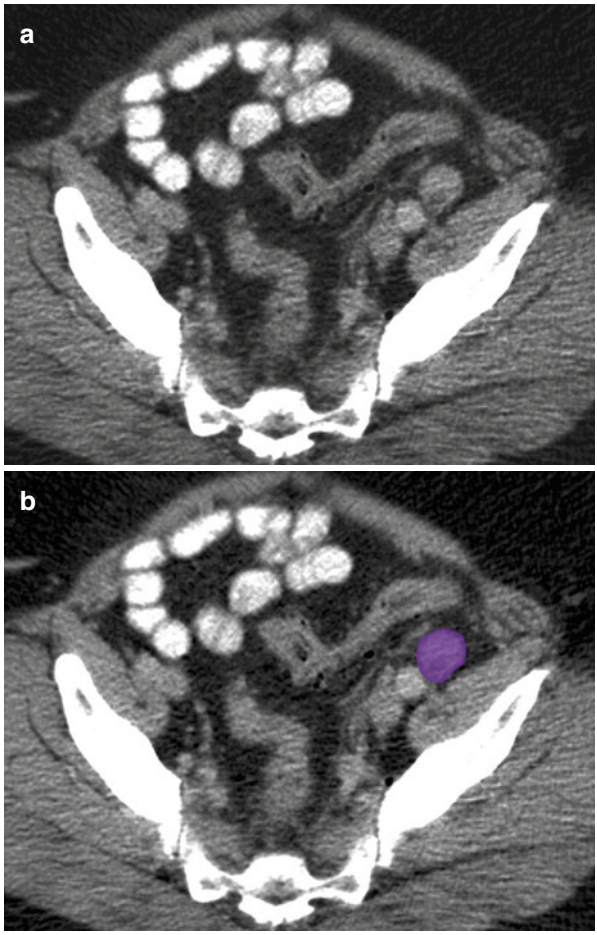

Fig. 4.58 (**a**, **b**) Axial CT image in a patient with bladder cancer shows metastatic left external iliac lymph node (*purple*)

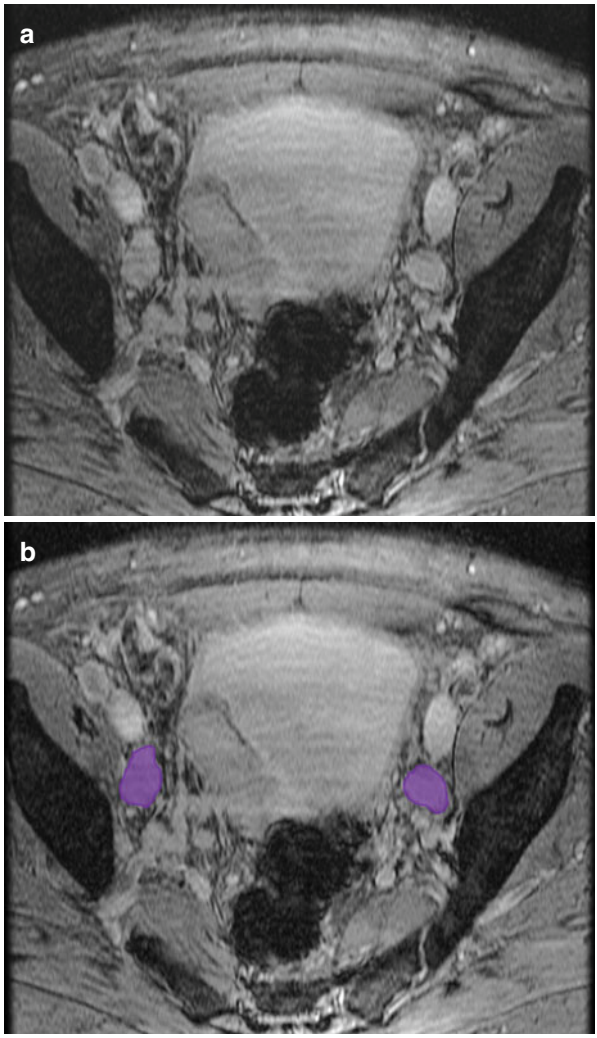

Fig. 4.59 (**a**, **b**) Axial T2-weighted gradient echo image shows bilateral external iliac lymph nodes (*purple*) in a patient with primary bladder cancer

Table 4.7 N-stage classification for bladder cancer

Stage	Findings
NX	Regional nodes cannot be assessed
N0	No regional nodal metastasis
N1	Single node metastasis <2 cm in greatest dimension
N2	Single node metastasis 2–5 cm or multiple node metastasis <5 cm in greatest dimension
N3	Metastasis in a single nodal >5 cm in greatest dimension

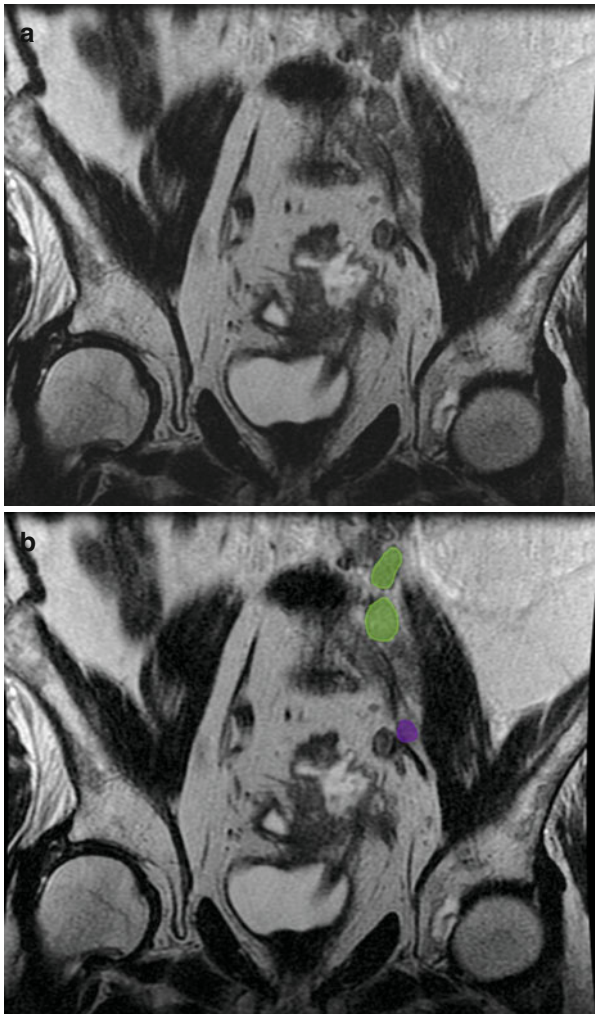

Fig. 4.60 (**a**, **b**) Coronal T2-weighted MRI showing ascending metastatic adenopathy in a patient with bladder cancer within a diverticulum. Metastatic nodes are seen in left external iliac (*purple*) and left common iliac lymph nodes (*green*)

References

1. Meyers MA, Charnsangavej C, Oliphant M. Meyers' dynamic radiology of the abdomen: normal and pathologic anatomy. New York: Springer; 2010.
2. Park JM, Charnsangavej C, Yoshimitsu K, Herron DH, et al. Pathways of nodal metastasis from pelvic tumors: CT demonstration. Radiographics. 1994;14:1309–21.
3. Fukuya T, Honda H, Hayashi T, et al. Lymph-node metastases: efficacy for detection with helical CT in patients with gastric cancer. Radiology. 1995;197:705–11.
4. Brown G, Richards CJ, Bourne MW, et al. Morphologic predictors of lymph node status in rectal cancer with use of high-spatial-resolution MR imaging with histopathologic comparison. Radiology. 2003;227:371–7.
5. Bipat S, Fransen GA, Spijkerboer AM, et al. Is there a role for magnetic resonance imaging in the evaluation of inguinal lymph node metastases in patients with vulva carcinoma? Gynecol Oncol. 2006;103:1001–6.
6. Ghurani GB, Penalver MA. An update on vulvar cancer. Am J Obstet Gynecol. 2001;185:294–9.
7. Klerkx WM, Bax L, Veldhuis WB, et al. Detection of lymph node metastases by gadolinium-enhanced magnetic resonance imaging: systematic review and meta-analysis. J Natl Cancer Inst. 2010;102:244–53.
8. Parikh S, Beriwal S. The integration of 3D imaging with conformal radiotherapy for vulvar and vaginal cancer. In: Viswanathan AN, Kirisits C, Erickson BE, Pötter RB, editors. Gynecologic radiation therapy. Berlin/Heidelberg: Springer; 2011. p. 85–95. Available from http://www.springerlink.com/content/q2357m067836822t.
9. Selman TJ, Luesley DM, Acheson N, et al. A systematic review of the accuracy of diagnostic tests for inguinal lymph node status in vulvar cancer. Gynecol Oncol. 2005;99:206–14.
10. McMahon CJ, Rofsky NM, Pedrosa I. Lymphatic metastases from pelvic tumors: anatomic classification, characterization, and staging. Radiology. 2010;254:31–46.
11. Adams M, Jasani B. Cancer metastasis: biological and clinical aspects, gynaecological cancer. In: Jiang WG, Mansel RE, editors. Cancer metastasis, molecular and cellular mechanisms and clinical intervention. Dordrecht: Kluwer Academic Publishers; 2004. p. 381–420. Available from http://www.springerlink.com/content/p21234wx75477150.
12. Berek JS, Hacker NF. Practical gynecologic oncology. Philadelphia: Lippincott Williams & Wilkins; 2005.
13. Narayanan P, Lyngkaran T, Sohaib SA, et al. Pearls and pitfalls of MR lymphography in gynecologic malignancy. Radiographics. 2009;29:1057–69.
14. Lai G, Rockall AG. Lymph node imaging in gynecologic malignancy. Semin Ultrasound CT MRI. 2010;31:363–6.
15. Mironov S, Akin O, Pandit-Taskar N, Hann LE. Ovarian cancer. Radiol Clin North Am. 2007;45:149–66.
16. Ricke J, Sehouli J, Hach C, et al. Prospective evaluation of contrast-enhanced MRI in the depiction of peritoneal spread in primary or recurrent ovarian cancer. Eur Radiol. 2003;13:943–9.
17. Bristow RE, Giuntoli 2nd RL, Pannu HK, et al. Combined PET/CT for detecting recurrent ovarian cancer limited to retroperitoneal lymph nodes. Gynecol Oncol. 2005;99:294–300.
18. Paño B, Sebastià C, Buñesch L, et al. Pathways of lymphatic spread in male urogenital pelvic malignancies. Radiographics. 2011;31:135–60.
19. Park JM, Charnsangavej C, Yoshimitsu K, et al. Pathways of nodal metastasis from pelvic tumors: CT demonstration. Radiographics. 1994;14:1309–21.
20. Morisawa N, Koyama T, Togashi K. Metastatic lymph nodes in urogenital cancers: contribution of imaging findings. Abdom Imaging. 2006;31:620–9.
21. Weckermann D, Holl G, Dorn R, et al. Reliability of preoperative diagnostics and location of lymph node metastases in presumed unilateral prostate cancer. BJU Int. 2007;99:1036–40.
22. Picchio M, Treiber U, Beer AJ, et al. Value of 11C-choline PET and contrast-enhanced CT for staging of bladder cancer: correlation with histopathologic findings. J Nucl Med. 2006;47:938–44.

23. Albers P, Bender H, Yilmaz H, et al. Positron emission tomography in the clinical staging of patients with stage I and II testicular germ cell tumors. Urology. 1999;53:808–11.
24. Singh AK, Saokar A, Hahn PF, Harisinghani MG. Imaging of penile neoplasms. Radiographics. 2005;25:1629–38.
25. Misra S, Chaturvedi A, Misra NC. Penile carcinoma: a challenge for the developing world. Lancet Oncol. 2004;5:240–7.
26. Ravizzini GC, Wagner M, Borges-Neto S. Positron emission tomography detection of metastatic penile squamous cell carcinoma. J Urol. 2001;165:1633–4.
27. Young RH. Testicular tumors – some new and a few perennial problems. Arch Pathol Lab Med. 2008;132:548–64.
28. Woodward PJ, Sohaey R, O'Donoghue MJ, Green DE. From the archives of the AFIP: tumors and tumorlike lesions of the testis: radiologic-pathologic correlation. Radiographics. 2002;22:189–216.
29. Ray B, Hajdu SI, Whitmore Jr WF. Proceedings: distribution of retroperitoneal lymph node metastases in testicular germinal tumors. Cancer. 1974;33:340–8.
30. Hilton S, Herr HW, Teitcher JB, et al. CT detection of retroperitoneal lymph node metastases in patients with clinical stage I testicular nonseminomatous germ cell cancer: assessment of size and distribution criteria. AJR Am J Roentgenol. 1997;169:521–5.
31. Lont AP, Horenblas S, Tanis PJ, et al. Management of clinically node negative penile carcinoma: improved survival after the introduction of dynamic sentinel node biopsy. J Urol. 2003;170:783–6.
32. Sharma S, Ksheersagar P, Sharma P. Diagnosis and treatment of bladder cancer. Am Fam Physician. 2009;80:717–23.
33. Husband JE. CT/MRI of nodal metastases in pelvic cancer. Cancer Imaging. 2002;2:123–9.
34. Abol-Enein H, El-Baz M, Abd El-Hameed MA, et al. Lymph node involvement in patients with bladder cancer treated with radical cystectomy: a patho-anatomical study – a single center experience. J Urol. 2004;172:1818–21.
35. Barentsz JO, Jager GJ, van Vierzen PB, et al. Staging urinary bladder cancer after transurethral biopsy: value of fast dynamic contrast-enhanced MR imaging. Radiology. 1996;201:185–93.

Pitfalls and Mimics of Lymph Nodes on Imaging

5

The important therapeutic and prognostic significance of lymph nodes in patients with cancer mandates accurate identification of lymph node involvement before commencing therapeutic approach. Anatomical approximation of different structures and anatomical variants can pose significant diagnostic dilemmas due to difficulty in delineating lymph nodes. In this section, we highlight these pitfalls and also focus on the characteristic appearance of the nodes.

Structures That Can Mimic a Lymph Node on Imaging

1. Bowel loops when not opacified with positive oral contrast agent (*see* Fig. 5.1) may be mistaken for lymph node [1].
2. Nodular and prominent diaphragmatic crura can imitate retrocrural or upper abdominal lymph node masses (*see* Fig. 5.2) [2].
3. Collateral vessels in the lienorenal or gastrohepatic regions region can appear like a conglomerate of lymph nodes on early enhanced or plain scans (*see* Figs. 5.3 and 5.4).
4. Paraesophageal varices can appear as enlarged lymph nodes (*see* Fig. 5.5) [3].
5. Cisterna chyli may appear as hypodense (water density) retrocrural lesion on CT imaging and can be mistaken for hypodense retrocrural lymph nodes (*see* Fig. 5.6).
6. Phleboliths (calcified veins) can mimic lymph nodes especially on MR scans. They are seen in the pelvis adjacent to the bladder and usually appear homogenously dark on T2-weighted images owing to susceptibility (*see* Fig. 5.7).
7. Renal or ureteric calculi sometimes can be confused with mesenteric lymph node calcification on plain radiographs [4].
8. Papillary process of the liver is the medial extension of the caudate lobe and can be mistaken for enlarged porta hepatis lymph nodes when it is oriented in the semicoronal plane (*see* Fig. 5.8); however, continuity with the caudate lobe helps differentiate the two [5].

M.G. Harisinghani, (ed.), *Atlas of Lymph Node Anatomy*,
DOI 10.1007/978-1-4419-9767-8_5, © Springer Science+Business Media New York 2013

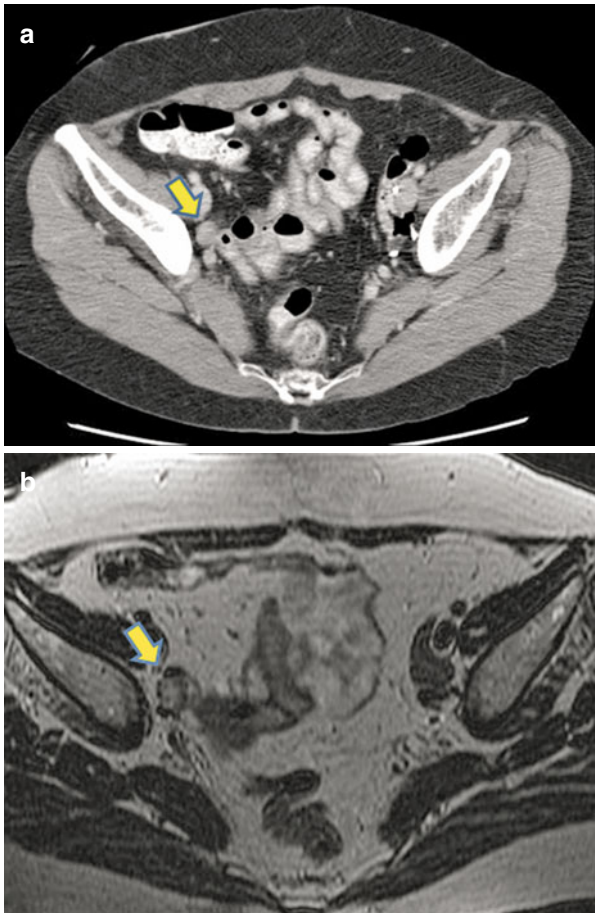

Fig. 5.1 Nonopacified bowel loop mimicking a lymph node. (**a**) Axial contrast-enhanced CT shows an ovoid lesion (*arrow*) in expected location of external iliac nodal location. (**b**) Axial T2-weighted MR in same patient shows the lesion to represent a bowel loop (*arrow*)

9. Small pulmonary nodules cannot be easily distinguished from intraparenchymal pulmonary lymph node (*see* Fig. 5.9) [6].
10. Mediastinal neural lesions can mimic lymph nodes [7].
11. Intrathoracic extension of the thyroid can mimic anterior mediastinal lymph node (*see* Fig. 5.10) [7].
12. Ectopic parathyroid adenoma can mimic lymph nodes in the neck [7].
13. Soft tissue hemangioma can mimic nodal masses (*see* Fig. 5.11) [7].
14. Focal parathyroid adenoma or hyperplasia can mimic neck nodes. However, classic location of the adenoma is the clue to the diagnosis (*see* Fig. 5.12) [7].
15. Extramedullary hematopoiesis can mimic mediastinal adenopathy [2].
16. Pericardial recesses can be mistaken for mediastinal lymph nodes (*see* Fig. 5.13); however, the cystic content, nonenhancement, and anatomical location are clues to differentiate the two [8].

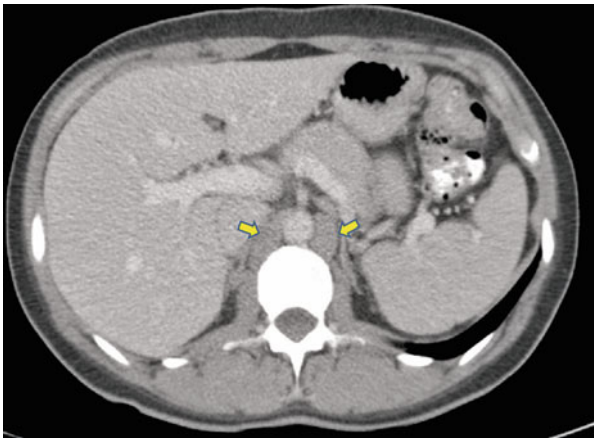

Fig. 5.2 Bilateral prominent diaphragmatic crura (*arrows*) that may mimic lymph nodes

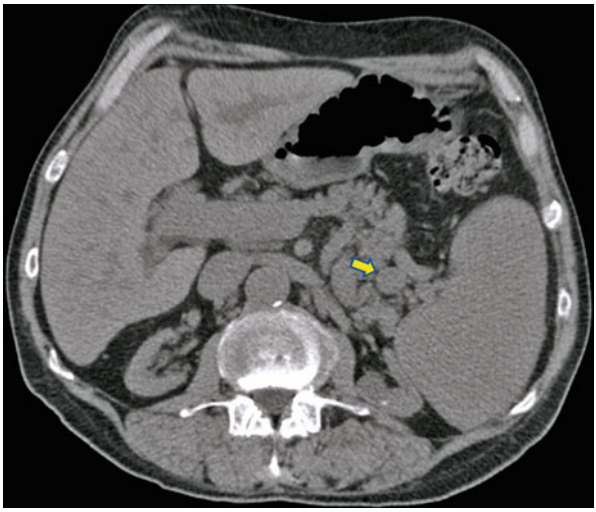

Fig. 5.3 Axial noncontrast CT scan shows nonopacified collateral vessel (*arrow*) in lienorenal region that may mimic lymph nodes

17. The scalene muscles that appear asymmetrical can mimic lymph nodes in the supraclavicular or lower neck location (*see* Fig. 5.14).
18. Bowel adhesion and close proximity of bowel to the inferior vena cava (IVC) and aorta can mimic adenopathy (*see* Fig. 5.15).
19. Mediastinal bronchogenic cysts can mimic mediastinal lymph nodes in pediatric patients (*see* Fig. 5.16) [2].
20. Foreign body granuloma mimicking axillary lymphadenopathy in a breast cancer patient [9].
21. Poorly opacified or nonenhanced vessels: tortuous vessels may be confused for lymph nodes on noncontrast images. This is especially seen when performing

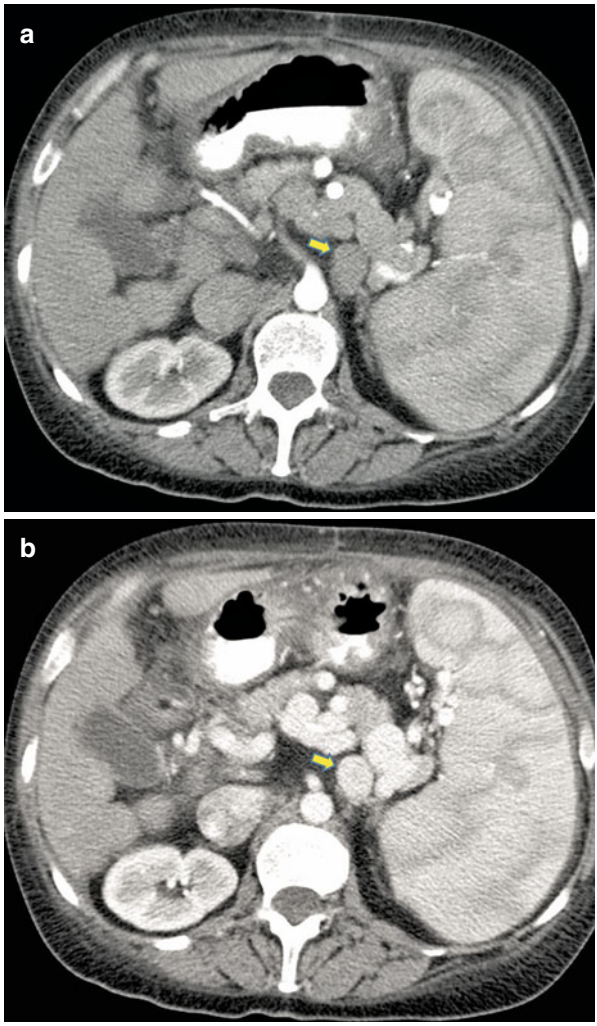

Fig. 5.4 (**a**) Axial contrast-enhanced early arterial phase CT shows splenic hilar collateral vessels (*arrow*) that may appear as nodal mass. Delayed arterial phase (**b**) shows opacification of the vessel (*arrow*) and confident diagnosis of non-nodal etiology

magnetic resonance imaging (MRI) for staging pelvic malignancies (*see* Fig. 5.17) [10, 11]. Evaluating the enhanced series helps differentiate nodes from vessels.

22. Localized hemorrhage when focal can mimic a lymph node [12].
23. Accessory spleen or splenule can mimic a lymph node (*see* Fig. 5.18) [13].
24. Ovary can be mistaken for pelvic side wall lymph node specifically in the luteal phase (*see* Fig. 5.19) [14]. Following the ovarian vein to the ovary may be useful for correct identification.
25. Undescended testis may be mistaken for lymph nodes within the pelvis (*see* Fig. 5.20) [15].

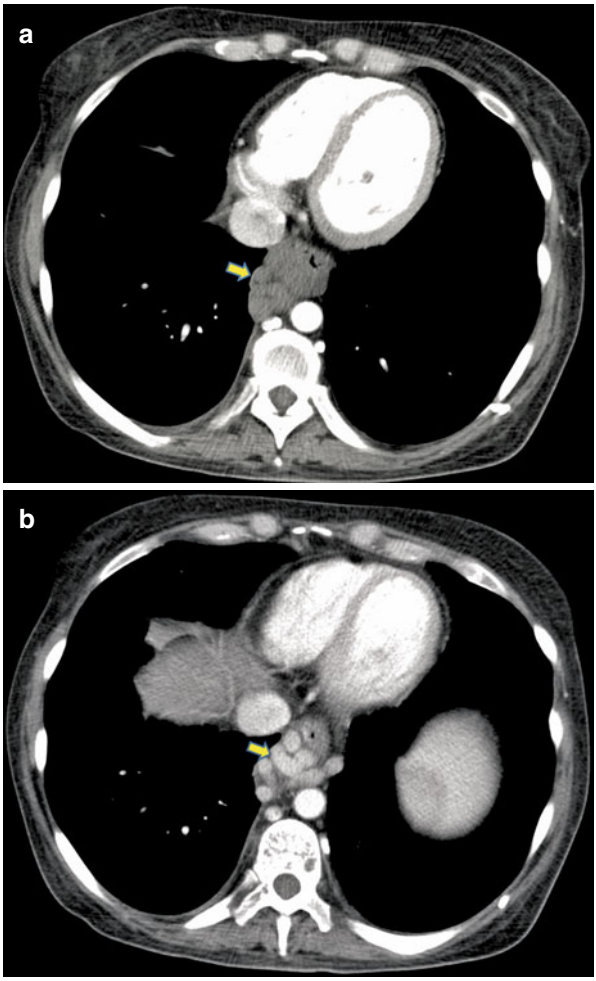

Fig. 5.5 Paraesophageal varices can mimic lymph nodes. (**a**) Early arterial phase shows nonopacification of the varicosities (*arrow*). (**b**) Delayed scan shows filling of the varices (*arrow*)

Commonly Overlooked Nodal Sites

The following nodal groups are commonly overlooked when there is diffuse involvement and not when they fall into the regional nodes category. The relevance is that it might affect the line of management.

(i) Retrocrural (*see* Fig. 5.21) and retrocaval
(ii) Internal mammary (*see* Fig. 5.22)
(iii) Pericardial/pericardiophrenic (*see* Fig. 5.23)
(iv) Adjacent to the gastroesophageal junction
(v) Internal iliac

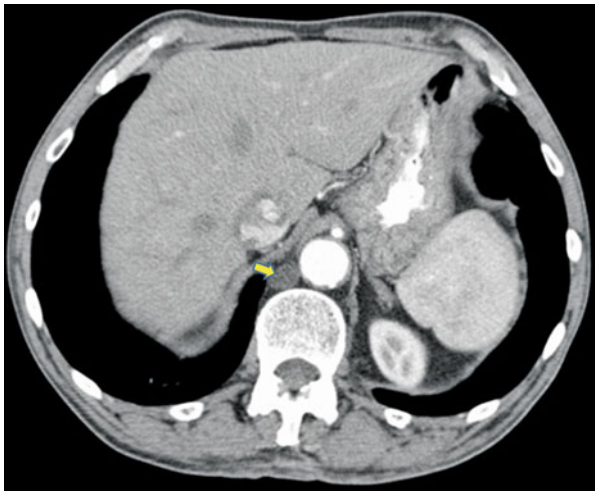

Fig. 5.6 Axial CT image showing low density retrocrural focal prominence of cisterna chyli (*arrow*)

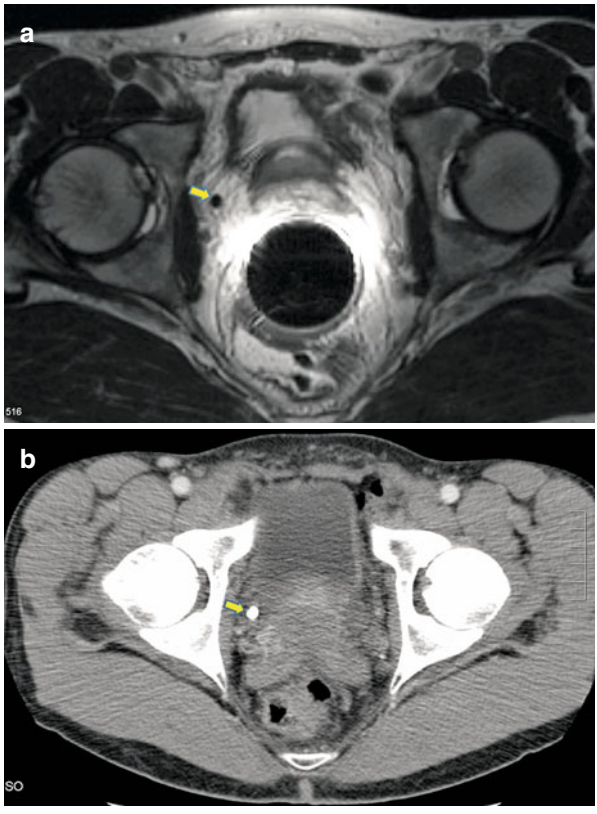

Fig. 5.7 Phleboliths mimicking lymph node on MRI. (**a**) Axial T2-weighted MRI in a patient with prostate cancer shows T2 dark focal lesion (*arrow*) to the right of the prostate. The clue is homogeneous dark signal on T2-weighted image, which is due to susceptibility from calcium. (**b**) Corresponding CT image in the same patient shows calcified phlebolith (*arrow*)

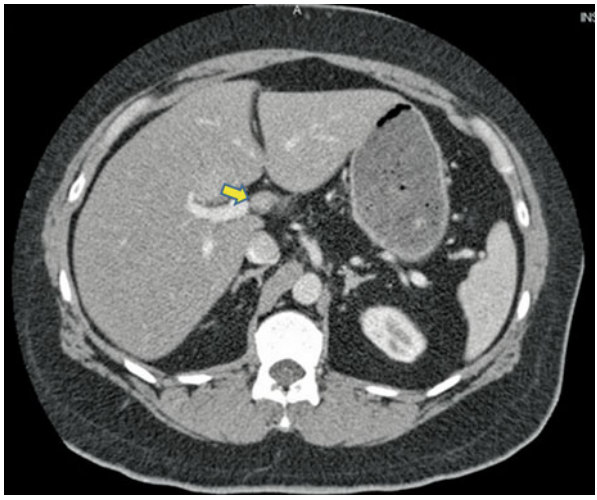

Fig. 5.8 Axial CT image of the upper abdomen shows prominent papillary process of liver (*arrow*) that may mimics peri-portal lymph node

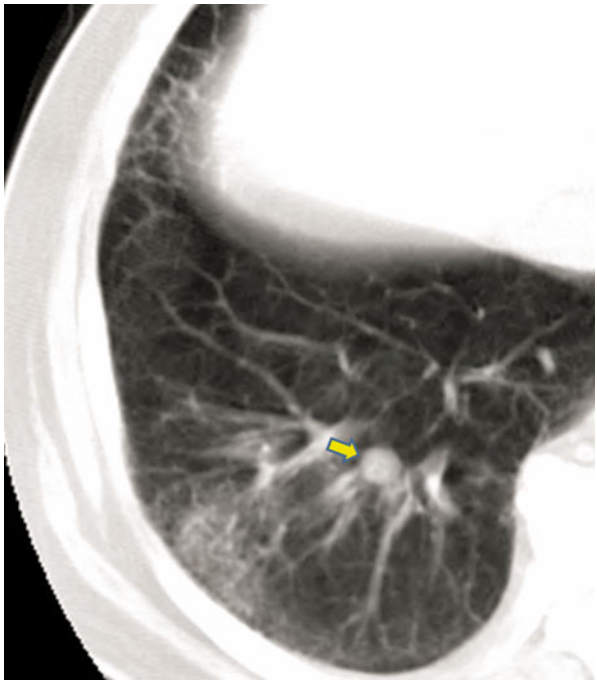

Fig. 5.9 Axial CT image showing an intraparenchymal lymph node (*arrow*)

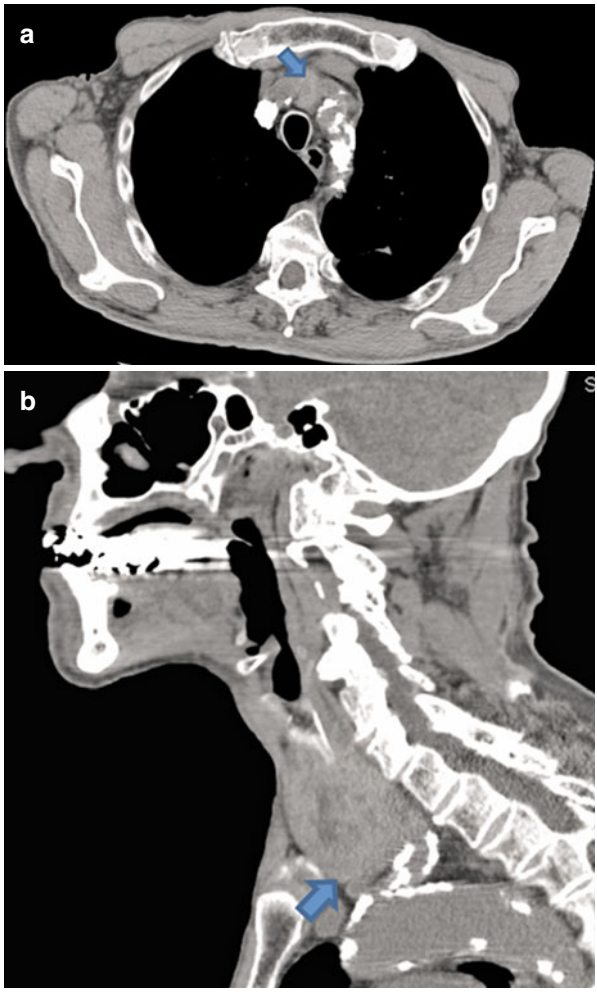

Fig. 5.10 (**a**) Axial CT image shows intrathoracic extension of the thyroid gland (*arrow*). (**b**) Sagittal image shows direct continuity with the thyroid gland (*arrow*)

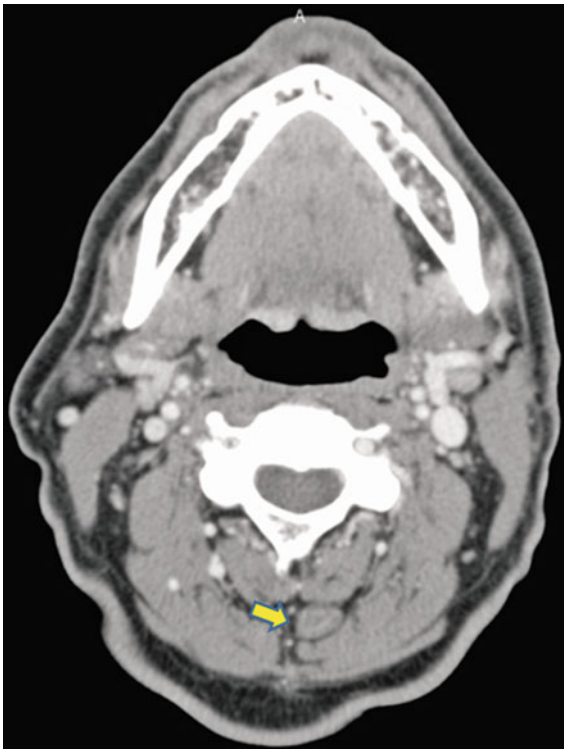

Fig. 5.11 Axial CT image showing a posterior cervical hemangioma (*arrow*) that may be mistaken for a cervical lymph node

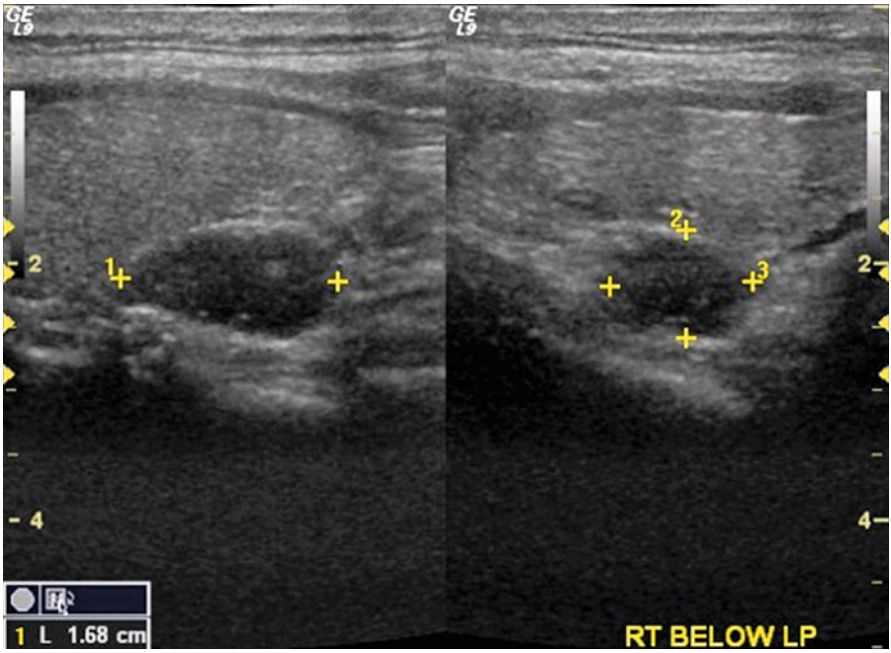

Fig. 5.12 Ultrasound image of the neck shows a hypoechoic lesion inferior to the thyroid; classic location for parathyroid adenoma should not be mistaken for a cervical lymph node

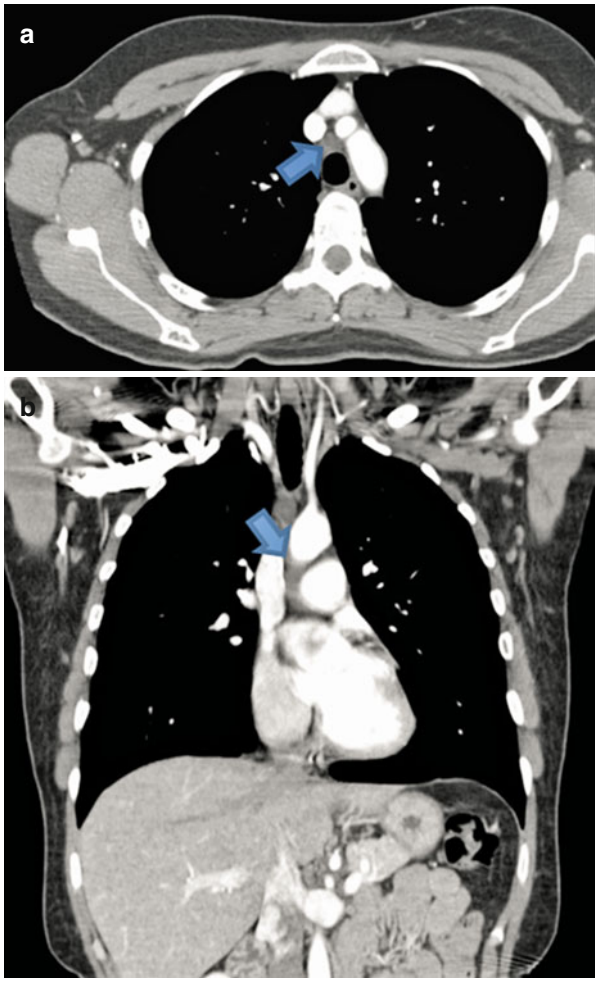

Fig. 5.13 Pericardial recess (*arrows*) as seen on axial (**a**) and coronal (**b**) CT images

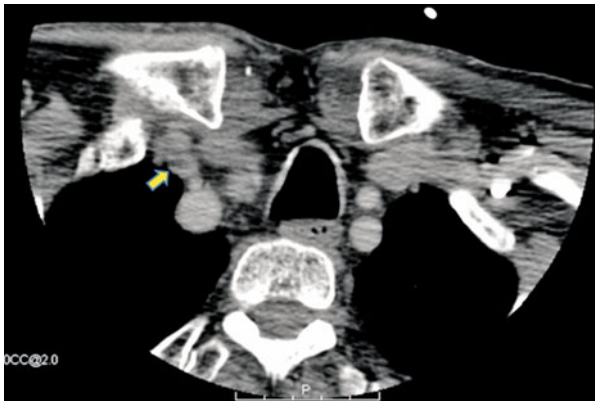

Fig. 5.14 Axial CT image showing asymmetric medial scalene muscle (*arrow*) that can mimic adenopathy

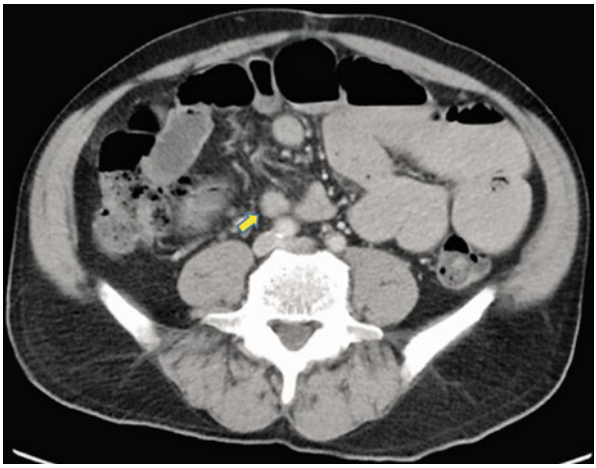

Fig. 5.15 Axial CT image showing close proximity of unopacified bowel (*arrow*) to the common iliac artery can mimic adenopathy. Careful attention to following the course of bowel will allow distinction from lymph nodes

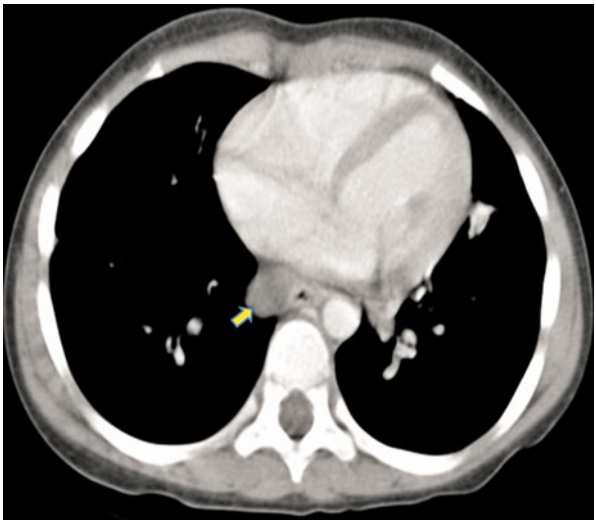

Fig. 5.16 Axial CT image shows low density bronchogenic cyst (*arrow*)

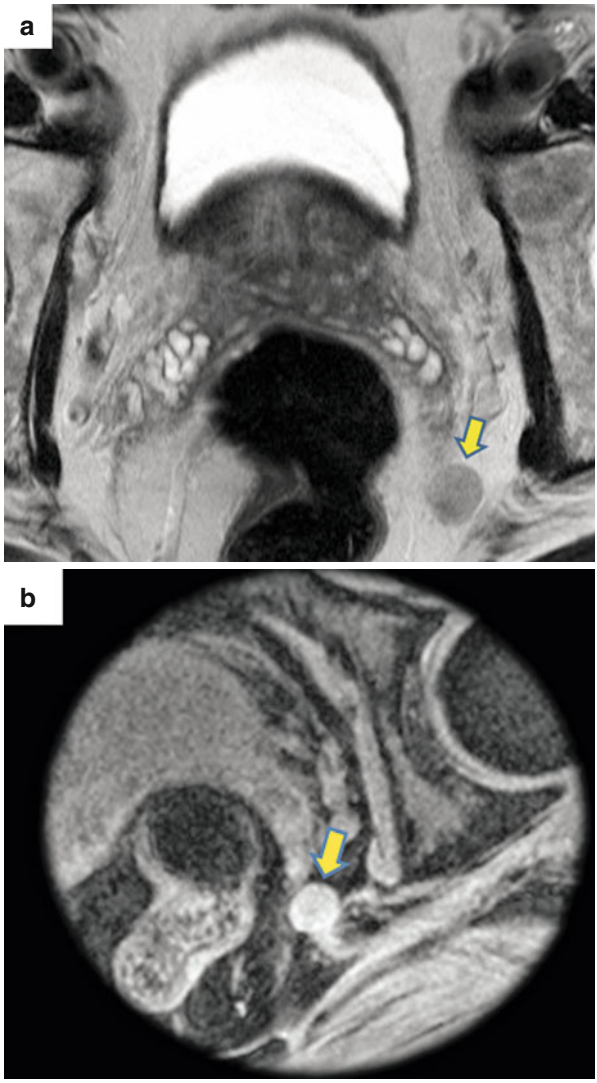

Fig. 5.17 (**a**) Axial T2-weighted image shows what looks like an enlarged internal iliac lymph node (*arrow*) in a patient with prostate cancer. Post-contrast T1-weighted images (**b**, **c**) show enhancement of this structure and continuity with internal iliac veins (*arrows*)

Fig. 5.17 (continued)

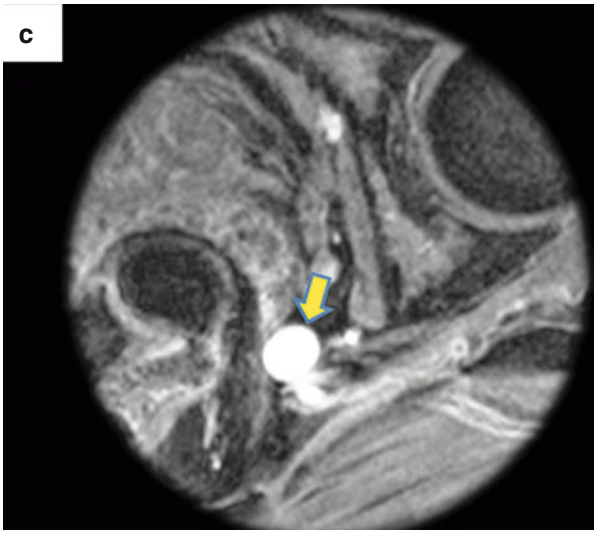

(vi) Retropharyngeal (node of Rouviere)
(vii) Femoral lymph nodes (*see* Fig. 5.24)

Missed Adenopathy on Imaging

1. Hypodense lymph nodes: they can be missed in the case of negative oral contrast administration.
    (i) The necrotic lymph nodes in malignancies like squamous carcinoma or germ cell tumors appear hypodense (*see* Fig. 5.25)
    (ii) In infectious condition such as Whipple's disease and mycobacterial tuberculosis (*see* Fig. 5.26) [2]
2. Small lymph nodes
3. Micrometastasis to lymph node

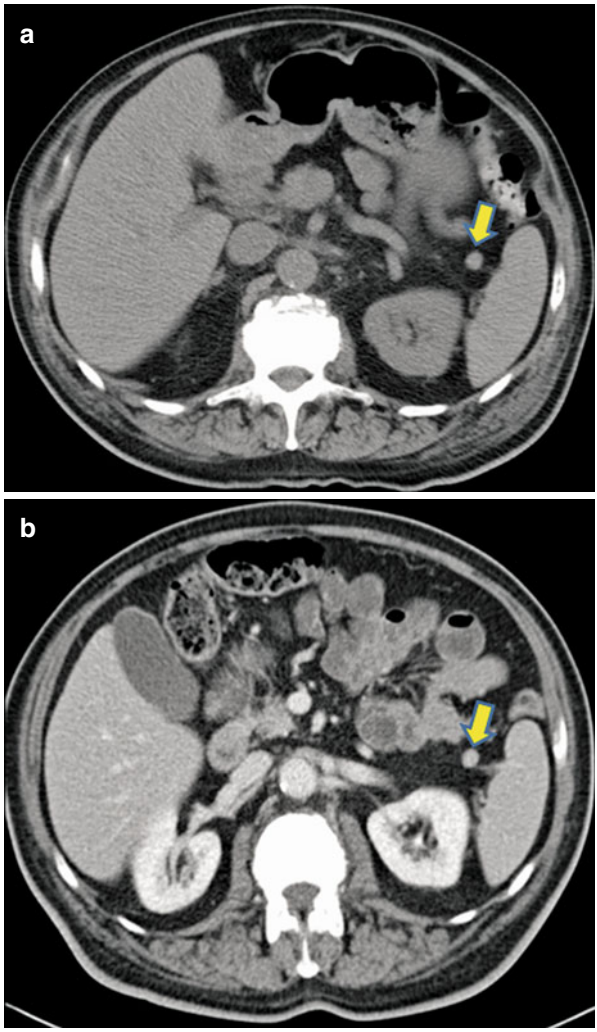

Fig. 5.18 Axial CT before (**a**) and after (**b**) intravenous contrast show presence of a small splenule (*arrow*) that can be confused for a lymph node

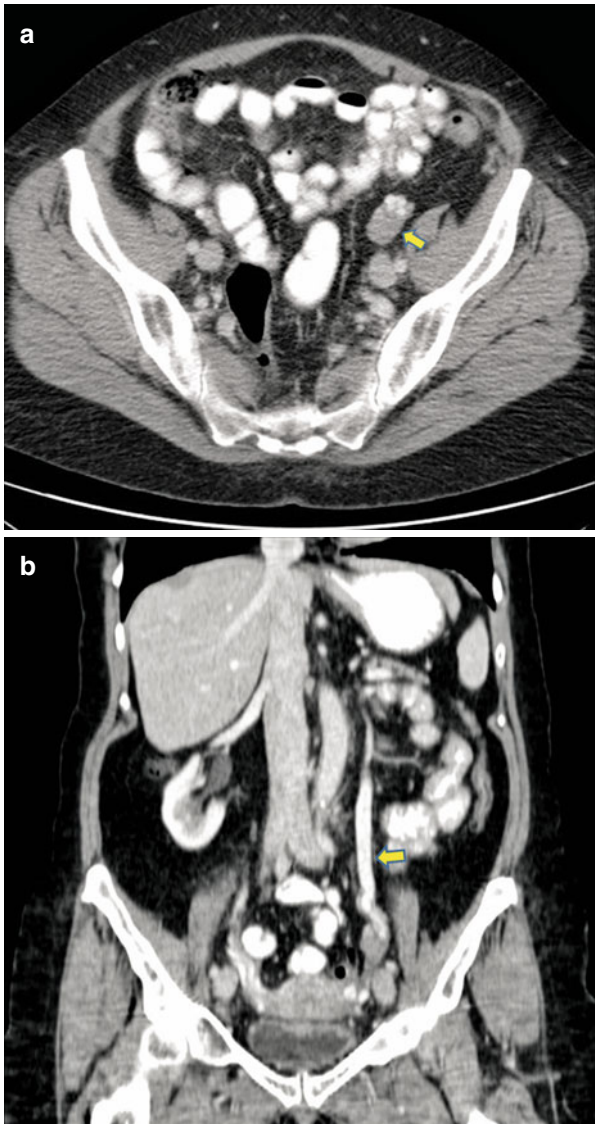

Fig. 5.19 Axial CT image (**a**) show left ovary (*arrow*) that can be mistaken for a pelvic side wall lymph node. Coronal reformatted image (**b**) shows left gonadal vein (*arrow*) that can be traced to the left ovary correctly identifying it as such

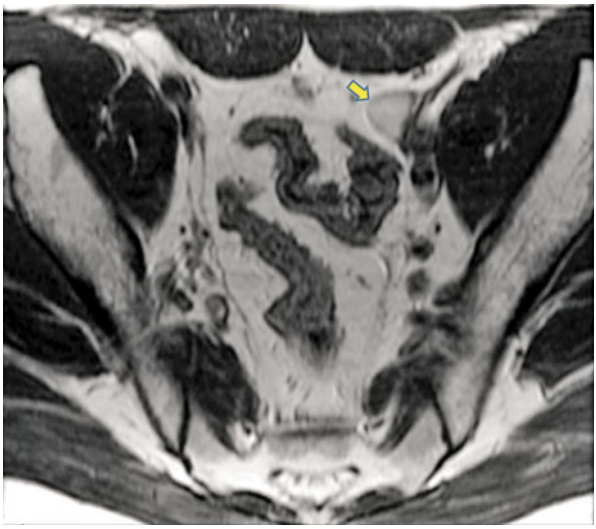

Fig. 5.20 Axial T2-weighted image show hyperintense undescended testis on the left (*arrow*) that can be mistaken for left pelvic lymph node

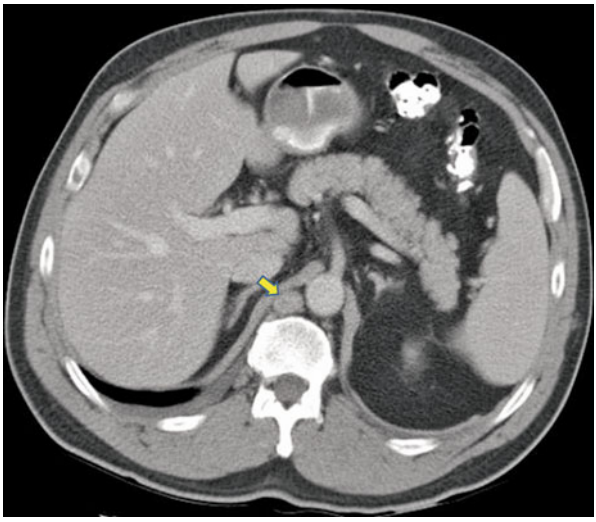

Fig. 5.21 Axial CT image shows enlarged right retrocrural lymph node (*arrow*) in a patient with metastatic lung cancer

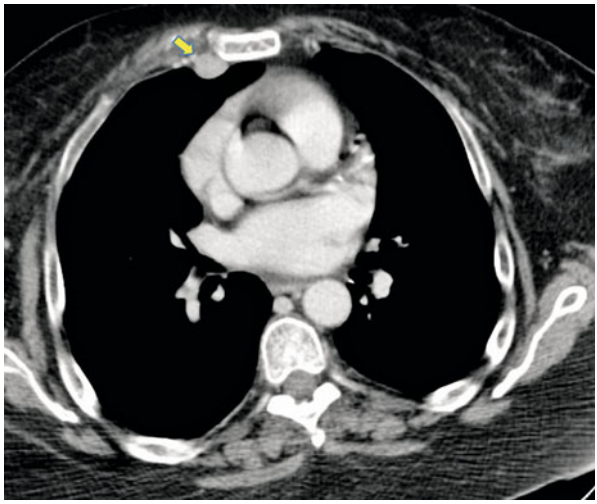

Fig. 5.22 Axial CT image shows enlarged right internal mammary lymph node (*arrow*) in a patient with breast cancer

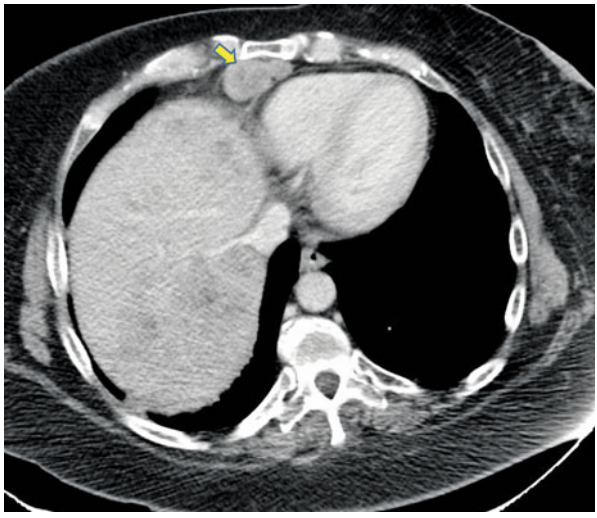

Fig. 5.23 Axial CT image shows enlarged right pericardial lymph node (*arrow*) in a patient with ovarian cancer

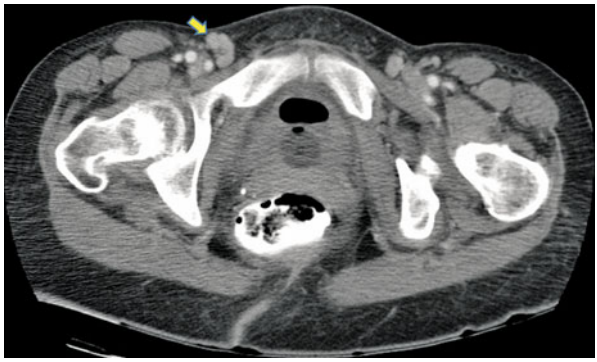

Fig. 5.24 Axial CT image shows enlarged right femoral node (*arrow*) in a patient with melanoma

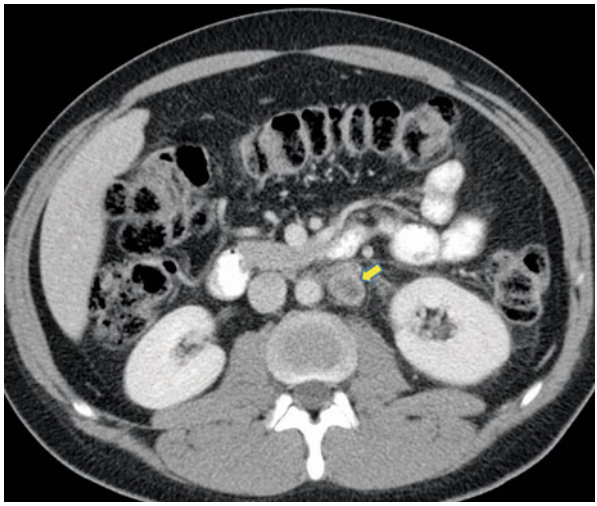

Fig. 5.25 Metastatic squamous cell carcinoma. Axial CT image shows enlarged left periaortic node (*arrow*) that shows central low density

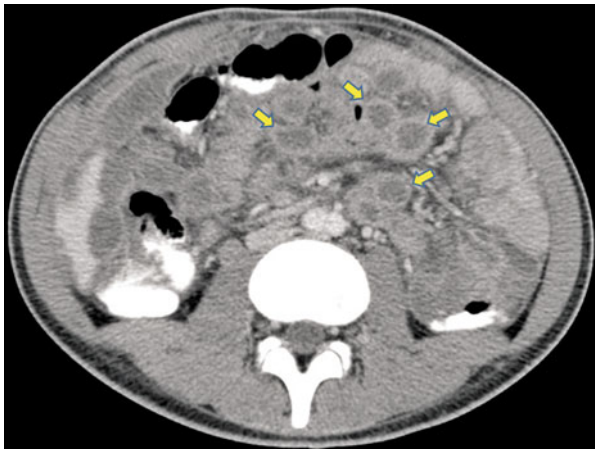

Fig. 5.26 Abdominal tuberculosis. Axial CT image shows multiple low density mesenteric lymph nodes (*arrows*)

Common Differential Diagnosis on Nodal Morphology

Characteristic appearance of lymph nodes:

Necrosis and cystic degeneration [2]:

(i) Germ cell tumor
(ii) Squamous cell cancer
(iii) Certain lymphomas and lymphoma post treatment
(iv) Infections such as *Mycobacterium tuberculosis* (MTB), *Mycobacterium avium-intracellulare* (MAI), fungal, Whipple's disease (*see* Fig. 5.27)

Enhancing [2]:

(i) Castleman's disease (*see* Fig. 5.28)
(ii) Melanoma
(iii) Carcinoid
(iv) Renal cell carcinoma
(v) Papillary cancer of thyroid
(vi) Kaposi's sarcoma (*see* Fig. 5.29)
(vii) Tuberculosis

Internal calcification [2]:

(i) Mucinous adenocarcinoma (*see* Fig. 5.30)
(ii) Papillary cancer of thyroid
(iii) Old granulomatous disease (*see* Fig. 5.31)
(iv) Sarcoidosis
(v) Silicosis
(vi) Amyloidosis
(vii) Osteosarcoma
(viii) Pneumocystis carinii
(ix) Lymphoma post radiation
(x) Bronchogenic carcinoma

Nonmalignant conditions leading to fludeoxyglucose (FDG) avid lymph nodes:

(i) Sarcoidosis (*see* Fig. 5.32)
(ii) Tuberculosis
(iii) Nodes draining sites of infection, inflammation, abscess (*see* Fig. 5.33)

Filling defect in lymph node on lymphangiogram [16]:

Common
(i) Granulomatous disease (*e.g.*, sarcoidosis; tuberculosis; fungus disease)
(ii) Idiopathic
(iii) Lymphoma
(iv) Metastatic neoplasm (*e.g.*, carcinoma; melanoma; sarcoma)

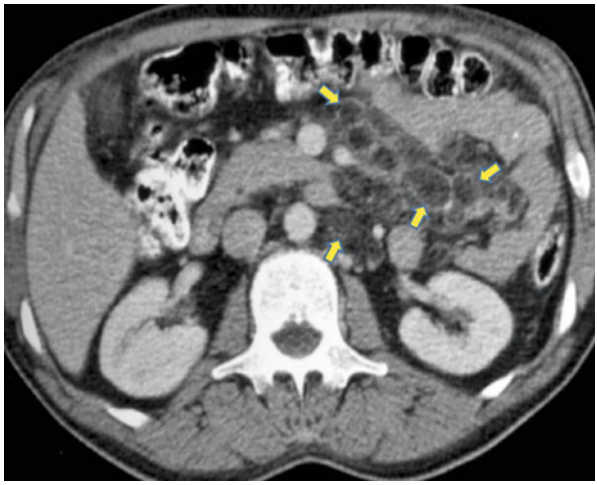

Fig. 5.27 Whipple's disease. Axial CT image shows multiple low attenuating (fat density) lymph nodes (*arrows*) within the mesentry

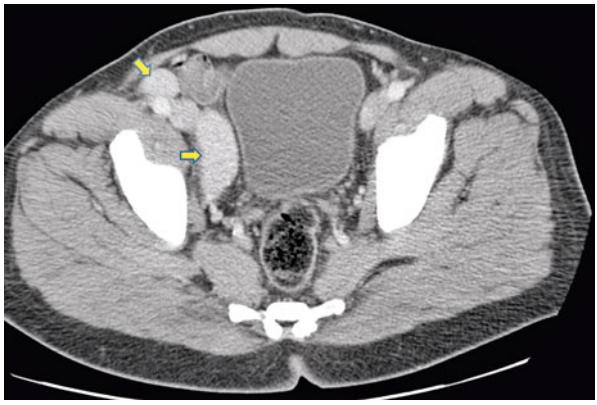

Fig. 5.28 Castleman's disease. Axial CT image shows enlarged right external iliac and right obturator nodes (*arrows*) that show vivid enhancement comparable to enhancement in adjacent external iliac vessels

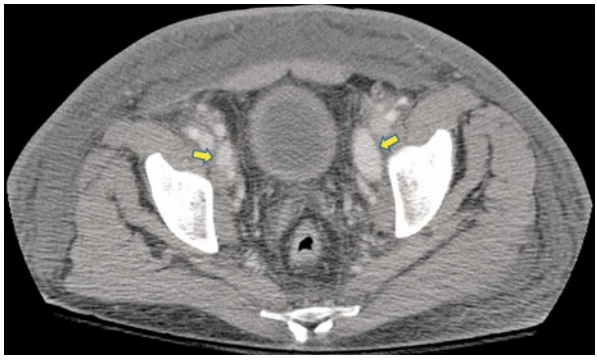

Fig. 5.29 Kaposi's sarcoma. Axial CT image shows diffuse soft tissue edema. There are enhancing bilateral obturator lymph nodes (*arrows*)

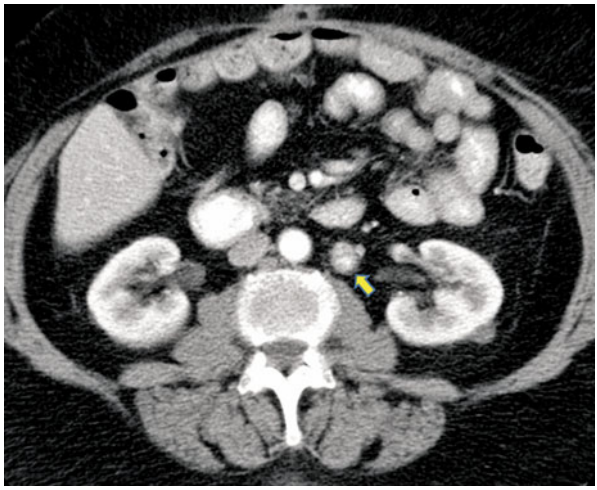

Fig. 5.30 Metastatic left paraaortic lymph node from primary mucinous ovarian cancer. Axial CT image shows calcified left periaortic lymph node (*arrow*)

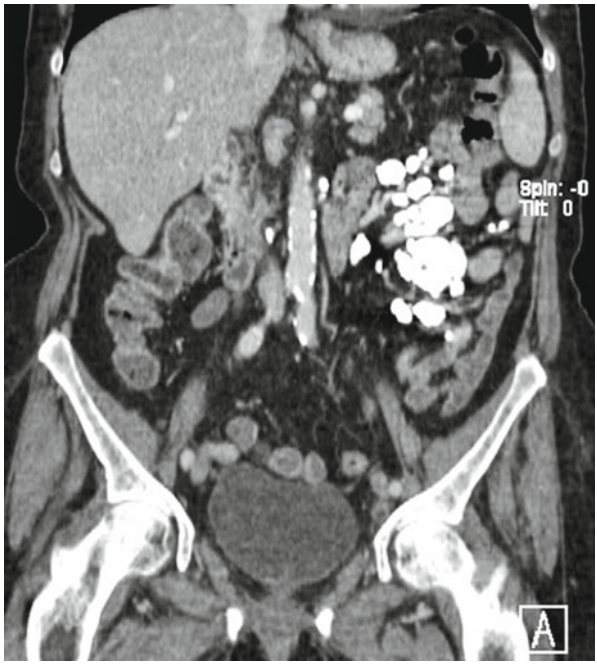

Fig. 5.31 Coronal reformatted CT image shows multiple calcified mesenteric lymph nodes from prior granulomatous disease

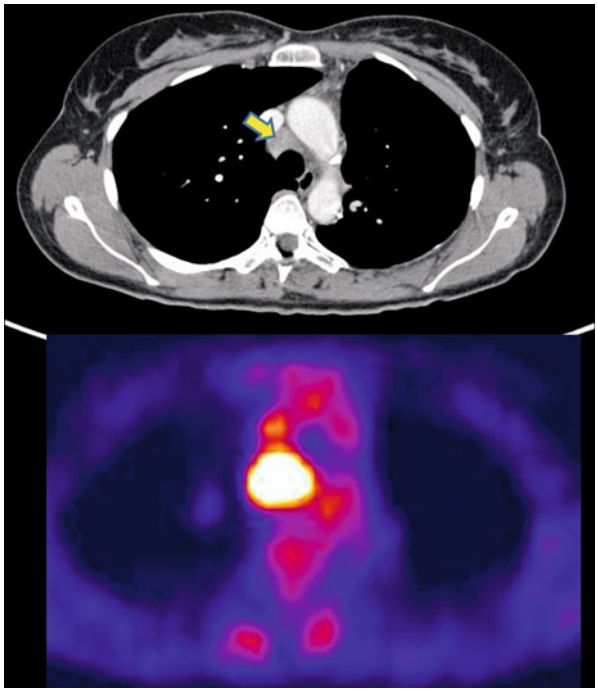

Fig. 5.32 Axial CT (*top*) and PET (*bottom*) image of the thorax shows an enlarged mediastinal lymph node (*arrow*) in a patient with sarcoidosis; the node shows intense FDG activity

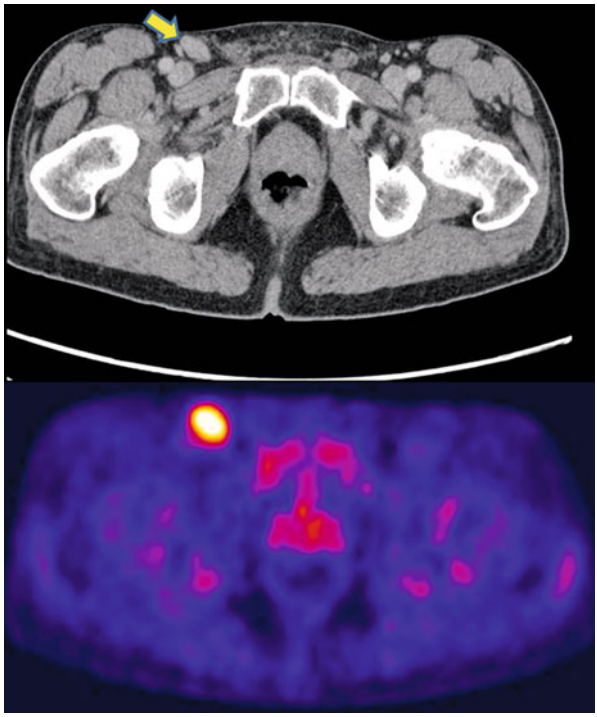

Fig. 5.33 Axial CT (*top*) and PET (*bottom*) image of the groin shows an enlarged right inguinal lymph node (*arrow*) in a patient with severe foot infection. The node shows intense FDG uptake

Uncommon
(i) Acute lymphadenitis (abscess)
(ii) Amyloidosis
(iii) Fatty replacement
(iv) Multiple myeloma
(v) Normal anatomic hilum
(vi) Reactive hyperplasia of connective tissue disease (collagen disease), especially rheumatoid arthritis
(vii) Sjögren disease

References

1. Feuerbach S, Lukas P, Gmeinwieser J. False interpretations of computed tomograms in malignant lymph node diseases of the pelvis and abdomen. Digitale Bilddiagn. 1984;4:176–80.
2. Suwatanapongched T, Gierada DS. CT of thoracic lymph nodes. Part II: diseases and pitfalls. Br J Radiol. 2006;79:999–1000.
3. Nyman R, von Sinner W, Mygind T, Kagevi I. Paraesophageal varices presenting as a retrocardiac mediastinal mass. A case report. Acta Radiol. 1994;35:255–7.
4. Resnick MI, Older RA. Diagnosis of genitourinary disease. 2nd ed. New York: Thieme; 1997.
5. Auh YH, Rosen A, Rubenstein WA, et al. CT of the papillary process of the caudate lobe of the liver. AJR Am J Roentgenol. 1984;142:535–8.
6. Reeder MM, Bradley W, Merritt CR. Gamuts in radiology. 4th ed. New York: Springer; 2003.
7. Glazer HS, Semenkovich JW, Gutierrez FR. Computed body tomography with MRI correlation. In: Lee JKS, Stanley RJ, Heiken JP, editors. Mediastinum. 3rd ed. Philadelphia: Lippincott-Raven Publishers; 1998. p. 261–349.
8. Santis MD, Strau G, Bachner M. Cross-sectional imaging techniques: the use of computed tomography (CT) and magnetic resonance imaging (MRI) in the management of germ cell tumors. In: Imaging in oncological urology. London: Springer; 2009. p. 287–303.
9. Hashim H, Alli K. Cotton-ball granuloma mimicking axillary lymphadenopathy in a breast cancer patient. Biomed Imaging Interv J. 2011;7:19.
10. Siewert B, Sosna J, McNamara A, et al. Missed lesions at abdominal oncologic CT: lessons learned from quality assurance. Radiographics. 2008;28:623–38.
11. Escott EJ, Branstetter BF. It's not a cervical lymph node, it's a vein: CT and MR imaging findings in the veins of the head and neck. Radiographics. 2006;26:1501–15.
12. Koehler PR, Mancuso AA. Pitfalls in the diagnosis of retroperitoneal adenopathy. J Can Assoc Radiol. 1982;33:197–201.
13. Lebtahi R, Cadiot G, Marmuse JP, et al. False-positive somatostatin receptor scintigraphy due to an accessory spleen. J Nucl Med. 1997;38:1979–81.
14. Ho KC, Ng KK, Yen TC, Chou HH. An ovary in luteal phase mimicking common iliac lymph node metastasis from a primary cutaneous peripheral primitive neuroectodermal tumour as revealed by 18-fluoro-2-deoxyglucose positron emission tomography. Br J Radiol. 2005;78:343–5.
15. Ko SW, Ko KS. Undescended testis appearing as a cecal mass in an adult. AJR Am J Roentgenol. 2002;179:1646–7.
16. Grant W. Lymphography – technique, indications and principles of interpretation. S Afr Med J. 1975;49:1341–6.

Index

M.G. Harisinghani (ed.), *Atlas of Lymph Node Anatomy*,
DOI 10.1007/978-1-4419-9767-8, © Springer Science+Business Media New York 2013